New Insights into Cenozoic Silicon Cycling in the Southern Ocean: Refined Application of Silicon Isotope Ratios in Biogenic Opal

Katherine E. Egan



Thesis submitted for the degree of Doctor of Philosophy in Earth Sciences

Trinity Term 2012

Department of Earth Sciences and Exeter College

Supervised by Prof. Rosalind E.M. Rickaby and Prof. Alex N. Halliday

Contents

Abstract 4

Extended Abstract 5

Chapter 1. Introduction 8

Abstract 8

1.1 Diatoms, Silicon, Carbon and Global Climate 11

1.2 Modern Ocean Silicon Dynamics 14

1.2.1 Summary 18

1.3 Reconstructing the Geological Silicon Cycle 21

1.3.1 Approaches to reconstructing the geological silicon cycle 21

1.4 Reconstructing the Cenozoic silicon cycle using biogenic opal $\delta^{30}Si$ 30

1.5 Thesis outline 33

Chapter 2. Methods 34

Abstract 34

2.1 Silicon Isotope analysis 36

2.1.1 MC-ICP-MS 36

2.1.2 Preparation of biogenic opal for MC-ICP-MS analysis 41

2.1.3 Mass dependency, precision and accuracy of MC-ICP-MS analyses 42

2.1.4 Vacuum-Line Fluorination IRMS 45

2.2 Opal extraction from sediments 48

2.2.1 Extraction of Sponge Spicules from Sediments 48

2.2.2 Existing Methods for Diatom Separation from Sediments and an Approach for Improvement 51

2.3 Summary 54

Chapter 3. Diatom Silicon Isotopes as a Proxy for Silicic Acid Utilisation: a Southern Ocean Core Top Calibration 55

Abstract 55

3.1 Introduction 56

3.2 Materials and methods 59

3.2.1 Materials 59

3.2.2 Methods 62

3.3 Results 68

3.3.1 Size Fraction Mass 68

3.3.2 Size Fraction Composition 70

3.3.3 Silicon Isotope Compositions 72

3.4 Discussion 76

3.4.1 Size Fraction Selection for Diatom $\delta^{30}Si$ Records 76

3.4.2 Diatom $\delta^{30}Si$ as a Proxy for Silicic Acid Utilisation 83
3.5 Conclusions 94
Chapter 4. Late Eocene CO_2 drawdown coincident with evolution of the Southern Ocean silicon cycle 96
Abstract 96
4.1 Introduction 97
4.2 Methods 102
4.2.1 Age Models 103
4.2.2 Opal Preparation and Analysis 104
4.3 Results 107
4.4 Discussion 108
4.4.1 Development of the Southern Ocean silicic acid concentration gradient 108
4.4.2 Development of ACC-type circulation and diatom radiation in the Late Eocene 111
4.4.3 Implications for carbon cycling and climate change at the Eocene-Oligocene Transition 114
4.5 Conclusions 117
Chapter 5. A Cenozoic record of Sponge $\delta^{30}Si$ 118
5.1 Introduction 119
5.2 Methods 123
5.3 Results 131
5.4 Discussion 134
5.4.1 Origin of noise in the Sponge $\delta^{30}Si$ Record 137
5.4.2 Low Silicic Acid Concentrations in the Oligocene and Miocene 140
5.4.3 Synthesis of Cenozoic Silicon Cycle Evolution 148
5.4.4 Links to pCO_2 through the Cenozoic 149
5.5 Conclusions 151
Chapter 6. Conclusions 152
6.1 Development of diatom $\delta^{30}Si$ as a proxy for silicic acid utilisation 152
6.2 The role of the Southern Ocean silicon cycle in the onset of Antarctic glaciation 154
6.3 The Cenozoic silicon cycle 155
6.4 Future Directions 155
7. References 157
Appendix 1: Silicon Isotope Data Tables 169
Appendix 2: Fragmentation during Microseparation 176
Appendix 3: Diatom Species Composition of Size Fractions 179
Acknowledgements 181

Abstract

The marine silicon and carbon cycles are intrinsically linked by a unique group of primary producers; the diatoms. These siliceous-walled phytoplankton play a significant role in carbon export, making them a critical component of the global biological carbon pump with the power to affect climatic change. In this thesis, the silicon isotope composition ($\delta^{30}Si$) preserved in diatom opal is used together with the $\delta^{30}Si$ of sponge opal, a powerful new proxy for deepwater silicic acid concentration, to document the Cenozoic Silicon cycle, shedding light on its role in carbon cycling and global climatic change. This study has developed a novel size-separation methodology to produce the first core top calibration of diatom $\delta^{30}Si$. The calibration demonstrates that diatom $\delta^{30}Si$ exhibits a strong negative correlation with surface water silicic acid concentration, supportive of its application as a proxy for silicic acid utilisation. The refined method is used to produce a diatom $\delta^{30}Si$ record, for the first time combined with sponge $\delta^{30}Si$, to gain insight into the Southern Ocean silicon cycle over one of the largest Cenozoic climatic shifts; the onset of Antarctic glaciation (~33.7 Ma). The two $\delta^{30}Si$ records yield the first geochemical footprint to demonstrate that diatom proliferation, coincident with the onset of Antarctic circumpolar current flow, was a precursor event to the Eocene-Oligocene Transition. Diatoms are shown to have played a role in climate cooling through enhanced export and burial of organic carbon on the seafloor. The first long term reconstruction of silicic acid concentration in subsurface waters of the Southern Ocean, which spans the Late Eocene to the earliest Pliocene, provides new evidence that oceanic vertical mixing rates, coupled with the efficient removal of silicon from the surface by the diatoms, have been the most important factor in controlling the silicon chemistry of the ocean over the Cenozoic.

Extended Abstract

The marine silicon and carbon cycles are intrinsically linked by a unique group of primary producers; the diatoms. These eukaryotes precipitate frustules of amorphous silica, and are a prolific component of the plankton community inhabiting turbulent, upwelling regions of the world's oceans. As photosynthetic organisms living in carbon dioxide venting regions of the ocean, diatoms possess the power to affect changes in the biological carbon pump. Their role in the export and eventual burial of organic carbon on the seafloor also bestows on them an ability to manipulate the long term carbon cycle. The formation of their silica frustules exerts a major control over the marine silicon cycle, and so through an understanding of the geological history of this cycle, insight may be gained into the effects of biogeochemical cycling on climate. In this thesis, the silicon isotope composition ($\delta^{30}Si$) preserved in diatom opal is used together with the $\delta^{30}Si$ of sponge opal, a powerful new proxy for deepwater silicic acid concentration, to document the Cenozoic Silicon cycle, shedding light on its role in carbon cycling and global climatic change.

Despite its continued use in palaeocanographic reconstructions, diatom $\delta^{30}Si$ has been, until now, without a clear methodology for the separation of pure diatom size fractions due to the small size of their frustules (on the order of 2-50μM). An advanced methodology for separating diatoms from sediments is presented here, and is applied to produce the first core top calibration of diatom $\delta^{30}Si$. This calibration demonstrates that diatom $\delta^{30}Si$ shows a strong negative correlation with surface water silicic acid concentration, highly supportive of the use of diatom $\delta^{30}Si$ as a proxy for silicic acid utilisation. Core top diatom $\delta^{30}Si$ agrees with mixed layer filtered diatom $\delta^{30}Si$ from published in situ studies, suggesting little to no effect of either dissolution during export through the water column, or early diagenesis, on sedimentary diatom $\delta^{30}Si$.

The refined method is further used to produce a diatom $\delta^{30}Si$ record from the Southern Ocean covering the Late Eocene to Early Oligocene. This time period witnessed the abrupt onset of Antarctic glaciation, in what was one of the most dramatic climate shifts of the Cenozoic. Declining pCO_2 levels are the most likely trigger of glaciation, yet it is still not clear what mechanisms were responsible for lowering pCO_2. In the modern Southern Ocean, the relationship between diatom productivity and overturning circulation driven by the Antarctic Circumpolar Current exerts a significant control over both global silicic acid distributions and the efficiency of the biological pump. The Eocene-Oligocene boundary is thought to encompass the development of this important relationship. The opening of two gateways to circumpolar flow, the Drake Passage and the Tasman gateway, created a 360˚ pathway for wind driven circulation. Diatom expansion to fully utilise silica has been suggested to have occurred over a similar time period, and the hypothesis put forward that the associated, diatom driven, burial of organic carbon may have played a role in the drawdown of atmospheric carbon dioxide. The Eocene-Oligocene diatom $\delta^{30}Si$ record is used for the first time in combination with a complimentary sponge $\delta^{30}Si$ record to yield important information regarding both the timing of diatom radiation and the onset of Antarctic circumpolar flow. Furthermore, the records infer that diatoms played a role in climatic deterioration by driving organic carbon burial, contributing to the observed pCO_2 drawdown not only at, but also prior to, Antarctic glaciation.

Finally, the Eocene-Oligocene sponge $\delta^{30}Si$ record is extended to produce the first long term reconstruction of silicic acid concentration in subsurface waters of the Southern Ocean covering a large portion of the Cenozoic (~38 Ma to ~4 Ma). The record, which spans the Late Eocene to the earliest Pliocene, provides new evidence that ocean circulation, coupled with the efficient removal of silica from the surface by the diatoms, has been the most important factor in controlling the silicon cycle over the Cenozoic. A three step history of the Late Eocene to modern Southern Ocean silicon cycle is proposed; 1) 38−31.5 Ma: Incursion of silicic acid rich deepwater into the Southern Ocean due to the subsidence of gateways, with associated expansion of the

diatoms to utilise silicic acid at near modern capacity; 2) 31 Ma−2.7 Ma: Sustained lower silicic acid concentrations caused by relatively high rates of surface-deepwater exchange that resulted mainly from the Eocene-Oligocene establishment of circum-Antarctic current flow; 3) 2.7 Ma onward: A return to higher silicic acid concentrations caused by reduced rates of overturning circulation associated with the onset of Northern Hemisphere glaciation.

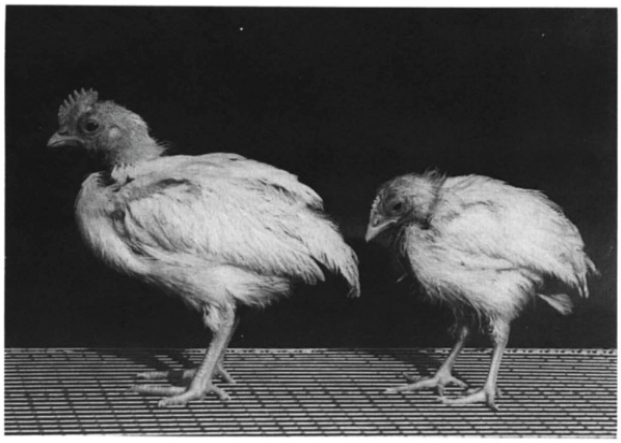
Valuable insight into the coupling of the global silicon and carbon cycles may in future be gained from the generation of Cenozoic coupled diatom-sponge $\delta^{30}Si$ records, at higher resolution, from the extremities of the meridional overturning circulation in the North Atlantic and North Pacific. The work undertaken here suggests that diatom radiation was an important driver of organic carbon burial and climatic change during the Late Eocene and Early Oligocene. Characterisation of diatom evolution and radiation prior to this, through the extension of diatom and sponge $\delta^{30}Si$ records into the Cretaceous, could further our understanding of how these micro-organisms may have shaped climate evolution.

Chapter 1. Introduction

Abstract

Silicon, element number fourteen of the periodic table, makes up around two thirds of Earth's mass. It is a nutrient element; you contain around 0.002% Si by mass. In humans and animals, silicon may play a role in bone formation, influence hair and nail strength, and decrease the risk of atherosclerosis (Prescha et al., 2012). However, our growth is never limited by its availability and its essentiality is far from established (EFSA, 2011, although, to be on the safe side, daily silicon intake can be increased using liquid dietary supplements*, Figure 1.1a and b). This is not the case for the diatoms, a group of photosynthetic algae which precipitate shells, or frustules, of amorphous silica (opal, $SiO_2.nH_2O$, Figures 1.1c and 1.2). For modern diatoms, the availability of silicon is more often than not the primary factor limiting the extent of their growth (Brzezinski and Nelson, 1996; De La Rocha, 2007). Many people have probably never heard of diatoms, but they surround us, inhabiting a vast range of environments from soils to puddles, through rivers, lakes, coastal environments, and into the open ocean. In the cold, turbulent seas surrounding Antarctica they are particularly prolific. At these polar latitudes, diatoms support a food-web which captures society's attention. Energy fixation through diatom photosynthesis feeds the krill, penguins and giant whales which feature in extensive swathes of footage included in television programs such as the BBC's 'frozen planet.' However, diatoms are likely to be of far greater significance to us than being simply the basis for a good nature documentary: They are often considered a key player in driving global climatic variation. Understanding the way in which diatoms, the silicon cycle and global climate are linked, and have evolved over geological time, is the motivation for this work.

a.



b.

Table 2. Silicon content of commercial beers

Category	Si, average (ppm)	Range (ppm)	*N*
All	29.4	6.4–56.4	100
Ales	32.8	11.1–55.5	67
Lagers	23.7	10.1–56.4	27
Regular lagers	23.8	14.5–40.4	9
Light lagers	17.2	14.1–23.4	5
IPA	41.2	26.2–55.5	15
Non-alcoholic	16.3	6.4–25.7	6
Wheat	18.9	14.3–23.4	7
Pale ale	36.5	16.8–50.7	18
Sorghum	27.3	23.9–30.7	2
USA	31.6	11.1–56.4	80
International	20.4	6.4–40.4	20
California	34.2	11.1–56.4	50
Colorado	20.8	14.1–26.2	10

c.

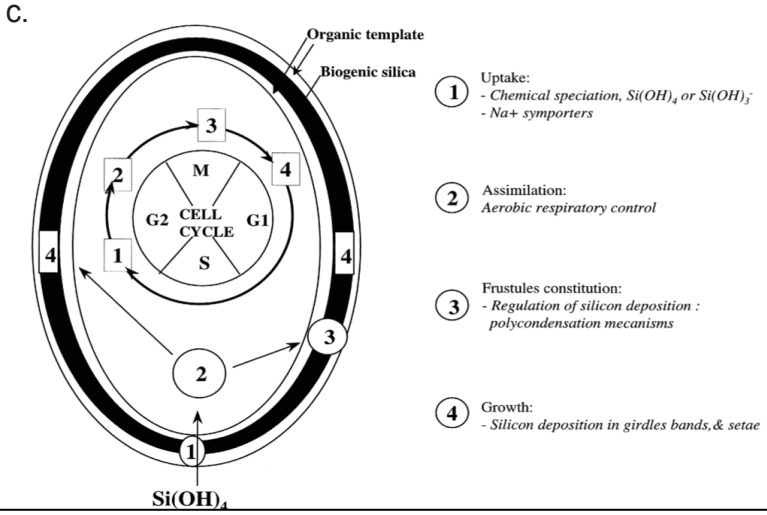


Figure 1.1a. 4 week old chicks on silicon supplemented diet (left) and low-silicon diet (right; Carlisle, 1988); **b.** Silicon content of commercially available beers (Casey and Bamforth, 2010); * please drink responsibly, http://www.drinkaware.co.uk/. Humans and animals are not limited by silicon intake, but this is not the case for diatoms, which have an absolute requirement for silicon driven by **c.** the formation of shells composed of amorphous opal ($SiO_2.nH_2O$). G1, G2, M and S are the stages of the diatom cell cycle representing Gaps 1 and 2, Mitosis and DNA replication (Ragueneau et al., 2000).

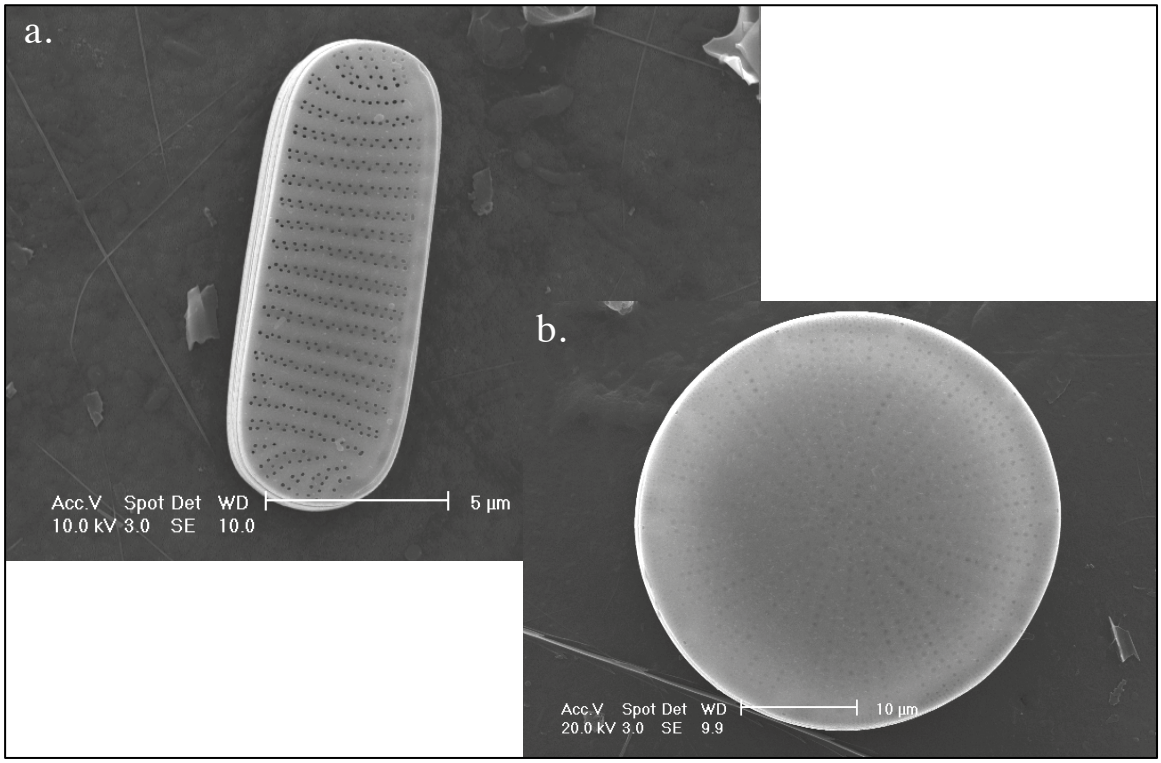


Figure 1.2 SEM images of the silica frustules produced by species representing the two orders of diatoms; **a.** the pennate diatom *Fragilariopsis curta* and; **b.** the centric diatom *Actinocyclus actinopyctus*.

1.1 Diatoms, Silicon, Carbon and Global Climate

Whilst diatoms utilise silicon in the formation of their frustules, as members of the phytoplankton they also fix carbon, dissolved in the ocean's surface, into organic molecules. They fundamentally tie the global silicon and carbon cycles (Ragueneau et al., 2000) and constitute an important part of the 'biological carbon pump' (Figure 1.3a). The term 'biological carbon pump' refers to the removal of organic carbon from the surface ocean when phytoplankton, and the higher life forms they support, die and sink (Volk and Hoffert, 1985; De La Rocha, 2007). In the deep ocean, this organic matter is remineralised, enriching the waters in nutrients and dissolved CO_2. The effect is to create a large carbon reservoir in the abyssal ocean, which is isolated from the atmosphere by phytoplankton carbon uptake in the surface. Having come full circle, it is evident that the biological carbon pump, by controlling the vertical distribution of carbon in the ocean, has great power to affect climatic change though mediation of ocean-atmosphere CO_2 balance (Figure 1.3b, CO_2 is an important greenhouse gas, e.g. Knox and McElroy, 1984; Sigman and Boyle, 2000). The biological pump is an important feature of the short term carbon cycle, which operates on thousand year timescales through the repartitioning of carbon between various surficial reservoirs. Furthermore, diatoms are involved in the long term carbon cycle where changes occurring over millions of years pertain to the balance between wholesale volcanic inputs and sedimentary outputs (Figure 1.3c). The link between diatoms and the long term carbon cycle is the burial of organic carbon in sediments accumulating on the seafloor, which acts to drawdown atmospheric CO_2 (Zachos et al., 1993; Sigman and Boyle, 2000; Berner, 2003; Zachos and Kump, 2005).

Diatoms account for ~40% of total primary production in the global ocean (Tréguer et al., 1995), and among the phytoplankton are considered particularly important to the biological pump (Falkowski et al., 1998; Smetacek, 1999; Sigman and Boyle, 2000). This is, in the first instance, because diatoms effectively export carbon from the surface ocean: Their silica frustules provide

ballast material, they are relatively large cells at the base of short food webs, and they form blooms which can terminate in the aggregation and the mass settling of cells (Buesseler, 1998; Smetacek, 1999; Ragueneau et al., 2000; Baines 2010). A second, and probably more significant reason, relates to the ecology of diatoms, which may contribute up to 75% to primary production in upwelling regions of the world's oceans (Nelson et al., 1995; De La Rocha et al., 1998). In these areas, nutrients and CO_2 sequestered in the deep ocean by the biological pump are resupplied to the surface. Diatom domination of the resident phytoplankton community makes them critical in determining the magnitude of the CO_2 flux to the atmosphere, explaining their importance to the biological pump. The reason diatoms inhabit these regions will become clear through the following discussion, and is related to the distribution of the silicon in the oceans.

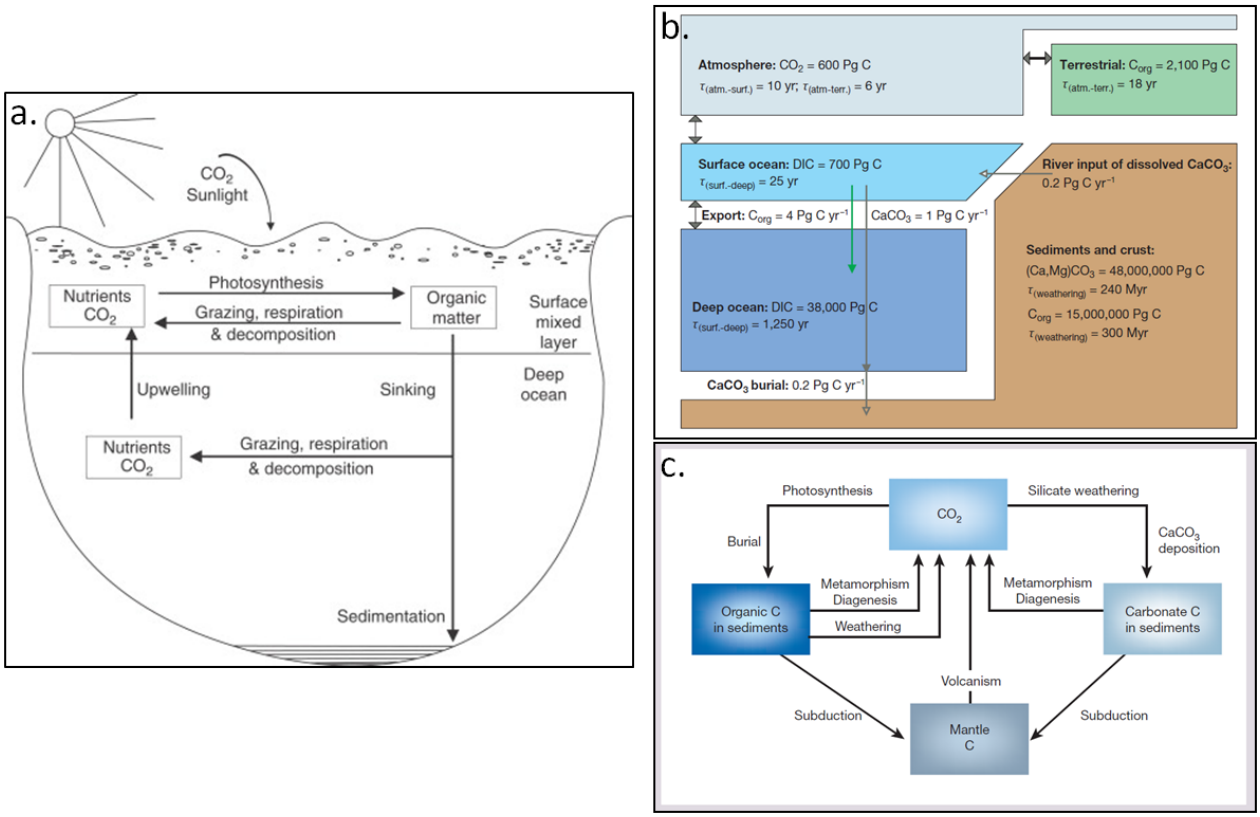


Figure 1.3a. The Biological Carbon pump. Carbon fixed in the surface ocean by phytoplankton is exported via sinking to the deep ocean, where the majority dissolves, enriching waters in dissolved carbon and other nutrients, whilst capping the exchange between the deep-CO_2 rich reservoir and the atmosphere. As a result of the greenhouse properties of CO_2 the biological pump plays a significant role in controlling global climate. Diatoms, which account for up to 75% of primary production in upwelling and coastal regions of the world's oceans, are an important component of this pump; Figure from De La Rocha (2007); **b.** Distribution of carbon between various reservoirs important in the short term carbon cycle where ocean circulation is important for climate; Figure from Sigman and Boyle (2000); **c.** The long term carbon cycle in which the burial of organic carbon is important in determining atmospheric CO_2 concentration; Figure from Berner (2003).

1.2 Modern Ocean Silicon Dynamics

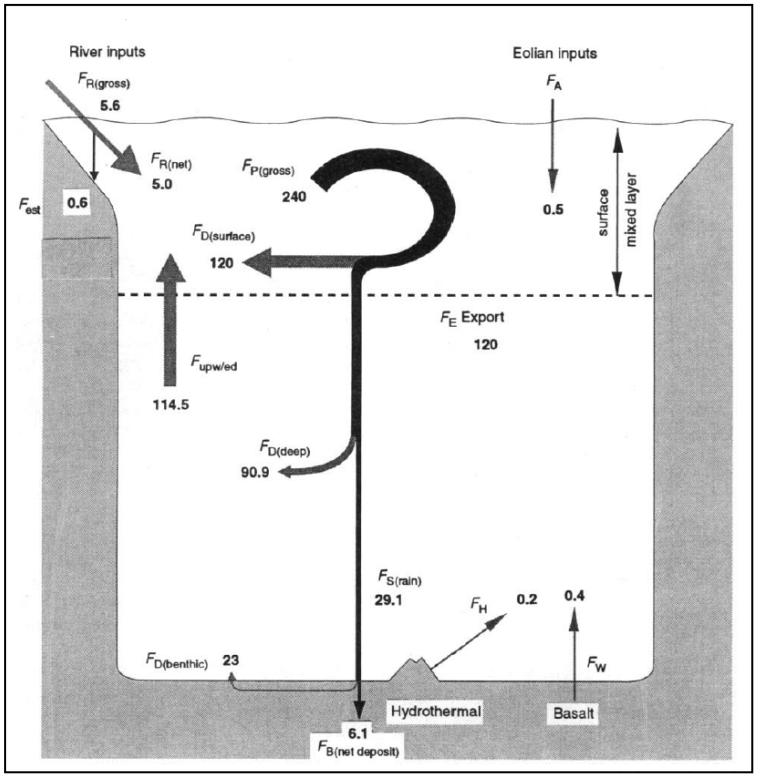


Figure 1.4 The modern marine silicon cycle (Tréguer et al., 1995). Grey arrows are silicic acid fluxes and black arrows are particulate silica fluxes.

Today, the marine silicon cycle is thought to be in steady state, with inputs to the ocean balanced by outputs. The ocean contains on the order of 10^{17} moles of Si, which exists predominantly in the form of silicic acid, $Si(OH)_4$ (Figure 1.4; Tréguer et al., 1995). Input of silicon to the ocean is almost entirely via the riverine transport of continental weathering products, which supplies around 6 Gt per year. There are additional small contributions from hydrothermal circulation, aeolian dust flux and sea floor weathering. These inputs are balanced by a sole output, being the burial of biogenic silica on the seafloor, again at ~6 Gt/yr. Given an average concentration of ~70μM, the residence time of silicon is estimated by Tréguer et al., (1995) to be around 15000 years. Probably the most remarkable feature of this system is its complete domination by

biological (almost entirely diatom) production, which fixes around 240 Gt Si/yr into amorphous opal (Tréguer et al., 1995; Nelson et al., 1995; Ragueneau et al., 2000). For the system to remain in steady state requires, as is the case, a large recycling of Si within the water column. Over half of the biological silica produced is regenerated in the surface, with a further ~91 Gt/yr dissolving in the deep ocean, and a net burial of around only 3.5%. This intense dissolution of opal occurs because the entire ocean is undersaturated with respect to biogenic opal, which at deep ocean temperatures has an equilibrium solubility of around 1000µM. A silicon residence time of 15000 years should produce an ocean homogeneous with respect to silicic acid (for a mixing time of 1000 years). However, interaction of the intense recycling loop created by diatom productivity with the ocean's circulation creates stark gradients in silicic acid concentration both vertically and horizontally (Figure 1.5; Tréguer et al., 1995; Sarmiento et al., 2004; Sarmiento et al., 2007).

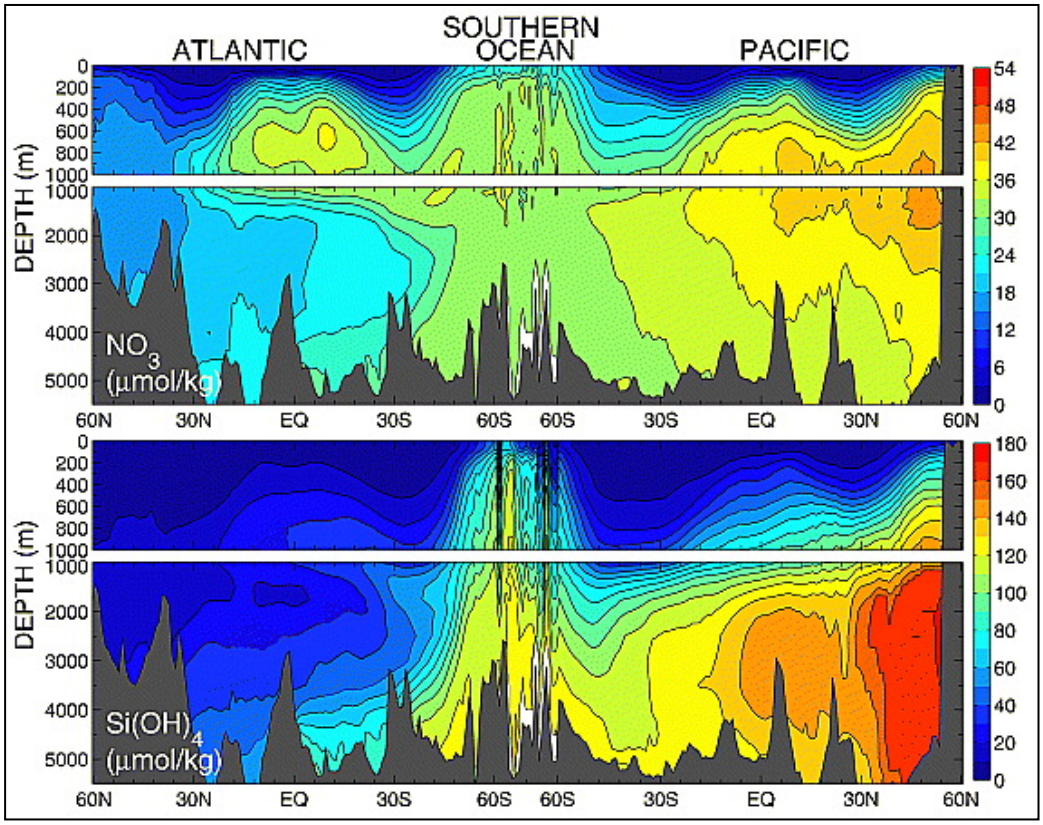


Figure 1.5 Nitrate (top) and silicate (bottom) distributions along the path of the global overturning circulation (Sarmiento et al., 2007).

To understand the distribution of silicic acid in the ocean, its relationship with the diatoms, and the links between the biological silicon cycle and climate, it is first necessary to consider the oceans circulation regime. Along the global 'conveyor belt' of thermohaline circulation (Figure 1.6a; Broecker, 1991) surface flow is directed toward the North Atlantic where cooling of salty waters results in sinking and the formation of deepwater. During transit, biological production removes nutrients from the surface, leaving deepwater formed in the North Atlantic (North Atlantic Deepwater, NADW) poor in silicic acid and other nutrients (Figure 1.5). As the newly formed deepwater travels south out of the Atlantic, through the Southern Ocean and eventually into the North Pacific, it ages and accumulates silicic acid and other nutrients exported from the surface. To first order, the conveyor provides a simple and convenient way to explain the distribution of nutrients such as silicic acid and nitrate in the ocean. Low concentrations in the young Atlantic deep water and high concentrations in old North Pacific subsurface water are clear in Figure 1.5. However, what it is also clear from Figure 1.5 is that high nutrient concentrations are present in the surface waters of the Southern Ocean, and that here the largest surface silicic acid gradient in the ocean exists. In addition it can be observed that over large regions of the ocean low silicic acid concentrations prevail to depths of around 1000m, far lower than the thermocline that supplies nutrient to the surface. On the other hand, the nitrate concentration gradient is close to the surface. This second observation can be partially explained by the deep regeneration depth of biogenic silica relative to organic matter (Ragueneau et al., 2000; Sarmiento and Gruber, 2006). However, it is also, along with the steep silicic acid gradient of the Southern Ocean, driven by the relationship between diatoms and circumpolar circulation in this region (Sarmiento and Gruber, 2006; de Souza et al., 2012).

An important feature not immediately obvious in the great conveyor cartoon is the Antarctic Circumpolar Current (ACC; Figure 1.6b). Uniquely in the modern ocean, the seas around Antarctica are open to flow of the ocean around the entire globe. The resultant wind driven current, the ACC, with a flow of around 100 Sv (Orsi et al., 1995; $1Sv = 10^6 m^3 s^{-1}$), transports the

largest mass of water of any current in the ocean. The flow is concentrated into three main fronts that span from the surface to the seafloor; the Sub-Antarctic Front (SAF), the Polar Front (PF), and the Southern ACC front (SACCF). The limit of ACC flow is defined by the southern boundary (SB; Figure 1.7, definitions follow Orsi et al., 1995). In the ACC nutrients are upwelled from the abyssal ocean as deepwater shoals south of the PF (Figure 1.7; Speer et al., 2000). This supplies silicic acid and other nutrients to the surface, explaining the high silicic acid and nitrate concentrations observed in the Southern Ocean (Figure 1.5). A portion of this upwelled water moves southwards, where it experiences limited primary productivity (Marinov et al., 2006), and subsequently forms nutrient rich Antarctic Bottom Water (AABW). This AABW fills large regions of the deep ocean as it flows northward into the Atlantic, Indian and Pacific Basins (Figure 1.5, bands of higher silicic acid and nitrate concentrations emanating from the Southern Ocean along the seafloor). This section of the ACC, to the south of the polar front, exposes CO_2 rich deepwater to the atmosphere, and as productivity does not keep up with nutrient supply, is a key region of CO_2 venting to the atmosphere. Diatoms are prolific in these waters (Nelson and Smith Jr., 1986; Tréguer et al., 1995) and as such are important in determining the extent of CO_2 efflux. A second portion of the upwelled water moves northwards via Ekman transport, eventually finding its way into the Antarctic Intermediate and Sub-Antarctic Mode Waters (AAIW and SAMW; Figure 1.7, Speer et al., 2000). These water masses subduct at the northern edge of the ACC and feed nutrients to a large portion of the lower latitude thermocline (Sarmiento et al., 2004). It is this region in that we find the answer to the second question, why low silicic acid concentrations penetrate to a much greater depth than those of nitrate. Diatom production that occurs during Ekman transport not only contributes to a marked band of carbon export (Figure 1.7; Ito et al., 2005), but also strips silica from the surface ocean to a much greater extent than nitrate (Sarmiento et al., 2004). This is due both to the deep regeneration depth of biogenic silica (de Souza et al., 2012), and to the unusually high uptake ratio of Si:N by Southern Ocean diatoms (Brzezinski et al., 2003; Baines et al., 2010). Waters that are exported to the lower latitudes are therefore enriched in nitrate with respect to silicic acid, and it is these waters that

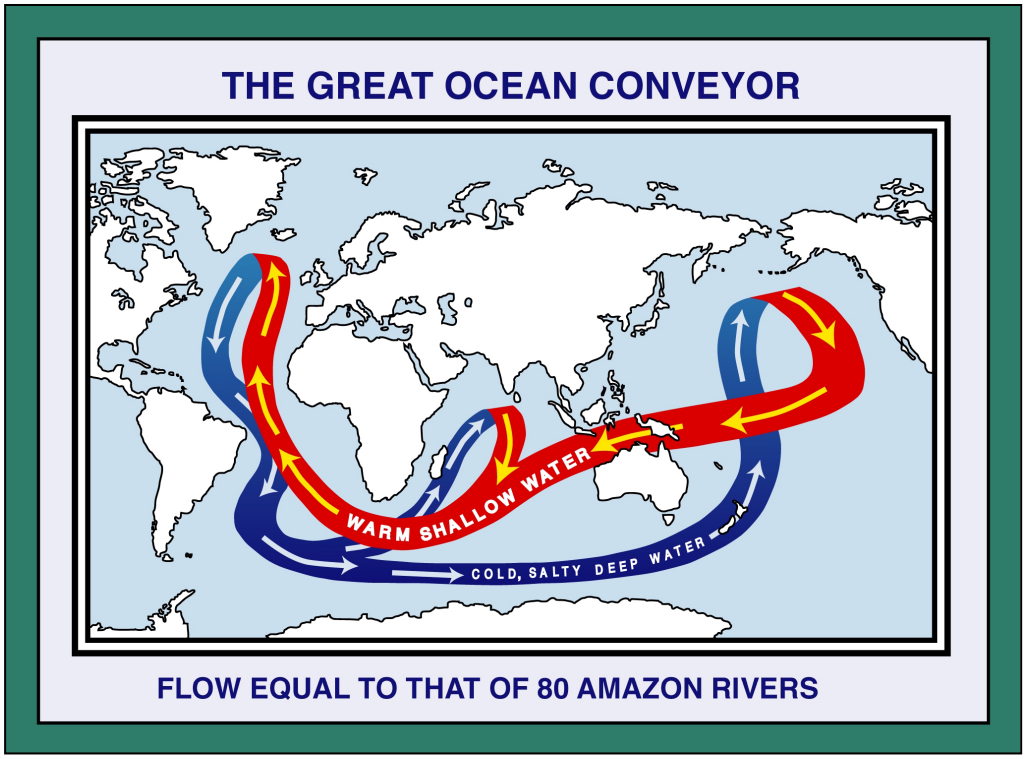
support up to three quarters of primary productivity north of 30˚S (Sarmiento et al., 2004). Silicic acid is effectively trapped in the Antarctic 'ring,' creating a narrow band of opal deposition and a strong north-south silicic acid gradient in the surface ocean. Thus, the Southern Ocean and the diatoms that reside within it exert a great control over the distribution of silicic acid in the world's oceans (Sarmiento et al., 2004), and also have a key role to play in the biological carbon pump (Marinov et al., 2006).

1.2.1 Summary

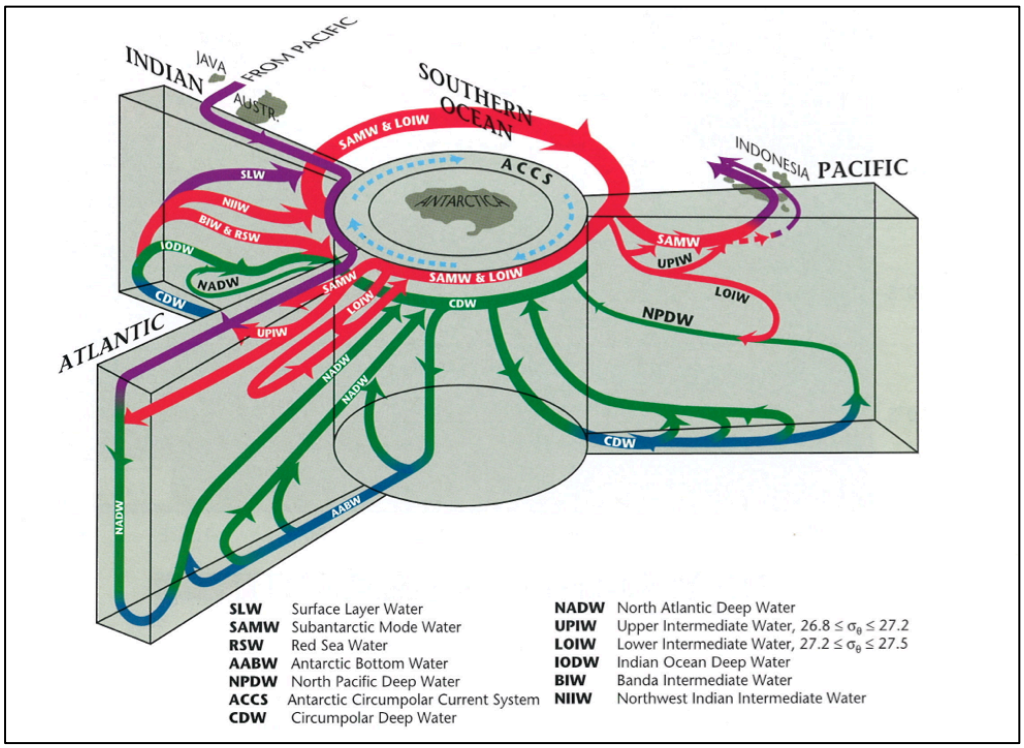
Weathering of continental silicate rocks is the dominant input of silicon to the ocean, and the burial of (primarily diatomaceous) biogenic opal on the seafloor is the singular output. The marine silicon cycle is overwhelmingly controlled by the biological silicon cycle. Near complete silicic acid utilisation by diatoms in the surface ocean and the intense regeneration of their silica frustules in undersaturated surface and deep waters drives strong vertical silicic acid gradients. Diatoms control, in combination with the global overturning circulation, the distribution of silicic acid through the oceans. Within the circulation regime, the Antarctic Circumpolar Current of the Southern Ocean exerts arguably the largest control over the partitioning of silicic acid between different water masses. Diatoms are selfAh limiting, confining themselves to deep upwelling regions like the Southern Ocean by limiting the export of silicic acid to the lower latitude thermocline and through the sequestration of dissolved silica at depths greater than 1000m.

Figure 1.6a. Cartoon of the 'ocean conveyor.' From Broecker (1991). This schematic of the ocean's overturning circulation lacks one critical feature: the Antarctic Circumpolar Current (ACC); **b.** schematic of the overturning circulation associated with the ACC (From Schmitz 2005).

a.


THE GREAT OCEAN CONVEYOR
WARM SHALLOW WATER
COLD, SALTY DEEP WATER
FLOW EQUAL TO THAT OF 80 AMAZON RIVERS

b.


INDIAN
JAVA
FROM PACIFIC
AUSTR.
SOUTHERN OCEAN
SAMW & LOIW
ACCS
ANTARCTICA
INDONESIA
PACIFIC
SLW
NIIW
BIW & RSW
IODW
NADW
CDW
SAMW
LOIW
UPIW
ATLANTIC
NPDW
AABW
SLW Surface Layer Water
SAMW Subantarctic Mode Water
RSW Red Sea Water
AABW Antarctic Bottom Water
NPDW North Pacific Deep Water
ACCS Antarctic Circumpolar Current System
CDW Circumpolar Deep Water
NADW North Atlantic Deep Water
UPIW Upper Intermediate Water, 26.8 ≤ σθ ≤ 27.2
LOIW Lower Intermediate Water, 27.2 ≤ σθ ≤ 27.5
IODW Indian Ocean Deep Water
BIW Banda Intermediate Water
NIIW Northwest Indian Intermediate Water

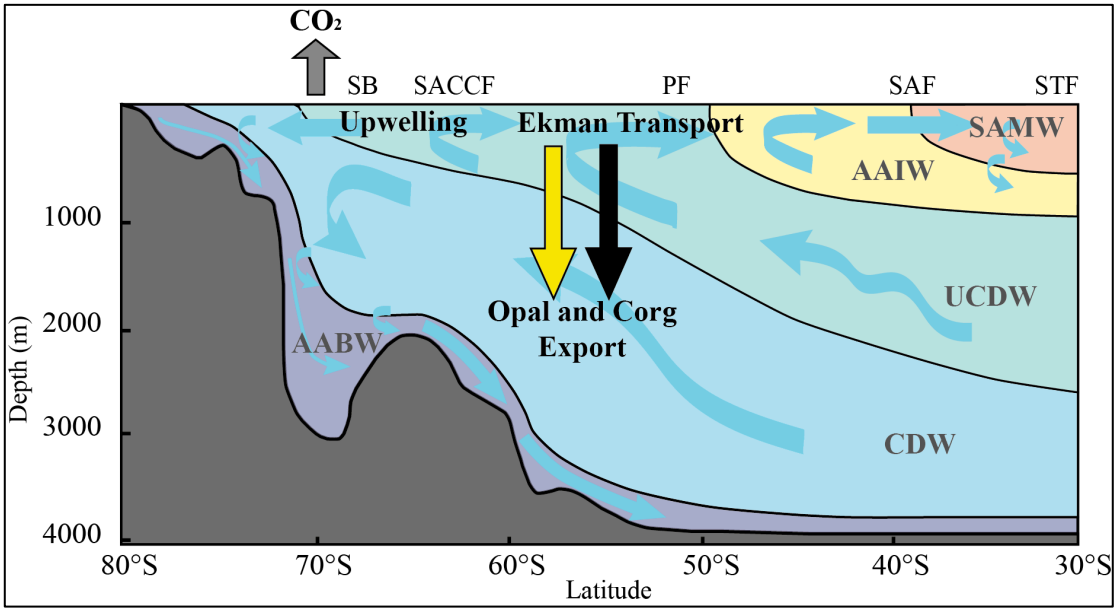


Figure 1.7 Schematic of the Southern Ocean overturning circulation (modified from Speer et al., 2000) and its relationship with diatoms, the biological pump, and atmospheric pCO_2. Upwelling to the south of the Polar Front (PF), driven by the Antarctic Circumpolar Current (ACC) supplies nutrient, CO_2 rich water to the surface. A portion of this water moves northwards via Ekman transport, where these nutrients are utilised by phytoplankton. Diatoms dominate production in the southern ACC, driving a marked belt of opal export and deposition (Yellow arrow, location based on Atlantic sector opal export in the model of Ito et al., 2005), whilst a combination of diatoms and smaller phytoplankton contribute to a broader belt of carbon export who's locus lies a few degrees northward (Black arrow, again based on Ito et al., 2005). A second portion of upwelled water moves southwards and eventually forms Antarctic Bottom Water (AABW). Along this pathway, limited primary production allows carbon dioxide venting to the atmosphere (Marinov et al., 2006). CDW = circumpolar deepwater; UCDW = upper circumpolar deepwater; AAIW = Antarctic intermediate water; SAMW = sub-Antarctic mode water; SB = southern boundary of the ACC; SACCF = southern ACC front; PF = Polar front; SAF = sub-Antarctic front; STF = sub-tropical front.

1.3 Reconstructing the Geological Silicon Cycle

The silicon cycle is controlled by two processes that may impact significantly on global climate. Silicate weathering, which controls the input of silicic acid to the oceans, is well established as a driver of long term (Ma) changes in atmospheric pCO_2 (Figure 1.3c; Berner, 1990). Importantly, silicate weathering also entails a negative feedback mechanism that maintains relative pCO_2 and climate stability (Berner and Caldeira, 1997). The relevance of the biological pump, of which the silica walled diatoms are a key component, is twofold. On long timescales, the deposition of organic carbon on the seafloor removes carbon from the dynamic surface reservoir and acts to drawdown atmospheric CO_2 (Figure 3c; Berner, 2003). Over shorter timescales, the extent to which the deep ocean reservoir of carbon and other nutrients is capped by surface productivity controls the atmosphere-ocean CO_2 balance (Figure 1.3b; Sigman and Boyle, 2000). The extent of deepwater isolation can be perturbed by either change in the rate of deepwater ventilation or in the efficiency of biological carbon export from the surface ocean.

1.3.1 Approaches to Reconstructing the Geological Silicon Cycle

Interest in understanding the history of the marine silicon cycle is not new. Prior to 1997, the main approach to this problem was to construct records of opal mass accumulation rate (Cortese et al., 2004) and to consider the nature of siliceous microfossils contained in sediments (Harper and Knoll. 1975). These techniques have provided us with tantalising glimpses and useful insight into silicon cycle evolution. Records of diatom diversity have been used to infer pulses of expansion in the Late Oligocene and the Miocene (Falkowski et al., 2004). Global compilation of opal mass accumulation rates has yielded evidence for dramatic changes in the location of the major opal burial sinks over the Cenozoic (Cortese et al., 2004). However, these records, in isolation, can be difficult to interpret. Processes controlling the rate of opal burial on the seafloor

are complex, and not fully understood (Ragueneau et al., 2000). As well as the obvious control of diatom production in the surface, the rate of opal export, the nature of the food chain, the deep to surface silicic acid gradient, the intensity of the bacterial regeneration loop, and differences in opal specific surface area and aluminium content are all examples of processes thought to influence the preservation of opal on the seafloor (Ragueneau et al., 2000; Van Cappellen, 2002). Accumulation of opal is also influenced by the focussing and winnowing of sediments as well as dilution by other sedimentary components such as clay and carbonate. Although this can be accounted for by normalising records to particle reactive nuclides such as ^{230}Th or ^{231}Pa (Kumar et al., 1995; De La Rocha et al., 1998) the short half lives of these nuclides mean such correction methods are not applicable on timescales longer than those of glacial-interglacial variation. Diatom diversity changes are problematic to interpret in terms of the global silicon cycle because they are not directly related to the productivity of diatoms, and can be highly biased by preservation and sample availability (Rabosky and Sorhannus, 2009).

The key event in 1997 was the publication of De La Rocha's paper titled 'Fractionation of silicon isotopes by marine diatoms during biogenic silica formation.' Although the silicon isotope composition (ratio of ^{30}Si to ^{28}Si) of diatom silica had previously been measured (Douthitt, 1982), it was this paper which demonstrated how these silicon isotope ratios reflected the extent of silicic acid utilisation by cultured diatoms. Subsequent studies went on to advance and substantiate the culture work, measuring the silicic acid composition of ocean waters and the diatom opal they contained (De La Rocha et al., 2000; Varela et al., 2004; Cardinal et al., 2005; Reynolds et al., 2006a; Cardinal et al., 2007; Fripiat et al., 2007; Beucher et al., 2008; Beucher et al., 2011; De La Rocha et al., 2011; Fripiat et al., 2011a; Fripiat et al., 2011b; Fripiat et al., 2011c; de Souza et al., 2012), testing the species dependence of the silicon fractionation factor (Milligan et al., 2004) and to applying the proxy to study glacial interglacial climate change (De La Rocha et al., 1998; Brzezinski et al., 2002; Beucher et al., 2007; Horn et al., 2011) and the onset of North Pacific stratification at 2.7Ma (Reynolds et al., 2008).

More recently in 2010, two papers in the same issue of Earth and Planetary Science letters outlined a new proxy for silicic acid concentration; the silicon isotope composition preserved in sponge spicules (Wille et al., 2010; Hendry et al., 2010). These two opal based proxies provide us with the necessary tools to study two key components of the past silicon cycle, the utilisation of silicic acid by diatoms in the surface, and the silicic acid concentration of the ocean's deep waters.

1.3.1.1 Silicon Isotope Fractionation and Notation

Silicon has three stable isotopes: ^{28}Si (92.2%), ^{29}Si (4.7%) and ^{30}Si (3.1%). The difference in mass between these isotopes imposes systematic variations in their reaction rate during chemical reactions. This mass dependant fractionation may be equilibrium or kinetic and results in the observed variation of silicon isotopic ratios in both terrestrial and extraterrestrial materials, including the biological fractionation by sponges and diatoms considered here. Isotope ratios are generally expressed using delta notation, and the fractionation between different phases is described using the fractionation factor, $\alpha = {}^{30}Si/{}^{28}Si_{product}/{}^{30}Si/{}^{28}Si_{substrate}$ (kinetic fractionation). Fractionation is also often expressed using the ε (‰) notation, which is related to α by the equations $\varepsilon = 10^3 \ln \alpha$ or $\varepsilon \sim (\alpha - 1)10^3$.

1.3.1.2 Diatom $\delta^{30}Si$

During silicification diatoms discriminate biologically against the heavier Si isotopes (^{30}Si and ^{29}Si) with a fractionation factor ($^{30}\varepsilon$) of −1.1±0.4‰ (De La Rocha et al., 1997; Milligan et al., 2004). In the oceans, this imparts a high $\delta^{30}Si$ ($\delta^{30}Si = ([(^{30}Si/^{28}Si)_{sample}/(^{30}Si/^{28}Si)_{std}]-1)*1000]$) signature on surface water silicic acid, and hence on any diatom silica which subsequently forms

from it. At depth, remineralisation of diatom silica releases silicic acid with a lower $\delta^{30}Si$ than the surface silicic acid, and creates a gradient between high $\delta^{30}Si$, low silicic acid surface water and high silicic acid, low $\delta^{30}Si$ deep water. Upwelling re-supplies the high silicic acid, low $\delta^{30}Si$ water to the surface ocean. Diatom $\delta^{30}Si$ is therefore a measure of diatom silicic acid utilisation, which is itself a balance between the amount of diatom silicification and the rates/composition of upwelled water. This is the basis of the diatom $\delta^{30}Si$ proxy, where high $\delta^{30}Si$ represents high utilisation (De La Rocha et al., 1997; De La Rocha et al., 1998; De La Rocha, 2006).

Diatom silicon isotope fractionation maybe modelled by considering either Rayleigh or steady state fractionation. Rayleigh fractionation (Figure 1.8) assumes a closed system with a single input of silicic acid to the surface ocean that is progressively utilised by diatoms. It is characterised by the following equations:

$$\delta^{30}Si(OH)_4 = \delta^{30}Si(OH)_{4\ initial} + {}^{30}\varepsilon \ln f \quad \text{(eq.1)}$$

$$\delta^{30}Si\text{-}bSiO_2 = \delta^{30}Si(OH)_4 + {}^{30}\varepsilon \quad \text{(eq.2)}$$

$$\delta^{30}Si\text{-}bSiO_{2\ acc} = \delta^{30}Si(OH)_{4\ initial} - {}^{30}\varepsilon \left(f \ln f / 1-f\right) \quad \text{(eq.3)}$$

Where $Si(OH)_4$ is silicic acid, $Si(OH)_{4\ initial}$ is initial silicic acid, $bSiO_2$ is diatom silica, $bSiO_{2\ acc}$ is accumulated diatom silica, and f is the fraction of silicic acid remaining in the surface ocean. In this model, sedimentary diatom silica should reflect accumulated diatom $\delta^{30}Si$ (eq.3).

The alternative steady state model assumes open system dynamics (Figure 1.8), whereby silicic acid is continuously supplied to the surface and is utilised to some degree by diatom uptake. This is represented by the equations:

$$\delta^{30}Si(OH)_4 = \delta^{30}Si(OH)_{4\ initial} - {}^{30}\varepsilon \left(1-f\right) \quad \text{(eq.4)}$$

$$\delta^{30}Si\text{-}bSiO_2 = \delta^{30}Si(OH)_{4\ initial} + {}^{30}\varepsilon f \quad \text{(eq.5)}$$

Rayleigh fractionation has been a key in understanding the nature of silicon isotope fractionation by diatoms in batch culture experiments (e.g. De La Rocha et al., 1997). Either model maybe applicable to the marine environment under certain conditions, for example Rayleigh fractionation has been shown to satisfactorily describe $\delta^{30}Si$ in diatom opal exported from the mixed layer on a seasonal scale in the Southern Ocean (Fripiat et al., 2011a). However regional scale investigations have demonstrated that the application of these simplistic models on a larger spatial scale and over longer time periods may be subject to some uncertainly. Spatial variation in the initial silicic acid concentration/$\delta^{30}Si$ supply term, caused by vertical and horizontal water mass mixing (Cardinal et al., 2005), and mixing and stratification events which drive deviation from pure open or closed system assumptions (Varela et al., 2004), are examples of the complexity introduced when modelling the natural environment.

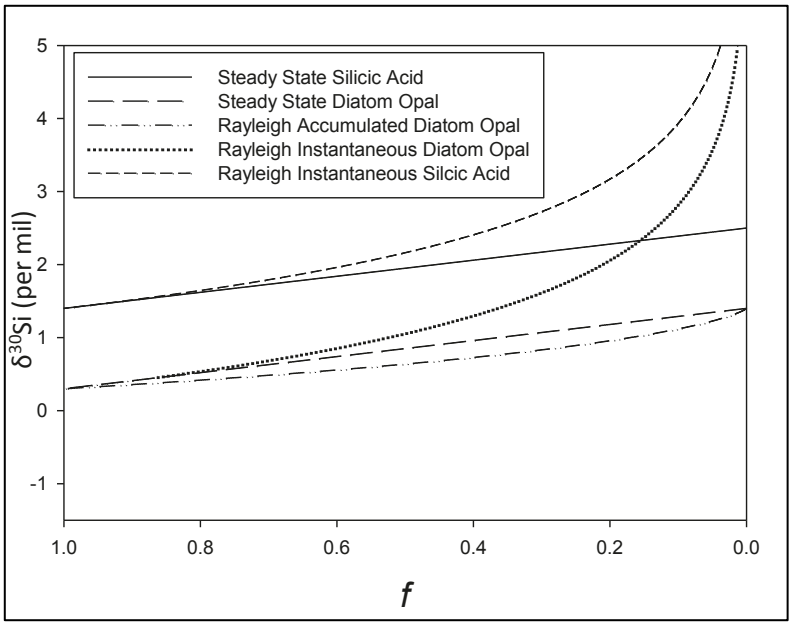


Figure 1.8 Rayleigh and Steady State models of diatom silicon fractionation. *f* is the fraction of silicic acid remaining in the surface ocean. Rayleigh fractionation describes a closed system from which silicic acid is progressively removed. Diatom $\delta^{30}Si$ produced at any given time is represented by the instantaneous product (eq.2), which parallels the silicic acid $\delta^{30}Si$ (eq.1). Diatom opal deposited in sediments integrates everything which has been produced up until a certain time, and is represented by the accumulated product (eq.3). The steady state model represents an open system with a continuous supply of silicic acid (eq. 4 and 5).

Although the diatom $\delta^{30}Si$ proxy has already been applied to palaeo-reconstructions, no modern sediment core top calibration of diatom $\delta^{30}Si$ as a proxy for silicic acid utilisation has been undertaken. Another important caveat of the use of the diatom $\delta^{30}Si$ proxy is that the impact of non-diatom components, such as radiolaria, sponge spicules and clay minerals, on diatom $\delta^{30}Si$ measurements is under-constrained. Due to their small size (generally 2-50μm), it is generally considered impractical to hand-pick diatom frustules (Swann et al., 2008) and a sequence of chemical and physical separation techniques are instead employed to purify diatom material (e.g. (Morley et al., 2004). However, samples will almost always contain some level of non-diatom material (Morley et al., 2004; Leng and Barker, 2006; De La Rocha, 2006; Swann and Leng, 2009). Non-diatom components may contribute silica with significantly different $\delta^{30}Si$ to diatom opal, for example sponges inhabiting the seafloor are known to fractionate silicon with $^{30}\varepsilon$ up to approximately −5‰, much greater than that of the diatoms (De la Rocha, 2003; Hendry et al., 2010). Assessment of the effect of non-diatom sedimentary components on measured $\delta^{30}Si$ is therefore required to ensure the reliability of silicic acid utilisation records based on diatom $\delta^{30}Si$. These issues, of methodology and core top calibration, are addressed in Chapter 3 of this thesis, before any application of the proxy is undertaken.

1.3.1.3 Sponge $\delta^{30}Si$

Sponges are benthic organisms, of which the Classes Dermospongea and Hexactinellida form skeletal structures by the precipitation of silica spicules. Work by Hendry et al., (2010), Wille et al., (2010) and Hendry and Robinson (2012) has shown that the $\delta^{30}Si$ composition of sponge spicules is dependent on the availability of silicic acid during spicule growth. This has been demonstrated empirically through calibration of both modern sponge specimens and core top spicules, and the relationship shown to be exponential. The sponge fractionation factor $^{30}\varepsilon$, has been documented to vary between –1 and –6.5‰ and no species specific differences have been

detected. As such sponge $\delta^{30}Si$ may be used as a proxy for bottom water silicic acid concentration (Hendry and Robinson, 2012).

1.3.1.4 Application of Diatom and Sponge $\delta^{30}Si$ to Palaeoenvironmental Reconstruction

To date, down core diatom $\delta^{30}Si$ studies have predominantly focussed on variations in silicic acid utilisation during glacial-interglacial cycles (Figure 1.9a; De La Rocha et al., 1998; Brzezinski et al., 2002; Beucher et al., 2007; Pichevin et al., 2009; Horn et al., 2011). The first glacial interglacial records documented a 0.6‰ negative excursion during the last glacial in the Southern Ocean, indicative of decreased diatom silicic acid utilisation (De La Rocha et al., 1998). Subsequently, Southern Ocean diatom $\delta^{30}Si$ records combined with the $\delta^{15}N$ (bulk) nitrate utilisation proxy were used to develop the 'silicic acid leakage' hypothesis (Brzezinski et al., 2002). This time, records spanning glacial-interglacial cycles back to ~300kyrs consistently documented low glacial $\delta^{30}Si$ coupled with high $\delta^{15}N$. At around the same time, iron fertilisation experiments (e.g. Boyd et al., 2000) had shown that diatoms relieved of iron limitation decreased their silicon uptake relative to nitrate. These results were interpreted to document glacial dust driven iron fertilisation of the Southern Ocean. This was suggested to have released silicic acid for use at lower latitudes, driving a change in the dominant phytoplankton from carbonate producers to silicate producers and facilitating glacial atmospheric CO_2 decline. Another study also found lower glacial $\delta^{30}Si$ and Si:C ratios in the Equatorial Pacific, again interpreted as relief from iron limitation (Pichevin et al., 2009). Only one significantly older study of diatom $\delta^{30}Si$ exists (Figure 1.9c): Reynolds et al. (2008) used a record from the sub-Arctic North Pacific to argue for increased silicon storage in Pacific deepwaters at the 2.7Ma initiation of northern hemisphere glaciation.

Until very recently, only one study of palaeo-sponge $\delta^{30}Si$ existed. De la Rocha (2003) produced a record from the high latitude Southern Ocean covering the Eocene-Oligocene boundary (Figure 1.9b). However, at this time, the dependency of sponge $\delta^{30}Si$ on ambient silicic acid concentration had not yet been documented, and a –2‰ shift across the boundary suggested further investigation was required. In addition to their 2010 sponge $\delta^{30}Si$ silicic acid concentration calibrations, both the Hendry et al., and Wille et al., groups produced glacial interglacial records of silicic acid concentration, with the aim of testing the silicic acid leakage hypothesis. Hendry et al. (2010) found no significant difference in glacial deepwater silicic acid concentrations in the Atlantic sector of the Southern Ocean compared to today, whereas in the Pacific sector Ellwood et al. (2010) found increased concentrations. However, in the Atlantic sector, Hendry et al. (2012) did find evidence for abrupt changes in the concentration of silicic acid exported at intermediate depths from the Southern Ocean during Heinrich stadials and the Younger dryas.

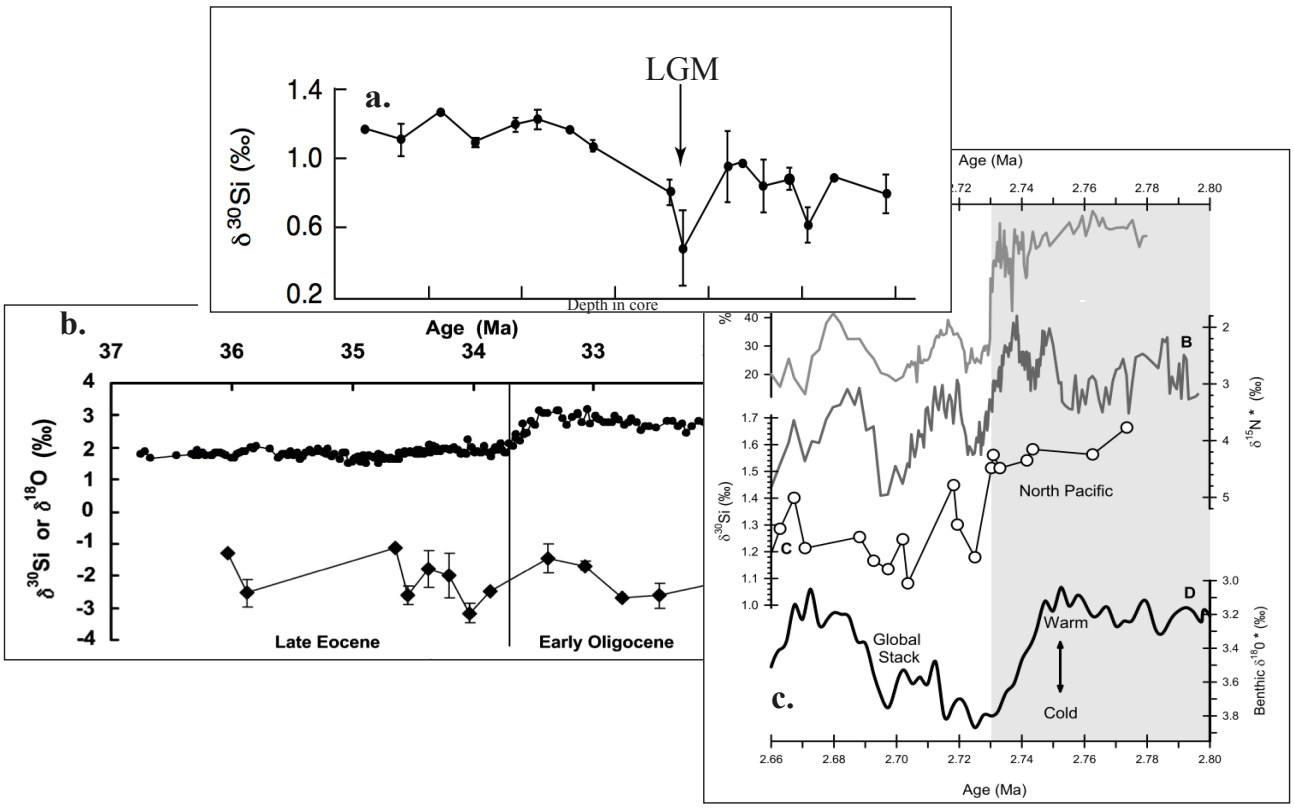


Figure I.9. Examples of previous palaeo-$\delta^{30}Si$ studies; **a.** Diatom $\delta^{30}Si$ record from the Atlantic sector of the Southern Ocean, showing approximately 0.6‰ lower values during the Last Glacial Maximum (LGM; De la Rocha., 1998); **b.** up to 2‰ shifts during the Late Eocene/Early Oligocene shown by the first down core sponge $\delta^{30}Si$ study, from the high latitude Southern Ocean (De la Rocha, 2003); and **c.** Diatom $\delta^{30}Si$ from the sub-Arctic North Pacific showing a decline of around 0.5‰ associated with northern hemisphere glaciation (Reynolds et al., 2008).

When considered in terms of the magnitude of changes in silicon cycling and CO_2 concentration thought to have occurred, for example, through the Cenozoic, variations during the heavily studied glacial interglacial periods are relatively small. The sponge spicule record of De La Rocha (2003) was constructed at a very low resolution before an understanding of the dependence of sponge $\delta^{30}Si$ on silicic acid concentration was developed. These pioneering studies have opened the door to the application of $\delta^{30}Si$ in the deeper geological past, where an understanding of the silicon cycle would be very valuable.

There have been no studies that have used diatom and sponge $\delta^{30}Si$ in combination, despite the powerful insights this could afford. Firstly, as diatom $\delta^{30}Si$ is a proxy for silicic acid utilisation, it is determined by both the extent of diatom production and the supply of silicic acid to the surface. Coordinated interpretation of diatom $\delta^{30}Si$ and sponge $\delta^{30}Si$ can be used to disentangle these upwelling and productivity effects by providing a constraint on the concentration of silicic acid supplied from the deep ocean. Perhaps an even more beneficial feature of combined sponge and diatom $\delta^{30}Si$ records is the ability to reconstruct vertical gradients of silicic acid in the oceans by defining the parameter $\Delta\delta^{30}Si$ (= diatom $\delta^{30}Si$ – sponge $\delta^{30}Si$). This parameter is described fully in Chapter 4, but for now it is suffice to say that it is important in allowing the elimination of whole ocean $\delta^{30}Si$ changes from the interpretation of diatom and sponge $\delta^{30}Si$ records.

1.4 Reconstructing the Cenozoic Silicon Cycle using Biogenic Opal $\delta^{30}Si$

The aim of this work is to reconstruct the Cenozoic silicon cycle, extending records of diatom and sponge $\delta^{30}Si$ into the deeper geological past. Study of this time period, over which both the silicon cycle and Earth's climate have undergone substantial modification, should further our knowledge of both the functioning of the marine silicon cycle and its role in global climate change.

The Cenozoic witnessed major changes in the state of Earth's climate system (Zachos et al., 2001). It is a period over which climate descended from the greenhouse world of the middle Eocene climatic optimum, when the world was free of ice caps, into the bipolar-glaciated icehouse of the modern day (Figure 1.10; Zachos et al., 2001). Cenozoic climate cooled gradually, potentially driven by ongoing pCO_2 decline associated with intensification of continental silicate weathering (Raymo and Ruddiman, 1992). The gradual cooling trend is punctuated by two major steps, first at the Eocene-Oligocene boundary, ~33.7 Ma ago (Coxall et al., 2005) when substantial ice sheets were emplaced on Antarctica, and again at 2.7 Ma by northern hemisphere glaciation (Raymo, 1994). That the silicon cycle was involved in these climate shifts has already been eluded to above, if increased silicate weathering was indeed the driver of Cenozoic pCO_2 drawdown. But the non linearity of pCO_2 decline (Pagani et al., 2005; Pagani et al., 2011) suggests additional mechanisms were at play.

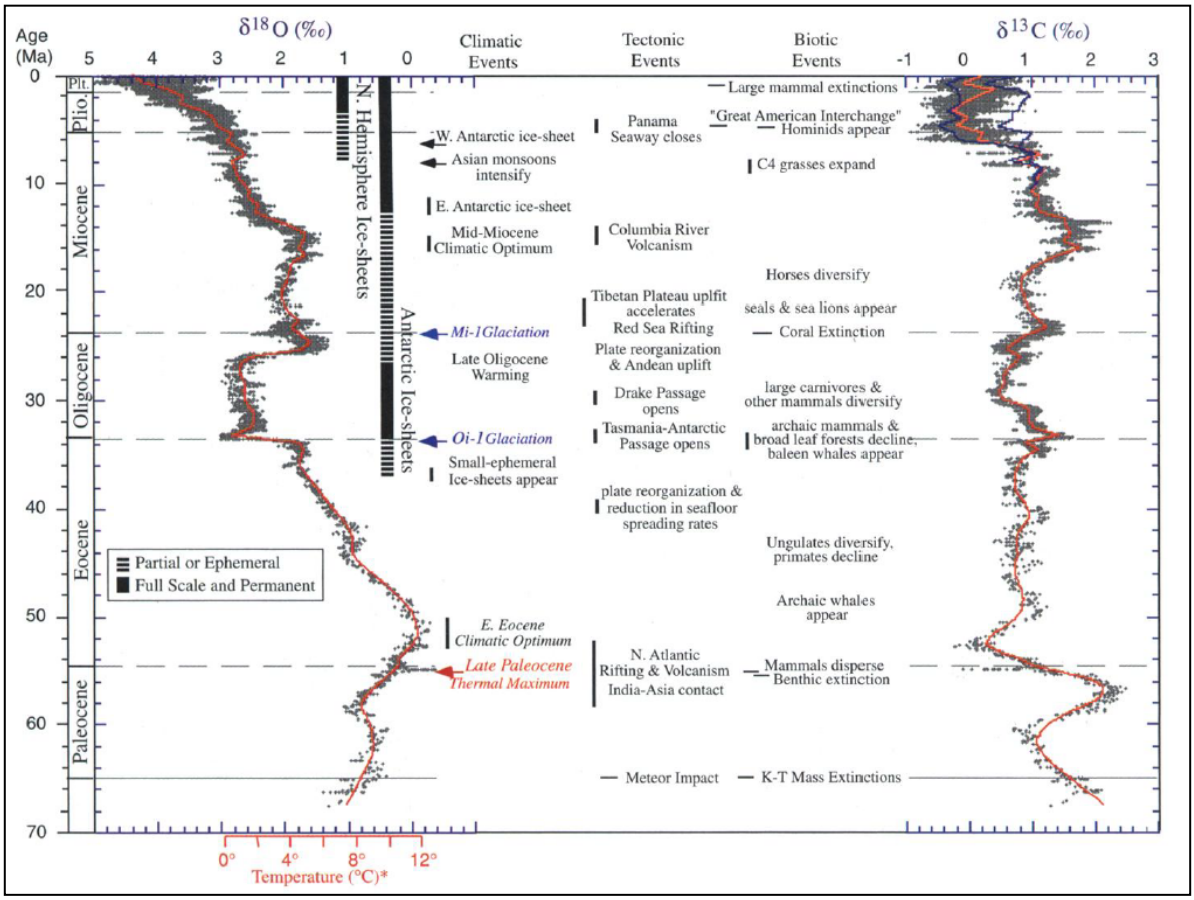


Figure 1.10 Benthic Foraminiferal $\delta^{18}O$ and $\delta^{13}C$ stacks, documenting cooling/glaciation and the oceans carbon cycle, respectively, over the Cenozoic. Figure from Zachos et al. (2001).

There are hints in the literature that the diatoms, with their links to carbon and the biological pump, may have contributed to climate deterioration and glaciation at the Eocene-Oligocene Boundary (DeConto and Pollard, 2003; Falkowski et al., 2004; Rabosky and Sorhannus, 2009). Diatoms have not always been the prolific phytoplankton they are today. They are thought to have evolved in the Jurassic, with their numbers increasing through the Cretaceous and undergoing great expansion through the Cenozoic (Falkowski et al., 2004). There is evidence to suggest that diatom diversification in the Cenozoic was pulsed, with intensification during the Late Eocene and the Middle to Late Miocene (Falkowski et al., 2004). It has been suggested that diatom radiation in the Late Eocene may have increase organic carbon burial and contributed to the pCO_2 drawdown thought to have triggered Antarctic Glaciation (Falkowski et al., 2004;

Rabosky and Sorhannus, 2009). Substantiation of this theory hinges on justifying the translation of diversity curves into an increase in diatom productivity. Miocene diatom radiation has been linked to an increased supply of silicic acid to the oceans, associated with the evolution of modern grasslands and grazing ungulates, which would have had an impact on the marine silicon cycle and has been suggested as a driver of cooling and expansion of the East Antarctic Ice sheet at this time (Falkowski et al., 2004).

The Cenozoic also encompasses the development of modern-style ocean circulation. The subsidence of two barriers to circumpolar flow, the Drake Passage and the Tasman gateway again during the Late Eocene and into the Oligocene, gradually unblocked the 360˚ latitudinal pathway that today allows the flow of the Antarctic Circumpolar Current (ACC). Between 15 Ma and ~3 Ma, the Central American seaway was gradually cut off by the emergence of the Ismuth of Panama (Poore et al., 2006; Cramer et al., 2009), allowing the development of a saline North Atlantic and the onset and invigoration of NADW formation. Lastly, the development of stratification in the North Pacific and Southern Ocean at ~2.7Ma (Haug et al., 1999; Sigman et al., 2004; Haug et al., 2005) added the final feature of modern circulation. The importance of the overturning circulation in setting the modern marine silicic acid distribution and in controlling the provenance of diatoms has been extensively discussed, and implies major changes should result from this piecing together of ocean circulation. Indeed, associated shifts in the location of major opal deposition sinks have already been documented (Cortese et al., 2004), pointing towards a wealth of information on the silicon cycle and climate locked in Cenozoic sediments. Chapter 5 of this work presents a first attempt to understand the longer term silicon cycle in a biogeochemical context.

1.5 Thesis outline

At the outset of work on this PhD, no core top calibration of diatom $\delta^{30}Si$ had been undertaken, and it was not clear from previously published work how best to separate diatoms from sediments in order to ensure that measured $\delta^{30}Si$ reflected robustly diatom $\delta^{30}Si$. Therefore, the first substantial task I undertook was to develop a methodology for extracting pure diatom fractions from sediments based on the coccolith separation technique of Minoletti et al. (2009). I then applied this technique to produce a core top calibration of the Southern Ocean. This work is published in GCA and appears in approximately this format in Chapter 3.

Having developed a robust diatom $\delta^{30}Si$ methodology, I moved on to apply diatom $\delta^{30}Si$, for the first time in combination with sponge $\delta^{30}Si$, to reconstruct the silicon cycle of the Late Eocene and Early Oligocene Southern Ocean. These records are presented in Chapter 4.

Lastly, I extended the sponge $\delta^{30}Si$ record of Chapter 4 through the Cenozoic to produce a long term record that I have used to assess the dominant controls on long term subsurface silicic acid concentration in the high latitude South Atlantic. This work is presented in Chapter 5.

Chapter 2. Methods

Abstract

The central tenet on which this thesis is founded is the accurate analysis of silicon isotope ratios in both diatom and sponge opal. There are a number of different methodological steps required in the generation of a silicon isotope value, beginning with the extraction of opal from raw sediments, through dissolution and matrix purification, and ending with the final generation of a ratio, denoted $\delta^{30}Si$, by mass spectrometry. Measurement of a reliable $\delta^{30}Si$ value, which faithfully records the environmental parameter of interest, is critically dependant not only on a sound calibration, but also on every stage of the methodology. This chapter outlines the techniques that have been employed to generate the $\delta^{30}Si$ values presented here and which are summarised in Figure 2.1. Section 2.1 considers the analysis of $\delta^{30}Si$ in biogenic opal by both Multi-Collector Inductively Coupled Plasma Mass Spectrometry (MC-ICP-MS) and vacuum-line fluorination coupled with gas source Isotope Ratio Mass Spectrometry (IRMS), which are now well developed techniques, alongside the relevant opal dissolution and purification methods. Section 2.2 is concerned with the extraction of biogenic opal from bulk sediment, which, in the case of diatom $\delta^{30}Si$, has aspects that require refinement. Such refinement has been one of the primary focuses of this thesis. The section therefore details first the rather simpler sponge extraction methodology and continues on to overview previously published diatom separation techniques, aspects of which are employed in this thesis. Some of the problems associated with existing diatom extraction methods are highlighted and an approach for refinement of the method, which is undertaken in Chapter 3, is advanced.

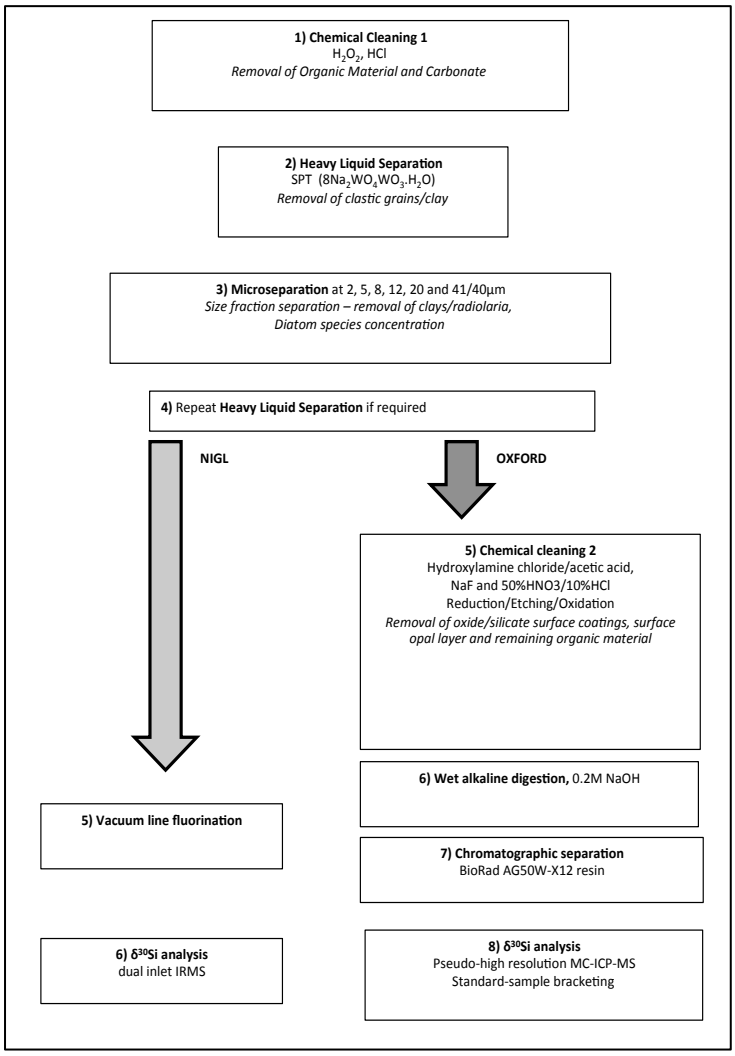


Figure 2.1 Summary of methods. Steps 1 to 4 are biogenic silica purification techniques common to analyses performed both in Oxford and at NIGL. Details on the use of the microseparation technique are included in Section 2.2.2 and Chapter 3. Steps 5 and 6 (left hand side) are NIGL analysis steps and 5 to 8 (right hand side) are clean up steps and analysis techniques used in Oxford. SPT = Sodium Polytungstate. MC-ICP-MS = Multi-collector inductively coupled plasma mass spectrometer.

2.1 Silicon Isotope analysis

At present, there are two main techniques employed in the measurement of silicon isotope ratios; vacuum-line fluorination coupled with gas source isotope ratio mass spectrometer (IRMS) and Multi-Collector Inductively Coupled Plasma Mass Spectrometry (MC-ICP-MS). The latter is more extensively employed, as it avoids the use of the explosive bromine pentafluoride (BrF_5) gas and analyses require a smaller amount of silica. MC-ICP-MS has been used to generate the bulk of the isotopic measurements in this thesis. However, vacuum line fluorination yields an equivalent precision, and has the added benefit of being able to analyse both silicon and oxygen isotope ratios from the same sample aliquot. For this reason, a small number of samples were analysed by vacuum-line fluorination by Melanie Leng and Hilary Sloane at the NERC Isotope Geochemistry Laboratories (NIGL), Nottingham (although the oxygen isotope data proved somewhat inconclusive, and is not discussed here). This section focuses primarily on MC-ICP-MS analytical procedures, with only a brief overview of the vacuum-line fluorination technique (greater detail can be found in Leng and Sloane (2008).

2.1.1 MC-ICP-MS

With the advent of plasma source mass spectrometry, which has the ability to efficiently ionise a large number of elements across the periodic table, silicon isotope measurements began to shift away from vacuum-line fluorination and IRMS towards the ICP-MS (De La Rocha, 2002; Cardinal et al., 2003). Initial measurements were somewhat problematic, but the use of mass spectrometers with high resolution or pseudo high resolution capacities and development of introduction methods (Cardinal et al., 2003; Georg et al., 2006) has made them more accessible.

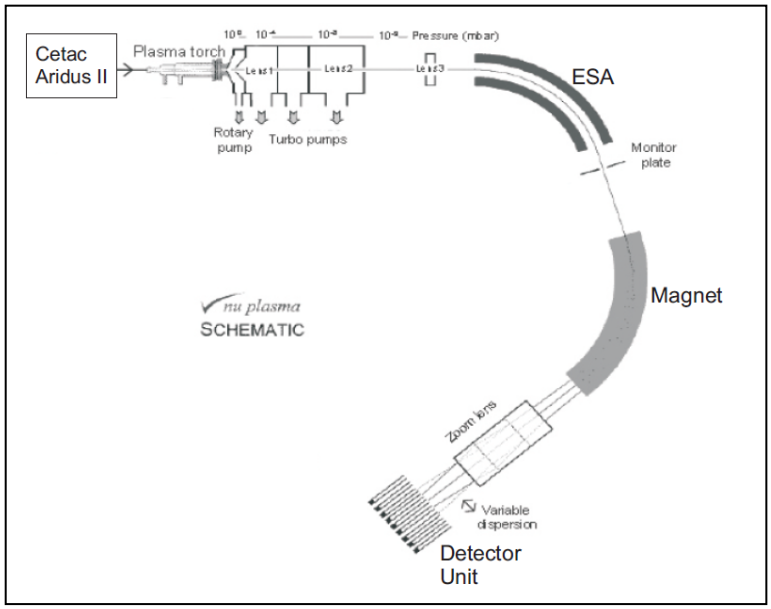


Figure 2.2 Schematic of the Nu Plasma HR-MC-ICP-MS; ESA – Electrostatic Analyser

Figure 2.2 shows a schematic of the Nu plasma instrument used in Oxford, with the specific set up detailed in Table 2.1. Silicon isotope analyses are carried out in dry-plasma mode (Cardinal et al., 2003), with samples introduced via a self-aspirating PFA microconcentric nebuliser (ESI) in a Cetac Aridus II desolvating unit, with an uptake rate of ~75µL/min. This generally yields a sensitivity of ~5V total Si on 750-1000ppb in medium resolution mode. Samples are introduced to the spray chamber of the Aridus as an aerosol produced by the nebuliser. In the spray chamber, the aerosol is heated, such that the solvent is separated in a gaseous form from the sample, in an aerosol form, by evaporation. This mixture then passes into a semi-permeable Teflon membrane, heated to 160˚C, through which the gaseous solvent may pass but within which the aqueous sample aerosol remains. The sample is subsequently conducted to the plasma by an argon gas flux. The benefit of this type of introduction system is the removal of large droplets of solvent that would otherwise compete for ionisation energy within the plasma, and to decrease the generation of isobaric interferences derived from the solvent. As a result, introduction in dry

plasma mode yields dramatically increased sensitivity (Cardinal et al., 2003) compared to wet plasma conditions (De La Rocha, 2002).

Parameter	Set up
Cones	Nickel B-type skimmer and sampler
Nebuliser uptake rate	75µL/minute
Cup configuration	L5, Ax, H6 (^{28}Si, ^{29}Si, ^{30}Si)
Cycles	20
Integration time	8 seconds
Sensitivity	5-6V on 750-1000ppb

Table 2.1 Oxford MC-ICP-MS set up

The sample is then introduced into an inductively coupled argon plasma, held within a quartz torch composed of three concentric cylinders. The torch is itself located within an induction coil through which an RF current is passed. Argon gas flows into the outer part of the torch, where a spark initiates the release of electrons. These electrons are accelerated by the RF field, and cause a chain reaction that generates the plasma ionisation source. The middle cylinder acts to separate the outer and inner cylinders and is also filled with argon gas. Through the central cylinder, the sample is introduced to the plasma (at >5000K) in a flow of argon gas via the quartz injector. It should be noted that there was no apparent change in background or sensitivity when using a quartz injector rather than a sapphire injector (e.g. Georg et al., 2006). Ionisation in the plasma not only effects silicon, but also produces a number of interferences, originating both from the plasma itself and from molecular species present in air. For silicon, important interferences are $^{14}N^{14}N^{+}$ and $^{12}C^{16}O^{+}$ on ^{28}Si, $^{14}N^{15}N^{+}$ on ^{29}Si and $^{14}N^{16}O^{+}$ on ^{30}Si. The most problematic of these is the interferences of $^{14}N^{16}O^{+}$ on the ^{30}Si beam. For a time, only δ^{29}Si was measured, but with the advent of pseudo high resolution/high resolution capabilities, this issue was overcome (Figure 2.3). Variations in sensitivity, and changes in the mass bias, can be introduced by the presence of other elements within the sample matrix that is also exposed to the plasma. For this reason,

column chromatography is undertaken to ensure purity of the sample (Georg et al., 2006, see below).

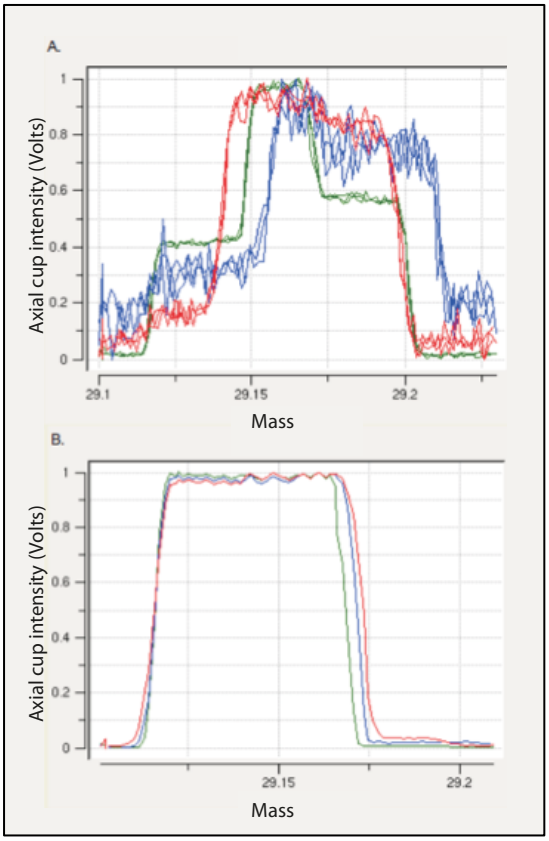


Figure 2.3 Peak shapes showing the signal created by scanning the ion beams across the three collectors used to measure silicon isotopes whilst running; **a.** an acid blank. Peak shape shows interferences on all three Si beams. The principle interferences are: $^{14}N^{16}O^{+}$ on ^{30}Si (red), $^{14}N^{15}N^{+}$ on ^{29}Si (blue), $^{14}N^{14}N^{+}$ and $^{12}C^{16}O^{+}$ on ^{28}Si (green); **b.** a silicon tuning solution, with the MC-ICP-MS running in medium resolution mode, showing resolution of Si beams from interferences. Measurements are made on the left hand shoulder of the peak in order avoid measuring the $^{14}N^{16}O^{+}$ interference on the ^{30}Si beam, which creates the slight intensity increase, just off centre, in the red collector scan.

Next, ions produced in the plasma, which is at atmospheric pressure, are transferred through the interface region into the mass spectrometer at ~3-4x10^{-9}bars. The interface consists of the sampler and skimmer cones, and in this case these are a nickel B-type skimmer and 540 sampler. This stage induces a large sensitivity decrease, with on average >99% of material lost. The ion beam is accelerated through a number of potentials and focussed into the mass analyser. In the

interface region and during movement of the ion beam through the mass spectrometer, significant mass bias occurs, whereby heavier ions are preferentially extracted and transmitted. To account for this mass bias, standard-sample bracketing is employed in the measurement of silicon isotope ratios. We typically measure 8 standards sample brackets (i.e. 16 consecutive, alternating analyses of the same two sample and standard solutions), with each measurement consisting of 20 or 25 integrations each of 8 seconds. The wash sequence between standard – sample brackets, and between each sample, is 50 seconds in 0.25M HCl and two x 50 seconds in 0.05M HCl.

In the mass analyser, where the pressure is ~10^{-8} millibars, ions are separated according to their mass to charge ratio (m/z). Double focussing is used to account for the production of ions in the plasma with a spread of kinetic energies. This involves the coupling of an Electrostatic Analyser (ESA) with a magnet. The ESA acts to deflect the ions according to their energy in an equal but opposite sense to the magnet, thus eliminating the effects of the initial energy spread. An adjustable source slit in front of the mass analyser allows for the pseudo high resolution capacity of the Nu-Plasma MC-ICP-MS. Setting this slit to, in the case of silicon, medium resolution ($m/\Delta m$ ~3500: because the machine is run is pseudo-high resolution, Δm represents the difference between the masses at 5% and 95% of the maximum signal intensity), narrows the apparent beam width, allowing the ^{30}Si beam to be separated from the interfering $^{14}N^{16}O^{+}$ (Figure 2.3). The medium resolution setting is used because it provides the best balance between resolution and loss of sensitivity cause by clipping the beam in this fashion.

Once the ion beams are separated, they are focussed into fixed position faraday detectors by an array of zoom lenses. This has the advantage of simultaneously measuring isotopic ratios, accounting for fluctuations in ion beam intensity associated with the plasma source. The cup separation for silicon isotope measurements is 1/7 mass units meaning the cup configuration used was L5, Ax, H6 (^{28}Si, ^{29}Si, ^{30}Si).

Prior to any measurement, the instrument is ideally left overnight with the magnet set to mass 29 to allow stabilisation. The Aridus II is likewise allowed to warm up for at least an hour, though preferable overnight and the whole system is run through with 0.25M HCl prior to analysis. The machine is then tuned to maximise sensitivity and peak shape, and the measurements carried out on the left hand side of the peak plateau to avoid the interferences on ^{29}Si and ^{30}Si (Figure 2.3). An initial self test of the tuning and mass setting is carried out by running a tuning solution against itself, which ideally should generate $\delta^{30}Si=\delta^{29}Si = 0$. Sixteen replicates of this self test are carried out (to reflect the 8 standard-sample brackets which are undertaken for sample measurements) and when the internal 2σSD error value produced is <0.2‰ and the mean is within error of zero, tuning is considered satisfactory.

2.1.2 Preparation of biogenic opal for MC-ICP-MS analysis

Purified opal is dissolved via wet alkaline digestion (Ragueneau et al., 2005; Cardinal et al., 2007) in 0.2M NaOH at 100˚C for 40 minutes in the case of diatoms, or up to 1 week for sponge spicules where regular sonication is also employed to aid dissolution. For diatoms, the opal is weighed, and 4mL NaOH was added per mg. In the case of the sponge spicules, ~100µL of NaOH is added per 10 spicules. However, some samples contained extremely large spicules, and in such cases it was often necessary to add more NaOH throughout the digestion process when spicules were not dissolving. Prior to column chromatography, the Si concentration of the samples is measured using the molybdenum-blue method. This allows a known concentration of silicon to be added to each column and sample and standard concentrations to be matched. Both bracketing standards and external standards undergo the same column chemistry as the samples, as they too are dissolved in NaOH (although using the alkali fusion method of Georg et al. (2006).

Samples are acidified to pH~2 with 0.2M thermally distilled hydrochloric acid (HCl) and separated from major ions using the chromatographic separation technique of Georg et al. (2006).

At pH 2-8, the main Si species present are $Si(OH)_4$ and $H_3SiO_4^-$. Chromatographic separation of Si can be achieved using a cation exchange resin (BioRad, DOWEX 50W-X12, 200-400 mesh), which retains neither of these species. Since there is no retention of Si species by the resin, elution requires only Milli-Q water. 0.8mL of resin for samples, and 1.8mL for standards, is required for effective chromatographic separation, although here all columns were loaded with 1.8mL. Tests by Hendry et al. (2010) demonstrated this method to result in 100% yields for both commercially available Si solutions and dissolved opal samples. Prior to being loaded onto columns, the resin is pre-cleaned 3-4 times with 6N HNO_3. Once in the columns, the resin is further cleaned using a series of steps with varying acid concentrations (Table 2.2). The concentration of the acid used for cleaning is gradually increased and decreased in this fashion to avoid expansion/contraction of the resin which may cause cracks or bubbles which will reduce its effectiveness. The last step of the cleaning, using Milli-Q water, is repeated until the elute is neutral. Sample and standards are loaded onto the columns. The volume of solution and amount of Milli-Q for elution are such that the end product is a 6mL solution with 500-1500ppb Si (the target concentration is decided depending on machine sensitivity at the time, and is adjusted to achieve a signal ideally of 4-9V on total Si).

Cleaning Stage	Cleaning Reagent	Volume
1	3N HNO3	3mL
2	6N HNO3	3mL
3	Conc HCl	1.5mL
4	6N HNO3	1.5mL
5	3N HNO3	1.5mL
6	Milli-Q water	6mL

Table 2.2. Resin cleaning procedure.

2.1.3 Mass dependency, precision and accuracy of MC-ICP-MS analyses

Stable isotope fractionations should be dependent on the masses of the isotopes involved, and thus should plot along a straight line in three isotope space. For the kinetic fractionation demonstrated for silicon isotopes using the standards diatomite, big batch and IRMM-018 (Reynolds et al., 2007), the theoretical relationship between $\delta^{30}Si$ and $\delta^{29}Si$ is $\delta^{30}Si$ =

0.5092*δ^{29}Si (calculated using the accurate masses of the three silicon isotopes equation $\beta = \ln(1/m(^{29}Si))/\ln(1/m(^{30}Si))$, Young et al., 2002). All the data produced in this thesis are in agreement with this line (Figure 2.4) providing confirmation of the data quality. Linear regression through the data yields a gradient of between 0.509 and 0.516 (at 95% confidence), in agreement with either kinetic or equilibrium fractionation.

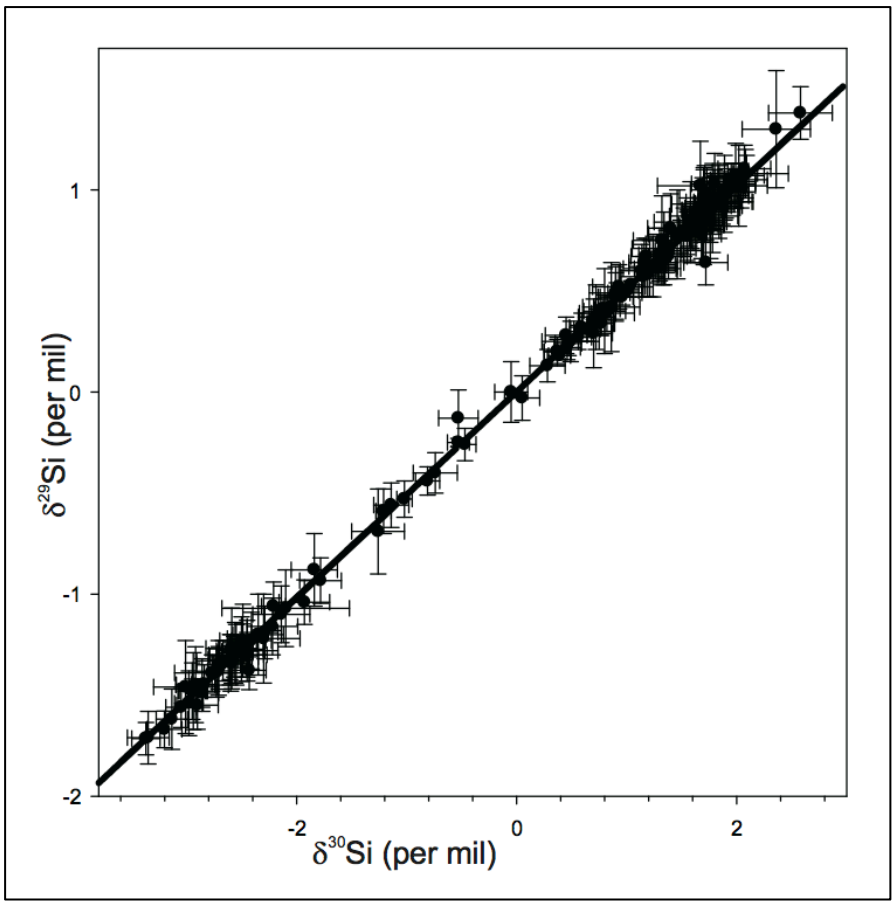


Figure 2.4 Three isotope plot of all values included in this thesis. Solid black line is the theoretical kinetic fractionation relationship between δ^{30}Si and δ^{29}Si. Error bars are the 2σSD internal error on each measurement. A linear regression through the data yield a gradient 0.513, and at the 95% confidence interval may range from 0.509 to 0.516.

All samples are measured relative to the silica sand NIST RM 8546 (NBS28) standard (Reynolds et al., 2006b), and from the 8 standard sample brackets measured a 2σSD and 2SE error are calculated for each sample measured, providing an estimate of the internal error. The bracketing

NIST RM 85646, as the sample itself, undergoes column chemistry prior to analysis. To assess the precision and accuracy of our measurements, the internationally utilised diatomite standard (1.26‰±0.2‰ (2σSD)), a natural diatomite sample originally deposited as marine biogenic opal, (Reynolds et al., 2007) is analysed during each session. To test the external reproducibility and to ensure the accuracy of analyses, the diatomite is analysed as a sample (again it is first subjected to column chemistry) bracketed against the NIST RM 8546 standard. At least one measurement of the diatomite consisting of 8 standard-diatomite brackets is made per session, and often one measurement of 4 brackets is run with each batch of 5 samples. From this, our long term reproducibility is 0.25‰ (2σSD, n=104), with a mean of +1.23‰ and average internal error of 0.19‰ (average 2σSD of the repeat standard sample measurements on each diatomite replicate). Repeat analyses of diatomite (this includes two separate batches of solution) covering the entire period of this study are shown in Figure 2.5. If the diatomite associated with a batch of samples did not produce an accurate value the data was discarded.

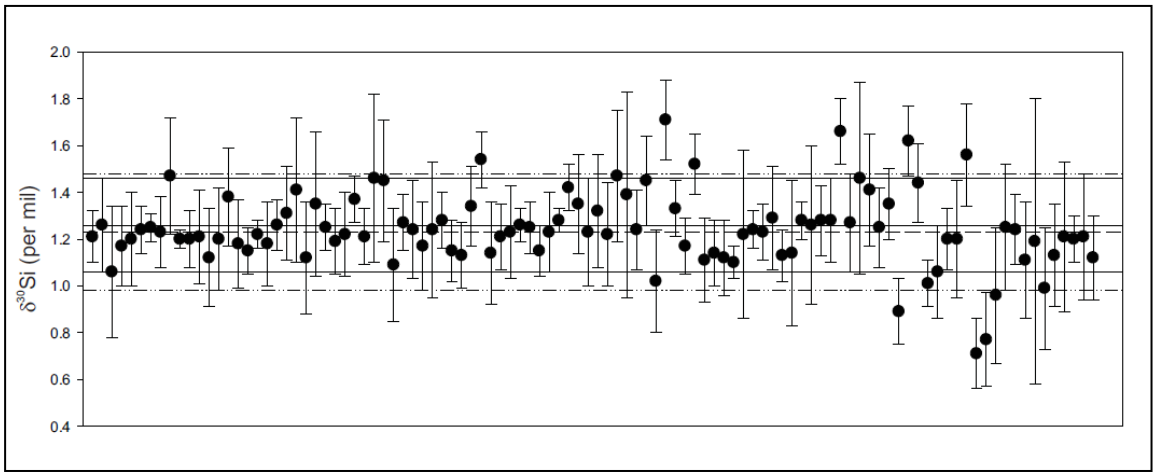


Figure 2.5 Long term diatomite reproducibility. Solid black lines are the mean and 2σSD from Reynolds et al. (2007); dashed black lines are the mean and 2σSD of diatomite measurements made in this study. Error bars are the 2σSD internal error on each measurement.

During the analysis of sponge spicules, I experienced some difficulty with sample replication. This was often associated with repeat analysis of the same sample aliquot, thus was not related to differences between individual batches of spicules. On inspection of the data, I noticed that the

sample-standard concentration matching on a portion of these analyses was poor, thus any sponge data not matched to within 20% were removed from the data set (Hendry et al., 2011). This, to a large extent, eliminated the issue of reproducibility, although it did mean that just under half the initial sponge dataset was removed.

2.1.4 Vacuum-Line Fluorination IRMS

The fluorination method used at NIGL involves the reaction of silica with bromine pentafluoride (BrF_5) to dissociate silica into the gaseous phases SiF_4 and CO_2 which can then be analysed by gas source IRMS. The technique for combined analysis of $\delta^{30}Si$ and $\delta^{18}O$ on the same aliquot of biogenic silica requires 5-10mg of silica, and was developed by Leng and Sloane (2008) based on much earlier work of e.g. Epstein and Taylor (1971) combined with the stepwise fluorination method of Leng and Barker (2006). Biogenic silica has a loosely bound outer hydroxyl layer that can be problematic for diatom $\delta^{18}O$ since it may be exchanged with surrounding water (in sediments and in the laboratory). This method, which yields both $\delta^{18}O$ and $\delta^{30}Si$ involves a pre-fluorination step to facilitate removal of the hydroxyl layer. The vacuum line fluorination method is described briefly below.

Reaction of silica with BrF_5 is carried out using a vacuum fluorination line, which consists of three sections under constant pressure (Figure 2.6); 1) BrF_5 storage section coupled to; 2) a manifold with 12 nickel reaction vessels, a trap for waste and cryogenic separation, and; 3) glass tubing and waste trap used for conversion of O_2 into CO_2 and collection of CO_2 and SiF_4. The silica is reacted in three steps, and subsequently the Si and O are extracted in two steps. Stage one involved 'outgassing' (dehydration) to remove surficial and loosely bound water in the reaction tubes at room temperature. In the reaction vessels of the vacuum line, stage two is carried out and involves a prefluorination step with a stoichiometric deficiency of the reagent (BrF_5) at low temperature to remove hydroxyl groups and loosely bound water. The third stage is a total reaction at 450^{o}C for 12 hours with an excess of reagent to dissociate the silica into O_2 and Si (as

SiF_4). Oxygen is then liberated into section 2 of the vacuum line while liquid nitrogen around the reaction vessels condenses other products, such as SiF_4. The O_2 then moves through two further nitrogen cooled traps that purify the gas, and eventually is reacted with a hot graphite rod to form the CO_2 collected for analysis. To extract SiF_4, the reaction vessels are surrounded by a dry ice/acetone sludge which liberates SiF_4 as a gas, but traps waste products such as BrF_3 and residual BrF_5. This gas is then purified using the two cooling traps, this time surrounded with the dry ice/acetone mixture. Using this method, silicon yields are between 97 and 99% and oxygen between 70 and 80% (due to the removal of the loosely bound hydroxyl layer). $\delta^{30}Si$ and $\delta^{18}O$ measurement of the SiF_4 and CO_2 gasses are carried out using a gas source IRMS (Thermo-Finnigan MAT253). $\delta^{30}Si$ is measured relative to NIST RM 8546 and $\delta^{18}O$ relative to VSMOW. The diatomite standard BFC (Chapligin et al., 2011) is run with each batch of samples to calibrate the sample data. From this, the long term reproducibility is 0.2‰ (2σSD). Duplicate samples had a mean reproducibility of 0.06‰ (2σSD).

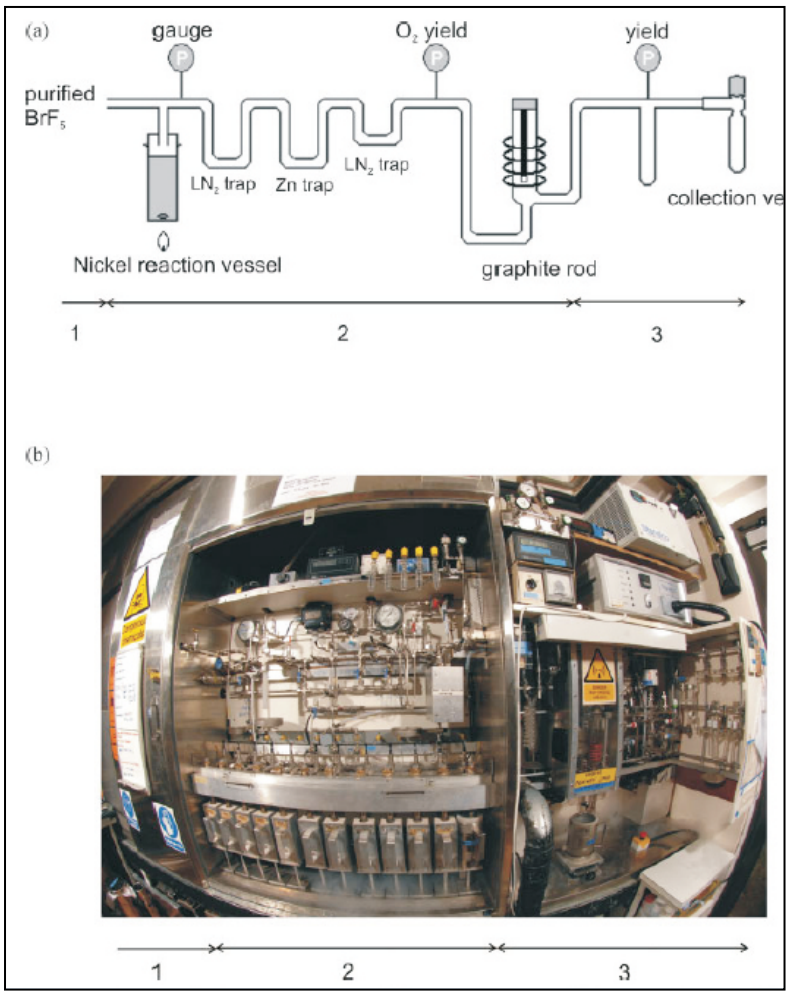


Figure 2.6 Fluorination line used at NIGL for the extraction of CO_2 and SiF_4 from biogenic silica for IRMS; **a.** Schematic; **b.** fish-eye lens image. From Leng and Sloane (2008)

2.2 Opal extraction from sediments

Before silicon isotope ratios can be measured it is essential to separate diatom frustules and sponge spicules from other sedimentary components. Firstly, any remnant contaminants, such as clays and organic matter, can produce matrix effects during MC-ICP-MS, leading to changes in sensitivity and mass bias yielding poor quality analyses. Secondly, in order to make a robust environmental interpretation, a pure fraction of the target opaline component must be analysed. The inclusion of, for example, sponge spicules in a diatom fraction may shift the measured $\delta^{30}Si$ away from diatom $\delta^{30}Si$ through the inclusion of silica with significantly different $\delta^{30}Si$ value. The first issue, of contamination, is largely dealt with through the use of existing sample preparation methodologies (see below). For the larger sponge spicules, silica contribution from other sedimentary components can be easily avoided by hand picking spicules. However for diatoms, the elimination of phases such as radiolaria, sponges, and clays is problematic due to the small size of the diatom frustules (generally 2-50μm, but up to >100μm for some species), which usually precludes hand picking. Outlined below are the techniques employed here for the extraction of sponge spicules, followed by an overview of the methods available for diatom purification, some of the problems associated with them, and the approach for the method development undertaken in Chapter 3.

2.2.1 Extraction of Sponge Spicules from Sediments

The sponge extraction methodology employed here is based on that of Hendry et al. (2010). However, this has been refined slightly to better suit the microseparation technique of Minoletti et al. (2009), used as a more convenient alternative to traditional sieving. As microseparation is more efficient when less sediment is used, initial sediment cleaning is conducted to concentrate the biogenic opal. Firstly, the bulk sediment is heated to 60˚C in a water bath with ~10-20mL of

30% hydrogen peroxide (H_2O_2). The reaction with H_2O_2 is also carried out to remove the majority of organic carbon from the samples. Secondly, 10% HCl is added until all carbonate is dissolved. If there is a large amount of carbonate present, the HCl step is carried out first. Both steps have the added benefit of deflocculating the samples. Samples are thoroughly rinsed between steps with deionised (DI) water. From this pre-cleaned sample, the >100μm fraction is separated using microseparation (Minoletti et al., 2009). The benefits of this technique over sieving are both the removal of adhered clays (See Chapter 3, Figure 3.4 for more details), and the ease of further separations at smaller sizes yielding fractions which can then be used to measure e.g. diatom $\delta^{30}Si$ (see below; although for the particular samples analysed for sponge $\delta^{30}Si$ here, the smaller fractions contained highly fragmented radiolarian opal, making robust diatom separation and $\delta^{30}Si$ analysis impossible). Between 50 and 100 spicules were picked per sample from the >100μm fraction. An example of the range of spicule morphologies present at the core site investigated is shown in Figure 2.7. Studies have demonstrated that neither spicule morphology or species composition creates a consistent offset in silicon isotopic composition or fractionation. Hendry et al., (2010 and 2011), working on modern Southern Ocean sponge specimens, demonstrate that different species from the same site have similar $\delta^{30}Si$ and that two specimens of the same species growing under different ambient silicic acid concentration have different $\delta^{30}Si$. The authors also show that spicules sampled from the internal and external layers of the same sponge specimen have $\delta^{30}Si$ within error of each other. Lastly, Hendry et al. (2010) show that core top measurements of megaspicules picked from Scotia Sea sediments are within error of modern mega and micro spicules extracted from sponges living near the core site. Therefore, when spicules are picked, no discrimination is made between different spicule morphologies. Although the methodology of Wille et al. (2010) includes homogenisation of sponge spicules prior to analysis, this is not consider this necessary here, as the work of Hendry et al. (2011) has shown spicules which have not undergone homogenisation produce replicable $\delta^{30}Si$ values between subsamples. The picked spicules are sonicated in reagent grade methanol to remove any remaining surface or internal contaminants and rinsed thoroughly with 18MΩ Milli-

Q water before drying down in 200µL of concentrated nitric acid (HNO_3) to ensure removal of organic matter (Hendry et al., 2010). Trace amounts of structural organic matter will remain, but as this comprises less than 0.1% of the sample any effect on plasma stability should be minimal.

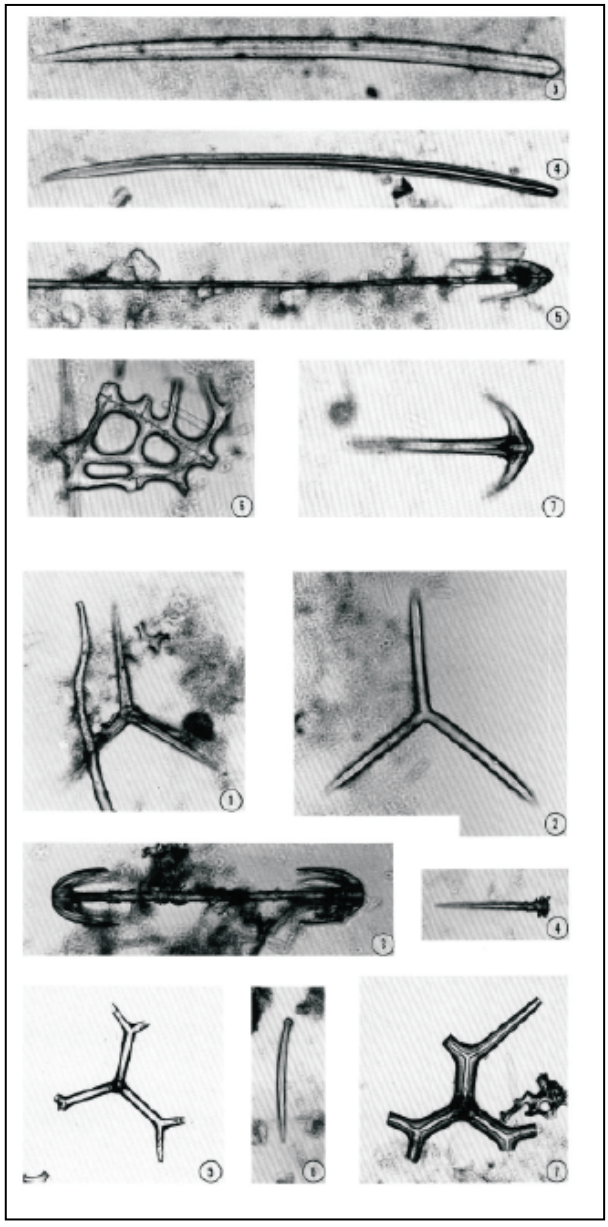


Figure 2.7 Examples of the variety of sponge spicule morphologies present in the sediments of ODP Leg113. This leg includes site 689 which is used to generate all the sponge $\delta^{30}Si$ values presented in this thesis. No discrimination between spicules morphologies is made when they are picked. Images from (McCartney, 1990).

2.2.2 Existing Methods for Diatom Separation from Sediments and an Approach for Improvement

Current diatom purification methodologies employ a sequence of chemical and physical separation techniques (e.g. Morley et al., 2004). In general, the existing chemical techniques and heavy liquid separation, which are employed throughout the work included in this thesis (Figure 2.1), are adequate to remove contaminant phases such as organic matter, surface oxides, and to some extent clay minerals, which can causes instabilities during MC-ICP-MS analysis. The established methodology used here follows the protocol of Hendry and Rickaby (2008), adapted from the methods of Shemesh et al. (1995 onwards), Ellwood and Hunter (1999), and Morley et al. (2004). Initial chemical cleaning steps use H_2O_2 and HCl to remove organic matter and carbonate respectively. These are followed by several heavy liquid separations using sodium polytungstate (SPT, $8Na_2WO_4WO_3.H_2O$) to remove clastic grains and clay minerals. After each stage opal is thoroughly rinsed with deionised water to remove any traces of reagents or heavy liquid. Prior to analysis by MC-ICP-MS, an additional chemical cleaning of diatom opal is carried out, following the protocol of Ellwood and Hunter (1999). This involves reductive cleaning (hydroxylamine hydrochloride/acetic acid solution), etching (sodium fluoride, NaF) and oxidative cleaning (strong acid solution of 50% HNO_3/10% HCl), to remove any remaining organic matter and surface contaminants respectively. This was not required for samples analysed at NIGL due to the different isotope extraction methods (section 2.1.4 above).

Traditionally, these techniques would have included sieving and/or differential settling in an effort to remove both clay minerals and the siliceous components of other organisms such as radiolaria and sponges (e.g. Shemesh et al., 1988). Methodologies in the literature which target diatom opal through sieving use a variety of different size ranges (<20μm, 10-38μm, <38μm), and no systematic study of the effect of size on measured $\delta^{30}Si$ has been undertaken. As such, the best size fraction to use when targeting diatom $\delta^{30}Si$ has been poorly constrained. An additional

issue is that in order to remove contaminating clay minerals, techniques often exclude the <10μm fraction, necessitating the loss of smaller diatom fractions (Morley et al., 2004). This not only removes a large portion of diatom opal that could otherwise be analysed, but may also introduce species specific biases. There are two ways in which species composition may alter $\delta^{30}Si$: Firstly, as with the $\delta^{13}C$ of foraminifera and coccolithophores (e.g. Erez, 1978; Minoletti et al., 2009), there may be species specific vital effects on silicon isotope fractionation. Although in general studies have found no evidence for species effects on diatom $\delta^{30}Si$ (De La Rocha et al., 1997; Milligan et al., 2004), there has recently been some suggestion from culture study that the genus *Chaetoceros* may have a much larger fractionation factor than other diatoms (Sutton, AGU 2011 abstract). Secondly, different species of diatom may thrive preferentially at different times of the year, recording different levels of silicic acid utilisation (De La Rocha. 2006). Species issues may pose a problem for diatom downcore $\delta^{30}Si$ records, as unless samples were initially monospecific, they will often contain a high number of diatom species the composition of which may change over time (Morley et al., 2004; De La Rocha, 2006; Leng and Barker, 2006; Swann and Leng, 2009).

One approach to addressing these issues is to assess the relationship of both size fraction and diatom species composition with measured $\delta^{30}Si$ in core top samples. Microfiltration (Minoletti et al., 2009, Figure 2.8) can be used to separate samples into narrow size fractions between 2μm and 100μm as an alternative to sieving, which is difficult below 63μm. The composition (both in terms of diatom:non-diatom silica ratios, and diatom species) and $\delta^{30}Si$ of each size fraction can then be analysed, establishing the existence and magnitude of size and composition effects on measured $\delta^{30}Si$. However, the technique of Minoletti et al. (2009) includes the use of ultrasonication, which can fragment sedimentary components. Therefore, before applying this technique, a preliminary test to establish both the degree of fragmentation which might be expected and the best setting to use in order to minimise its extent was carried out as follows. A suspension of mainly centric diatoms (dominantly *Thalassiosira lentiginosa*) in the size range 20-

50µm was subjected to the two lowest (20% and 40%) power settings of the bath for up to 2 hours. The suspension was placed in a beaker and on the bottom of the bath. Smear slides were made from material removed at 5min, 15min, 20min, 1hr and 2hrs and from the sample prior to sonication. Fragmentation was then analysed by counting the numbers of fragments in the ranges >75% of a valve (i.e. whole valves), 50-<75%, 25-<50%, and <25% using ImageJ sofware. Fragmentation at 20% power does not become significant until greater than 30 minutes of sonication, with the number of whole valves decreasing from 50% to 45% in that time, but subsequently to 25% after 1hour (Appendix 2). At 40% power (Appendix 2), fragmentation is much quicker, with the number of whole valves decreasing from the initial 50% to 30% after 15 minutes, 20% after 30 minutes and to only 10% after 2 hours.

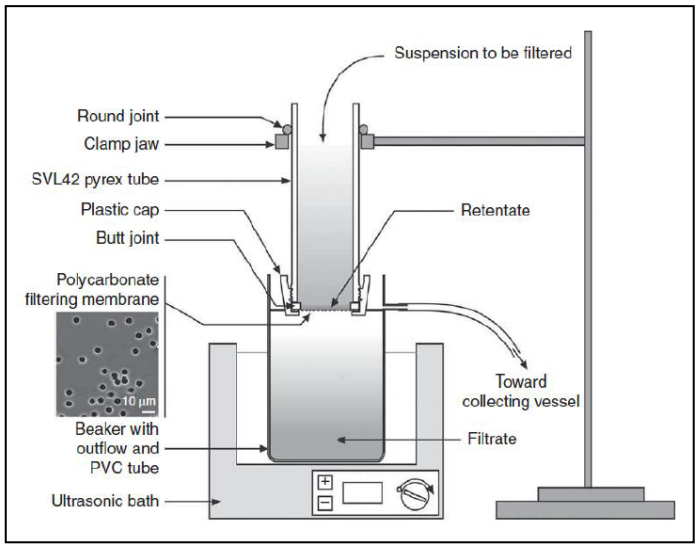


Figure 2.8 Ultrasonic filtration setup, Figure from Minoletti et al., (2009). The opal suspension is poured into the Pyrex tube. Larger particles are retained on either a polycarbonate membrane (<20µm) or nylon mesh (20-100µm). The filtrate is collected and can then be re-filtered at a smaller size if required. A variable power ultrasonic bath is used to minimize valve fragmentation.

These are maximum estimates of fragmentation for two reasons; firstly, the large centric diatoms that make up the bulk of this sample are probably the most susceptible to fragmentation, and secondly because the suspension is placed directly in the bath and is subjected to sonication for the entire 2 hours. In reality, the suspension moves through the beaker suspended in the bath into

another beaker that is not in the bath – so the suspension is not subjected to sonication for the entire time the separation is taking place (Figure 2.8). Nonetheless the experiment shows that fragmentation is a justified concern, and likely does occur to some extent during the filtrations. As such the time material is subjected to sonication is kept as minimal as possible and only the lowest power (20%) setting used. Filtrations at >20μm take less than 5 minutes, and therefore are highly unlikely to fragment large, non- diatom components such as radiolaria, which would lead to more of their fragments being incorporation into smaller size fractions than for normal sieving. Therefore, as long as the above considerations are taken into account, it is appropriate to apply this technique to testing the effect of size fraction on measured $\delta^{30}Si$.

2.3 Summary

Well established techniques exist for the measurement of silicon isotope ratios in biogenic opal using both MC-ICP-MS and vacuum-line fluorination/IRMS, which have been applied to produce the $\delta^{30}Si$ values included in this thesis. Robust, tested, techniques also exist for the extraction of sponge spicules from sediments, and extensive core top calibration in the modern ocean has been undertaken elsewhere. However, current diatom preparation methods, although ensuring the removal of contaminants such as organic carbon and surface oxides, do not wholly ensure the removal of biogenic silica derived from non-diatom sources such as radiolaria. Additionally, no core top calibration exists for diatom $\delta^{30}Si$ as a proxy for silicic acid utilisation. Chapter 3 documents the application of microseparation to sediments from Southern Ocean core tops, with the aim of developing a method that ensures the consistent extraction of pure diatom fractions. Diatom $\delta^{30}Si$ measured in these core tops is used to produce a marine diatom $\delta^{30}Si$ calibration.

Chapter 3. Diatom Silicon Isotopes as a Proxy for Silicic Acid Utilisation: a Southern Ocean Core Top Calibration*

Abstract

Despite a growing body of work that uses diatom $\delta^{30}Si$ to reconstruct past changes in silicic acid utilisation, few studies have focused on calibrating core top data with modern oceanographic conditions. In this study, a microfiltration technique is used to divide Southern Ocean core top silica into narrow size ranges, separating components such as radiolaria, sponge spicules and clay minerals from diatoms. Silicon isotope analysis of these components demonstrates that inclusion of small amounts of non-diatom material can significantly offset the measured from the true diatom $\delta^{30}Si$. Once the correct size fraction is selected (generally 2-20μm), diatom $\delta^{30}Si$ shows a strong negative correlation with surface water silicic acid concentration (R^2=0.92), highly supportive of the qualitative use of diatom $\delta^{30}Si$ as a proxy for silicic acid utilisation. The core top diatom $\delta^{30}Si$ matches well with mixed layer filtered diatom $\delta^{30}Si$ from published in situ studies, suggesting little to no effect of either dissolution on export through the water column, or early diagenesis, on diatom $\delta^{30}Si$ in sediments from the Southern Ocean. However, core top diatom $\delta^{30}Si$ shows a poor fit to simple Rayleigh or steady state models of the Southern Ocean when a single source term is used. The data can instead be described by these models only when variations in the initial conditions of upwelled silicic acid concentration and $\delta^{30}Si$ are taken into account, a caveat which may introduce some error into quantitative reconstructions of past silicic acid utilisation from diatom $\delta^{30}Si$.

*Published in Geochimica et Cosmochimica Acta, 96, p.174-192.

3.1 Introduction

Reliable palaeoproductivity and nutrient utilisation proxies are essential to our knowledge of the role played by the marine biosphere in climatic change. Such records are of particular importance in regions such as the Southern Ocean, the Equatorial and Sub-Arctic Pacific, and areas of coastal upwelling which have a direct influence on atmospheric CO_2 concentration and are sensitive to changes in biological carbon pumping (Sarmiento and Toggweiler, 1984; Elderfield and Rickaby, 2000; Sigman and Boyle, 2000; Takahashi et al., 2002; Kohfeld et al., 2005; De La Rocha, 2006). In these areas, a lack of carbonate preservation limits the use of traditional nutrient utilisation or productivity proxies based on foraminifera (e.g. Benthic Foraminiferan Accumulation Rates, $\delta^{13}C$; Swann and Leng, 2009). As a result we must turn to less conventional media, such as biogenic silica, to gain insight into past variation in nutrient utilisation.

Diatoms, siliceous walled phytoplankton, are the dominant contributor to modern biogenic silica deposition (Tréguer et al., 1995). Diatoms play an important role in carbon export; in nutrient rich and coastal environments they may account for up to 75% of primary production (Nelson et al., 1995; De La Rocha et al., 1998). Their silica frustules also provide an effective ballast material for sinking organic matter (Buesseler, 1998; Baines et al., 2010). As primary producers making an important contribution to the biological carbon pump, and which have an absolute requirement for silicon, diatoms represent an important link between the silicon and carbon cycles.

The silicon isotope signature preserved in diatom opal may be used as a proxy for their silicic acid utilisation (De La Rocha et al., 1997; De La Rocha et al., 1998; De La Rocha, 2006). During silicification diatoms discriminate biologically against the heavier Si isotopes (^{30}Si and ^{29}Si) with a fractionation factor ($^{30}\varepsilon$) of $-1.1\pm0.4‰$(De La Rocha et al., 1997; Milligan et al., 2004). This imparts a high $\delta^{30}Si$ signature on surface water silicic acid, and hence on diatom silica that subsequently forms from it. At depth, remineralisation of diatom silica releases silicic acid with a

lower δ^{30}Si than the surface silicic acid, and creates a gradient between high δ^{30}Si, low silicic acid surface water and high silicic acid, low δ^{30}Si deep water. Upwelling re-supplies the high silicic acid, low δ^{30}Si water to the surface ocean. Diatom δ^{30}Si is therefore a measure of diatom silicic acid utilisation, which is itself a balance between the amount of diatom silicification and the rates/composition of upwelled water. This is the basis of the diatom δ^{30}Si proxy, where high δ^{30}Si represents high utilisation. However, diatom δ^{30}Si is still a developing proxy, with areas of both methodology and calibration that require some refinement.

One important caveat is that the impact of non-diatom components on diatom δ^{30}Si measurements is under-constrained. Due to their small size, it is generally considered impractical to hand-pick diatom frustules (Swann et al., 2008) and a sequence of chemical and physical separation techniques are instead employed to purify diatom material (e.g. Morley et al., 2004). However, samples will almost always contain some level of non-diatom material (Morley et al., 2004; De La Rocha, 2006; Leng and Barker, 2006; Swann and Leng, 2009). Non-diatom components may contribute silica with significantly different δ^{30}Si to diatom opal, for example sponges are known to fractionate silicon with $^{30}\varepsilon$ up to approximately −6‰, much greater than that of the diatoms (De la Rocha, 2003; Hendry et al., 2010; Wille et al., 2010). Assessment of the effect of non-diatom sedimentary components on measured δ^{30}Si is therefore required to ensure the reliability of silicic acid utilisation records based on diatom δ^{30}Si.

Additionally, little work has been undertaken to establish how well modern sedimentary diatom δ^{30}Si reflects silicic acid utilisation in the surface ocean or the associated uncertainties involved in reconstructing utilisation from downcore records (De La Rocha et al., 2011; Fripiat et al., 2011b). The δ^{30}Si of both silicic acid and diatom opal may be described using either a Rayleigh or steady state fractionation model (e.g. De La Rocha et al., 1998). Rayleigh fractionation considers the surface ocean to have a finite pool of silicic acid that is progressively depleted by diatoms and exported to the deep ocean. With increasing export both silicic acid and diatom δ^{30}Si become progressively higher. In the steady state model, a continuous supply of

silicic acid from the deep ocean to the surface is matched by diatom uptake and export. These models may allow the reconstruction of past changes in surface water silicic acid utilisation by diatoms, but require knowledge of the initial conditions from which fractionation occurs i.e. the starting silicic acid concentration and its $\delta^{30}Si$ value. It is currently not clear whether such models, with one fixed set of initial conditions, are applicable over large areas of the modern ocean, and if so, which are the most appropriate starting conditions to use in reconstructions. To this end, a body of work has been published on the $\delta^{30}Si$ of both silicic acid and filtered biogenic opal (De La Rocha et al., 2000; Varela et al., 2004; Cardinal et al., 2005; Reynolds et al., 2006a; Cardinal et al., 2007; Fripiat et al., 2007; Beucher et al., 2008; Beucher et al., 2011; De La Rocha et al., 2011; Fripiat et al., 2011a; Fripiat et al., 2011b; Fripiat et al., 2011c; de Souza et al., 2012), but despite this opinion is divided over whether the Southern Ocean may be modelled as a single system. Given the growing number of oceanic studies available for comparison, the step of core top calibration is overdue.

Here, we aim to develop the diatom $\delta^{30}Si$ proxy both in terms of methodology and calibration, which, especially if used in combination with other proxies such as the $\delta^{30}Si$ of sponge spicules (deep water silicic acid concentration, Hendry et al., 2010; Wille et al., 2010), and diatom $\delta^{15}N$ (nitrate utilisation, Sigman et al., 1999; Brzezinski et al., 2002; De La Rocha, 2006), has great potential for the reconstruction of past productivity and nutrient dynamics. Core top calibration of the Southern Ocean, representing a first assessment of the contribution made by different components to measured $\delta^{30}Si$, is presented. Through comparison of this latitudinal transect of core top diatom $\delta^{30}Si$ with modern surface water silicic acid concentrations, the extent to which simple models may allow quantitative reconstruction of past silicic acid utilisation is assessed.

3.2 Materials and methods

3.2.1 Materials

I have analysed sediments from both the Atlantic and Pacific sectors of the Southern Ocean covering a range of silicic acid concentrations from annual averages of ~80μM in the Firth of Tay (NBP07-03-KCO8A) to ~10μM just north of the Polar Front (TAN0803-127) (Figure 3.1, Table 3.1). The Western Antarctic Peninsula cores, JCR112-BC383 (383), JCR112-BC385 (385) and JCR112-BC391 (391) were collected as part of an Antarctic Funding Initiative Project (AFI4-02) in collaboration with the Rothera Biogeochemical Time Series (Hendry and Rickaby, 2008). They represent approximately 10 years of modern sediment accumulation, as evidenced by: i) the presence of photo-detrital fluff near site 383, and ii) sedimentation rates of 0.14cm/yr and 0.13cm/yr at two proximal sites (^{210}Pb dating, JCR112-BC388 and JCR112-BC391 respectively in Hendry and Rickaby, 2008). NBP07-03-KCO8A (08A) was collected as part of the 2006 SHADRILL II cruise to the north-western Weddell Sea; its top has been ^{14}C dated to 1706AD. Samples from the Pacific sector of the Southern Ocean were supplied by the New Zealand National Institute of Water and Atmospheric Research (TAN0803-127 (TAN127) and TAN0803-124 (TAN124)) and Oregon State University (in subsequent text 'NZ samples': KN7812-04BC (NZ4), NBP9802-05MC1 (NZ5), KN7812-06BC (NZ6), NBP9802-07MC1 (NZ7), KN7812-11BC (NZ11)) and have been ^{14}C dated to <10 k yrs.

To test the relationship between geological samples and core top size fractions, we have analysed four downcore samples from the Eocene and Oligocene of Ocean Drilling Program Site 177-1090 in the Atlantic Sector of the Southern Ocean (Table 3.1). The site has a palaeodepth of 3700m and is currently situated just south of the Subtropical Front. The age model is from Channell et al. (2003) on the timescale of Cande and Kent (1995).

Site (Text Reference)	Latitude	Longitude	Depth (m)	Age	Modern Annual Silicic Acid Range and (annual average) (μM)	Core Type	Source
JCR112-BC383 (383)	-66.72	-70.44	578	Modern Accumulation (Photodetrital fluff)	34-74 (55)	Box	AFI 4/02
JCR112-BC385 (385)	-68.02	-70.52	845	<10 years (^{210}Pb)	43-92 (70)	Box	AFI 4/02
JCR112-BC391 (391)	-67.86	-68.23	814	<10 years (^{210}Pb)	55-65 (60)	Box	AFI 4/02
NBP07-03-KC08A (08A)	-63.34	-55.87	629	1706AD (^{14}C)	76-101 (90)	Kaston	Shadrill
TAN0803-124 (TAN124)	-58.69	160.23	4358	47600±1800 Radiocarbon years at 11cm	7-26 (15)	Gravity	NIWA
TAN0803-127 (TAN127)	-57.56	160.87	3830	7567±100 Radiocarbon years at 1cm	5-20 (10)	Gravity	NIWA
KN7812-04BC (NZ4)	-61.77	174.42	4240	<10Ka (^{14}C)	3-39 (25)	Box	OSU
NBP9802-05MC1 (NZ5)	-63.11	-169.74	2927	<10Ka (^{14}C)	19-52 (40)	Multi	OSU
KN7812-06BC (NZ6)	-63.29	174.78	2429	<10Ka (^{14}C)	22-58 (40)	Box	OSU
NBP9802-07MC1 (NZ7)	-60.42	-170.19	3860	<10Ka (^{14}C)	6-31 (20)	Multi	OSU
KN7812-11BC NZ11)	-63.63	-169.32	2738	<10Ka (^{14}C)	19-52 (40)	Box	OSU
ODP177-1090B	-41.81	8.9	3700m (palaeodepth)	25.5Ma, 27.1Ma, 33.8Ma, 35.9Ma	N/A	Hydraulic Piston Core/Extended Core Barrel	Ocean Drilling Program

Table 3.1. Core Site Summary.

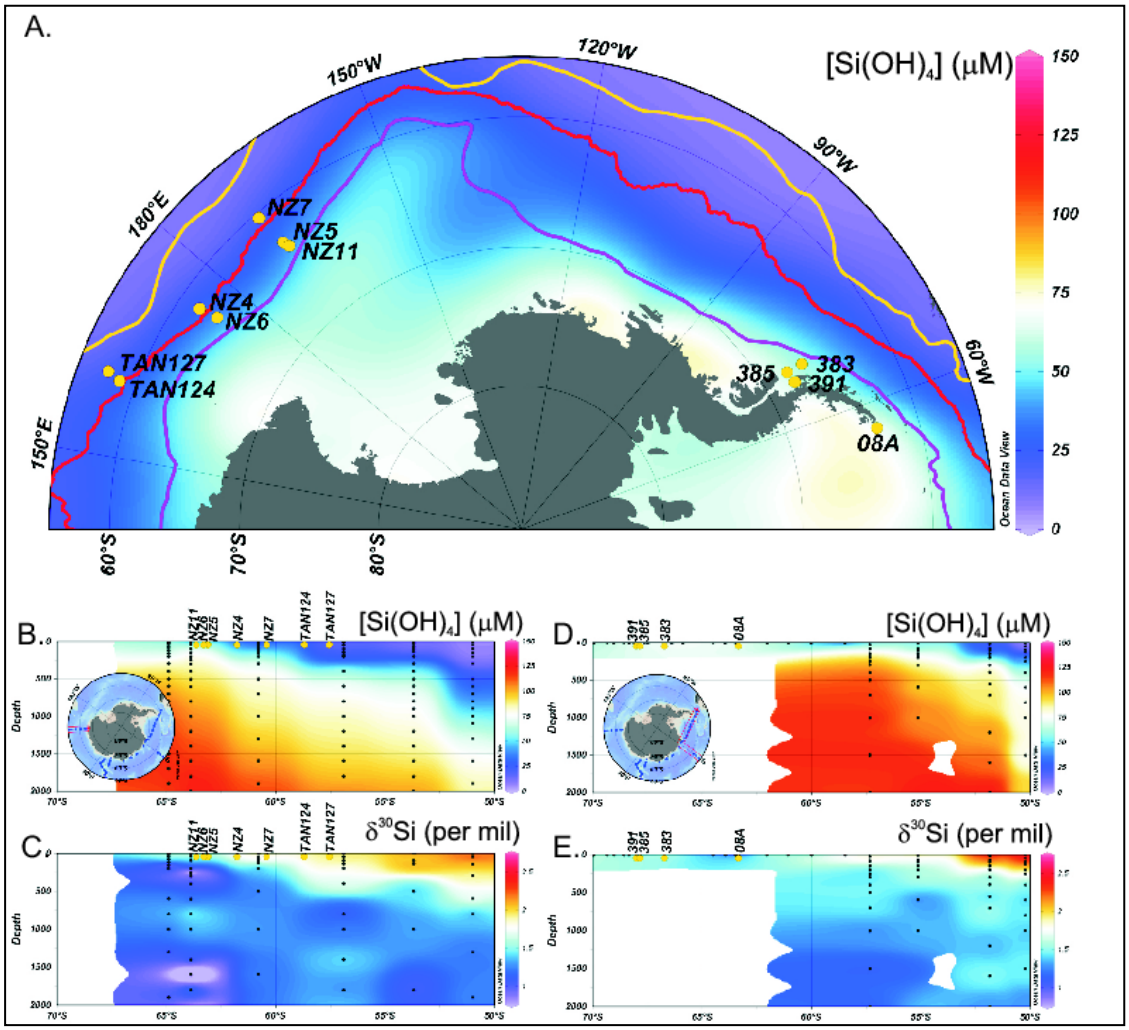


Figure 3.1a. Core top locations with annual surface water silicic acid concentration (World Ocean Atlas 2009, http://www.nodc.noaa.gov/OC5/WOA09/pr_woa09.html) and Southern Ocean Antarctic Circumpolar Current (ACC) Fronts (Orsi, 1995). Purple = ACC Southern Boundary (SB), Red = Polar Front (PF), Yellow = Sub-Antarctic Front (SAF); **b and c.** Pacific Sector Silicic acid concentration and $\delta^{30}Si$, respectively, above 2000m (Cardinal et al., 2005) with core top locations plotted at respective latitude; **d and e**. Atlantic Sector Silicic acid concentration and $\delta^{30}Si$, respectively, above 2000m (Fripiat et al., 2011b, De La Rocha et al., 2011) with core top locations plotted at respective latitude. Note core tops are compared to the nearest transect available and that as such longitudes are not exactly the same.

3.2.2 Methods

3.2.2.1 Biogenic Silica Extraction and Size Separation

Biogenic opal was separated from sediments using both chemical and physical techniques following the protocol of Hendry and Rickaby (2008), adapted from the methods of Shemesh et al. (1995 onwards), Ellwood and Hunter (1999), and Morley et al. (2004), with the addition of the novel microseparation technique of Minoletti et al. (2009). The 8 stage methodology is outlined in Figure 3.2 and described below:

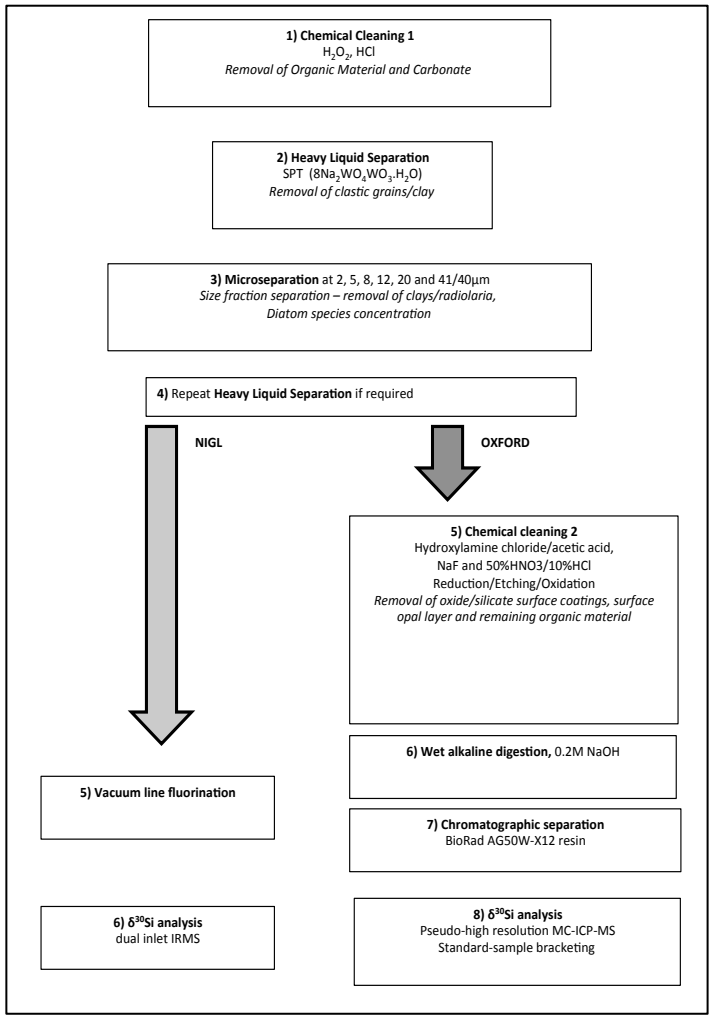


Figure 3.2 Summary of Methods. Steps 1 to 4 are biogenic silica purification techniques common to analyses performed both in Oxford and at NIGL. Steps 5 and 6 (left hand side) are NIGL analysis steps and 5 to 8 (right hand side) are clean up steps and analysis techniques used in Oxford. SPT = Sodium Polytungstate. MC-ICP-MS = Multi-collector inductively coupled plasma mass spectrometer.

3.2.2.2 Chemical cleaning stage 1 and heavy liquid separation

Initial chemical cleaning steps used H_2O_2 and HCl to remove organic matter and carbonate respectively. This was followed by several heavy liquid separations using sodium polytungstate (SPT, $8Na_2WO_4WO_3.H_2O$) to remove clastic grains and clay minerals. After each stage opal was thoroughly rinsed with deionised water to remove any traces of reagents or heavy liquid.

3.2.2.3 Microseparation

In traditional methods, sieving is employed either before or after initial chemical cleaning with the aim of removing clay minerals and the siliceous components of other organisms such as radiolaria and sponges (e.g. Shemesh et al., 1995; Morley et al., 2004). Here, rather than sieving, which is difficult below 63µm, microfiltration was employed (described in Minoletti et al., 2009), allowing the samples to be separated into a range of size fractions between 2µm and 100µm. The technique involves filtering sediment suspensions through a series of nylon meshes or Millipore® polycarbonate membranes with the aid of an ultrasonic bath (Figure 3.3). The gentle ultrasonication continuously re-suspends the sediment and prevents clogging of the membrane/mesh, ensuring effective separation. Separations were made at 50 or 41µm, 20µm, 12µm, 8µm, 5µm and 2µm, and a sample of the bulk silica (purified silica prior to size fraction separation) was removed for analysis. As only the <63µm fraction was available from the NZ samples (Table 3.1), separations for these samples were made at 2µm and 20µm. Size fractions were dried and weighed. Smear slides of each fraction were analysed for relative proportions of diatoms to other siliceous organisms, as well as for diatom specific abundances. If at this stage any clastic grains were observed, a repeat heavy liquid separation was undertaken. For 08A some clastic contamination proved impossible to remove.

For the Antarctic Peninsula sites, a comparison of bulk silica (i.e. no microseparation) with separated diatom size fractions, using a scanning electron microscope, showed that the microseparation removed clay minerals which were adhered to and clogging the pores of

frustules in the bulk samples (Figure 3.4). At all sites, optical and SEM observations of the <2µm fraction showed abundant clay.

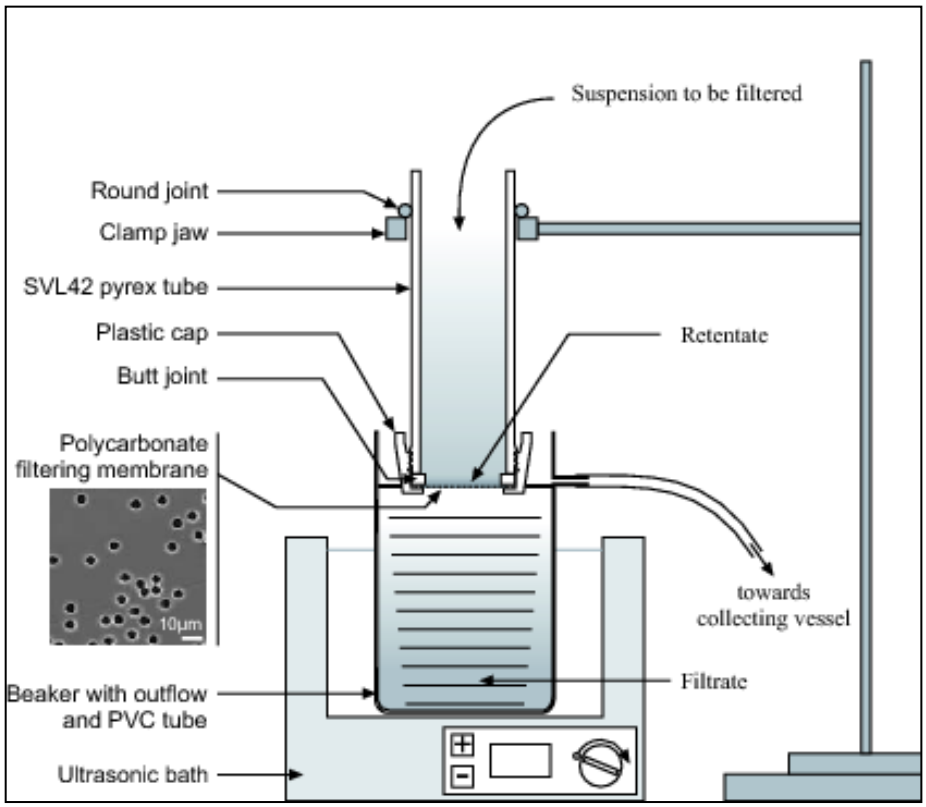


Figure 3.3 Ultrasonic filtration setup, from Minoletti et al., (2009). The opal suspension is poured into the Pyrex tube. Larger particles are retained on either a polycarbonate membrane (<20µm) or nylon mesh (20-100µm). The filtrate is collected and can then be re-filtered at a smaller size if required. A variable power ultrasonic bath is used to minimize valve fragmentation (Appendix 2).

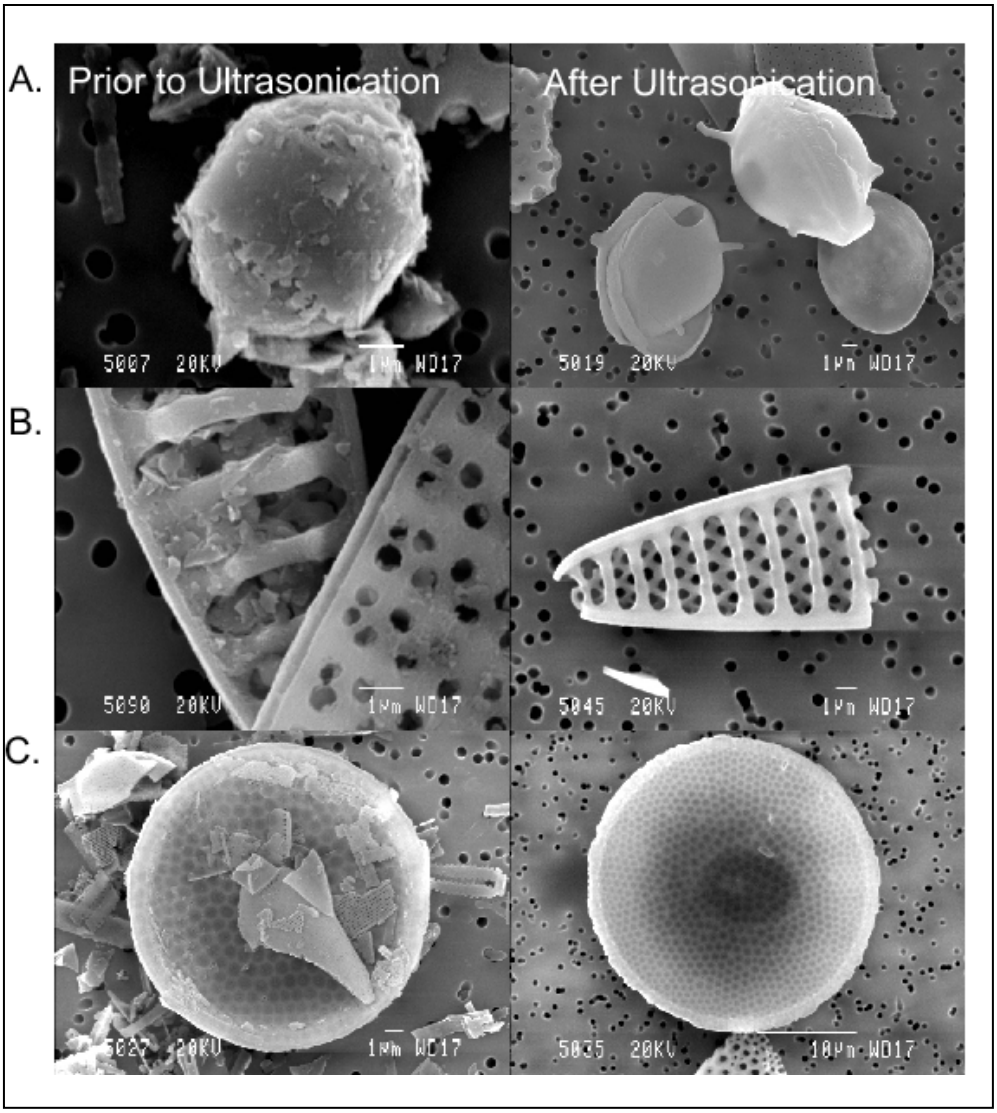


Figure 3.4 SEM images of diatoms before (left) and after (right) microseparation **a.** *Cheatoceros* resting spores; **b.** *Fragilariopsis kerguelensis* and; c. *Thalassiosira* sp. Images demonstrate the removal of adhered clays and clays lodged in the pores of diatom frustules (particularly b). Images from Antarctic Peninsula sites.

Fragmentation of siliceous components limits the ability of microseparation to partition them on merit of their size and/or shape. Fragmentation has two sources; initial fragmentation during sinking and early diagenesis, and fragmentation occurring during ultrasonication as part of the microseparation technique. Initial fragmentation is particularly high in coastal Antarctic Peninsula samples, while the Pacific sector samples tend to have relatively low numbers of fragments. To determine optimal sonication settings and potential fragmentation, an experiment subjecting whole diatom valves to different levels of sonication, over various lengths of time, was undertaken (Appendix 2). This shows that fragmentation is directly related to both time and power setting, but that use of the lowest power setting on the ultrasonic bath minimises fragmentation during microseparation.

3.2.2.4 Chemical cleaning stage 2 (Oxford only)

Silicon isotope analyses were conducted at both Oxford University and at the NERC Isotope Geochemistry Laboratory, Nottingham (NIGL). Si isotope data from the two laboratories have been shown to be comparable (Hendry et al., 2010). The samples analysed in Oxford underwent an additional chemical cleaning stage, following the protocol of Ellwood and Hunter (1999) (Figure 3.2). This involves reductive cleaning (hydroxylamine hydrochloride/acetic acid solution), etching (NaF) and oxidative cleaning (strong acid solution of 50% HNO_3/10% HCl), to remove any remaining organic matter and surface contaminants respectively. This was not required for NIGL due to the different isotope extraction methods (see section 3.2.2.6 below).

3.2.2.5 Digestion and Chromatographic Separation (Oxford only)

The purified opal was dissolved via wet alkaline digestion (Ragueneau et al., 2005; Cardinal et al., 2007) in 0.2M NaOH at 100˚C for 40 minutes. The samples were then acidified to pH~2 with 0.2M thermally distilled HCl and separated from major ions using cation exchange resin (BioRad AG50W-X12; Georg et al., 2006).

3.2.2.6 Vacuum line fluorination (NIGL only)

At NIGL a fluorination method was employed to convert the silica into SiF_4 (and O_2) using a fluorine based reagent. The diatom silica was reacted in three steps, and subsequently the Si was extracted. Stage one involved 'outgassing' (dehydration) to remove surficial and loosely bound water in the reaction tubes at room temperature. Stage two involved a prefluorination step with a stoichiometric deficiency of the reagent (BrF_5) at low temperature which removes the hydroxyl and loosely bound water. The third stage was a total reaction at 450^{o}C for 12 hours with an excess of reagent to dissociate the silica into O_2 and Si (as SiF_4) (Leng and Sloane, 2008).

3.2.2.7 Mass Spectrometry and δ^{30}Si analysis

At Oxford, δ^{30}Si analysis was carried out using a Nu Instruments Nu-Plasma HR multi-collector Inductively Coupled Plasma Mass Spectrometer (HR-MC-ICP-MS). Samples were introduced via a self-aspirating PFA microconcentric nebuliser (ESI) in a Cetac Aridus II desolvating unit. The HR-MC-ICP-MS was run in medium resolution mode (m/Δm ~3500, at 5 and 95%) in order to resolve interferences on ^{29}Si and ^{30}Si. Standard-sample bracketing was used to account for mass bias, and 8 repeats of 20 x 8 second integrations were made. Samples were measured relative to the NIST RM 8546 standard. The Diatomite standard (1.26‰±0.2‰ (2σSD); Reynolds et al., 2007) was analysed with each batch of samples. From this, the long term reproducibility is 0.24‰ (2σSD, n=52), with a mean of +1.26‰ and an average internal error of 0.18‰ (2σSD of the 8 repeat standard sample measurements).

At NIGL δ^{30}Si measurement was carried out using a Thermo-Finnigan MAT253 gas source mass spectrometer. The gaseous silicon tetrafluoride (SiF_4) was produced off line and introduced via a manifold. Samples were again measured relative to NIST RM 8546. The diatomite standard BFC (Chapligin et al., 2011) was run with each batch of samples to calibrate the sample data. From this, the long term reproducibility is 0.2‰ (2σSD). Duplicate samples had a mean reproducibility of 0.06‰ (2σSD). All measurement values quoted in the text and figures have

error values equal to the 2σSD external reproducibility, except where the internal reproducibility was greater, in which case this is quoted instead.

3.2.2.8 Size fraction composition analysis

Area analysis of smear slides images (taken with a high-resolution ZeissTM Scope A1 optical microscope and Zeiss AxioCam ICc1 camera) for both diatom to non-diatom component ratios and diatom species were carried out using ImageJ software (free to download from http://rsb.info.nih.gov/ij/index.html). It is noted that there are significant errors associated with area analysis, particularly due to differences in biovolume between the various components (especially between diatoms and radiolaria/sponge spicules).

3.3 Results

In order to determine the size fraction most appropriate to use to represent diatom $\delta^{30}Si$ in future downcore studies, it is necessary to consider the mass, composition and isotope signature of each size fraction.

3.3.1 Size Fraction Mass

For sites on the Antarctic Peninsula (383, 385, 391 and 08A), the <2μm fraction contained the greatest mass of silica, ranging from 40% at 383 to 70% at 08A (Figure 3.5a and b). In contrast, sites in the Pacific sector of the Southern Ocean had <2μm fractions that contained <1% (TAN124) to 15% (NZ4, TAN127) of the total (Figure 3.5c and d). SEM observations of the <2μm fraction showed it to contain significant amounts of clay at all sites.

The Antarctic Peninsula sites display a general decrease in the amount of silica contained in a size fraction with increasing size e.g. from 15% in the 2-5μm size fraction, to <1% in the >50μm at site 383 (Figure 3.5a and b). However, there is a small relative peak in silica mass in the 8-12

or 12-20µm size fractions at all four sites (e.g. 25% in the 12-20µm at site 383). For TAN127 and 124, there is a decrease in the mass of silica from 35% and 70% (respectively) in the 2-5µm fractions, to 5% in the 12-20µm fractions (Figure 3.5c). The >50µm fractions contain 5% of the total at sites TAN127 and TAN124 respectively, in contrast to the <1% found in the >50µm fraction at any of the Antarctic Peninsula sites. For the NZ sites most silica is contained in the 2-20µm size fraction which contributes between 75% (NZ7) and 90% (NZ11) to the total mass of silica (Figure 3.5d).

In the downcore samples, 1090-18, 26 and 31 have 20% to 25% of material contained in the <2µm size fraction, compared to 65% in 1090-20. The 2-10µm size fraction contains between 20% (1090-20) and 55% (1090-26), the 10-20µm size fraction between 6% (1090-20) and 25% (1090-31) and the 20-41µm size fraction up to ~10% (1090-26).

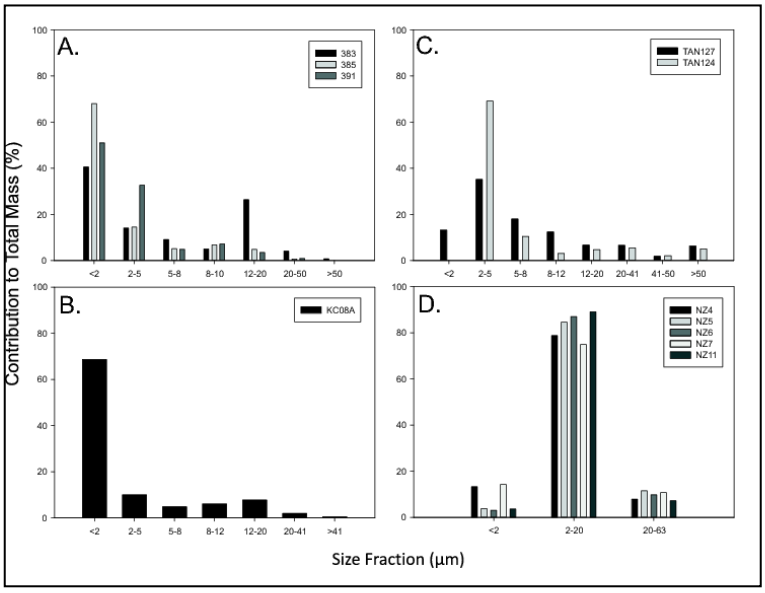


Figure 3.5 Size fraction contributions to total silica (% by mass) for; **a.** Sites 383, 385 and 391, and; **b.** Site 08A on the Antarctic Peninsula; **c.** Pacific Sector sites TAN127 and 124, and; **d.** Pacific Sector NZ sites. For sites on the Antarctic Peninsula, the <2µm size fraction contains the most silica, and subsequently silica contribution decreases with increasing size fraction. For Pacific sites TAN127 and 124, the greatest mass is contained in the 2-5µm fraction, and contribution again decreases with increasing size. NZ sites all have the most opal contained in the 2-20µm fraction.

3.3.2 Size Fraction Composition

At all of the core top sites studied for a full range of size fractions, relative diatom abundance shows the same trend, with diatom percentage lowest in the two largest size fractions (Figure 3.6) and closer to 100% in the smaller size fractions (2-20μm). The small size of material and dominance of clay in the <2μm fractions meant it was not possible or informative to carry out area analysis, and they are not considered further.

For the Antarctic Peninsula sites (Figure 3.6a to c), diatom percentage is highest between 2 and 20μm, in all cases being between 90% (e.g. site 383, 8-12μm) and 100% (e.g. site 385, 2-5μm, 5-8μm, 12-20μm). The non-diatom contribution between 2 and 20μm comprises (in the case of sites 383 and 385) radiolaria, sponge spicules and silicoflagellates. Individually these components never account for more than 5%. In the 2-20μm range at 08A, the non diatom material is dominantly clastic grains, with a small contribution from sponge spicules. The percentage of diatom material decreases significantly in the larger size fractions, dropping to only 5% in the >50μm fraction of site 383 and the >41μm of site 08A (the >50μm fraction contained almost no material at site 385 and so was not analysed). The diatom percentage contained in the 20-50/20-41μm fractions falls between that of the 2-20μm and >50/41μm fractions, containing 55% to 80% diatom material at 08A and 383, 385 respectively. At all sites except 08A the largest size fraction is dominated by radiolaria, which contribute up to 95% of silica (e.g. >50μm fraction at site 383). At 08A, clastic grains account for 65% of the >41μm fraction.

At TAN127, the pattern is again very similar (Figure 3.6d), although diatoms are more abundant in the 20-41μm fraction, accounting for approximately 90% of the silica. Non-diatom material in all size fractions is almost exclusively radiolarian, which constitute 94% of the >50μm size fraction. NZ samples were only analysed in the 20-63μm range, but are dominantly diatom material (82% at NZ4 to 99% at NZ6). Non-diatom material is generally radiolarian (e.g. 16% at NZ4), with minor contributions from sponge spicules and silicoflagellates.

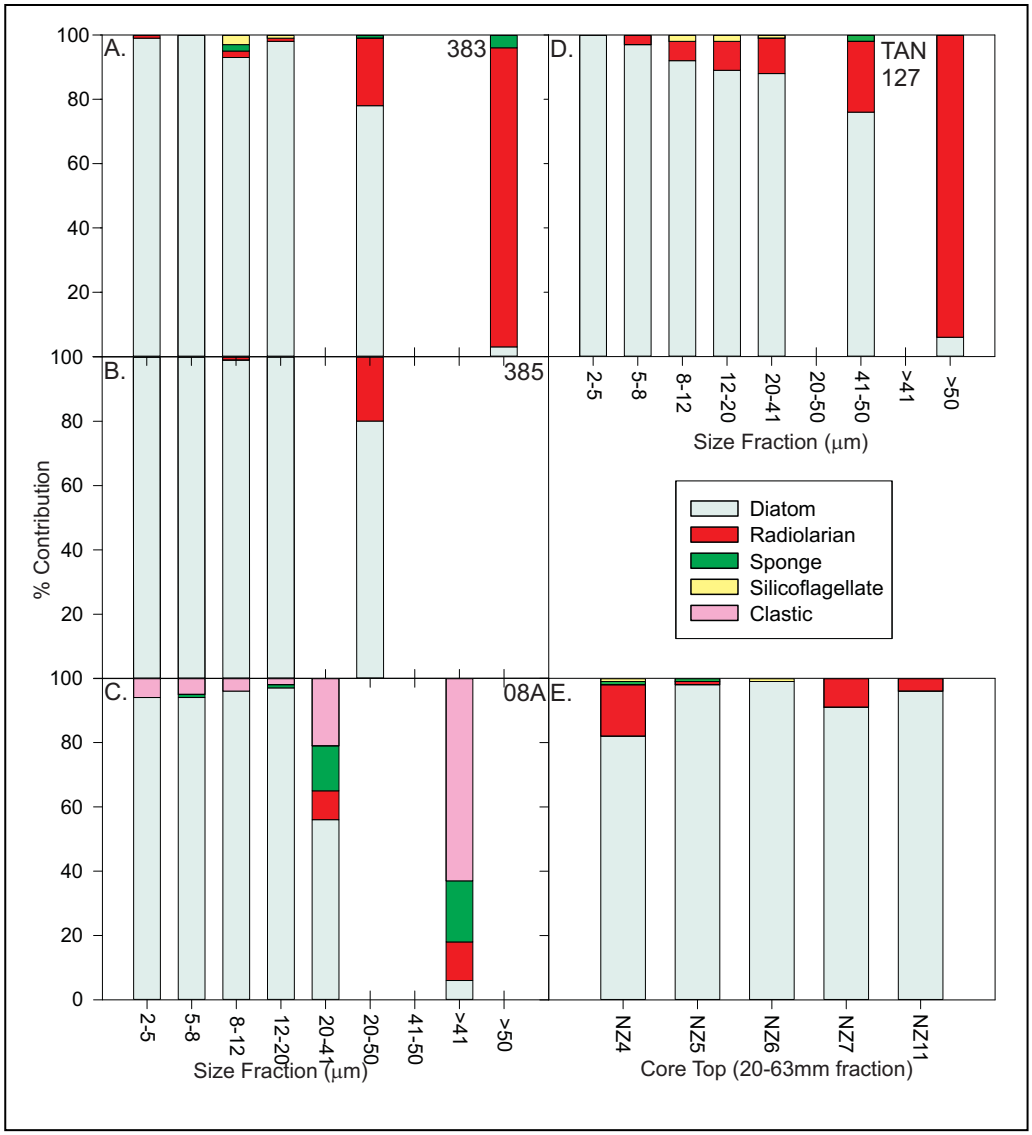


Figure 3.6 Size fraction composition by area analysis; **a.** Site 383; **b.** Site 385; **c.** Site 08A; **d.** Site TAN127; and **e.** 20-63μm size fractions only for NZ sites; a - d. Total diatom percentage is lowest in the >50μm size fraction, which is dominated by radiolaria (or clastic grains at site 08A (c)), and is highest between 2 and 20μm.

3.3.3 Silicon Isotope Compositions

Size fractions in the range 2-20μm have a higher average $\delta^{30}Si$ of +0.97±1.20‰ with values ranging from −0.47±0.24‰ (08A, 12-20μm) to +1.99±0.26‰ (TAN124, 8-12μm), than size fractions >20μm which average +0.23‰±1.97‰ and range from −1.84±0.20‰ (391, >50μm) to +1.4±0.24‰ (TAN124, 41-50μm) (Figure 3.7). In general the greatest disparity is between the 2-5μm fraction and the largest size fraction (>41 or >50μm) e.g. at site 383 the 2-5μm fraction has $\delta^{30}Si$ of +1.04±0.20‰ and the >50μm a $\delta^{30}Si$ of −1.21±0.24‰. $\delta^{30}Si$ of the 2-5μm, 5-8μm, 8-12μm and 12-20μm fractions is high and stable, with these size fractions being within at least external error at all sites except 08A where the 12-20μm fraction is significantly lower (Figure 3.7). The $\delta^{30}Si$ of the <2μm fractions is lower than that measured in the 2-20μm (e.g. −1.14±0.24‰ for KC08A) at all sites except TAN127 where it is more positive (+2.35±0.31‰). There was insufficient material in the <2μm fraction at TAN124 for analysis.

The NZ 2-20μm $\delta^{30}Si$ ranges between +1.14±0.24‰ at NZ6 and +1.94±0.24‰ at NZ4 (Figure 3.9, Appendix 1). At NZ4 and NZ5, the 20-63μm fractions are significantly lower than the 2-20μm, with offsets of 1.22‰ and 0.63‰ respectively. At sites NZ6 and NZ11 there is no resolvable offset between the two.

All four 1090 downcore samples have 20-41μm fractions with significantly lower $\delta^{30}Si$ values than the 2-10μm fraction by between 1.79‰ (1090-18) and 1.19‰ (1090-26) (Figure 3.8). For two samples, 1090-18 (25.5 Ma) and 1090-20 (27.1 Ma), the 10-20μm size fraction was also analysed, and is within error of the 2-10μm fraction, e.g. for 1090-18, 2-10μm $\delta^{30}Si$ = +1.87±0.24‰, 10-20μm $\delta^{30}Si$ = +1.87±0.24‰.

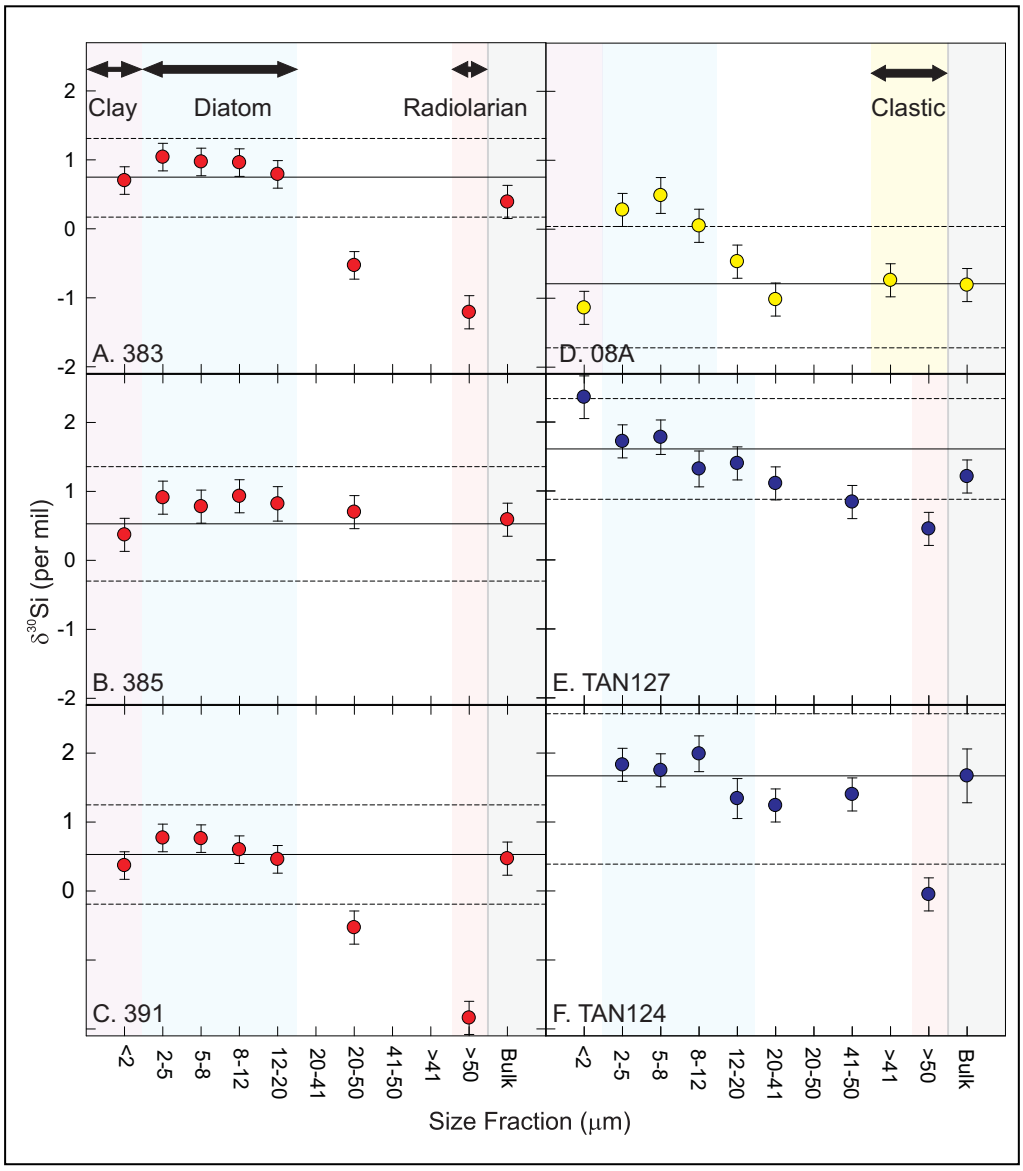


Figure 3.7 Core top size fraction $\delta^{30}Si$; **a.** Site 383; **b.** Site 385; **c.** Site 391; **d.** Site KC08A; **e.** Site TAN127; **f.** Site TAN124. Shading denotes areas with $\delta^{30}Si$ compositions considered in the text to represent diatoms + clay (pink), predominantly diatom (blue), predominantly radiolaria (orange) and predominantly clastic grains (yellow). Solid lines show estimates of bulk sample $\delta^{30}Si$ calculated by mass balance of the individual size fraction $\delta^{30}Si$. Dashed lines show the propagated error on the mass balanced bulk from the 2σSD internal error of the $\delta^{30}Si$ of each size fraction, neglecting error on the mass of the size fractions; these bounds therefore represent a minimum estimate of the actual error on this calculation, nevertheless the measured bulk $\delta^{30}Si$ is still within error of the calculated bulk $\delta^{30}Si$.

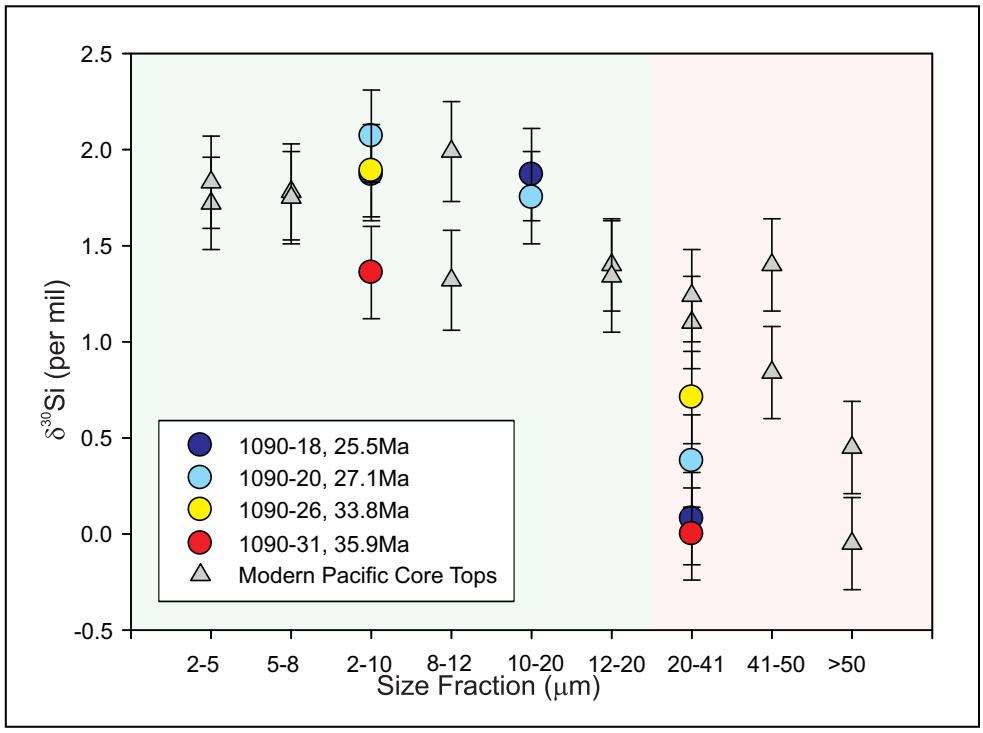


Figure 3.8 Size fraction $\delta^{30}Si$ from four downcore samples at ODP site 1090 (coloured circles) compared to TAN124 and 127 (grey triangles). Site 1090 and these core tops are located north of the modern Polar Front. The decrease in $\delta^{30}Si$ with increasing size fraction observed in modern core tops is also found in downcore samples, despite an age difference of between 26-36Ma. Additionally, the size-$\delta^{30}Si$ relationship is consistent in the downcore samples even across the major climatic shift which occurred at the Eocene-Oligocene Boundary (~34Ma). Green shading represents the size range considered to represent diatom $\delta^{30}Si$ in the downcore samples, and red shading that considered effected by non-diatom components (dominantly radiolarian).

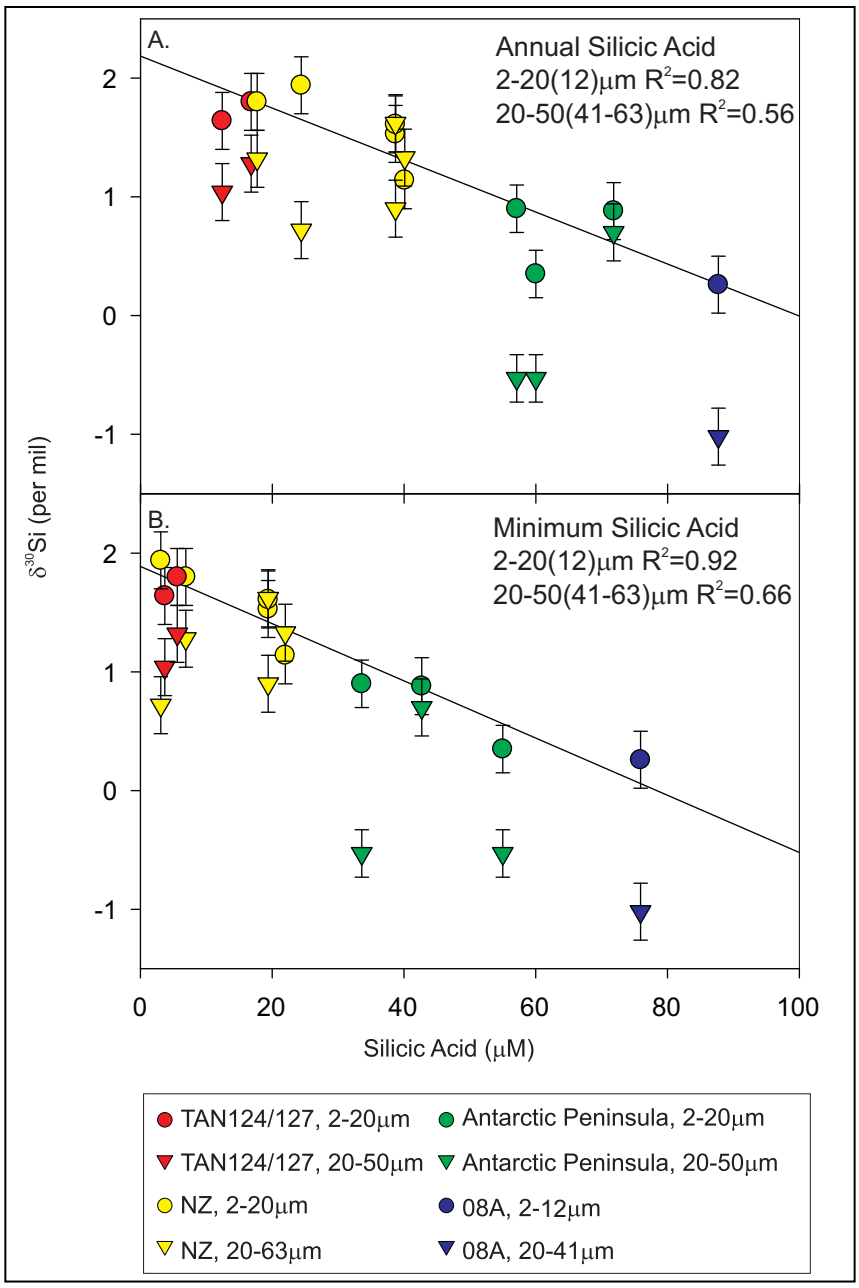


Figure 3.9 Core top δ^{30}Si of size ranges comprised of predominantly diatoms (circles) or a combination of diatoms and non-diatom components (triangles); **a.** Compared to the annual surface water silicic acid concentration at each site taken from the World Ocean Atlas (2009); **b.** Compared to the minimum silicic acid concentration observed yearly, taken from monthly surface water silicic acid concentrations in the World Ocean Atlas (2009). Black lines are the linear regressions through the smaller size fraction at each site ((2-20(12)μm), as represented by the circles). R^2 values are based on linear regression through the respective data set. Error bars represent the long term reproducibility of 0.25 (Oxford) or 0.2 (NIGL) ‰.

3.4 Discussion

3.4.1 Size Fraction Selection for Diatom $\delta^{30}Si$ Records

It is clear from Figures 3.7, 3.8 and 3.9 that a consistent relationship exists between the size fraction of silica analysed and $\delta^{30}Si$. The smallest (<2µm) and largest (> approximately 20µm) size fractions tend to have lower $\delta^{30}Si$ than those between 2µm and approximately 20µm (although the exact size-$\delta^{30}Si$ association differs slightly at TAN127 and 08A). Size fractions with lower $\delta^{30}Si$ contain non-diatom silica which is variably composed of radiolarian tests, sponge spicules, lithogenic components and clay minerals (Figures 3.6 and 3.7), consistent with published $\delta^{30}Si$ ranges of the components present (Figure 3.10). Using the size fraction $\delta^{30}Si$ values and area analyses presented in this study, the size range which most robustly represents diatom $\delta^{30}Si$ at each site can be established, and the potential for these non-diatom components to bias diatom $\delta^{30}Si$ assessed.

The $\delta^{30}Si$ of the <2µm fraction at sites on the Antarctic Peninsula (−1.14±0.24‰ to +0.7±0.20‰, Figure 3.7) is consistent with the fraction being composed of a combination of diatom fragments with a higher $\delta^{30}Si$ (e.g. 2-5µm $\delta^{30}Si$ +1.04±0.20‰ at site 383) and lower $\delta^{30}Si$ clay minerals (Figure 3.10). Douthitt (1982) reports a kaolinite clay with $\delta^{30}Si$ = +1.9‰, indicating that the high $\delta^{30}Si$ of the <2µm fraction at TAN127 is potentially compatible with Si contribution from clay, but since the <2µm fraction can contain components other than clay minerals the offset may not be entirely of clay mineral origin. Clay minerals are much more likely to offset diatom $\delta^{30}Si$ in sediments such as those from the Antarctic Peninsula, where the <2µm fraction contributes a large mass of silica to the bulk sample, than the open ocean Pacific sites where it is only a minor component (Figure 3.5). Clay minerals adhered to, or lodged in, diatom frustules have been problematic to remove in the past and have required sieving at 10µm, necessitating the loss of smaller diatom fractions (Morley et al., 2004). This problem can be

overcome using the microseparation technique, which effectively dislodges (Figure 3.4) and concentrates clays in the <2µm size fraction.

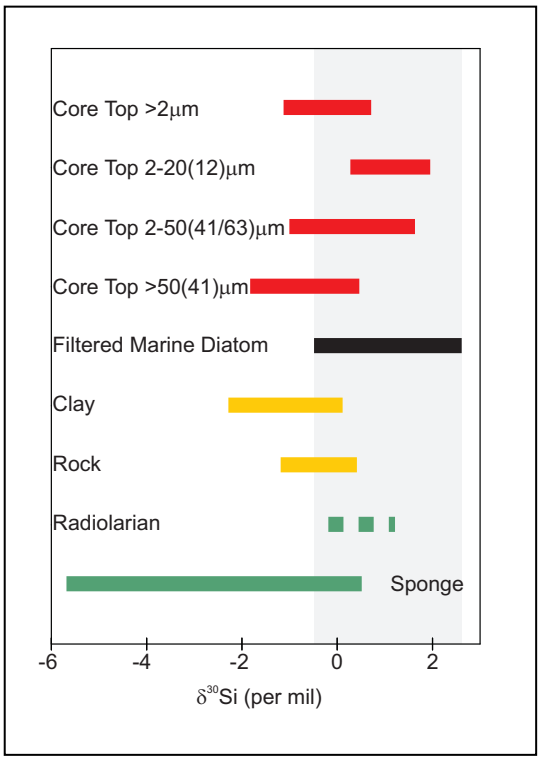


Figure 3.10 Published $\delta^{30}Si$ ranges for the type of non-diatom components present in our core tops and for diatoms filtered from the modern ocean. Also plotted are the $\delta^{30}Si$ ranges of size fractions from the core tops which contain diatoms (2-20 or 2-12µm), clay + diatoms (<2µm, but TAN 127 not included), radiolaria/sponges/clastics + diatoms (20-41/50/63µm) and radiolaria/clastics (>41/50µm). See Section 3.3.2 for details of size fraction contents at each site. Filtered marine diatom $\delta^{30}Si$ between −0.5 and +2.6‰ (Cardinal et al., 2007; Fripiat et al., 2011c; Varela et al., 2004). It should be noted that inclusion of radiolarian tests in this filtered opal cannot be ruled out (Cardinal et al., 2007). Sponge $\delta^{30}Si$ between +0.5 and −5.7‰ (Hendry and Robinson. 2012). Clay $\delta^{30}Si$ from +0.1‰ to −2.3‰ (Basile-Doelsch, 2006). Sedimentary, mafic and felsic rock $\delta^{30}Si$ observations between ~+0.4 and −1.2‰, −0.1 and −0.4‰, and +0.4‰ and −0.4‰, respectively (Reynolds, 2011). Few measurements of radiolarian $\delta^{30}Si$ exist: Ding et al. (1996), measure three samples of radiolaria from mid-Pacific sediments ($\delta^{30}Si$ of +0.3 to −0.2‰), and a set of radiolarian siliceous rocks from the Cambrian to Jurassic ($\delta^{30}Si$ of +0.8‰ to −0.6), and Wu et al. (1997) measure a range of +0.2 to +1.2‰ in downcore Pacific samples. The scarcity of measurements and dominance of geological samples makes it difficult to assess the actual range of radiolarian $\delta^{30}Si$.

At 383 and 385 the 2-20μm size range consists of ≥90% diatom silica. The size fractions found in this range have the highest $\delta^{30}Si$ at their respective site, are all within error of each other, and are considered the most representative of diatom $\delta^{30}Si$. The low $\delta^{30}Si$ of the >50μm fraction at sites 383 and 391 is attributed to the presence of abundant radiolaria (Figsure 3.6, 3.7 and 3.10). On this basis, and considering the low $\delta^{30}Si$ of the radiolarian dominated fractions at other our core top sites (Table 3.2) we suggest that the published range of radiolarian $\delta^{30}Si$ extends to lower values than previously documented. The $\delta^{30}Si$ of the 20-50μm size fractions at sites 383 and 391 is intermediate between the 2-20μm and >50μm fractions, suggesting that it represents a mixture of diatoms and radiolaria. The area analysis shows this fraction contains around 20% radiolaria at site 383, and from this an expected value for the 20-50μm fraction can be calculated; a 20% contribution of silica with $\delta^{30}Si = -1.2‰$ (>50μm $\delta^{30}Si$ i.e. radiolaria) to silica with a $\delta^{30}Si$ = 0.9‰ (the mass-balanced 2-20μm $\delta^{30}Si$ i.e. diatom) yields a value of +0.5‰, around 1‰ higher than the measured 20-50μm $\delta^{30}Si$ (−0.53±0.20‰). This difference probably occurs for two reasons. Firstly, area analysis is likely to underestimate the contribution of radiolarian silica, since radiolarian tests generally have a larger volume than diatom frustules. Secondly, because of difficulty in the homogenisation of biogenic silica samples, it is possible that heterogeneity in analysed material led to over representation of radiolaria in the measured silicon.

Site	2-20μm averaged (diatom)	>50μm/>41μm (Radiolarian)	Offset
383	0.9	-1.21	2.11
391	0.72	-1.84	2.56
127	1.64	0.45	1.19
124	1.80	-0.05	1.85

Table 3.2 Diatom/Radiolarian $\delta^{30}Si$ offsets.

The 2-20μm range at 08A also contains >90% diatom by area (Figure 3.6), in agreement with the highest $\delta^{30}Si$ in the 2-5μm, 5-8μm and 8-12μm size fractions. However, the 12-20μm fraction has significantly lower $\delta^{30}Si$ which tends towards the $\delta^{30}Si$ of the 20-41μm and >41μm fractions (Figure 3.7) despite containing significantly more diatom material (Figure 3.6). The $\delta^{30}Si$ of the 20-41μm and >41μm fractions (−1.02±0.24‰ and −0.74±0.24‰) is in keeping with silicon supplied from clastic grains and sponge spicules, although again the 20-41μm fraction appears to contain significantly more diatom material than the >41μm fraction. As discussed above, inconsistency between area analysis and measured $\delta^{30}Si$ is probably due to inhomogeneous sampling or underestimation of the contribution from non-diatom components by area analysis. In particular, the low $\delta^{30}Si$ of the 12-20μm fraction may be due to sponge spicules, which, because they are generally long and thin could carry a substantial volume of dense silica through a 20μm mesh. At this site the 2-12μm fraction is most representative of diatom $\delta^{30}Si$.

At TAN124 and TAN127 a large, radiolarian rich >50μm size fraction with low $\delta^{30}Si$ relative to the smaller, diatom rich size fractions is again observed (Figure 3.7), implying that radiolaria consistently form with a lower $\delta^{30}Si$ than diatoms at a similar location (Figure 3.10, Table 3.2). At both sites, the 2-5 and 5-8μm fractions have high $\delta^{30}Si$, and Figure 3.6 shows that they are the fractions with most pure diatom silica. By assuming the average $\delta^{30}Si$ of the 2-8μm size range is exclusively diatom, an appropriate upper size limit can be determined: The $\delta^{30}Si$ of the 8-12μm and 12-20μm size fractions at both sites is within error (internal or external) of the 2-8μm range, and so are considered to record diatom $\delta^{30}Si$. At both sites the 20-41μm fraction is outside this range, and so the 2-20μm fraction in this region, as for the Antarctic Peninsula, is considered the most representative of diatom $\delta^{30}Si$. Although the 41-50μm fraction at TAN124 is within error of the 2-20μm range, it will likely be subject to the previously discussed issues with sample heterogeneity and as such is best excluded.

For all NZ sites where a resolvable offset is observed, the 2-20μm fraction has a higher $\delta^{30}Si$ than the 20-63μm fraction, and is taken to record diatom $\delta^{30}Si$ (Figure 3.9, Appendix 1). The

magnitude of the offset between the two fractions at these sites is qualitatively related to the type and amount of non-diatom component present, but is again much greater than would be predicted from the area analysis (Figures 3.6e and 3.9, Appendix 1). The two sites with the greatest $\delta^{30}Si$ offset, NZ4 (offset = −1.22‰) and NZ5 (offset = −0.63‰) are the only two sites containing sponge spicules in the 20-63μm fraction (both 1% by area), with NZ4 having a larger radiolarian component (16%) than NZ5 (1%). This is consistent with the larger offset at NZ4, but the low levels of contamination would not be expected to produce an offset at all if the sample analysed had silicon ratios equivalent to the area analysis. Of NZ 6, 7 and 11, NZ7 has the largest radiolarian contribution to 20-63μm silica (9%) and is the only one of the three to show any offset.

The pattern of $\delta^{30}Si$ across size fractions from downcore analysis of 1090 is very similar to TAN124 and 127, which are located in a similar oceanographic setting north of the modern Polar Front (Figures 3.1 and 3.8), indicating that this relationship holds as far back as 36Ma. The $\delta^{30}Si$ of the 1090 20-41μm fractions is generally lower than that of the modern core tops, suggesting more influence from non-diatom silica. For these downcore samples the 2-20μm range is again the most appropriate for targeting diatom $\delta^{30}Si$.

For core top sediments analysed in this study, 2-20μm appears to be the size fraction most consistently representative of diatom $\delta^{30}Si$. However, the low $\delta^{30}Si$ of the 12-20μm fraction at 08A highlights the need to tailor size fraction selection to sediment composition. Another important observation is the extent to which very minor amounts of sponge and radiolarian silica can offset the $\delta^{30}Si$ of a sample that under the microscope appears to be almost entirely composed of diatom silica. The presence of non-diatom material down to a relatively small size is not a result of fragmentation of these components during microseparation (Appendix 2), and has previously been noted by Singer and Shemesh (1995) and Crosta and Shemesh (2002), who remove the >20μm fraction from their samples to avoid radiolarian contamination. Samples should be carefully examined and the appropriate size fractions selected prior to analysis to

ensure that measured $\delta^{30}Si$ represents robustly diatom $\delta^{30}Si$. An initial test of $\delta^{30}Si$ from a set of size fractions in representative downcore samples may be useful in such an assessment. Additionally, running two size fractions (e.g. the 2-10μm and 10-20μm) from the same sample at selected intervals will help to ensure measured $\delta^{30}Si$ consistently reflects diatom $\delta^{30}Si$ downcore.

Diatom species composition has been suggested as a factor that may influence $\delta^{30}Si$ (De La Rocha, 2006). The species composition of our size fractions is shown in Appendix 3. Size fractions in the 2-20μm range, with consistent $\delta^{30}Si$, contain different diatom assemblages, indicating that diatom vital effects are unlikely to affect $\delta^{30}Si$. However, because it was not possible to separate 100% species specific size fractions we cannot as yet draw any firm conclusions regarding this issue.

3.4.1.1 Implications for published $\delta^{30}Si$ records

The potential for common sedimentary components to bias measured $\delta^{30}Si$ away from diatom $\delta^{30}Si$ could lead to misrepresentation of palaeo-environmental changes. This is especially significant as geological studies tend to focus on climatic boundaries, when the abundance of taxa such as radiolaria and sponges relative to diatoms may change rapidly, as well as the ratio of biogenic to non biogenic components such as clay. Additionally, downcore, the preservation of biogenic opal may change significantly, and of particular relevance to the separation of diatoms from radiolarian/sponges, the degree of fragmentation may change, something that can complicate the separation of radiolarian and diatom silica.

Low $\delta^{30}Si$ is generally recorded at the Last Glacial Maximum (LGM; De La Rocha et al., 1998; Brzezinski et al., 2002). The LGM is frequently defined by a peak in relative abundance of the radiolarian *Cycladophora davisiana* (De La Rocha, 1998), raising the possibility of an increased glacial contribution from low $\delta^{30}Si$ radiolarian silica. Examples of negative offsets observed during glacial stages in published records are 1.5‰ (De La Rocha et al., 1998), 1.7‰ (Beucher et al., 2007) and 2‰ (Brzezinski et al., 2002) (Table 3.3), and would require 30-50% radiolarian

contribution to explain the entirety of the offset (calculated by taking diatom $\delta^{30}Si$ to be the most positive value observed in the records and offsetting this by −2‰ (Table 3.2) to give the radiolarian $\delta^{30}Si$). It seems unlikely that such levels of contamination are present in any of the published records, since authors are generally careful to eliminate non-diatom components. Although it is not always clear exactly what size fraction has been analysed, diatom $\delta^{30}Si$ studies generally follow methods such as those of Shemesh et al. (1988), Singer and Shemesh (1995), and Crosta and Shemesh (2002) which use the <20μm or <38μm fractions, and should exclude the majority of radiolarian or sponge silica.

Paper	Time Period	Maximum $\delta^{30}Si$ (Diatom) (‰)	Minimum $\delta^{30}Si$ (‰	Offset (‰)	Required Radiolarian Contamination (%)
De La Rocha *et al*. (1998)	LGM	1.5	0.8	0.7	35
Brzezinski *et at.* (2002)	0-300 Ka	2	1	1	50
Beucher *et al.* (2007)	LGM	1.7	1.1	0.6	30

Table 3.3 Mass balance calculations of the percentage radiolarian silica required to produce published palaeoceanographic offsets.

3.4.2 Diatom δ^{30}Si as a Proxy for Silicic Acid Utilisation

In section 3.4.1 the size range most representative of diatom δ^{30}Si was determined to be the 2-20μm (or 2-12μm for 08A) and in this section either the δ^{30}Si of this size fraction or the mass balanced δ^{30}Si from size fractions within this range will be referred to as core top diatom δ^{30}Si.

Core top diatom δ^{30}Si correlates well with both the annual average silicic acid concentration and the minimum annual silicic acid concentration at each site (Figure 3.9, $R^2 = 0.82$ and 0.92 respectively). The silicic acid concentrations were estimated from the nearest grid point to the core site in the World Ocean Atlas 2005. The poorer correlation between silicic acid concentration and the 20-50/20-41/20-63μm (depending which was measured at each site) δ^{30}Si (Figure 3.9, $R^2 = 0.55$ or 0.66) confirms that this fraction should be excluded from silica analysed in studies targeting silicic acid utilisation. Figure 3.9b shows a particularly robust relationship between core top diatom δ^{30}Si and the minimum surface water silicic acid concentration when the correct size fraction of sedimentary silica is analysed, validating the use of diatom δ^{30}Si as a proxy for silicic acid utilisation and highlighting the need for careful size fraction selection. Core top δ^{30}Si is remarkably consistent with mixed layer filtered diatom δ^{30}Si from the equivalent sector of the Southern Ocean (Figure 3.11), indicating that surface diatom δ^{30}Si is faithfully recorded in the sediments, with minimal effect of either dissolution, which should act to increase the δ^{30}Si of the diatom opal (Demarest et al., 2009), or of early diagenesis. Minimal effect of dissolution is consistent with sediment trap δ^{30}Si and filtered diatom δ^{30}Si-depth profiles, which have found no evidence for δ^{30}Si modification during sinking (Varela et al., 2004; Cardinal et al., 2007; Fripiat et al., 2011a). This is again supportive of the qualitative use of diatom δ^{30}Si as a proxy for silicic acid utilisation. It should be noted that as we plot our core top data against minimum silicic acid concentration, they are less comparable to the spring data measured in the

Pacific by Cardinal et al. (2005), and the spring data included in Varela et al. (2004). This likely explains why a portion of these filtered data are offset somewhat from the core top δ^{30}Si data.

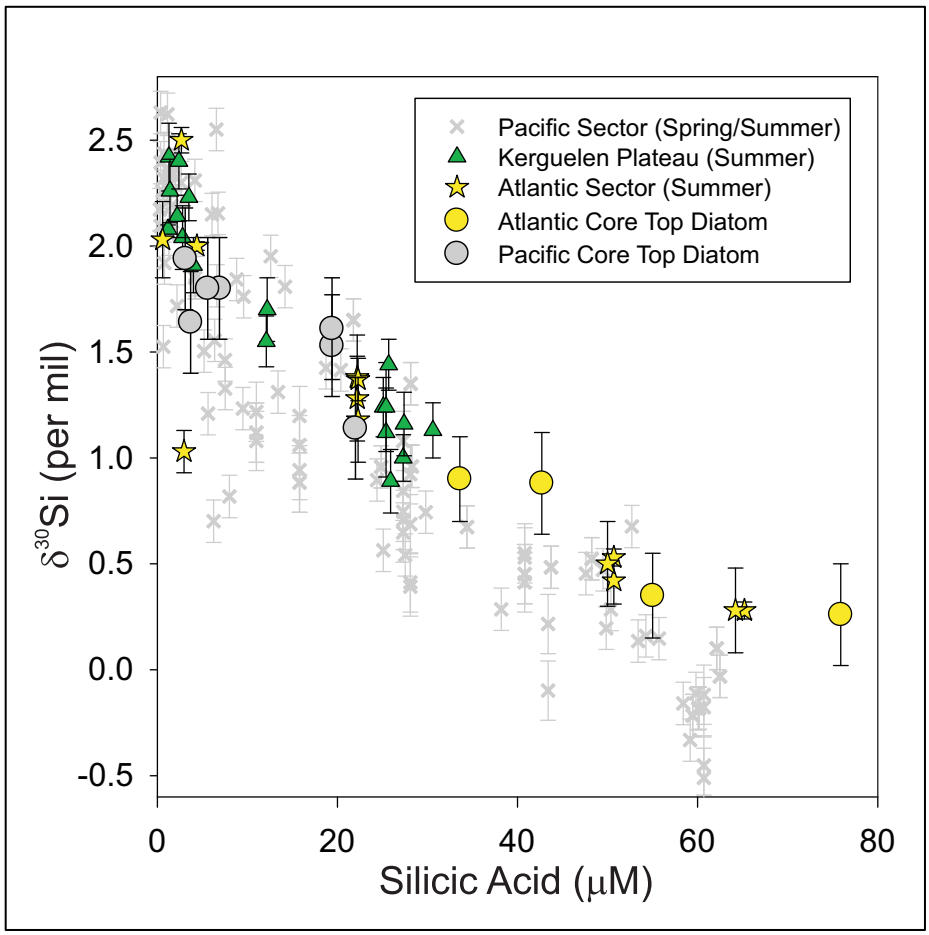


Figure 3.11 Core top diatom δ^{30}Si (2-20μm or 2-12μm) compared to filtered diatom δ^{30}Si collected during in situ studies from the top 100m of the water column (Varela et al., 2004; Cardinal et al., 2007; Fripiat et al., 2011a). Core top diatom δ^{30}Si is plotted against minimum annual silicic acid concentration, and the filtered δ^{30}Si against the silicic acid concentration measured at the time of sampling. Core top diatom δ^{30}Si and filtered diatom δ^{30}Si are remarkably consistent, especially when they are from the same ocean basin.

However, there are still some important considerations that should be taken into account when interpreting diatom δ^{30}Si records. Firstly, there is a significantly better correlation ($p>0.95$) between core top diatom δ^{30}Si and minimum silicic acid concentration (Figure 3.9b) compared to the mean annual silicic acid concentration (Figure 3.9a; $R^2 = 0.92, 0.82$ respectively). The

significance of the difference in goodness-of-fit between the minimum and mean annual models was estimated using a bootstrapping method which accounts for the error bars on the $\delta^{30}Si$ measurements (bootstrapping analysis was carried out by Jorn Bruggeman). Unfortunately, I have been unable to obtain good error estimates for the silicic acid concentrations from the World Ocean Atlas (2005), which has precluded these being taken into account when testing this significance. This difficulty stems from two main issues. Firstly, the World Ocean Atlas is a gridded field, meaning that for a number of our core top locations, the silicic acid estimates are based on 1 or fewer actual measurements. Secondly, the error bars which are quoted in the World Ocean Atlas are determined not only by the actual variation in silicic acid on an annual basis, but by both the number of measurements and, for the mean annual estimates, the seasonality of a given location, making their inclusion rather uninformative. Nevertheless, the better correlation between minimum silicic acid concentration and 2-20μm diatom $\delta^{30}Si$ suggests that sedimentary diatom $\delta^{30}Si$ documents seasonal diatom silicic acid utilisation. This could be explained by sedimentary diatom $\delta^{30}Si$ recording silicic acid utilisation only at the time when diatoms are growing (e.g. during summer stratification in the Southern Ocean, when silicic acid is driven to a minimum and $\delta^{30}Si$ to high values; Varela et al., 2004; Fripiat et al., 2011c), whereas average annual silicic acid concentration may include large portions of the year when diatom production is minimal and surface silicic acid concentration is high (e.g. during winter mixing), and so will be biased towards higher silicic acid concentrations. The extent to which the annual silicic acid concentration is offset from the minimum will be dependent on the degree of seasonality at a given location, creating the observed variation in the R^2. At sites such as 383 and 385, the minimum silicic acid concentration is much lower than the annual average indicating there is a seasonal nature to diatom driven silicic acid drawdown (Table 3.1). In contrast, at core top locations where production is either more continuous throughout the year (e.g. near TAN127/124; Sigmon et al., 2002) or where the extent of seasonal drawdown is very small (e.g. 391; Clarke et al., 2008), the annual silicic acid concentration is more similar to the minimum (Table 3.1). That the seasonal maximum of silicic acid utilisation is being recorded in

sedimentary diatom $\delta^{30}Si$ is an important point to acknowledge when interpreting downcore records, since the season of diatom productivity may be as little as only 3 months in some regions south of the Polar Front (Sigmon et al., 2002). If diatom $\delta^{30}Si$ records are produced from cores located in regions where silicic acid uptake is highly seasonal or if seasonality changes through time, changes in silicic acid utilisation recorded by diatom $\delta^{30}Si$ may exaggerate the change in silicic acid concentration of the wider, annually integrated surface ocean. This is also something that should be kept in mind when interpolating results between cores located in different oceanic regimes.

Secondly, the reliability of quantitative silicic acid reconstructions from diatom $\delta^{30}Si$ pivots on the assumption that simple Rayleigh or steady state models, with a single silicic acid concentration/$\delta^{30}Si$ source term and a consistent diatom fractionation factor are sufficient to describe the Southern Ocean $\delta^{30}Si$ distribution. This would appear not to be the case for our core top data.

Rayleigh Fractionation is characterised by the following equations;

$$\delta^{30}Si(OH)_4 = \delta^{30}Si(OH)_{4\ initial} + {}^{30}\varepsilon \ln f \quad \text{(eq.1)}$$

$$\delta^{30}Si\text{-}bSiO_2 = \delta^{30}Si(OH)_4 + {}^{30}\varepsilon \quad \text{(eq.2)}$$

$$\delta^{30}Si\text{-}bSiO_{2\ acc} = \delta^{30}Si(OH)_{4\ initial} - {}^{30}\varepsilon \left(f \ln f / 1-f\right) \quad \text{(eq.3)}$$

Where $Si(OH)_4$ is silicic acid, $Si(OH)_{4\ initial}$ is initial silicic acid, $bSiO_2$ is diatom silica, $bSiO_{2\ acc}$ is accumulated diatom silica, and *f* is the fraction of silicic acid remaining in the surface ocean. In this model, sedimentary diatom silica should reflect the accumulated diatom $\delta^{30}Si$ (eq.3).

For the steady state model:

$$\delta^{30}Si(OH)_4 = \delta^{30}Si(OH)_{4\ initial} - {}^{30}\varepsilon\ (1-f) \quad \text{(eq.4)}$$

$$\delta^{30}Si\text{-}bSiO_2 = \delta^{30}Si(OH)_{4\ initial} + {}^{30}\varepsilon\ f \quad \text{(eq.5)}$$

In order to test how well core top diatom $\delta^{30}Si$ fits these models, an estimate of the initial conditions from which fractionation occurs must be made. Upper Circumpolar Deepwater (UCDW) is probably the most ubiquitous ultimate source of silicic acid to the mixed layer, either by upwelling or Ekman Transport, over the latitudinal range of our Southern Ocean core tops (Whitworth et al., 1994; Pollard et al., 2002; Clarke et al., 2008; Fripiat et al., 2011b; with the exception of 08A where Lower Circumpolar Deepwater and Antarctic shelf water are more likely to control silicic acid supply; Whitworth et al., 1994). We have therefore used two different estimates of the silicic acid concentration/$\delta^{30}Si$ signature of UCDW (Cardinal et al., 2004; Fripiat et al., 2011b) to represent initial conditions (Figure 3.12a). The expected Rayleigh and steady state $\delta^{30}Si$ evolution from UCDW were calculated assuming a fractionation factor of –1.1‰ (De La Rocha et al., 1997), and are shown compared to our core top diatom $\delta^{30}Si$ in Figure 3.12a. Values of ${}^{30}\varepsilon$ and initial silicic acid $\delta^{30}Si$ were also calculated (Table 3.4) from the gradient and intercept of the linear regression of core top diatom $\delta^{30}Si$ against either *f* or $(f*\ln f)/(1-f)$ for steady state and Rayleigh accumulated opal respectively (Equations 3 and 5). *f* was set as the minimum

silicic acid concentration at each site divided by the UCDW concentration. Quoted errors for $^{30}\varepsilon$ and $\delta^{30}Si(OH)_{4\ initial}$ are ±1SE on the gradient and intercept of the regression line respectively.

Data set	Fractionation Factor ε (‰)	Initial Silicic Acid $\delta^{30}Si(OH)_{4\ initial}$ (‰)	R^2
2-20(12)µm Core Top UCDW Fripiat et al., 2011b	-1.9±0.2(Steady State) -1.8±0.2 (Rayleigh)	2.0±0.1(Steady State) 2.2±0.1 (Rayleigh)	0.92 0.88
2-20(12)µm Core Top UCDW Cardinal et al., 2005	-2.2±0.2 (Steady State) -2.1±0.2 (Rayleigh)	1.9±0.1(Steady State) 2.2±0.1 (Rayleigh)	0.92 0.92
Top 100m Silicic Acid Compilation (Frip UCDW)	-0.9±0.1 (Steady State)	1.6±0.05 (Steady State)	0.48
Top 100m Silicic Acid Compilation (Card UCDW)	-1.1±0.1 (Steady State)	1.4±0.05 (Steady State)	0.47
Mixed Layer Filtered Diatoms (Frip UCDW)	-2.5±0.1 (Steady State)	2.0±0.05 (Steady State)	0.82
Mixed Layer Filtered Diatoms (Card UCDW)	-3.2±0.1 (Steady State)	2.0±0.05 (Steady State)	0.82

Table 3.4 Estimated ε and $\delta^{30}Si(OH)_{4\ initial}$.

Estimates of $^{30}\varepsilon$ from our core top diatom $\delta^{30}Si$ vs. minimum silicic acid concentration are between −1.9±0.2‰ and −2.2±0.2‰ (both models are in agreement, Table 3.4). The gradient of the core top $\delta^{30}Si$ is therefore too large to be compatible with a fractionation factor of –1.1‰ using these simple models, explaining the lack of coherence with any of the model fractionations illustrated in Figure 3.12a. This is highlighted by the high estimates of $\delta^{30}Si(OH)_{4\ initial}$ from the core top diatom $\delta^{30}Si$ (Table 3.4). In situ studies have also observed a steeper than expected increase in surface filtered diatom $\delta^{30}Si$ with silicic acid concentration when using $^{30}\varepsilon$ = –1.1‰ and simple single source models (Varela et al., 2004; Cardinal et al., 2007; Fripiat et al., 2011a). Varela et al. (2004) estimate $^{30}\varepsilon$ to be −2.1±0.2‰ for filtered biogenic silica, using a steady state model starting from 65µM, which is remarkably consistent with our estimate from the core top data. Taking all the Southern Ocean mixed layer filtered diatom $\delta^{30}Si$ data published to date, and using either UCDW estimate as a starting point, the steady state model yields $^{30}\varepsilon$ = −2.5±0.1‰ or

−3.2±0.1‰ (Table 3.4), which is again very high. On the contrary $^{30}\varepsilon$ estimates made in the same way assuming the single source steady state model and published silicic acid $\delta^{30}Si$ from the Southern Ocean mixed layer are −0.9±0.1‰ or −1.1±0.1‰. This is very similar to the compiled Antarctic Circumpolar Current $^{30}\varepsilon$ estimate of −1.2 ±0.2‰ from Fripiat et al. (2011c), despite the fact that this estimate includes studies which considered fractionation from a variable source targeted at the specific location being considered (Cardinal et al., 2007; Fripiat et al., 2011c). The large difference in $^{30}\varepsilon$ estimates from core top diatom $\delta^{30}Si$ and silicic acid $\delta^{30}Si$ leads to an increase in the apparent fractionation factor (offset between $\delta^{30}Si$ of silicic acid and of core top/filtered diatoms) with increasing latitude (silicic acid concentration) (Varela et al., 2004; Cardinal et al., 2007; Fripiat et al., 2011a) which can be clearly seen in Figure 3.12. Such observations demonstrate that the simple fractionation models cannot account for the $\delta^{30}Si$ distribution recorded in Southern Ocean sediments.

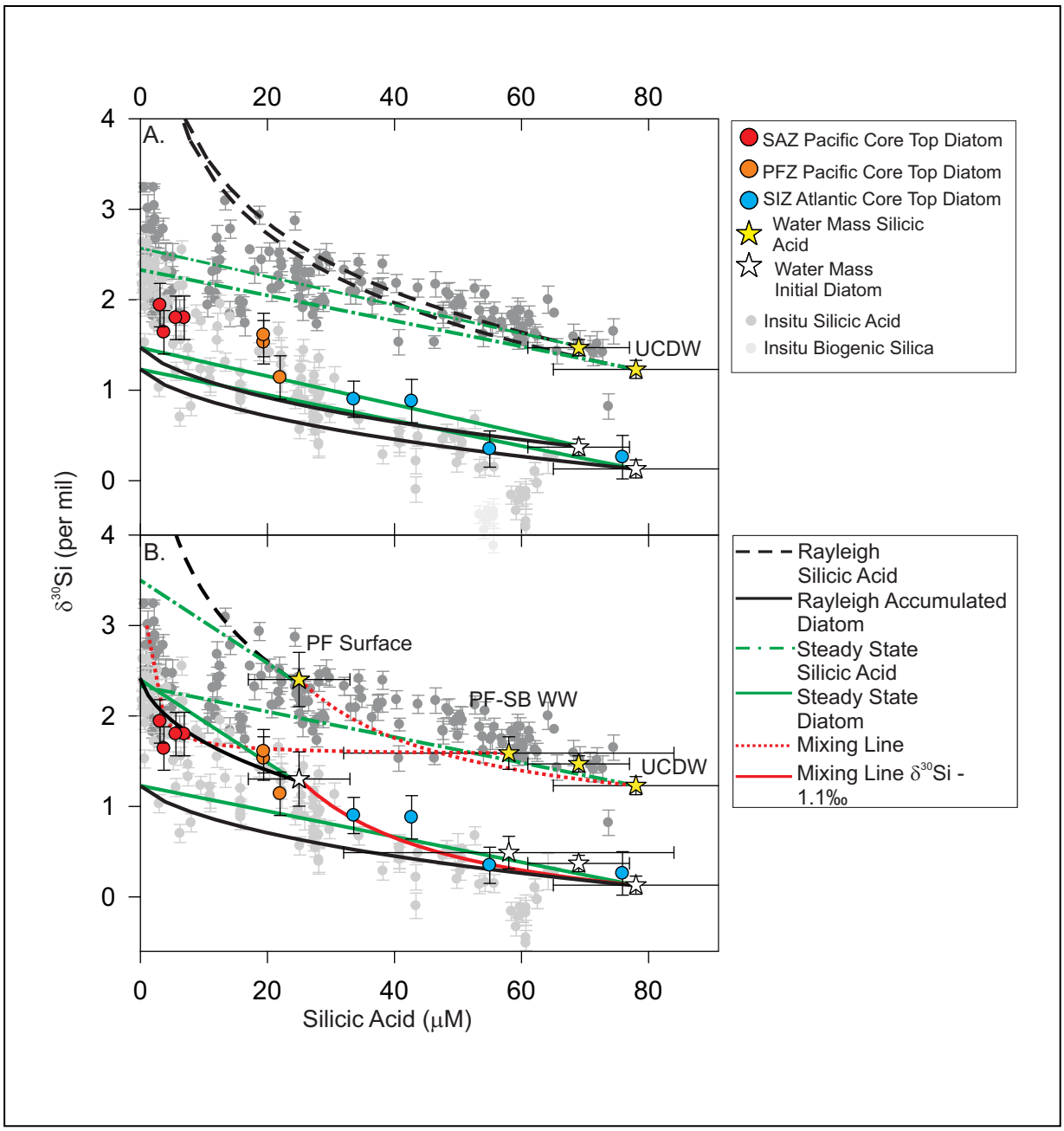

A.
B.
UCDW
PF Surface
PF-SB WW
UCDW
δ30Si (per mil)
Silicic Acid (μM)
SAZ Pacific Core Top Diatom
PFZ Pacific Core Top Diatom
SIZ Atlantic Core Top Diatom
Water Mass Silicic Acid
Water Mass Initial Diatom
Insitu Silicic Acid
Insitu Biogenic Silica
Rayleigh Silicic Acid
Rayleigh Accumulated Diatom
Steady State Silicic Acid
Steady State Diatom
Mixing Line
Mixing Line δ30Si - 1.1‰

Figure 3.12 Core top diatom $\delta^{30}Si$ (coloured circles), shown with filtered diatom $\delta^{30}Si$ and silicic acid $\delta^{30}Si$ measured during in situ studies of the Southern Ocean (top 100m of the water column, grey circles; Varela et al., 2004; Cardinal et al., 2005; Cardinal et al., 2007; Fripiat et al., 2011a; Fripiat et al., 2011b; Fripiat et al., 2011c and De La Rocha et al., 2011); **a.** With Rayleigh and steady state $\delta^{30}Si$ evolution of silicic acid and diatom silica (accumulated product for the Rayleigh model), assuming a fractionation factor of −1.1‰ and taking the silicic acid concentration and $\delta^{30}Si$ of Upper Circumpolar Deep Water (UCDW) as initial conditions. Two estimates for UCDW composition were considered; these encompass the range of values quoted for this water mass in the literature: UCDW (Pacific) = 78±13µM, 1.23±0.13‰ (In Fripiat et al., 2011b, from the data of Cardinal et al., 2005) and UCDW (Atlantic) = 69±8µM, 1.47±0.37‰ (Fripiat et al., 2011b; error bars as quoted in Fripiat et al., 2011b). Neither model can explain the range of $\delta^{30}Si$ observed in our core top data, particularly at sites north of the Polar Front with silicic acid concentrations of <20µM; **b.** Rayleigh and steady state evolutions, but in this case with initial conditions taken as either the Pacific UCDW composition, or an estimate of the Pacific Polar Front surface water composition (25±8µM, 2.4±0.3‰; PF-Surface; calculated using data from 60-63˚S in Varela et al., 2004, error bars are 1σSD, n = 16). The mixing line between these two end members (red dashed line between UCDW and PF-surface stars) can be taken to represent the source waters from which diatom silicification occurs in the Southern Ocean. Rayleigh or steady state fractionation curves from anywhere on this mixing line will plot between those shown for UCDW and PF surface. These fractionation lines satisfactorily explain the variation in $\delta^{30}Si$ of our core tops, and the majority of the filtered diatom $\delta^{30}Si$. Also plotted is a mixing line between the Pacific Winter Water (averaged between the Polar Front and the Southern Boundary of the Antarctic Circumpolar Current; PF-SB WW; Fripiat et al., 2011b; Cardinal et al., 2005, error bars as quoted in Fripiat et al., 2011b), and an evolved composition from north of the Polar Front (1µM, 3‰, based on the estimate of Fripiat et al. (2011b); no data are available for summer conditions north of the Polar Front in the Pacific). This fractionation and mixing can account for the low apparent fractionation factor at low silicic acid concentrations. It should be noted that these mixing lines would not look significantly different using Atlantic end member estimates, but since the majority of our core tops are located in the Pacific, we have chosen to use the Pacific end members.

Two main hypotheses on the cause of such deviations from the idealised models can be considered. Firstly, the assumption of a single source is likely to be wrong, given the significant mixing that occurs both vertically and horizontally in the Southern Ocean mixed layer from which diatoms produce their silica (Cardinal et al., 2005; Cardinal et al., 2007; Fripiat et al., 2011b). Secondly, the assumption of a constant fractionation factor with latitude may be incorrect (Varela et al., 2004; Cardinal et al., 2007; Hendry and Robinson, 2012). Although a change in the diatom fractionation factor with latitude cannot be ruled out, it can be demonstrated that when the effects of water mass mixing are taken into account, variation in the core top diatom $\delta^{30}Si$ can be satisfactorily explained using a constant fractionation factor of approximately −1.1‰ (Figure 3.12b). Fripiat et al. (2011a) have shown that in the Atlantic Sector of the Southern Ocean, the sub-surface (Winter Water) silicic acid concentration and $\delta^{30}Si$ plot on a mixing line between the characteristic signatures of UCDW and the seasonally depleted mixed layer. This Winter Water may be considered the starting point for diatom silicon isotope fractionation over large areas of the Southern Ocean (Cardinal et al., 2005, Fripiat et al., 2011a; De La Rocha et al., 2011). Simplistically, a mixing line of this type, for example between Pacific UCDW and the Polar Front surface ocean (Figure 3.12b), can be taken to represent the possible range of silicic acid concentration and $\delta^{30}Si$ which may be present at the beginning of seasonal diatom production (this line would not appear significantly different using Atlantic end member estimates from Fripiat et al., 2011a). Steady state or Rayleigh fractionation models can then be used to calculated the evolution of silicic acid and diatom $\delta^{30}Si$ from anywhere on this spectrum of initial conditions (following Cardinal et al., 2005 and Fripiat et al., 2011a). Any such fractionation will plot somewhere between the fractionation lines from UCDW and the Polar Front surface water silicic acid which are illustrated in Figure 3.12b. The core top diatom $\delta^{30}Si$ data are compatible with such a model (i.e. fractionation, either Rayleigh or steady state, from an initial water mass composition described by mixing between UCDW and surface waters at the Polar Front) of Southern Ocean silicon isotope distributions (Figure 3.12b), which also describes much of the variation in surface water silicic acid and filtered diatom $\delta^{30}Si$ from in situ studies (with the

exception of some very low filtered diatom $\delta^{30}Si$ values at high silicic acid concentration in the Pacific). In particular, this description of the system can provide an explanation for the relatively high core top diatom $\delta^{30}Si$ at silicic acid concentrations <20μM (Figure 3.12b). The fit between this mixing model and the core top diatom $\delta^{30}Si$ is in good agreement with Fripiat et al. (2011a). Their modelling of seasonal mixed layer $\delta^{30}Si$ evolution at the Polar Front shows that biogenic silica exported from the mixed layer can be satisfactorily replicated by a Rayleigh accumulated product. As demonstrated by Fripiat et al. (2011a), the unexpectedly low $\delta^{30}Si$ of the surface water silicic acid at low silicic acid concentrations, which also contributes to the low apparent fractionation factor, can be explained by mixing of an evolved water mass having very low silicic acid concentration and high $\delta^{30}Si$ (driven by diatom production), with subsurface waters sourced from the Polar Front having higher silicic acid concentration and lower $\delta^{30}Si$. This is illustrated on Figure 3.12b by a mixing line between the Pacific Winter Water (averaged between the Polar Front and the Southern Boundary of the ACC in Fripiat et al. (2011b), from the data of Cardinal et al. (2005)) and a hypothetical mixed layer from north of the Polar Front (1μM, 3‰, based on the estimate of Fripiat et al. (2011b); no data are available for summer conditions north of the Polar Front in the Pacific). Such a mixing line is a good example of how the relationship between physical mixing and biological uptake might control the $\delta^{30}Si$ distribution in the surface waters of the Southern Ocean.

Since dissolution acts to increase the $\delta^{30}Si$ of diatom silica (Demarest et al., 2009), it could provide an alternative explanation for the relatively high $\delta^{30}Si$, and the small apparent fractionation factor, at core top locations with silicic acid <20μM. However, good agreement between our core top diatom $\delta^{30}Si$ and mixed layer filtered diatom $\delta^{30}Si$, and the preservation of surface diatom $\delta^{30}Si$ signatures in both deep sediment traps (Varela et al., 2004) and through depth profiles of filtered diatoms (Cardinal et al., 2007; Fripiat et al., 2011a) all argue against dissolution as the driver of these relatively high values. Additionally, the modelling results of

(Fripiat et al., 2011a) indicate that there should be no significant effect of dissolution on the $\delta^{30}Si$ of accumulated diatom silica.

Reconstruction of surface water silicic acid concentrations from diatom $\delta^{30}Si$ does appear to be robust (Figure 3.9). However, any attempt to fully quantify changes in the degree of silicic acid utilisation will be subject to major uncertainties regarding the initial surface water mass composition and mixing regime. A particularly optimistic note from this study is that the diatom $\delta^{30}Si$ signal appears unaltered by dissolution over million year timescales (Figure 3.8).

3.5 Conclusions

A consistent size-$\delta^{30}Si$ pattern, related to the proportions of diatom and non-diatom components in a sample, has been demonstrated. This study highlights the great potential for small amounts of non-diatom silica to significantly offset measured $\delta^{30}Si$ to lower values than diatom $\delta^{30}Si$. In order to create reliable downcore records of diatom $\delta^{30}Si$, it is essential to eliminate such contamination by selecting the correct size fraction for analysis. In general the 2-20μm fraction has been found most appropriate for core tops in this study, although this is not a hard and fast rule, and rather must be tailored to the sediment composition of each sample set.

When a pure diatom size fraction is selected, an extremely good correlation with surface water minimum annual silicic acid concentration is documented (R^2=0.92). In comparison, larger size fractions (~20-50μm) exhibit a poorer correlation (R^2=0.66), again emphasising the need for size targeted analyses.

Correlation with surface silicic acid concentration, and a good agreement between core top diatom $\delta^{30}Si$ and surface filtered diatom $\delta^{30}Si$, are highly supportive of the use of sedimentary diatom $\delta^{30}Si$ as a proxy for surface water silicic acid utilisation and indicate no significant effect of dissolution or early diagenesis. The better correlation with minimum annual silicic acid

reflects the fact that diatom $\delta^{30}Si$ records the seasonal extent of silicic acid utilisation by diatoms, which should be kept in mind when interpreting diatom $\delta^{30}Si$ records.

Core top diatom $\delta^{30}Si$ can be satisfactorily explained using steady state or Rayleigh fractionation without the need to invoke a variable diatom fractionation factor, as long as changes in the silicic acid concentration and $\delta^{30}Si$ from which diatom uptake occurs are properly accounted for i.e. it is not possible to model the entire Southern Ocean with a single set of initial conditions. This represents a major source of error in quantitative silicic acid utilisation reconstructions. However, it should not detract from the strong relationship that exists between sedimentary diatom $\delta^{30}Si$ and surface water silicic acid concentration, proving this to be a reliable qualitative proxy for silicic acid utilisation.

Acknowledgements. Many thanks to Nick Belshaw and Bastian Georg for their help with silicon isotope analysis, to Jenny Pike for her training in diatom identification, to Jorn Bruggeman for his statistical analyses, and to George Swann and Fatima Mokadem for their help with lab protocols/setup. Thanks to the Ocean Drilling Program for supplying downcore samples from site 177-1090. The Oxford isotope geochemistry lab is supported by an ERC grant to Halliday. This work was carried out as part of Natural Environmental Research Council (NERC) grant NE/F005296/1, and Antarctic Peninsula core tops collected thanks to the Antarctic Funding Initiative grant AFI4-02.

Chapter 4. Late Eocene CO_2 drawdown coincident with evolution of the Southern Ocean silicon cycle

Abstract

The abrupt onset of Antarctic glaciation ~34 Ma ago has been linked to a decline in atmospheric pCO_2 levels below a critical threshold. Oxygen isotope records document rapid growth of Antarctic ice sheets superimposed on a more gradual long term cooling trend that began around 50 Ma ago. Despite the obvious importance of understanding this non-linear climate shift, the mechanisms that forced pCO_2 decline remain somewhat elusive. The biogenic silicon cycle is inextricably linked to the ocean-atmospheric pCO_2 balance through diatom primary production, especially in the Southern Ocean. The silicon isotope composition ($\delta^{30}Si$) preserved in diatom and sponge opal provides a window to the Eocene-Oligocene silicon cycle. Novel combination of these proxies from two sites in the Southern Atlantic Ocean (ODP 689 and 1090) demonstrates major reorganisation of silicon cycling during the Late Eocene and Early Oligocene. Sponge $\delta^{30}Si$ documents increasing silicic acid concentration at intermediate depths in the Antarctic Zone of the Southern Ocean, which is attributable to an intensification of upwelling resulting from the initiation and maturation of a circum-Antarctic current. The late Eocene also saw a major radiation of diatoms, documented by rising diatom $\delta^{30}Si$ and the onset of Southern Ocean opal deposition. Together, changing circulation and diatom proliferation facilitated the gradual development of a Southern Ocean silicic acid gradient, with a modern-type configuration established by ~31.5 Ma, coincident with the completion of a circum-Polar deepwater connection. These changes in the silicon cycle are accompanied by evidence for increasing primary productivity and organic carbon deposition in the high southern latitudes. Here, it is

suggest that radiation of the diatoms, coupled with tectonically driven changes in Southern Ocean circulation, may have triggered organic carbon burial, contributing to pCO_2 drawdown which triggered the onset of Antarctic glaciation.

4.1 Introduction

The Eocene-Oligocene Transition marks the onset of modern icehouse conditions as continental scale ice sheets enveloped Antarctica (the 'Oi1 event') (Ehrmann and Mackensen, 1992; Robert et al., 2002; Coxall et al., 2005). The nature of the Oi-1 glaciation is of particular interest as rapid ice expansion punctuated a more gradual cooling trend initiated subsequently to the Early Eocene Climatic Optimum (Zachos et al., 2001; Lear et al., 2008; Cramer et al., 2009; Bohaty et al., 2012). Declining pCO_2 levels are the most likely driver for the accelerated onset of Southern Hemisphere glaciation. Models have demonstrated that when a certain threshold concentration of atmospheric pCO_2 is crossed, ice sheet mass balance feedbacks prevail and Antarctic ice expands rapidly (DeConto and Pollard, 2003). This view has been to some extent corroborated by recent pCO_2 reconstructions across the Eocene-Oligocene boundary, which document a decline beginning prior to glaciation itself (Pagani et al., 2011). However, it is still not clear what mechanisms were responsible for the lowering of pCO_2. I consider the hypothesis that radiation of the diatoms, coupled with tectonically driven changes in Southern Ocean circulation, are likely to have played a role by facilitating increased organic carbon burial.

In the modern Southern Ocean, the relationship between diatom productivity and overturning circulation associated with the Antarctic Circumpolar Current (ACC) exerts a significant control over both the efficiency of the biological carbon pump and the air-sea pCO_2 balance (Sarmiento et al., 2004; Marinov et al., 2006). In the Southern Ocean, nutrients and CO_2 are upwelled from the abyssal ocean as deepwater shoals south of the Polar Front (PF, Figure 4.1; Speer et al.,

2000). A portion of this upwelled water moves southwards, where limited primary productivity allows venting of CO_2 to the atmosphere (Marinov et al., 2006), and the subsequent formation of nutrient rich Antarctic Bottom Water (AABW). As diatoms are a major component of the phytoplankton in this region (Nelson et al., 1995), the balance between the rate of upwelling and diatom primary production is important in determining the magnitude of pCO_2 release to the atmosphere (Ragueneau et al., 2000). A second portion of the upwelled water moves northwards via Ekman transport, eventually finding its way into the Antarctic Intermediate and Sub-Antarctic Mode Waters (AAIW and SAMW, Figure 4.1; Speer et al., 2000). These water masses subduct at the northern edge of the ACC and feed nutrients to a large portion of the lower latitude thermocline (Sarmiento et al., 2004). Diatom production that occurs during Ekman transport not only contributes to a marked band of carbon export (Ito. 2005), but also strips silica from the surface ocean to a much greater extent than nitrate (Sarmiento et al., 2004). This is due both to the deep regeneration depth of biogenic silica (de Souza et al., 2012), and to the unusually high uptake ratio of Si:N by Southern Ocean diatoms (Brzezinski et al., 2003; Baines et al., 2010). The waters that are exported to the lower latitudes are therefore enriched in nitrate with respect to silicic acid, and these waters support up to 75% of primary productivity north of 30˚S (Sarmiento et al., 2004). Silicic acid is effectively trapped in the Antarctic 'ring,' creating a narrow band of opal deposition and a strong north-south silicic acid gradient in the surface ocean.

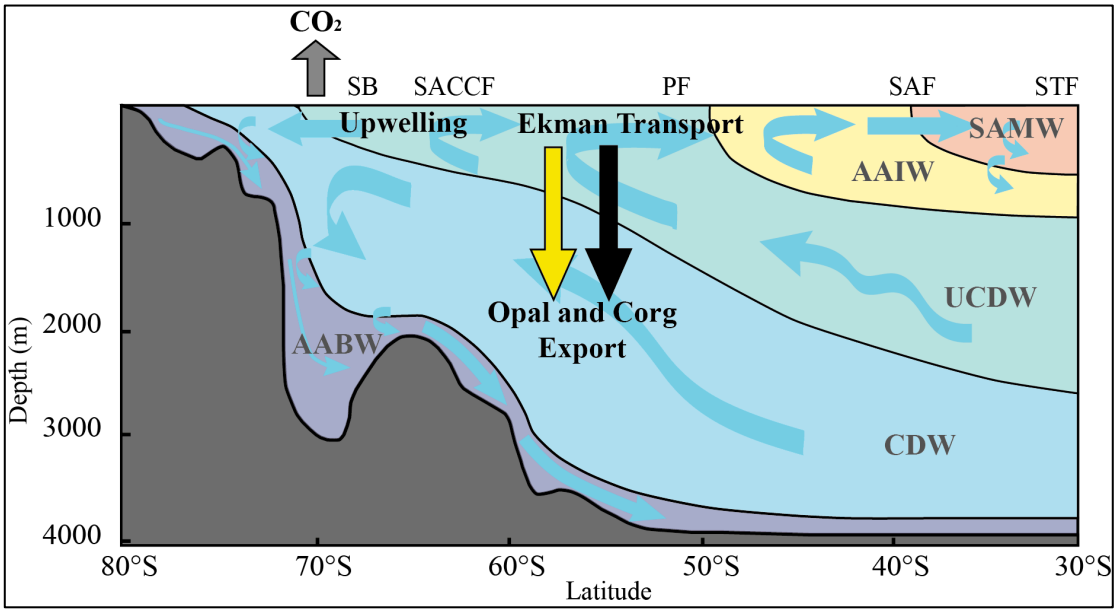


Figure 4.1 Schematic of Southern Ocean overturning circulation (modified from Speer et al., 2000) and its relationship with diatoms, the biological pump, and atmospheric pCO_2. Upwelling to the south of the Polar Front (PF), driven by the Antarctic Circumpolar Current (ACC) supplies nutrient, CO_2 rich water to the surface. A portion of this water moves northwards via Ekman transport, where nutrients are utilised by phytoplankton. Diatoms dominate production in the southern ACC, driving a marked belt of opal export and deposition (Yellow arrow, location based on Atlantic sector opal export in the model of Ito et al., 2005), whilst a combination of diatoms and smaller phytoplankton contribute to a broader belt of carbon export who's locus lies a few degrees northward (Black arrow, again based on Ito et al., 2005). A second portion of upwelled water moves southwards and eventually forms Antarctic Bottom Water (AABW). Along this pathway, limited primary production allows carbon dioxide venting to the atmosphere (Marinov et al., 2006). CDW = circumpolar deepwater; UCDW = upper circumpolar deepwater; AAIW = Antarctic intermediate water; SAMW = sub-Antarctic mode water; SB = southern boundary of the ACC; SACCF = southern ACC front; PF = Polar front; SAF = sub-Antarctic front; STF = sub-tropical front.

The ACC, which is a key component of this system, exists due to the complete zonal pathway present in the Southern Ocean. The subsidence of the two major Southern Ocean gateways, the Drake Passage and the Tasman gateway, occurred gradually through the Late Eocene and into the Oligocene (Stickley et al., 2004; Mackensen, 2004; Livermore et al., 2007). From the time when these gateways opened, even to a relatively shallow depth, a complete pathway for wind driven currents would have begun to effect Southern Ocean circulation, gradually intensifying upwelling

as subsidence progressed (Livermore et al., 2007; Sijp et al., 2011). Thus, the Late Eocene is likely to have witnessed the initiation and development of Southern Ocean circulation patterns that would eventually form the ACC. The late Eocene is also thought to have witnessed the proliferation of diatoms (Figures 4.2 and 4.3), with both dramatic species diversification (Rabosky and Sorhannus, 2009; Falkowski et al., 2004) and the rise of Southern Ocean biogenic opal burial (Diester-Haass, 1991; Salamy and Zachos, 1999; Schumacher and Lazarus, 2004; Diekmann et al., 2004; Lazarus et al., 2008). The development of an ACC-type circulation coupled with diatom radiation may have substantially increased the efficiency of the biological pump, facilitating organic carbon burial and contributing to the atmospheric CO_2 drawdown hypothesised to have driven Antarctic Glaciation (Scher and Martin, 2006; Rabosky and Sorhannus, 2009).

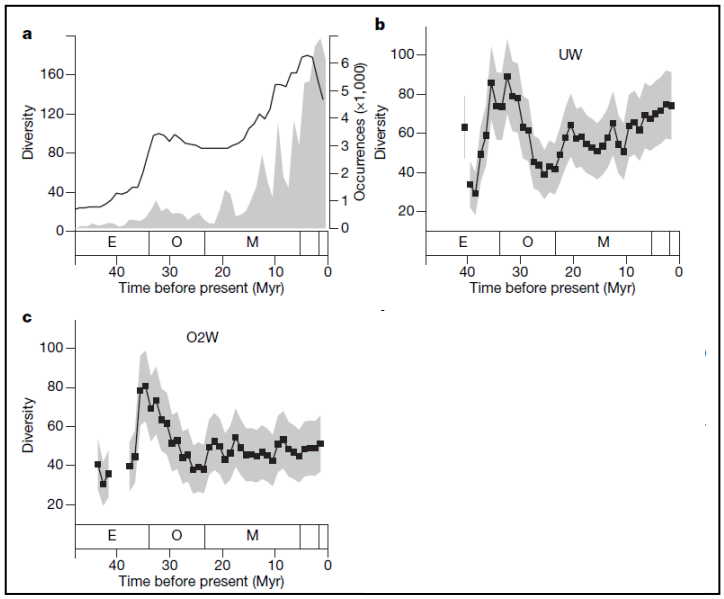


Figure 4.2 Diatom diversity curves from Rabosky and Sorhannus (2009); **a.**Traditional, non-standardized diatom diversity curves and; **b-c.** sampling-standardised diatom diversity curves accounting for the increasing availability of records with time. Estimates based on the Neptune Database. Regardless of the method of sampling used, a robust result of these curves is the dramatic increase in diatom diversity during the Late Eocene

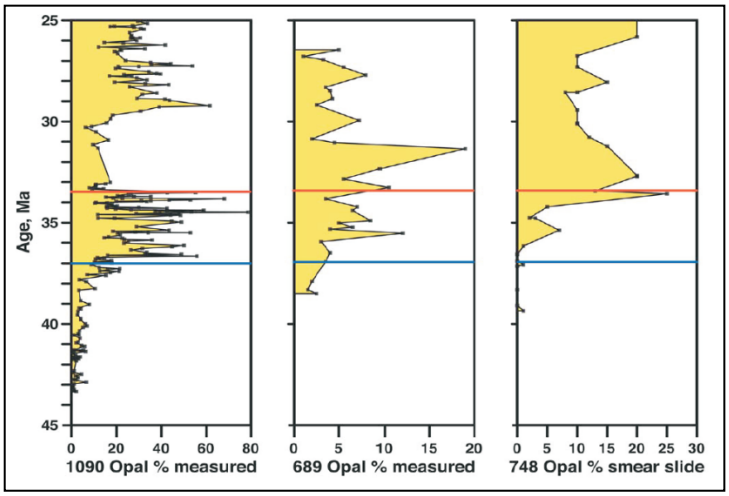


Figure 4.3 Opal abundance through the Eocene-Oligocene for three Southern Ocean sections. Data were replotted from Diekmann et al. (2004) (Site 1090) and Schumacher and Lazarus (2004) (Sites 689 and 748) by Lazarus et al. (2008). Lines at 37 Ma and 33.7 Ma are the beginning of the Late Eocene and the Eocene-Oligocene Boundary, respectively.

Deciphering the role of Southern Ocean diatom expansion in Eocene - Oligocene climatic change hinges on justifying the translation of Late Eocene diatom diversification and opal deposition into diatom expansion, and on establishing that there is a valid relationship with the carbon cycle. To this end I have used the novel combination of two silica based proxies, diatom and sponge $\delta^{30}Si$ (Figure 4.4). Diatom $\delta^{30}Si$ is a proxy for diatom silicic acid utilisation (De La Rocha et al., 1997), which is related to both diatom productivity and silicic acid supply to the surface ocean (Figure 4.4a). Sponge $\delta^{30}Si$ is a proxy of bottom water silicic acid concentration (Hendry and Robinson. 2012, Figure 4.4b). The comparison of these proxies between two key sites in the Southern Ocean (ODP sites 689 and 1090, Figure 4.5) additionally allows investigation of the evolution of the relationship between ACC-type circulation and diatom productivity through reconstruction of the Southern Ocean silicic acid gradient.

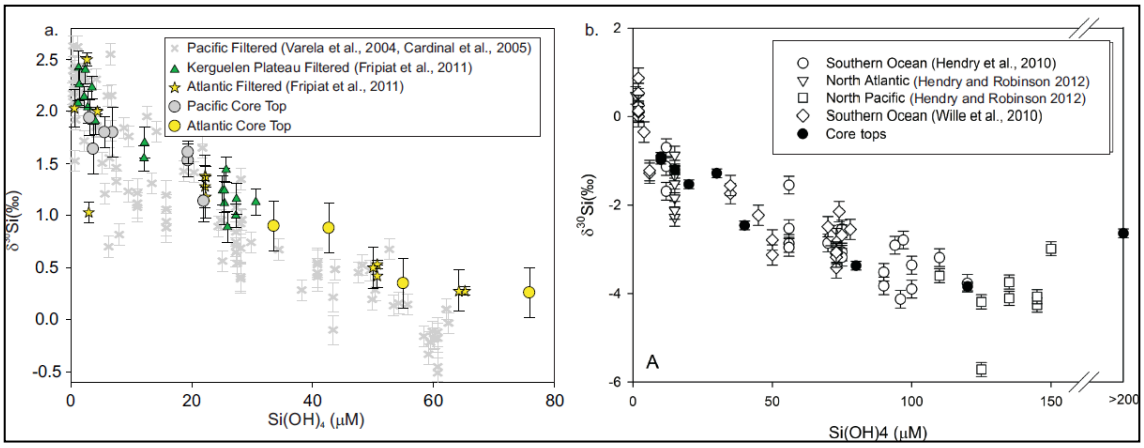


Figure 4.4 Modern Diatom and Sponge $\delta^{30}Si$ calibrations; **a.** Diatom $\delta^{30}Si$ vs. surface water silicic acid concentration in different sectors of the Southern Ocean in diatoms filtered from the top 100m of the water column during in situ studies (crosses, triangles and stars; Varela et al., 2004, Cardinal et al., 2007, Fripiat et al., 2011a,c) and core top diatom opal (circles). During silicification diatoms discriminate against ^{30}Si with a fractionation factor ($^{30}\varepsilon$) of −1.1±0.4‰ relative to ^{28}Si (De La Rocha et al., 1997, Milligan et al., 2004). This imparts a high $\delta^{30}Si$ on surface water silicic acid, and hence on diatom silica that sebsequently forms from it. At depth, remineralisation of diatom silica releases silicic acid with a lower $\delta^{30}Si$, and creates a $\delta^{30}Si$ gradient between surface and deep water. Upwelling re-supplies high silicic acid, low $\delta^{30}Si$ water to the surface ocean. Diatom $\delta^{30}Si$ is therefore a measure of diatom silicic acid utilisation, which is a balance between diatom uptake and the rates/composition of upwelled water; **b.** Sponge $\delta^{30}Si$ vs. ambient silicic acid concentration (Hendry and Robinson 2012), sponge spicules from modern sponges (open symbols) and core tops (solid symbols) in different ocean basins. Sponge $\delta^{30}Si$ is a function of ambient silicic acid concentration due to an increase in the sponge $^{30}\varepsilon$ with increasing concentration

4.2 Methods

Diatom $\delta^{30}Si$ was analysed in sediment from ODP site 177-1090, located just south of the modern Sub-Tropical Front, in the Sub-Antarctic Zone of the Southern Ocean (Figure 4.5; Gersonde et al., 1999). Sponge $\delta^{30}Si$ is reconstructed at ODP site 113-689 on the Maud Rise (Figure 4.5; Barker et al., 1990). Site 689 has a palaeodepth of approximately 1500m (Bohaty and Zachos, 2003), thus sponge $\delta^{30}Si$ from this site will yield intermediate water silicic acid concentration.

4.2.1 Age Models

The magnetostratigraphic age models of Spiess (1990) and Florindo and Roberts (2005) were used for site 689 and the model of Channell et al. (2003) for 1090, on the timescale of Cande and Kent (1995). Comparison of benthic foraminiferan $\delta^{13}C$ and $\delta^{18}O$ from site 689 with bulk carbonate stable isotopes generated in this study from site 1090 shows generally good agreement and provides an independent corroboration of the correlation between the two sites (Figure 4.6).

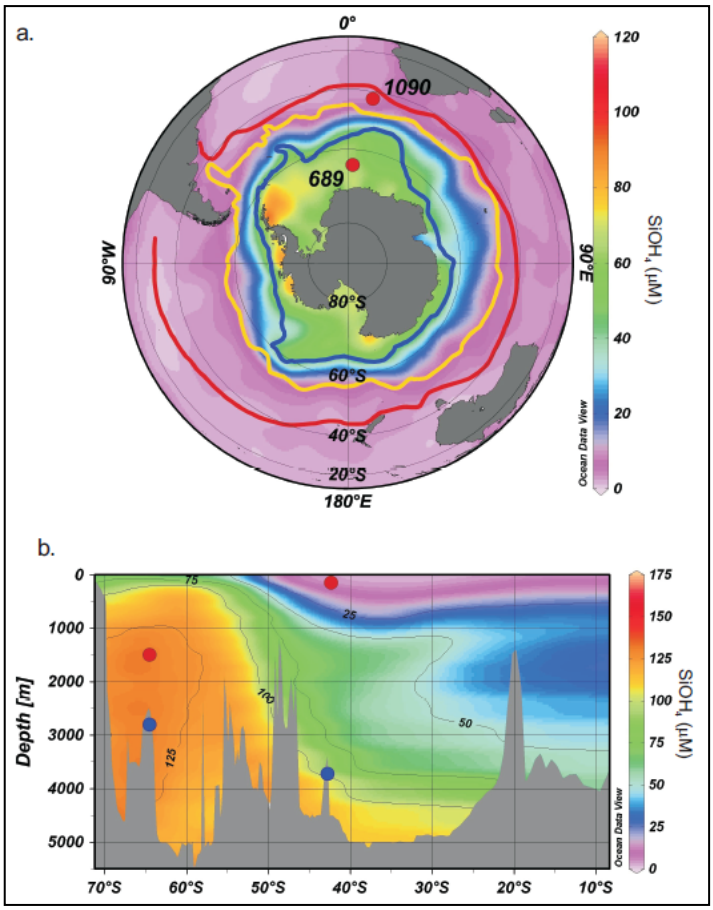


Figure 4.5 a. Map and **b.** transect showing the location of ODP sites 1090 and 689. Blue circles represent the modern depths of the two sites, and red circles the depth in the palaeocean at the time period reconstructed using silicon isotopes. Diatom $\delta^{30}Si$ is measured in sediments from site 1090, thus surface water silicic acid utilisation is reconstructed at this site. Sponge $\delta^{30}Si$ is from site 689 which has an intermediate palaeodepth of ~1500m, and therefore represents intermediate depth silicic acid concentration. Figure made with ocean dataview software and silicic acid concentrations from the World Ocean Atlas 2009.

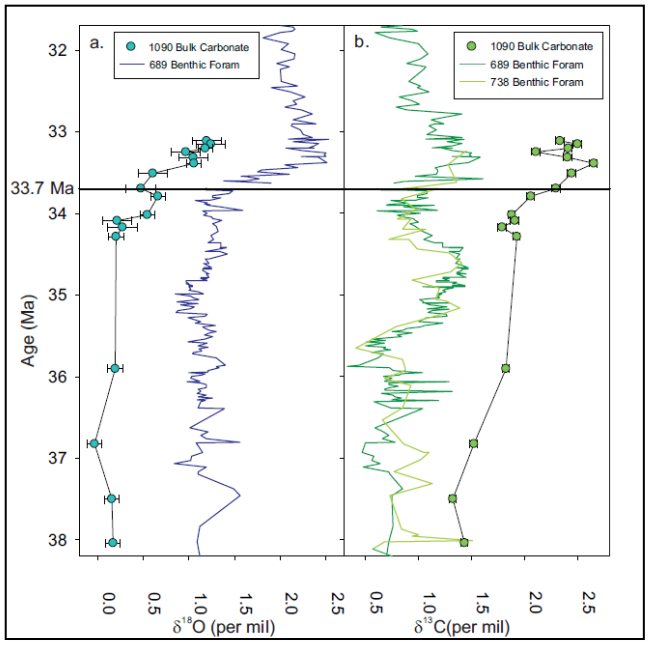


Figure 4.6 Comparison of benthic foram **a.** $\delta^{13}C$ and **b.** $\delta^{18}O$ with bulk carbonate records provide an independent test of the age model correlation between the sites.

4.2.2 Opal Preparation and Analysis

Methodologies already outlined in Chapter 2 are not reiterated in this section. XRD was carried out on Eocene-Oligocene sponge spicules from this site by De la Rocha (2003), who found them to be composed of amorphous opal. My data are generally in good agreement with the data generated at this site by De la Rocha (2003, Figure 4.7). However, there are some intervals at which the values do not agree. Due to the much larger error bars on the De La Rocha data, and because the data produced here show consistent values over the regions of disagreement, I choose to interpret only my own data in the following discussion. It is perhaps not surprising that there is some disagreement between values generated by different labs using different preparation techniques and different sample splits. However, it should be noted that the trend of both datasets, with sponge $\delta^{30}Si$ moving to lower values across the Late Eocene-Early Oligocene, is the same, thus inclusion of the De La Rocha (2003) data would not change the interpretation.

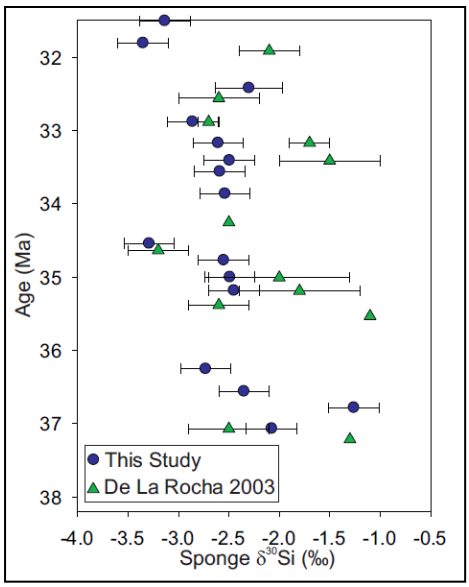


Figure 4.7 Comparison of sponge $\delta^{30}Si$ generated in this study (dark blue circles) and those from De La Rocha (2003) (green triangles). In general, there is agreement between this study and De La Rocha (2003). Given that these are complete repeats, on different sample splits, in different laboratories using different preparation techniques, the disagreement on three points is not considered problematic.

Analysis of core top opal has shown that the 2-20µm size range is generally most representative of diatom $\delta^{30}Si$ and that size fractions within this range produce consistent $\delta^{30}Si$ values (Chapter 3). Therefore, the 2-10µm fraction was generally used, but in order to test for reproducibility the 10-20 µm fraction was also run for some samples. For four samples, the 20-41µm size range was also analysed to affirm the correct size fraction for diatom $\delta^{30}Si$ had been selected. Smear slides were made to check the composition of size fractions. Figure 4.8 shows these results in the context of core top samples from similar oceanic regime to 1090 (although in the Pacific). The pattern of $\delta^{30}Si$ with size fractions is consistent between the downcore samples and the core tops, with more negative values in the largest size fractions due to contamination by radiolaria and sponge spicules. The 2-10µm size fractions are almost always within error of the 10-20µm fractions, confirming the choice of these fractions to reconstruct diatom silicic acid utilisation. As the 2-10µm fraction was run at all depth intervals, the following discussion and three point averages in figures are based on these $\delta^{30}Si$ and not that of the 10-20µm. XRD was run on three samples covering the entire age range, and all three showed the diffuse peak representative of

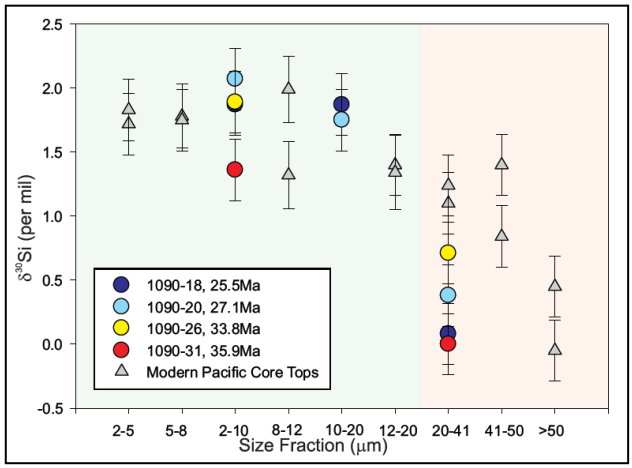


Figure 4.8 Size fraction $\delta^{30}Si$ from four downcore samples at ODP site 1090 (coloured circles) compared to TAN124 and 127 (grey triangles). Site 1090 and these core tops are located north of the modern Polar Front. The decrease in $\delta^{30}Si$ with increasing size fraction observed in modern core tops is also found in downcore samples, despite an age difference of between 26-36Ma. Additionally, the size-$\delta^{30}Si$ relationship is consistent in the downcore samples even across the major climatic shift that occurred at the Eocene-Oligocene Boundary (~34Ma). Green shading represents the size range considered to represent diatom $\delta^{30}Si$ in the downcore samples, and orange shading that considered affected by non-diatom components (dominantly radiolaria).

amorphous opal. The maintenance of distinct isotopic signatures in the diatom and sponge records produced here, with the offset in the direction expected from studies of the modern ocean, adds additional confidence to our results (see Figure 4.9).

The diatomite standard (1.26±0.2‰, Reynolds et al., 2007) was measured to assess external reproducibility for both diatom and sponge $\delta^{30}Si$, and yields a mean of 1.23±0.25‰ (2σSD, n=104). Error bars are quoted as the 2σSD external reproducibility, except where the 2σSD internal error on the 6-8 standard sample brackets was larger, in which case this is instead quoted, both in the text and in figure.

4.3 Results

Diatom $\delta^{30}Si$ increases from +1.2±0.25‰ at 38Ma to average values of +1.76±0.3‰ between 33.8 and 32.9Ma with a maximum of +1.9±0.25‰ at 33.2Ma (Figure 4.9c). The magnitude of this rise, ~0.6‰, may appear relatively small, but it should be emphasized that as the diatom $^{30}\varepsilon$ = −1.1‰, this represents a significant increase in diatom silicic acid utilisation. In the modern Atlantic sector of the Southern Ocean, diatom $\delta^{30}Si$ of ~+1.4‰ (i.e. the average diatom $\delta^{30}Si$ between 38Ma and 36Ma, Figure 4.9c), occurs where surface water silicic acid concentrations are ~20µM, compared to 2-10µM at +1.9‰ (peak $\delta^{30}Si$ at 33.2Ma) (Figure 4.4a). Modern diatom $\delta^{30}Si$ at site 1090 is estimated to be around 2‰ (Fripiat et al., 2001a). Downcore diatom $\delta^{30}Si$ comes consistently within error of the estimated modern value subsequent to ~33.5Ma, during the onset of glaciation (Grey shading in Figure 4.9c shows the modern diatom $\delta^{30}Si$ at site 1090, and dark green shading indicates the onset of glaciation as defined by the rise in benthic $\delta^{18}O$). Thus, diatom $\delta^{30}Si$ documents increasing silicic acid utilisation across the Late Eocene achieving near modern values during Antarctic glaciation.

Sponge $\delta^{30}Si$ shows a fairly steady decline from maximum values of −2.08±0.25 and −1.26±0.25‰ at around 37Ma to an Early Oligocene minimum at ~31.5Ma where values reach −3.35±0.25‰ (Figure 4.9b). Based on the modern calibration of Hendry and Robinson (2012), this translates to an increase in silicic acid concentration at intermediate depths from 10-50µM to 50-100µM. Modern sponge $\delta^{30}Si$ at site 689 is estimated to be between −3 and −4‰, based on a concentration of ~125µM (World Ocean Atlas 2009, Figure 4.5b) and the modern calibration of Hendry and Robinson 2012, Figure 4.4b). Sponge $\delta^{30}Si$ comes into the range of modern values at around ~32Ma (grey bar in Figure 4.9b), somewhat after diatom $\delta^{30}Si$ (Figure 9c).

4.4 Discussion

4.4.1 Development of the Southern Ocean silicic acid concentration gradient

For the combined interpretation of sponge and diatom $\delta^{30}Si$ records it is useful to define the term $\Delta\delta^{30}Si$ (= diatom $\delta^{30}Si$ – sponge $\delta^{30}Si$) and to understand what this value represents in the modern ocean. As diatom $\delta^{30}Si$ is a measure of the degree of diatom silicic acid utilisation it can be broadly interpreted as a measure of the surface silicic acid concentration (Figure 4.4a). Sponge $\delta^{30}Si$ is dependent on the silicic acid concentration of bottom waters at the site of measurement (Figure 4.4b) and thus, in defining $\Delta\delta^{30}Si$ we are approximating a measure of the oceans vertical silicic acid gradient. A particularly valuable aspect of $\Delta\delta^{30}Si$ is that it accounts for whole ocean/secular changes in the $\delta^{30}Si$ of seawater (as these should affect sponge and diatom $\delta^{30}Si$ to the same degree).

In the case of the new diatom and sponge $\delta^{30}Si$ records, $\Delta\delta^{30}Si$ is not a simple measure of this vertical gradient because the sites are at disparate locations. Although it would be ideal to have sponge and diatom $\delta^{30}Si$ at both sites, this was not possible due to a lack of large spicules at site 1090 and the highly fragmented nature of biogenic opal at site 689 (making it difficult to separate diatoms from radiolaria). Nevertheless, the core localities, and opal medium available at each, are ideally set up to document the evolution of the diatom-ACC controlled silicic acid concentration gradient present in the modern Southern Ocean (Figure 4.5), and hence the development of the system itself. Site 689 is situated at the eastern extremity of the Weddell gyre (Barker et al., 1990), monitoring the nutrient status of upwelling and re-subducting waters in the Antarctic Zone of the Southern Ocean. (Barker et al., 1990, Figures 4.1 and 4.5). Site 1090 is situated between

the modern Sub-Antarctic and Sub-Tropical fronts (Gersonde et al., 1999) and underlies the silicic acid depleted surface water created by diatom silicic acid utilisation during Ekman transport (Figure 4.1 and 4.5). The $\Delta\delta^{30}Si$ between sites 689 (sponge) and 1090 (diatom) in the modern ocean is critically dependant on the balance between upwelling of deepwater in the Antarctic zone and the amount of diatom silicic acid utilisation occurring during Ekman transport (Figure 4.5b). Neither of these sites has moved significantly over the course of the Cenozoic (Gersonde et al., 1999), and as such the $\Delta\delta^{30}Si$ between them should record shifts in the Southern Ocean silicic acid gradient.

$\Delta\delta^{30}Si$ calculated using the three point averages of the diatom and sponge $\delta^{30}Si$ increases from a low of ~3.5‰ at around 37Ma to a high of ~4.5‰ at ~34.5Ma, just prior to the onset of Antarctic glaciation (Figure 4.9d). This divergence is statistically significant, with $p = 2.4\times10^{-5}$ for non-divergence of the two linear regressions between 38 and 34 Ma using a maximum likelihood method (pers. comm. Jorn Bruggeman). $\Delta\delta^{30}Si$ stabilizes across the interval of glaciation itself (dark green shading Figure 4.9). Today this $\Delta\delta^{30}Si$ is ~5.5‰, based on the modern values of diatom and sponge $\delta^{30}Si$ estimated at each site.

Through the Late Eocene $\Delta\delta^{30}Si$ shifts towards, though does not achieve, the modern value. Although diatom $\delta^{30}Si$ does reach to within error of the modern level during Antarctic glaciation, sponge $\delta^{30}Si$ does not achieve this until ~31.5Ma (Figure 4.9). Unfortunately a hiatus at site 1090 between 32.8 and 28.7Ma precludes knowledge of the diatom $\delta^{30}Si$ at this time. However, based on measurements made subsequent to the hiatus (data not shown here, see Chapter 5 Figure 5.6), which average +1.9±0.35‰ between 28.7 and 24.2Ma, diatom $\delta^{30}Si$ seems likely to have remained high. Thus, it is inferred that modern $\Delta\delta^{30}Si$ is reached at approximately 31.5Ma, and that the increase in this value which occurs between the onset of Antarctic glaciation, at ~34Ma, and 31Ma is primarily driven by decreasing sponge $\delta^{30}Si$ rather than any further substantial increase in diatom $\delta^{30}Si$.

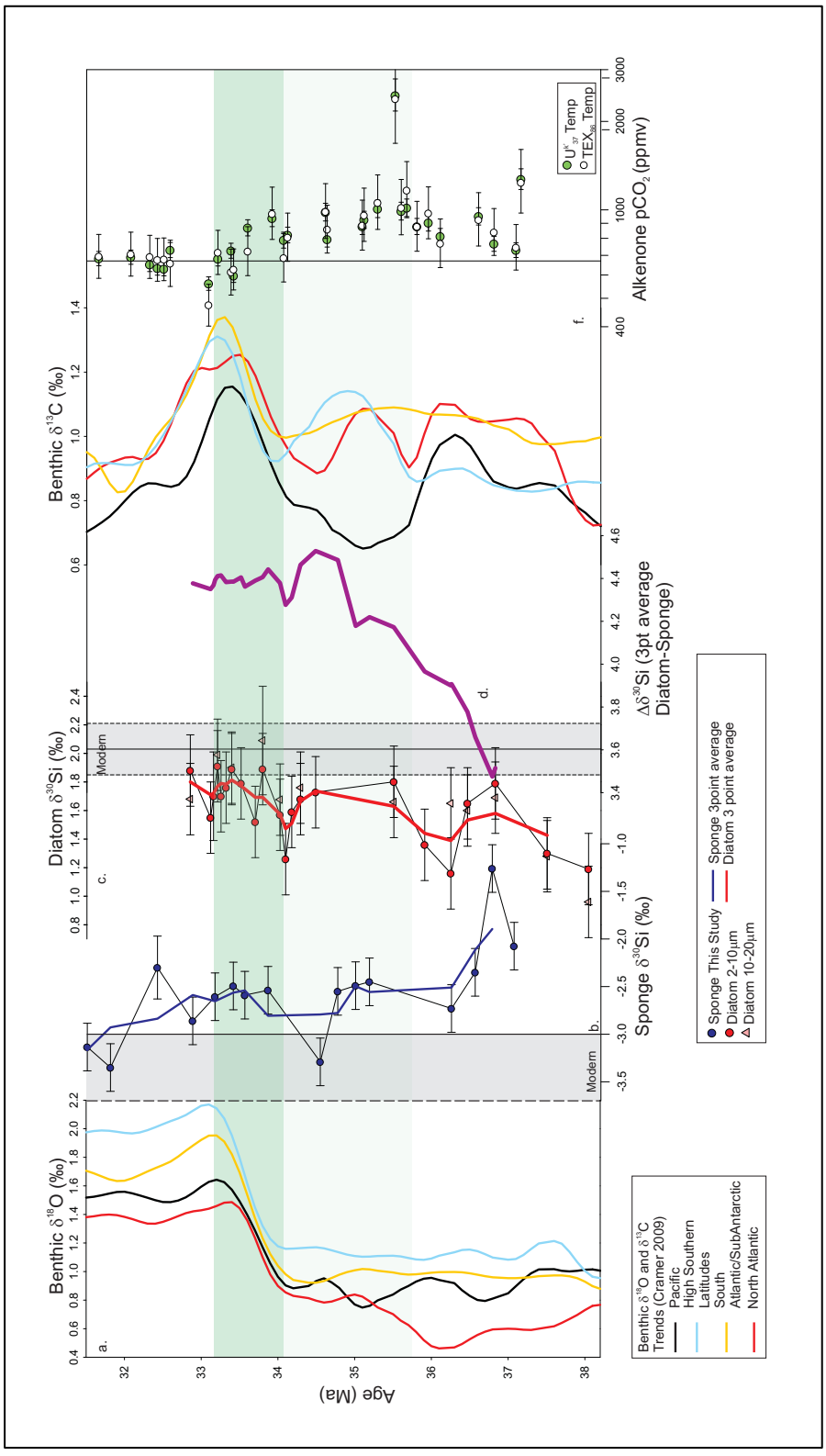

Benthic δ18O (‰)
Benthic δ13C (‰)
Diatom δ30Si (‰)
Sponge δ30Si (‰)
Δδ30Si (3pt average Diatom-Sponge)
Alkenone pCO2 (ppmv)
Age (Ma)
Modern
a.
b.
c.
d.
f.
Benthic δ18O and δ13C Trends (Cramer 2009)
Pacific
High Southern Latitudes
South Atlantic/SubAntarctic
North Atlantic
Sponge This Study
Diatom 2-10µm
Diatom 10-20µm
Sponge 3point average
Diatom 3 point average
U37K' Temp
TEX86 Temp

Figure 4.9 Palaeoceanographic records of the Eocene-Oligocene silicon and carbon cycles, with; **a.** the Oi1 event indicated by ~1.5‰ positive excursion in benthic foram $\delta^{18}O$ (stacks from Cramer et al. (2009)); **b.** Sponge $\delta^{30}Si$, dark blue line = three point running mean, grey bar is the modern value estimated using a silicic acid concentration of ~125µM and the modern calibration of Hendry and Robinson (2012); **c.** Diatom $\delta^{30}Si$; red circles = 2-10µm fraction, pink triangles = 10-20µm fraction, red line = 3 point running mean. Good agreement at all but one interval confirms that diatom $\delta^{30}Si$ is consistently measured downcore. Grey bar is the modern value of +2.03±0.18‰ measured by Fripiat et al. (2011) at a proximal location; **d.** $\Delta\delta^{30}Si$ calculated by interpolation of the three point running means of diatom and sponge $\delta^{30}Si$ **e.** $\delta^{13}C$ benthic foram stacks for each ocean basin from Cramer et al. (2009) and; **f.** pCO_2 reconstructions at ODP sites 925 and 929 from Pangani et al. (2011). Dark Green shading represents Antarctic Glaciation as defined by $\delta^{18}O$ stacks, light green and dark green together the period of pCO_2 decline inferred from e.

4.4.2 Development of ACC-type circulation and diatom radiation in the Late Eocene

The new $\delta^{30}Si$ records infer that a modern-type silicic acid gradient existed in the Southern Ocean by ~31.5Ma. Today, the existence of this feature owes both to the abundance of Southern Ocean diatoms and to the particular circulation of the ACC. Using the diatom and sponge $\delta^{30}Si$ records in combination with several other lines of evidence, it is suggested that both of these features were either initiated and/or undergoing substantial rearrangement over the Late Eocene and Early Oligocene.

The Eocene-Oligocene rise in diatom $\delta^{30}Si$ can only be interpreted in isolation as an increase in the degree of diatom silicic acid utilisation, which could be driven either by increased diatom uptake or by a decrease in the supply of silicic acid to the surface. We can determine with some confidence that for our records it is the former process that is driving the diatom $\delta^{30}Si$ rise, at least through the Late Eocene. Decreasing silicic acid supply is in conflict with two important observations: Firstly, the coincident decline in sponge $\delta^{30}Si$ shows an increase in intermediate water silicic acid concentration (Figures 4.1b and 4.9b) suggesting supply to the surface is more

likely to have increased. Secondly, lower silicic acid supply resulting from higher stratification cannot easily be reconciled with increasing opal contribution to Southern Ocean sediments that occurs thorough the Late Eocene and at the Eocene/Oligocene Boundary (Figure 4.3; Schumacher and Lazarus, 2004; Salamy and Zachos, 1999). Stratification would have decreased nutrient supply and is likely to limit diatom production, thus reducing the supply of opal to the seafloor. Diatom expansion as the driver of rising $\delta^{30}Si$ at this time is also in good agreement with substantially increased diatom diversity (Rabosky and Sorhannus, 2009). It appears that a major proliferation of diatoms occurred in the Late Eocene, putting into place an important component in control of the modern Southern Ocean over both global nutrient distributions and the biological carbon pump.

Increased silicic acid concentration at site 689 is well reconciled, temporally, with the subsidence of both the Tasman gateway and the Drake Passage. The Tasman gateway is thought to have undergone initial subsidence prior to 35.5 Ma and increased deepening between 35.5 and the Eocene-Oligocene Boundary, with a deepwater connection established between 33.5 and 30.2 Ma (Stickley et al., 2004). Seafloor complexities in the Drake Passage make the timing of subsidence somewhat difficult to constrain. However, initial opening may have occurred as far back as 50 Ma ago (Livermore et al., 2007), followed by continued subsidence, with a deep connection established by around 32 Ma (Mackensen, 2004; Livermore et al., 2007). Greater flow through these gateways was thus occurring across the interval during which silicic acid concentration at site 689 increases. Peak silicic acid at ~31.5 Ma is well reconciled with the establishment of a deepwater pathway for circumpolar current flow. It is hypothesized that the incursion of a new Pacific sourced water mass into the high latitude South Atlantic, as the gateways subsidised (Scher and Martin, 2006), was ultimately responsible for the increase in silicic acid concentration. Prior to the onset of upwelling associated with the initiation of circum-polar current flow, sedimentological and modelling studies have shown that the Southern Ocean was likely to have been a region dominated by sinking of surface water (Diester-Haass, 1995; Heinze

and Crowley, 1997; Sijp et al., 2011). This would have created a southern hemispheric circuit that drew in warm and salty water from the low latitudes, in a situation analogous to the modern day North Atlantic. There would have been little to no upwelling in the Southern Ocean, no exchange between the Pacific and Atlantic basins, and thus ocean overturning would have been sluggish (Cramer et al., 2009). During this time of decreased circulation, silicic acid may have become trapped in the deep ocean as the result of a low rate of exchange between deepwater and the surface. With it being the largest of the Eocene basins, this silicic acid may well have been concentrated in old deep Pacific waters (Cramer et al., 2009). With the increased upwelling caused by the development of a circum−Antarctic current, and an influx of waters from the Pacific, these nutrients would have been supplied to the Southern Atlantic and hence to site 689. This in agreement with the work of Schumacher and Lazarus which suggests that at or before the EO boundary there was a shift from opal deposition in the Equatorial Pacific to the Southern Ocean. I cannot exclude entirely the possibility that intensification of continental weathering, inferred from $^{87}Sr/^{86}Sr$ ratios (Zachos et al., 1999), may have increased the supply of silicic acid to the whole ocean. Additionally, with global cooling and the onset of Antarctic glaciation during the Eocene Oligocene transition, it may be that sea ice cover increased at site 689, whilst given its northerly location this would not have been the case for site 1090. There is no reason to believe a change in sea ice would have directly influence the $\delta^{30}Si$ of sponge spicules, as may have been the case if diatom $\delta^{30}Si$ had been measured at this site (sea ice diatoms have distinct $\delta^{30}Si$ values; Fripiat et al., 2007). It is unclear whether increased sea ice cover would have affected directly the silicic acid concentration at intermediate depths on Maud Rise, for example by changing the surface silicic acid utilisation by diatoms and their regeneration at intermediate depths. However, in the modern ocean there is little evidence that local diatom dissolution controls the silicic acid concentration/isotopic signature underlying a given site, but rather that this is a feature of oceanic circulation and silica regeneration on a global scale (de Souza et al., 2012). Hence it is far more likely that the increase in silicic acid documented at site 689 results from a circulation change in the wider Southern Ocean rather than from a change in sea ice cover.

4.4.3 Implications for carbon cycling and climate change at the Eocene-Oligocene Transition

The establishment of diatoms as dominant Southern Ocean phytoplankton and the inception of an ACC-type circulation documented here are expected to have had implications for the global carbon cycle. With intensification of overturning, and higher nutrient availability, in the Southern Ocean during the Late Eocene and into the Early Oligocene, the potential of the biological pump to export and bury organic carbon is likely to have increased. In particular, proliferation of the diatoms to fill the newly developed, turbulent, nutrient-rich niche associated with ACC-type circulation (Tozzi et al., 2004) may have facilitated major organic carbon burial (Rabosky and Sorhannus, 2009). Indeed, there is an extensive body of evidence that suggests increased Southern Ocean primary productivity occurring during the Late Eocene and across the Eocene-Oligocene Boundary (Diester-Haass, 1991; Diester-Haass et al., 1993; Salamy and Zachos, 1999; Diester-Haass and Zahn, 2001; Latimer and Filippelli, 2002; Diekmann et al., 2004; Schumacher and Lazarus, 2004; Anderson and Delaney, 2005; Zachos and Kump, 2005), with some studies pointing to an associated burial of organic carbon (Diester-Haass and Zahn, 2001; Diekmann et al., 2004; Anderson and Delaney, 2005). Further evidence comes from benthic $\delta^{13}C$ stacks (Cramer et al., 2009), which show an overall trend toward higher $\delta^{13}C$ values across the Late Eocene, although there is not exact coherency between the various ocean basins and a somewhat fluctuating nature to the individual basin records. The trend towards heavier values is consistent with a general increase in organic carbon burial and diatom radiation (as inferred from diatom $\delta^{30}Si$) at this time. The fluctuating nature of the $\delta^{13}C$ records in the Late Eocene is perhaps not surprising if this period is interpreted to be one of both increasing organic carbon burial, which will tend to drive $\delta^{13}C$ to heavier values, and of changing circulation and nutrient redistribution, which may shift $\delta^{13}C$ in either direction dependant on the circulation regime and oceanic location. The Late Eocene may represent a period of re-equilibration in the carbon cycle. Initially, increased upwelling may have vented CO_2 to the atmosphere, and arguably redistributed light

carbon through the oceans. At the same time, increased organic carbon burial would have worked to drawdown atmospheric CO_2. It is only when biological carbon pumping outstrips the effect of increased nutrient and CO_2 supply from depth that the system can facilitate an overall decrease in pCO_2. The pCO_2 reconstruction of Pagani et al. (2011) shows a decline which begins around 35.5Ma, proceeding a slight rise (Figure 4.9f). This is in keeping with a re-equilibration of the effects of upwelling and diatom driven organic carbon burial on atmospheric pCO_2 during the Late Eocene, with burial becoming dominant from around 35.5Ma.

Associated with the onset of glaciation itself, there is a positive carbon isotope excursion coherent across all ocean basins (Cramer et al., 2009), which is indicative of a major pulse of organic carbon burial (Salamy and Zachos, 1999). The beginning of the excursion occurs just subsequent to flattening of the rise in $\Delta\delta^{30}Si$ in our records, and coincident with the final approach of diatom $\delta^{30}Si$ towards consistently modern values. A further shift to increased opal accumulation is observed at some sites in the Southern Ocean (Salamy and Zachos, 1999; Anderson and Delaney, 2005) and there is additional microfossil and sedimentological evidence for further increased primary productivity and organic carbon burial here and further afield (Diester-Haass and Zahn, 2001; Anderson and Delaney, 2005; Coxall and Wilson, 2011). It seems likely, then, that this was a time of extremely high biological productivity in the Southern ocean and perhaps the globally. The emplacement of an ice sheet and thus an enhanced meridional temperature gradient is likely to have further increased the rate of upwelling (Salamy and Zachos, 1999). The proceeding establishment of the diatoms, which favour high nutrient, turbulent regions, would have allowed for utilisation of the higher nutrient supply and contributed to further pCO_2 decline.

Subsequent to glaciation, $\delta^{13}C$ values drop (Figure 4.9e), and deposition of opal declines at some sites in the Southern Ocean (Salamy and Zachos, 1999; Anderson and Delaney, 2005). However, diatom $\delta^{30}Si$ remains high (Chapter 5, Figure 5.6), and sponge $\delta^{30}Si$ continues to decline. This may be indicative of a system that has become self-limiting – high biological productivity would

have stripped nutrients from the whole ocean, limiting productivity and driving the system back towards steady state (Salamy and Zachos, 1999). In the case of the silicon cycle it is interesting that major export of opal coupled with the development of a more structured overturning circulation may have become limiting to the diatoms. Today, the Southern Ocean traps silica due to both deep regeneration of biogenic opal (de Souza et al., 2012) and the high Si:N ratio of Southern Ocean diatoms (Baines et al., 2010). This leaves large swaths of the thermocline devoid of silica, limiting diatom productivity (Sarmiento et al., 2004). The progressive trapping of this silica in the deep ocean may have eventually begun to limit diatoms at more northerly locations such as site 1090, thus decreasing productivity. Such ideas relating to the control of ocean circulation and diatom adaptation over the nutrient distribution of the world's oceans are highly relevant to understanding the role played by the biological pump in climatic change through the Cenozoic. Exploration of these questions warrants further study, and my initial attempts to develop an understanding the Cenozoic silicon cycle form the basis of Chapter 5.

4.5 Conclusions

In this chapter I present the first reconstruction of the Eocene-Oligocene marine silicon cycle achieved through novel combination of diatom and sponge $\delta^{30}Si$. Increasing diatom $\delta^{30}Si$, interpreted in light of both opal accumulation rates and sponge $\delta^{30}Si$, provides convincing evidence for diatom radiation during the Late Eocene of the Southern Ocean. Sponge $\delta^{30}Si$ shows increasing silicic acid concentrations at intermediate depths in the Antarctic Zone throughout the Late Eocene and the Early Oligocene, coincident with the timing of subsidence of Southern Ocean land bridges. The concomitant development of these two components, which are key in controlling the marine silicic acid distribution, also had major implications for organic carbon burial and global climate. A mechanistic link between the development of this system and Eocene-Oligocene pCO_2 drawdown exists through diatom driven burial of organic carbon triggered by intensified upwelling, supportive of the initial hypothesis that the biological carbon pump may have had a role to play in the onset of Antarctic glaciation. In particular, this mechanism implies a drawdown of CO_2 associated with events of a precursor nature to the glaciation, as is required from both modeling and pCO_2 proxy reconstructions.

Chapter 5. A Cenozoic record of Sponge $\delta^{30}Si$

Abstract

Across the Late Eocene and Earliest Oligocene, the subsurface silicic acid concentration of the high latitude South Atlantic increased to near modern values by ~31.5Ma. To investigate the subsequent evolution of Southern Ocean silicon cycling, an extended sponge $\delta^{30}Si$ record from site 689 spanning 27Ma of the Oligocene, Miocene and very earliest Pliocene is presented here. The record documents an increase in sponge $\delta^{30}Si$, tracking a decrease in silicic acid concentration, almost immediately after the earliest Oligocene peak (sponge $\delta^{30}Si$ of ~−3.3‰ at 31.5Ma). Although there is a great deal of oscillation in the sponge $\delta^{30}Si$ record through the Oligocene and Miocene, average values remain remarkably stable at around −2.6 to −2.7‰. After the 4Ma end of this sponge $\delta^{30}Si$ record, silicic acid concentrations at site 689 must have increased in order to achieve modern levels, which are equivalent to a sponge $\delta^{30}Si$ of ~−3.5‰. With the aid of a simple two box model, I interpret low silicic acid concentrations during the Oligocene and Miocene, as compared to today, to result from enhanced surface-deepwater exchange. It is suggested that the shift towards modern, high silicic acid concentrations occurred at ~2.7Ma and was caused by the onset of stratification in the North Pacific and Southern Ocean. This stratification, associated with Northern Hemisphere Glaciation, is hypothesised to have decreased the rate of exchange between the deep and surface ocean, limiting diatom production and leading to a build up of silicic acid in the deep ocean. A three step history of the Late Eocene to modern Southern Ocean silicon cycle is proposed as follows; 1) A Late Eocene to Earliest Oligocene influx of silicic acid rich deep water from the Pacific, driven by the subsidence of Southern Ocean gateways and coincidence diatom radiation; 2) Oligocene, Miocene and Pliocene periods which entailed high rates of surface-deepwater exchange, enhanced diatom production and a steady state ocean driven to lower silicic acid concentrations; 3) Decreased surface-deep water exchange from 2.7Ma leading to sequestration of silicic acid in the deep ocean. I suggest

that the relationship between ocean circulation and diatom productivity exerts a dominant control over Cenozoic silicon cycling.

5.1 Introduction

In the previous chapter, a fundamental shift in the Southern Ocean silicon cycle across the Eocene-Oligocene Boundary was inferred from combined sponge and diatom $\delta^{30}Si$ records. The silicic acid concentration recorded by sponge $\delta^{30}Si$ in subsurface waters had increased to near modern values by ~31.5Ma. Coincidentally, diatom $\delta^{30}Si$ demonstrates that this pool of silicic acid was increasingly utilised, reaching an extent similar to that of today at the Eocene-Oligocene boundary, thus establishing the diatom production belt. Between the end of this record and the present day, there have been a number of events with the potential to perturb the marine silicon cycle, in particular subsurface silicic acid concentrations. These fall into two categories, those with the potential to alter the whole ocean silicon inventory (i.e. shifts in the input and output fluxes), and those which could act to redistribute silicic acid through the oceans.

The intensification of continental weathering inferred to have occurred through the Cenozoic (Figure 5.1) from reconstructions of marine lithium (Misra and Froelich. 2012), osmium (Pegram et al., 1992) and strontium (e.g. Hodell et al., 1991) isotope ratios, falls into the first category. A simple translation of intensified weathering is a higher flux of silicon to the ocean via rivers, which modelling suggests would increase subsurface silicic acid concentration by increasing the whole ocean silicon content (De La Rocha and Bickle, 2005).

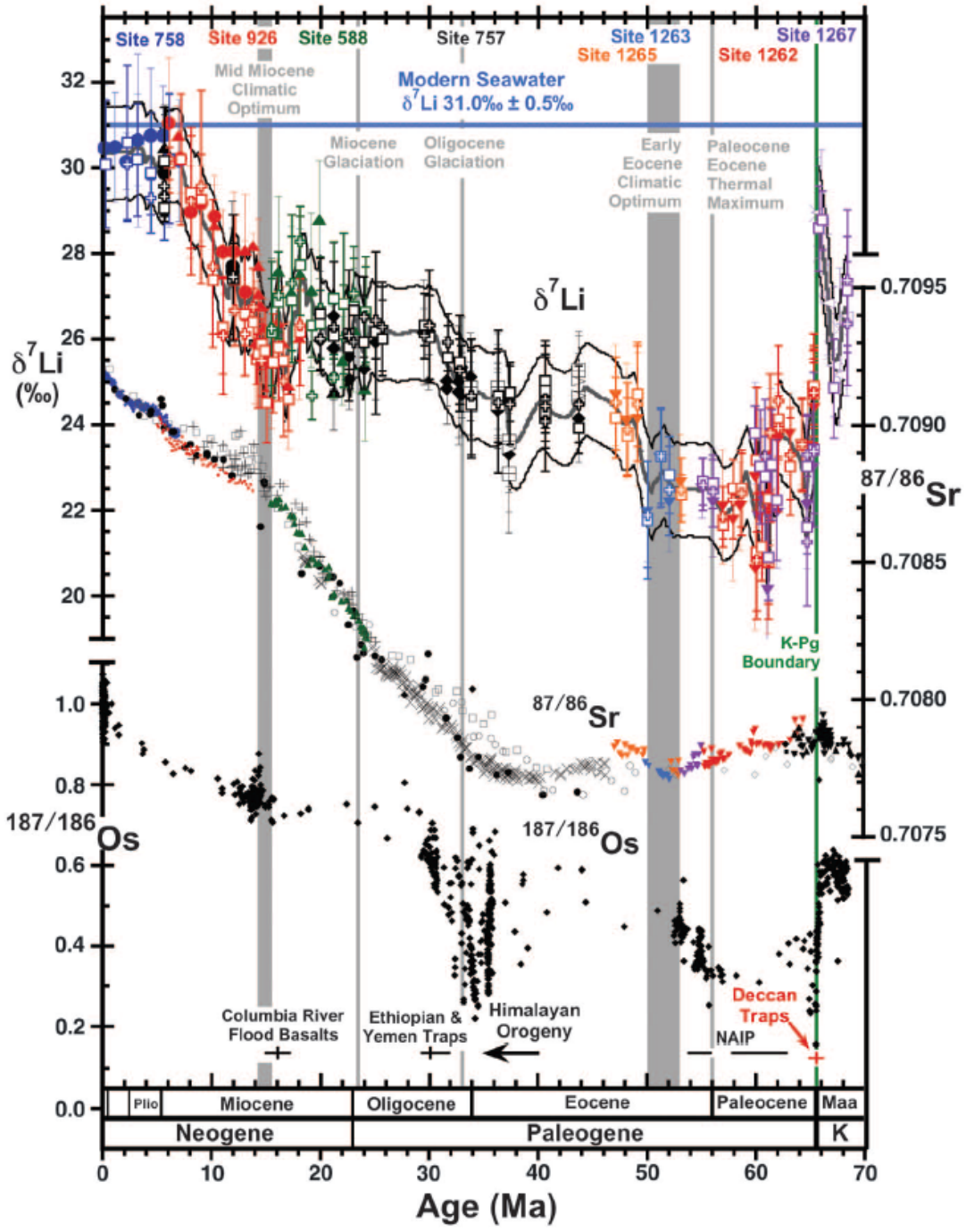


Figure 5.1 Strontium, lithium and osmium isotope records covering the Cenozoic. Considered together, the increase observed in all three isotope ratios can be taken to indicate escalating rates of continental weathering from the Late Eocene to the modern. Figure from Misra et al. (2012).

The rise of the diatoms to dominate the silicon cycle, although considered to have occurred mainly between the Cretaceous and Early Oligocene (Harper and Knoll, 1975; Maldonado et al., 1999; Rabosky and Sorhannus, 2009), is also hypothesised to have continued through the Middle to Late Miocene (Falkowski et al., 2004). This type of change constitutes one of two mechanism expected to alter silicon output from the oceans. De La Rocha and Bickle (2005), using a two box model, explored the effects of diatom radiation by considering a situation in which the output of diatom opal is higher than the input of silicon by rivers. This acts to remove silicon from the oceans and thus drives subsurface silicic acid concentrations to lower values. A model employing this type of forcing can never produce an ocean in steady state because the output term is fixed to be greater than the input. In this case the silicic acid concentration of the ocean is eventually drawn down to zero, and diatoms are no longer able to produce opal for burial. In reality, a steady state is presumably achieved when the burial of opal declines in response to the limitation of silicic acid in the surface. The second form of output mechanism relieves diatom limitation in the surface ocean by increasing the rate of exchange between silicic acid rich deep water and the surface, driving a pulse of opal burial that acts to drawdown silicon from the ocean. This situation is expected to push the ocean into a new steady state with lower silicic acid concentrations at depth. An example of this type of change, occurring as we approach the modern day, might be the onset of stratification in the North Pacific and Southern Ocean at 2.7Ma (decrease in the surface-deepwater exchange rate, Haug et al., 1999; Sigman et al., 2004; Haug et al., 2005; de Boer et al., 2007). At this point a distinction is made between changes in the deep-surface exchange and the configuration of the oceans overturning circulation, which although not necessarily mutually exclusive, have separate effects on silicic acid in the deep ocean.

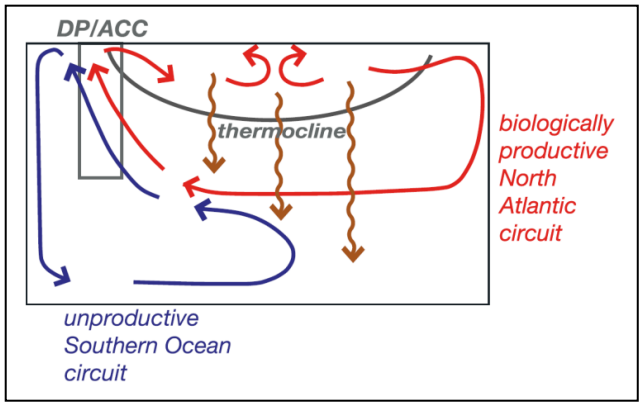


Figure 5.2 Schematic of circulation in the Atlantic Ocean from Toggweiler et al. (2006). The blue loop represents Southern sourced deepwater (i.e. in the present day Antarctic Bottomwater), and the red loop the Northern sourced waters (i.e. the present day North Atlantic Deepwater). Today, the blue loop is rich in silicic acid, as silicic acid upwelling in the Southern Ocean is trapped within the Antarctic circumpolar current by diatom silicification. Simplistically, if the rate of surface-deepwater exchange were to increase, the upwelling of silicic acid would increase, enhancing diatom productivity in the wider ocean. This would increase deposition of opal on the seafloor and drawdown the deep ocean silicic acid inventory. The red loop contains nutrient poor waters sourced from the surface of the north Atlantic. It is possible that changes in the speed of the northern loop would increase the supply of silicic acid poor waters into the Southern Atlantic.

Whist the deep-surface exchange mechanism outlined above works to drawdown silicic acid from the deep ocean, the configuration of the overturning circulation (in combination with diatom silicic acid utilisation) controls the partitioning of silicic acid between the various deepwater masses (Figure 5.2; Cortese et al., 2004; Sarmiento and Gruber, 2006; Fripiat et al., 2011b; de Souza et al., 2012). Configuration of the overturning circulation falls into the category of local, rather than whole ocean, change in silicic acid concentration. Shifts in silicic acid concentration related to circulation may be due either to a change in the partitioning of silicic acid between oceanic watermasses, or to a change in the watermass overlying a given site. The geological record provides evidence that significant shifts in overturning circulation have occurred through the Cenozoic with, for example, the onset and strengthening of NADW formation occurring through the latter Miocene (overturning circulation change; Poore et al., 2006; Cramer et al., 2011).

In order to investigate the response of the silicon cycle to the types of event outlined above, the sponge silicon isotope record from site 689 presented in the previous chapter has been extended into the Oligocene, Miocene and the very earliest Pliocene. As the silicon and carbon cycles are fundamentally linked both through continental silicate weathering and photosynthesis by diatoms, shifts in the Cenozoic silicon cycle may have had implications for atmospheric pCO_2 and global climate. The diatom $\delta^{30}Si$ record from site 1090 has also been extended into the Late Oligocene. A two box model of the oceanic silicon cycle developed by De La Rocha and Bickle (2005) has been employed to explore which processes are important in setting the deep ocean silicic acid concentration, with the ultimate aim of aiding interpretation of the long term sponge $\delta^{30}Si$ record presented in this chapter.

5.2 Methods

5.2.1 Silicon Isotope Ratios

As detailed in Chapters 2 and 5, sediments were cleaned using H_2O_2 and HCl, before the >100μM fraction was separated using microseparation. Between 20 and 100 spicules were handpicked, sonicated in methanol and thoroughly rinsed with deionised and 18MΩ Milli-Q water. The spicules were dried down in concentrated HNO_3 and dissolved in NaOH. As also outlined in Chapters 2 and 5, diatom preparation methods employ a number of chemical and physical separation stages, including the microseparation technique detailed in Chapter 3, to produce pure diatom fractions for $\delta^{30}Si$ analysis. Again, both the 2-10μm and 10-20μm fractions were analysed to ensure that quality data were produced, and the diatoms were dissolved in NaOH. Silicon isotopes ratios were measured using a Nu-Instruments HR multi-collector inductively coupled plasma mass spectrometer. The age model of site 689 is based on magntostratigraphy (Spiess,

1990; Censarek and Gersonde, 2002; Florindo and Roberts, 2005) and the calibration of Cande and Kent (1995).

Within the extended sponge $\delta^{30}Si$ record, the three points highlighted in red on Figure 5.3 differ from their respective replicates (in pink) by –1.64, –0.9 and –0.84‰, which is outside the acceptable offset given an external reproducibility of 0.25‰. The two youngest red data points also lie outside 2σSD of the mean of all data younger than 18Ma, indicating they are outliers at the 95% confidence interval (Figure 5.3, grey dashed lines). This simple test represents an underestimate of confidence, as it does not take into account any temporal trends in the data. Therefore, although it is less clear that the oldest anomolous point is a genuine outlier, this is still suggested to be the case given its offset from surrounding data points. The average offset between all other sponge replicates made at site 689 is 0.28‰ (n=20, including Eocene-Oligocene data) indicating this issue is probably not related to a difference in the accuracy of sponge spicule vs. diatom opal analyses. These three outliers all constitute complete replicates, i.e. they were measured on a newly separated and picked set of sponge spicules, and the two replicates do not agree. The lower $\delta^{30}Si$ for all the outlying values is in the direction expected for incomplete dissolution. The dissolution fractionation factor for mixed assemblages of diatoms is ~0.55‰ (Demarest et al., 2009), which is too low to explain the offset of the sponge spicules. However, it is possible that dissolution of sponge spicules induces a greater fractionation than that of the diatoms. It is also possible that the difference is due to vital effects, driving an offset between individual batches of spicules. Another possibility is that changes in the deep water silicic acid concentration at this site may have occurred over timescales shorter the sedimentation rate (which averages around 5m/Ma between 18 and 4Ma), meaning that the spicules picked could possibly have been deposited under differing silicic acid concentrations. It may be useful in future to study both the fractionation of silicon isotopes associated with sponge spicule dissolution and the variation of sponge $\delta^{30}Si$ in downcore samples. However, given the generally good agreement between re−picked samples through the rest of our record (Appendix 1), the

outliers are not considered to be problematic for either the record presented here or the more general use of sponge $\delta^{30}Si$ as a proxy for silicic acid concentration. In all three cases one of the two replicates agrees well with the surrounding data. Thus, the outliers have been excluded from further discussion and figures.

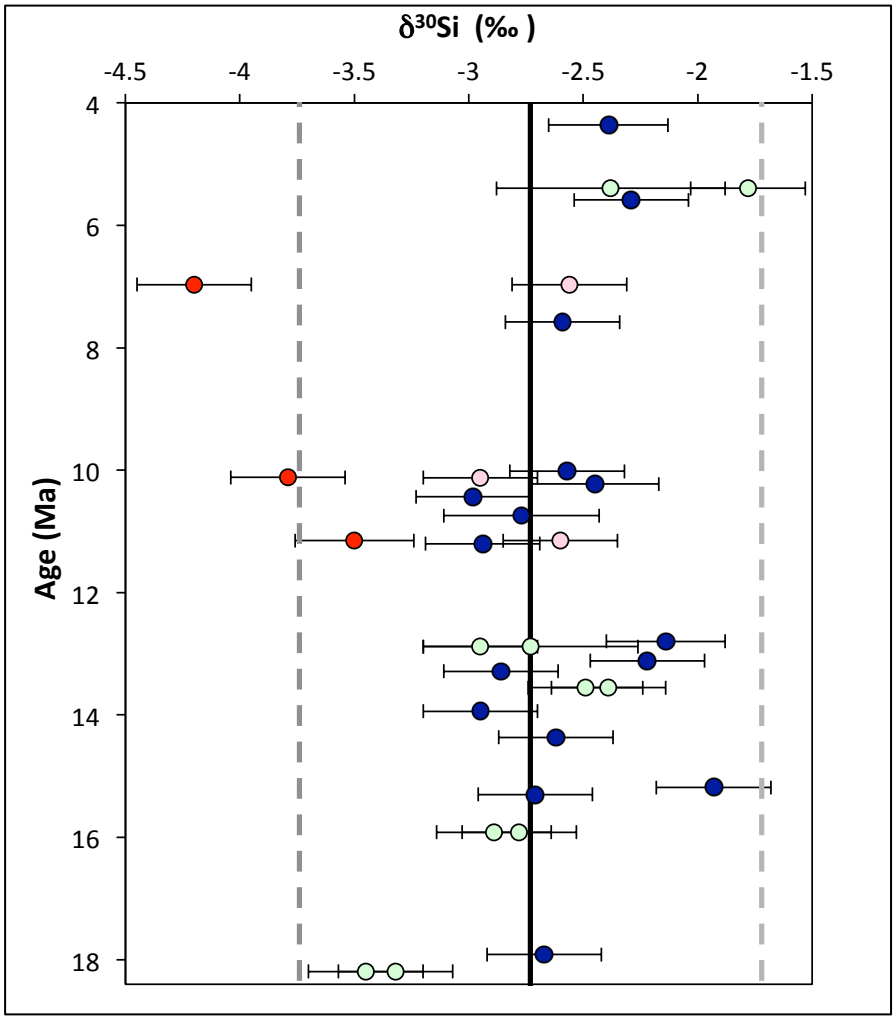


Figure 5.3 Three outliers in the Miocene sponge $\delta^{30}Si$ data set (red dots). These are all complete replicates measured on a new batch of sponge spicules. Red points are suspected outliers, and the pink pints are their corresponding replicates. Blue dots are samples that were not replicated, whilst pale green points are replicates that are in agreement with one another. The solid black line is the mean of all data younger than 18Ma, and the grey dashed lines are the 2σSD. The two younger points lie outside 2 standard deviations of the mean, and therefore may be considered outliers at the 95% confidence interval. Although the older data point does not fall outside the 2σSD, it may also be considered an outlier on the grounds of it being outside the external reproducibility of the surrounding data points, however whether this is a genuine outlier is more debateable.

5.2.2 Model Description

The model employed here is that of De La Rocha and Bickle (2005) and was run in Matlab (J.Bruggeman, pers. comms). An overview of its configuration is shown in Figure 5.4. The model has a deep box and a 100m surface box. Silicon is incorporated into diatom opal in the surface and can be set either as a function of silicic acid concentration or dictated to be a certain proportion of the input value (which will drive the model out of steady state). A portion of this opal is then dissolved in the surface ocean. Dissolved silicon is exchanged between the deep and surface boxes (upwelling/downwelling), with the flux rate set for a deep ocean mixing time of 1000yrs. Inputs to the model are from riverine and hydrothermal fluxes, and the single output is opal deposition on the seafloor. Further details of the model may be found in De La Rocha and Bickle (2005). The constants, variables and calculated variables used in the model are detailed in Table 5.1.

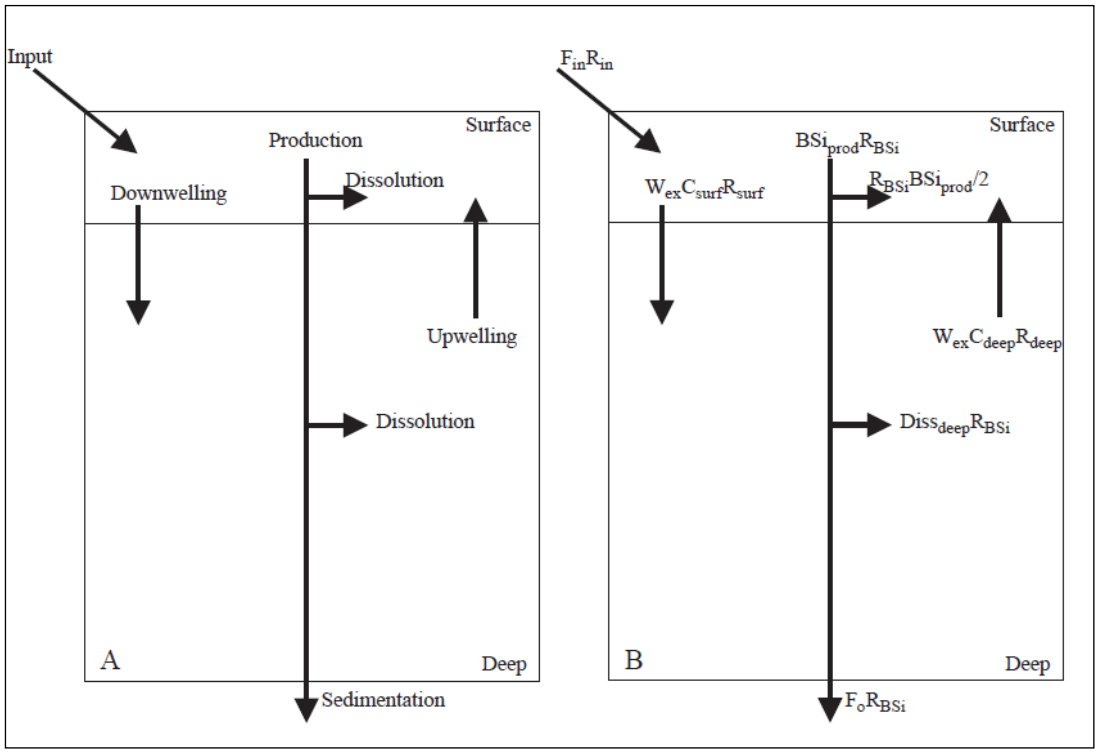


Figure 5.4 Two box model of De La Rocha and Bickle (2005). A flux of dissolved silicon, with a magnitude and isotopic ratio determined by the balance between riverine and hydrothermal inputs, enters the surface box. Biogenic silica is produced in the surface box, of which some portion immediately dissolves and the remainder sinks to the deep ocean. In the deep ocean, most of the exported biogenic silica dissolves. The small remaining amount is buried in the sediments and output from the model. Water is exchanged between surface and deep boxes via upwelling and downwelling. The silicon isotopic ratio is traced through the model, and depends ultimately on the isotopic compositions of the inputs and outputs. $V_{surf/deep}$ = volume of the surface/deep boxes; $C_{surf/deep}$= [Si] in the surface/deep boxes; F_{in} = flux of Si into the model; BSi_{prod}= biogenic silica produced; D_{diss} = the fraction of BSi_{prod} which dissolves in the deep box; W_{ex}=volume upwelled/downwelled each year; R = $^{30}Si/^{38}Si$.

The equations that determine the concentration of silicic acid in the surface and deep boxes are:

$$V_{surf}\,dC_{surf}/dt = F_{in} - BSi_{prod}*(1-S_{diss}) - W_{ex}C_{surf} + W_{ex}C_{deep} \quad \text{(eq. 1)}$$

$$V_{deep}dC_{deep}/dt = W_{ex}C_{surf} - W_{ex}C_{deep} + Diss_{deep} \quad \text{(eq. 2)}$$

(Where $V_{surf/deep}$ = volume of the surface/deep boxes; $C_{surf/deep}$= [Si] in the surface/deep boxes; Fin = Flux of Si into the model = $F_{river}*f_{river} + F_{hydrothermal}*f_{hydrothermal}$; F_{river}= river flux; $F_{hydrothermal}$ = hydrothermal flux; f_{river} = riverine proportion of input; $f_{hydrothermal}$ = hydrothermal proportion of input; BSi_{prod}= biogenic silica produced; S_{diss}=fraction of BSi_{prod} which dissolves in the surface box; P_{eff} = preservation efficiency; D_{diss} = the fraction of BSi_{prod} which dissolves in the deep box; W_{ex}=volume upwelled/downwelled each year)

Biogenic opal production is dictated by equation 3 when diatom production is to set to be a function surface silicic acid concentration ('Diatom use' is the fraction of silicic acid used by diatom production).

$$BSi_{prod} = C_{surf}*V_{surf}*\text{Diatom use} \quad \text{(eq. 3)}$$

Alternative, to bury a given fraction of the input flux and push the model out of steady state equation 4 is used ('$F_{input\ used}$' is the amount of the input flux which is to be buried, and can be set to either less than or greater than one).

$$BSi_{prod} = F_{in} * F_{input\ used} / P_{eff} \quad \text{(eq. 4)}$$

Dissolution in the surface ocean (S_{diss}) is set at a fixed percentage of the biological production, and for standard runs is 50% (Nelson et al., 1995). The preservation of opal (P_{eff}) is also a set term for standard runs, here 3.5% (Trueger et al., 1995). These two parameters dictate the extent of deep dissolution according to:

$$D_{diss} = [BSi_{prod}) 1\text{-}S_{diss}] - [BSi_{prod}.P_{eff}] \quad \text{(eq. 5)}$$

Silicon isotopes are traced through the model using the terms ($R = {}^{30}Si/{}^{28}Si$):

$$V_{surf} C_{surf} dR_{surf}/dt = F_{in}R_{in} - BSi_{prod} * (1 - S_{diss}) R_{BSi} - W_{ex} C_{surf} R_{surf} + W_{ex} C_{deep} R_{deep} \quad \text{(eq. 6)}$$

$$V_{deep} C_{deep}\ dR_{dep}/dt = W_{ex} C_{surf}\ R_{surf} - W_{ex} C_{deep} R_{deep} + R_{BSi} Diss_{deep} \quad \text{(eq.7)}$$

It is acknowledged that tracing fractions through the model is an approximation that introduces a small error into the outputs.

The isotopic outputs of the original model were the $\delta^{30}Si$ of the dissolved silicic acid in the surface and deep boxes (above) and the $\delta^{30}Si$ of diatom opal (calculated assuming Rayleigh fractionation using equation (8), DSi = dissolved silicic acid, f=fraction of silicic acid consumed by diatoms in the surface)

$$R_{Diatom} = R_{DSi}\ (1 - f\alpha)/(1 - f) \quad \text{(eq.8)}$$

I have added a term to output the $\delta^{30}Si$ of sponges (equation 9) according to a linear relationship based on the calibration of Hendry et al. (2012). Although the relationship is generally agreed to be exponential, in the case of this model it is deemed acceptable to use the simple linear equation, as the two models only deviate at the extremes of silicic acid concentration.

$\delta^{30}Si = (C_{deep} + 115.18 / -45.3) + \delta^{30}Si_{deep}$ (eq.9)

Thus, the $\Delta\delta^{30}Si$ (=diatom $\delta^{30}Si$ − sponge $\delta^{30}Si$) may also be calculated.

A 'quaternary' run, in which the model is allowed to reach steady state from an initial whole ocean concentration of 70μM (De La Rocha and Bickle, 2005) is shown in Figure 5.5, and the output conditions at steady state are recorded in Table 5.2. In the following discussion the model setup is as that in Table 5.1 unless otherwise stated. The initial conditions of surface and deep silicic acid concentration and $\delta^{30}Si$ are set to be the quaternary equilibrium at the beginning of each subsequent run.

Prescribed terms	**Nominal Value (unless perturbed for a given run)**	**Units**	**Equation**	**Description**
F_{in}	7×10^{12}	mol yr^{-1}	$F_{river}+F_{hyrothermal}$	Si input
R_{std}	0.0335320			$^{30}Si/^{28}Si$ of the standard NIST RM 8564
R_{in}	0.0335589		$F_{river} \times R_{river} + F_{hydrothermal} \times R_{hydrothermal}$	$^{30}Si/^{28}Si$ of the input
α	0.9989			Diatom fractionation factor
V_{surf}	3.6×10^{19}	L		Volume of the surface box
V_{deep}	1.334×10^{21}	L		Volume of the deep box
W_{ex}	1.37×10^{18}	L yr^{-1}		Upwelling/downwelling volume
P_{eff}	0.035			Preservation efficency
S_{diss}	0.5			Fraction of BSi dissolved in surface
Variables				
C_{surf}		μM		Surface concentration
C_{deep}		μM		Deep concentration
R_{surf}				$^{30}Si/^{28}Si$ of the surface
R_{deep}				$^{30}Si/^{28}Si$ of the deep
Calculated Variables				
f			$1-BSi_{prod}/C_{surf}V_{surf}$	fraction of surface Si remaining after BSi prod
R_{BSi}			$R_{DSi}(1-f^{\alpha})/(1-f)$	$^{30}Si/^{28}Si$ of BSi
$Diss_{deep}$		mol yr^{-1}	$BSi_{prod} \times (1-S_{diss}) – Bsiprod \times P_{eff}$	amount of BSi dissolved in the deep box
$\delta^{30}Si_{surf}$		‰	$(R_{surf}/R_{std}-1) \times 10^3$	$\delta^{30}Si$ of surface Si
$\delta^{30}Si_{deep}$		‰	$(R_{deep}/R_{std}-1) \times 10^3$	$\delta^{30}Si$ of deep Si
$\delta^{30}Si_{diatom}$		‰	$(R_{Bsi}/R_{std}-1) \times 10^3$	$\delta^{30}Si$ of diatoms
$\delta^{30}Si_{sponge}$		‰	$(C_{deep} + 115.18 / -45.3) + \delta^{30}Si_{deep}$	$\delta^{30}Si$ of sponges
$\Delta\delta^{30}Si$		‰	diatom $\delta^{30}Si$ − sponge $\delta^{30}Si$	

Table 5.1 Model Parameters

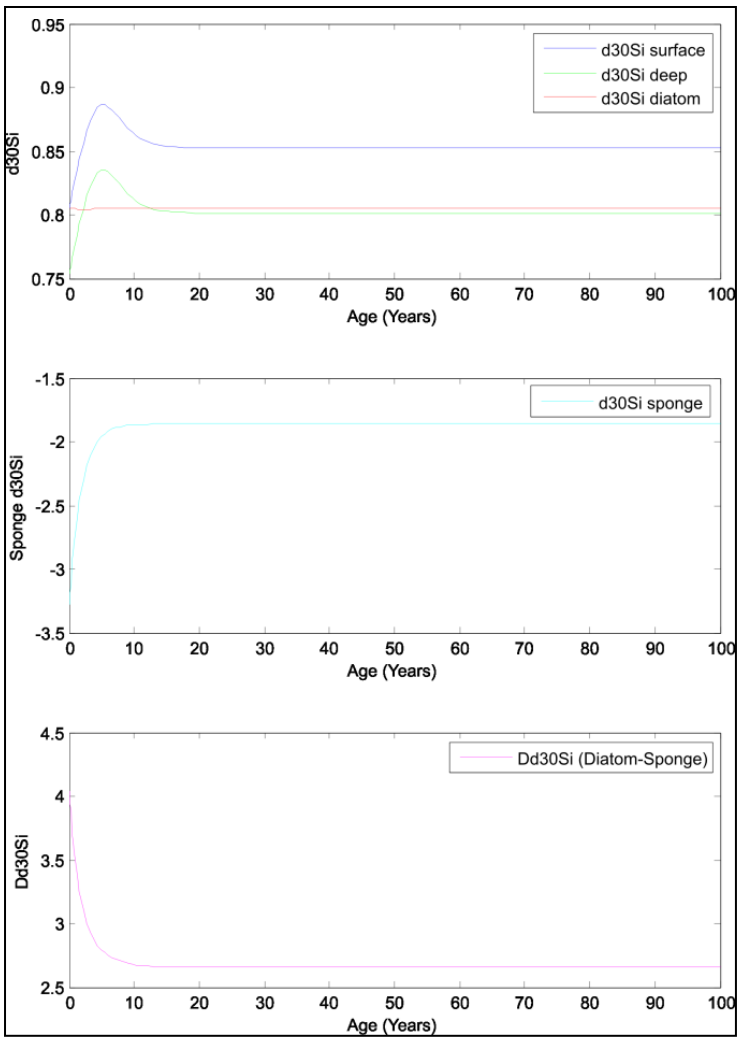


Figure 5.5 The model was allowed to equilibrate from an initial condition of 70μM. Our model closely approximate match the original outputs of De La Rocha and Bickle (see Table 5.2 for steady state outputs).

Model Run	Time to equilibrate (kyrs)	Surface [Si] (µM)	Deep [Si] (µM)	Surface $\delta^{30}Si$ (‰)	Deep $\delta^{30}Si$ (‰)	Diatom $\delta^{30}Si$ (‰)	Sponge $\delta^{30}Si$ (‰)	$\Delta\delta^{30}Si$ (‰)	Opal produced (Tmol yr-1)	Opal buried (Tmol yr-1)
'Quaternary' run.	300	5.6	73.5	0.86	0.81	0.81	-3.35	4.16	200	7
Double riverine input flux (moles)	400	10.4	136	0.95	0.90	0.89	-4.65	5.5	370	12.95
Double riverine input, Peff = 7%	200	5.2	63.3	0.94	0.9	0.89	-3.04	3.93	185	12.95
Double riverine input flux, Peff = 14%	80	2.6	26.9	0.95	0.90	0.89	-2.24	3.13	93.5	12.95
Halved surface-deep exchange	600	5.6	141	0.86	0.81	0.81	-4.86	5.66	200	7
Doubled surface-deep exchange	80	5.6	39.6	0.86	0.81	0.81	-2.6	3.4	200	7
Doubled surface-deep exchange, Peff = 2	200	9.8	71.0	0.86	0.81	0.81	-3.3	4.1	350	7
Doubled surface-deep exchange, Peff = 7	50	2.8	18.56	0.86	0.81	0.81	-2.14	2.94	100	7
Doubled surface-deep exchange, diatom use = 0.6	300kyrs	9.3	43.2	1.48	0.95	0.81	-2.55	3.35	200Tmol/yr	7Tmol/yr
Doubled surface-deep exchange, surface dissolution = 25%	200kyrs	5.6	21.3	0.86	0.82	0.81	-2.19	2.3	200Tmol/yr	7Tmol/yr
Doubled circulation surface dissolution = 75%	300kyrs	5.6	57.8	0.86	0.81	0.81	-3.01	3.81	200Tmol/yr	7Tmol/yr

Table 5.2 Steady state model outputs.

5.3 Results

From the minimum in sponge $\delta^{30}Si$ at ~32 Ma, which was documented in the previous chapter, values rebound from −3.35‰ at ~31.8 Ma to an average of −2.77±0.29‰ between 30 Ma and 25.5 Ma (n=6, Figure 5.6). The average of values during the period of the Miocene and very earliest Pliocene presented here (18 and 4 Ma) is −2.58±0.38‰ (n=25). Thus, there is no discernible difference between the Oligocene subsequent to 31.5Ma and the Miocene/earliest Pliocene. However, these averages are higher than the minimum of the Early Oligocene, and are also higher than the modern value at this site, which was estimated in the previous chapter to be around −3.5‰ (Grey bar, Figure 5.6). It is noted that the data are very noisy, sometimes oscillating around the average value by as much as 0.8‰ between subsequent data points. This

noise is likely to be an inherent component of the silicon system and this will be expanded on below. In as far as an interpolation can be made across the gap in the record encompassing the Oligocene−Miocene boundary, the average silicic acid concentration at site 689 appears to have been relatively stable between 31 Ma and 4 Ma. This requires that between the last point of the record at approximately 4 Ma, and the modern day, the silicic acid concentration at intermediate depths in the Atlantic Sector of the Southern Ocean must have increased by between 40 and 80μM (using the modern calibration of Hendry and Robinson, 2012).

Diatom $\delta^{30}Si$ remains stable at values very similar to, though slightly higher than, those measured just subsequent to the Eocene−Oligocene Boundary. An average of 1.91±0.16‰ (n=6) occurs between 28.6 and 24.2Ma, as compared to +1.76±0.3‰ between 33.8 and 32.9Ma. The straightforward interpretation of this data is that diatom utilisation at site 1090 remained relatively constant across the Oligocene, despite the shift to lower silicic acid concentrations at site 689 at around 31Ma. It is reiterated that, as noted in the previous chapter, these values are very similar to modern diatom $\delta^{30}Si$ measured in the vicinity of this site (Grey bar, Figure 5.6). This is supportive of the hypothesis submitted therein that by the beginning of the Oligocene, diatoms had adapted to be prolific users of surface water silicic acid in the Southern Ocean north of the polar front, as they are in the modern day.

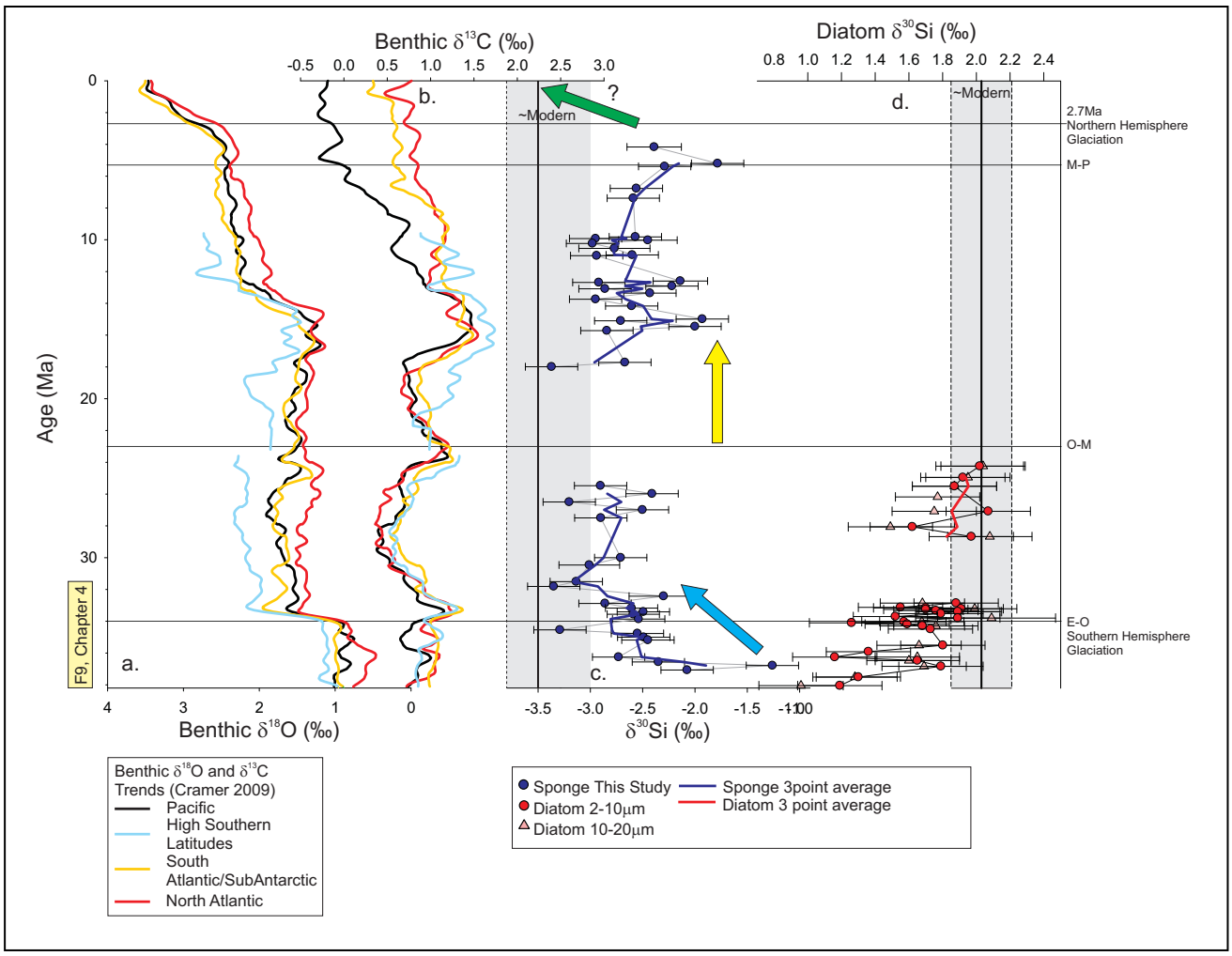


Figure 5.6 Cenozoic record of sponge $\delta^{30}Si$ with the Oi1 event indicated by ~1.5‰ positive excursion in; **a.** benthic foram $\delta^{18}O$ at ~33.7Ma, and the onset of Northern hemisphere glaciation by a further increase at ~2.7M (stacks from Cramer et al. (2009)); **b.** $\delta^{13}C$ benthic foram stacks for each ocean basin from Cramer et al. (2009); **c.** Sponge $\delta^{30}Si$, dark blue line = three point running mean, grey bar is the modern value estimated using a silicic acid concentration of ~120μM and the modern calibration of Hendry and Robinson (2012); **d.** Diatom $\delta^{30}Si$; red circles = 2−10μm fraction, pink triangles = 10−20μm fraction, red line = 3 point running mean. Grey bars are the estimated modern $\delta^{30}Si$ diatom or sponge values.

5.4 Discussion

Average silicic acid concentrations between 31 and 4 Ma at site 689 appear stable and high relative to the modern day. After an initial consideration of the noise observed in the sponge $\delta^{30}Si$ dataset, the following discussion explores why the silicic acid concentration at site 689 may have been driven to lower values for such a long period of time compared to the modern day, and what mechanisms may have facilitated the return to high concentrations. Finally, this portion of the record will be considered in concert with the Eocene−Oligocene record presented in the previous chapter to provide an overview of the evolution of the Cenozoic Southern Ocean silicon cycle. However, before beginning the discussion, two key points must be made.

First, it is necessary to establish which water mass site 689 is believed to have sampled over the time period of interest. A cross section of the Southern Ocean showing the maximum and minimum palaeodepth for site 689 is presented in Figure 5.7a. Site 689 is situated at the eastern extremity of the Weddell Gyre (Barker et al., 1990). The Weddell Gyre is an important region of deepwater formation feeding Antarctic Bottom Water (AABW). Thus, today the site monitors the nutrient status of upwelled Circumpolar Deepwater (CDW) that sinks in the Weddell Gyre and contributes to AABW (Figures 5.7a). This feature of the Southern Ocean circulation is a direct result of the presence of the Antarctic Circumpolar Current (ACC). As eluded to in Chapter 4, a deepwater connection and a resultant circum−Antarctic current were likely in place by the Early Oligocene (Stickley et al., 2004; Mackensen, 2004; Livermore et al., 2007; Cramer et al., 2011; Katz et al., 2011) and the sponge $\delta^{30}Si$ record subsequent to 31Ma is thus considered to record the silicic acid concentration of CDW (or its precursor water mass) and the subsequently formed Southern Component Water (SCW, likened to modern day AABW). Site 689 subsided from around 1200m at 60 Ma (approximately 1500m at the Eocene-Oligocene Boundary) and at the modern day is situated at 2080m. There is no change in silicic acid concentration over this depth today (Figure 5.7a), and as a result subsidence is not considered to be a controlling factor of sponge $\delta^{30}Si$ evolution.

Secondly, it is noted that two of the mechanisms described in the introduction have implications for whole ocean $\delta^{30}Si$, which would shift sponge $\delta^{30}Si$. If large changes in the riverine flux occurred, they would cause a shift in the relative importance of river silicon inputs, with $\delta^{30}Si$ of ~+1‰, compared to the hydrothermal input of ~−0.3‰. The maximum possible change in deepwater $\delta^{30}Si$ caused by changes in riverine input was found to be around 0.4‰ in the modelling work of De La Rocha and Bickle (2005). In the same work, increasing the output of opal relative to the riverine input was found to drive a maximum deepwater $\delta^{30}Si$ shift of ~0.8‰. Whole ocean changes in $\delta^{30}Si$ are considered highly unlikely to have caused the changes in sponge $\delta^{30}Si$ in the Cenozoic record. None of the suggested mechanisms have the power to change the whole ocean isotopic signature of silicic acid in the deep ocean without changing its concentration. The magnitude of $\delta^{30}Si$ shifts (0.2-0.8‰) modelled by De La Rocha and Bickle (2005) has a negligible effect on sponge $\delta^{30}Si$ compared to the change in the sponge fractionation factor (−1 to −6.5‰) brought about by changes in silicic acid concentration. Other changes, such as the balance of water supplied via rivers and ground water, can also only produce isotopic shifts on the magnitude of ~0.3‰, and would also be associated with changes in silicic acid supply. Therefore whole ocean changes are not further discussed here. It should also be noted that in the equation for sponge $\delta^{30}Si$ used in this version of the De La Rocha and Bickle (2005) model, any change in the silicon isotope composition of the deepwater from which sponge spicules form is already accounted for.

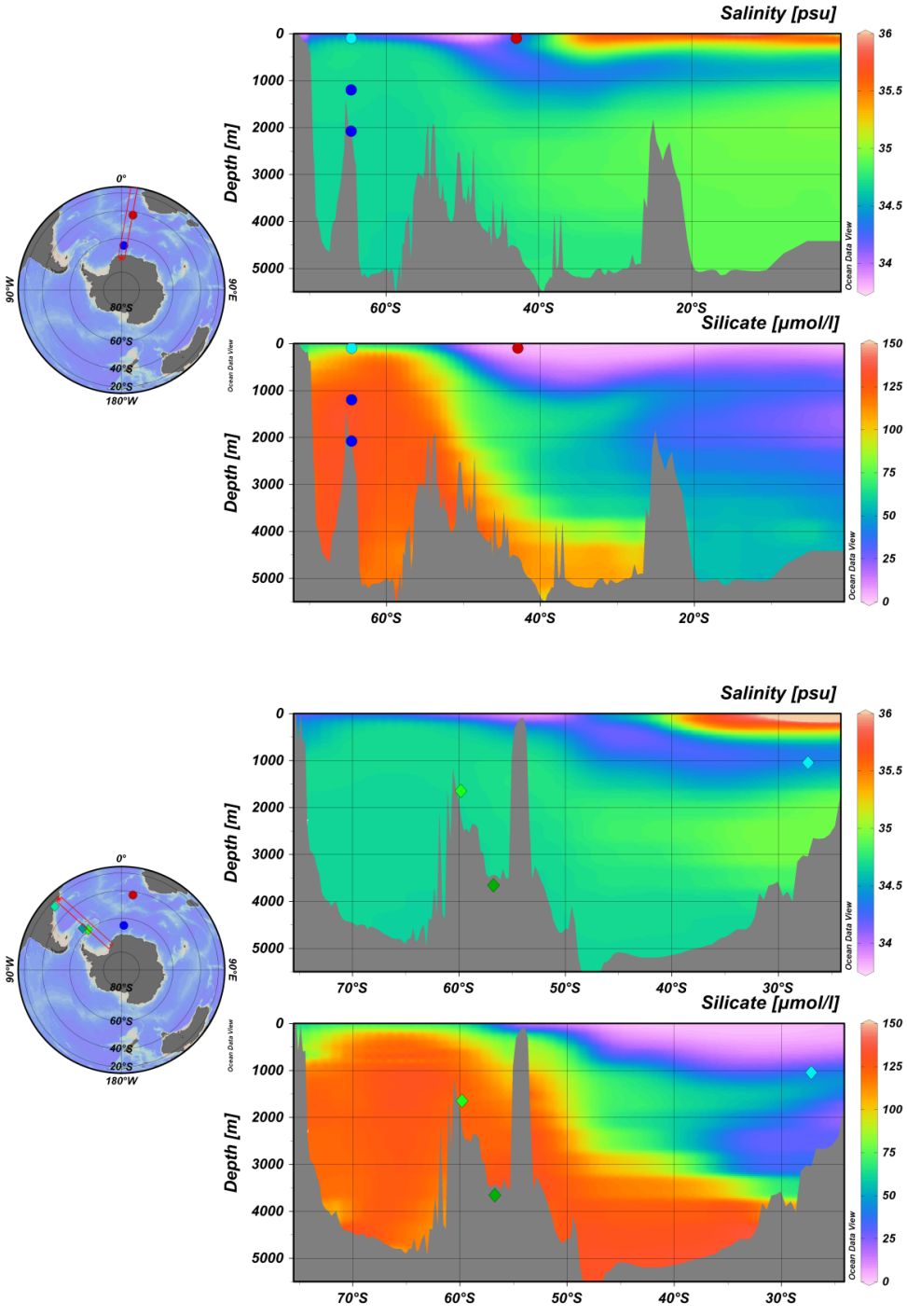


Figure 5.7 a. Location of sites 689 (dark blue) and 1090 (red) on profiles of salinity and silicic acid concentration. The two blue dots show the total range of subsidence of site 689 through the Cenozoic, over which neither salinity nor silicic acid changes; **b**. Locations of the sites used to produced the three Glacial−Interglacial records compared to the Miocene of site 689 in Figure 5.8 (below). It can be seen that in the modern ocean, the two more southerly sites sample similar high silicic acid Circumpolar Deepwater to site 689. Latitudes and longitudes of the sites discussed are given in Table 5.3. Figure produced using ODV and the World Ocean Atlas 2009.

5.4.1 Origin of noise in the Sponge δ^{30}Si Record

Miocene sponge δ^{30}Si is compared to three Glacial−Interglacial records from the South Atlantic (Figure 5.7 and Table 5.3) in Figure 5.8 (Hendry et al., 2010; Hendry et al., 2012). Miocene δ^{30}Si values at site 689 do not stray outside the range of glacial−interglacial sponge δ^{30}Si observed at the two sites in the Southern Ocean that sample CDW (Figures 5.7a and 5.8, labelled CDW−N and CDW−S). Average Miocene values are more akin to the higher deglacial sponge δ^{30}Si, recorded at the more northerly site, than to modern values. This provides some confidence that although the δ^{30}Si record is generated from some of the oldest sponge spicules used to date, their isotopic composition is robust. Over the 20kyrs encompassed by the glacial-interglacial records there are variations in sponge δ^{30}Si of greater than 1‰. Given the resolution of the Cenozoic record is around 500kyrs, it is not surprising to observe seemingly rapid fluctuations of the same magnitude. It is noteworthy that in contrast, diatom δ^{30}Si remains relatively stable (given analytical precision of ±0.25‰), once modern day values are reached (acknowledging that Oligocene data is sparse).

The variability in subsurface silicic acid concentration recorded by sponge δ^{30}Si, and the stability of diatom δ^{30}Si observed subsequent to ~33.5M, may be inherent features of the marine silicon cycle. Chapter 4 argues that diatoms underwent major expansion around the Eocene-Oligocene boundary. Once dominant, diatoms almost completely stripped silicon from the surface ocean, as is the case in the majority of the modern ocean (Brzezinski and Nelson, 1996; De La Rocha, 2007). Therefore, when more silicic acid is supplied to the surface, diatoms utilise it to the same extent and diatom δ^{30}Si remains reasonably constant. Subsurface silicic acid concentrations, as monitored by sponge δ^{30}Si, are more sensitive to changes in the inputs and outputs of silicon to and from the ocean (De La Rocha and Bickle, 2005) and, at a given location, to changes in ocean circulation (Hendry and Robinson, 2012). The contrasting response of sponge and diatom δ^{30}Si to perturbations of the marine silicon cycle can be demonstrated using the model of De La Rocha

and Bickle (2005) by increasing the input flux to the oceans by 1.5 times. The new steady state, with significantly increased deepwater silicic acid but identical diatom $\delta^{30}Si$ compared to the 'modern' conditions, is reached by 200 kyrs (Table 5.2). Due to the relatively short residence time of silicon in the ocean (~15000 years Treguer et al, 1995), and because the distribution of silicic acid is influenced by the overturning circulation (occurring today on a timescale of around 1000 years), changes in deepwater silicic acid concentration either of this nature, or driven by a redistribution of silicic acid between water masses, will appear to be instantaneous at the resolution of the Cenozoic record. This is further highlighted by noting that in Table 5.2 any perturbation considered reaches equilibrium in less than the 500 kyr resolution of the sponge $\delta^{30}Si$ record.

Site	Latitude	Longitude	Depth
113-689	-64.52	3.10	1200(60Ma)-2080m(modern
177-1090	-42.91	8.90	3702m
GeoB2107-3	-27.18	-46.45	1048m
PC034	-59.79	-39.69	1652m
KC081	-56.74	-42.97	3662m

Table 5.3 Locations and depths of cores referred to in this chapter.

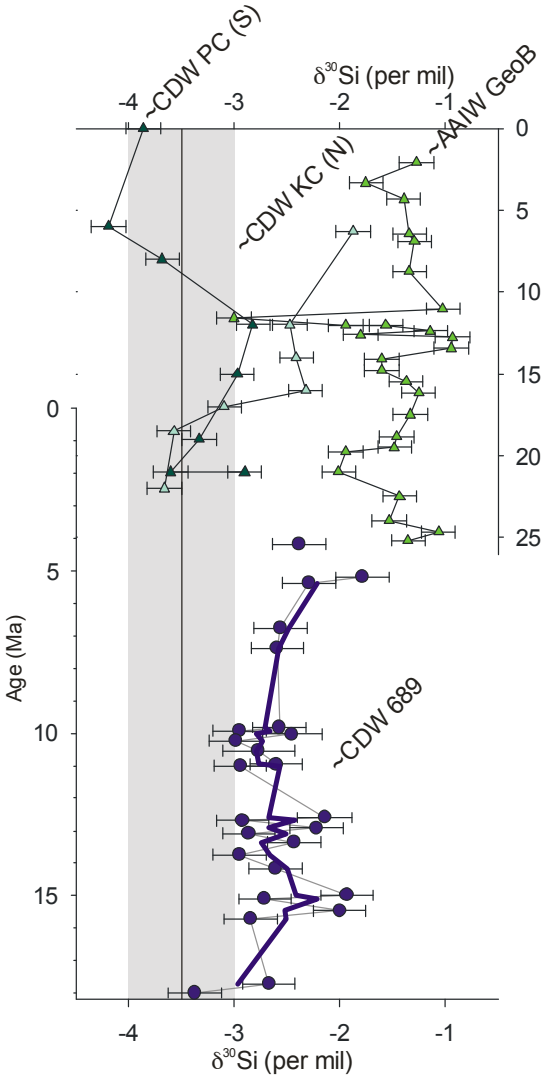


Figure 5.8 Comparison of Miocene $\delta^{30}Si$ from site 689 with the glacial−interglacial records of Hendry et al. (2012) from the South Atlantic (locations in Figure 5.7). Miocene $\delta^{30}Si$ is within the range of glacial interglacial values from the two southern most glacial-interglacial core locations. CDW−N and CDW−S correspond to the two sites sampling Circumpolar Deep Water, N being the more northern site, and S being the more southern site. AAIW = Antarctic Intermediate Water, which is the water mass inferred to predominantly bath this site. Core codes correspond to those given in Table 5.3.

5.4.2 Low Silicic Acid Concentrations in the Oligocene and Miocene

The sponge $\delta^{30}Si$ record demonstrates that for the majority of the Oligocene, through the Miocene, and into the earliest Pliocene, silicic acid concentrations in the subsurface high latitude south Atlantic were lower than they are today (an interpretation in terms of silicic acid is justified by its much larger effect on sponge $\delta^{30}Si$ than whole ocean $\delta^{30}Si$ change, as discussed above). In this section mechanisms that may have driven sustained low silicic acid concentration are examined. Initially, straightforward changes in the input and output of silicon to and from the ocean are considered, but are found to be incompatible with observations. Consequently, changes in ocean circulation are demonstrated to be a plausible explanation for the observed silicon isotope record, consistent with the previous interpretation of the Eocene-Oligocene boundary data in Chapter 4.

5.4.2.1 Input and output fluxes of silicon

Arguably the simplest way to explain low silicic acid concentrations during the Oligocene and Miocene would be a sustained minimum in the supply of silicic acid via riverine runoff. However, this would appear to be at odds with osmium, lithium and strontium isotope records which when considered together indicate enhanced continental silicate weathering through the Cenozoic (Hodell et al., 1991; Pegram et al., 1992; Misra and Froelich, 2012). In particular, lithium isotopes indicate rather stable values through the Oligocene followed by a dramatic rise during the Miocene, and a levelling at around 6 Ma. This in turn implies an increase in the supply of silicic acid to the oceans through the Miocene compared to the Oligocene, which is at odds with the stable values. An increased supply of silicic acid to the ocean may alternatively be considered to have increased opal preservation efficiency (both due to diatom production and deepwater silicic acid concentration). The model sensitivity to changing preservation efficiency when riverine inputs were increased was tested, and the results are shown in Table 5.2. In order to decrease silicic acid concentration with increased riverine inputs, opal preservation efficiency

had to be tripled to 14% preservation. Whilst 14% preservation is not outside the range of modern observations (from 0 up to 15-24% in areas with diatom rich sediments (Nelson et al., 1995)), given the modern average of 3%, globally this value seems unrealistically high. In addition, the effect of increasing preservation efficiency in the model is to decrease silicic acid concentration and diatom production, both of which would be expected to lower preservation efficiency (Van Capellen et al., 2002). This effect is suggestive of a negative feedback loop that limits the degree to which oceanic silicic acid concentrations can be drawn down by increased preservation of diatom opal. Thus, although this result raises a potential caveat to ruling out a weathering input mechanism driving higher sponge $\delta^{30}Si$, it seems unlikely to have been plausible in the real ocean. These observations suggest that changing riverine silicon inputs to the oceans did not cause the sustained low silicic acid concentrations of the Oligocene and Miocene. An increase in the weathering rate between 4Ma and the modern day, which would explain the implied return to today's high concentrations, is also not supported by the isotopic records, as the lithium record does not change during this time, and the gradient of the strontium curve is decreased relative to the Oligocene and Early Miocene.

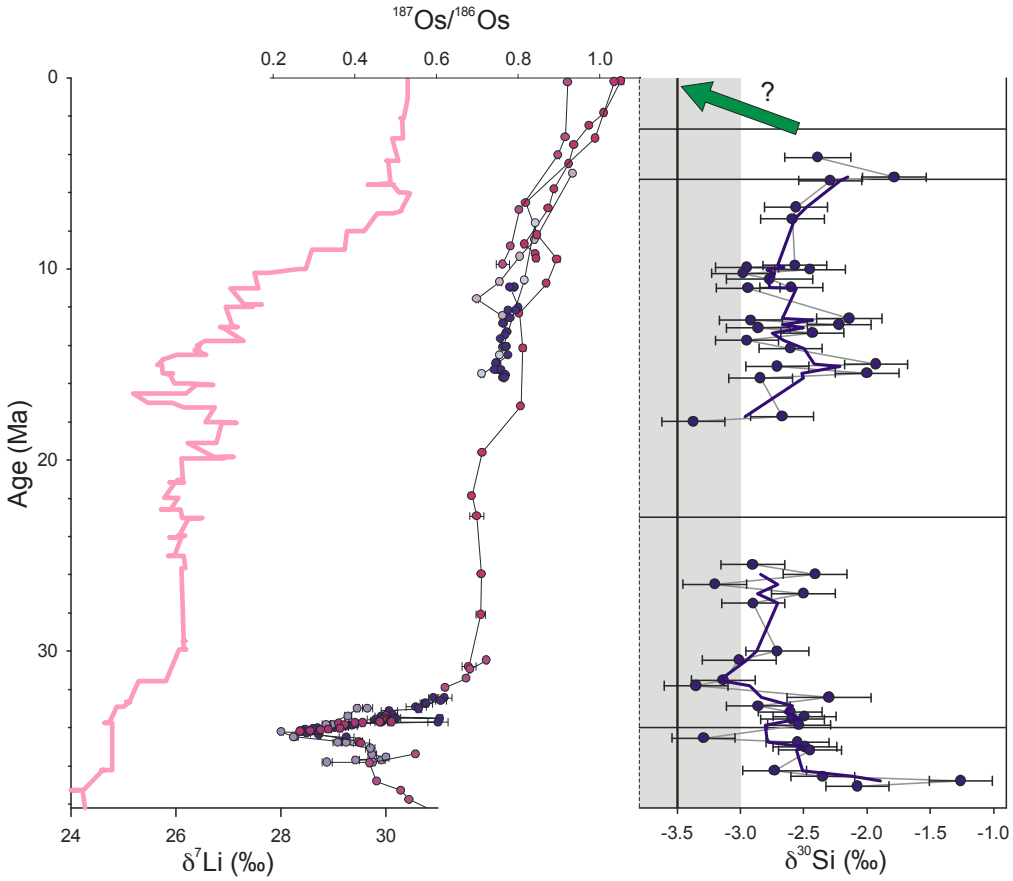


Figure 5.9 Comparison of Cenozoic sponge $\delta^{30}Si$ to lithium and osmium isotope records (Misra and Froelich, 2012 and references therein). There is no clear correspondence between sponge $\delta^{30}Si$ record either of these systems.

An alternative mechanism able to drive lower subsurface silicic acid concentrations is high diatom production (and therefore opal burial) relative to the input of silicic to the ocean (De La Rocha and Bickle. 2005). As documented in Chapter 4 and further demonstrated by the extended diatom $\delta^{30}Si$ record in Figure 5.6, high levels of diatom silicic acid utilisation were established by the Early Oligocene. In Chapter 4, diatom expansion is invoked to have played a major role, through this mechanism, in depositing opal on the floor of the Southern Ocean during the Late Eocene and the Early Oligocene. Indeed, it may well have drawn down the silicic acid concentration of the oceans. However, as has also been demonstrated in Chapter 4, the silicic acid concentration at site 689 over this time period was almost certainly controlled by a switch in the water mass bathing the locality, not by changes in the whole ocean silicic acid concentration. As

such the rise in silicic acid concentration that occurred at around 31 Ma is likely due to a mixture of processes entailing diatom utilisation and ocean circulation. This will be further discussed in section 5.4.3, and the following consideration, of the influence of whole ocean changes in the silicon cycle, will be limited to considering the difference in silicic acid concentration between the modern day (~120μM), and the low values (~40-80μM) prevailing though the majority of the Oligocene and Miocene. What can be stated in this regard is that a mechanism involving diatom radiation does not seem able to explain the shift to the higher concentrations of the modern, as this would require a decrease in relative silicic acid utilisation at odds with the observation that diatoms are still predominantly silica limited (De La Rocha, 2007; Brzezinski and Nelson, 1996).

5.4.2.2 Ocean Circulation as a driver of low silicic acid concentrations

If neither the stable low in average silicic acid concentrations, nor the increase in silicic acid concentration between the Oligocene-Miocene subsurface ocean and that of the modern, can be explained by changes in riverine flux or the relative utilisation of surface ocean silicic acid by diatoms, the next obvious route to explore is changing ocean circulation. An interesting feature of the box model is that increasing the upwelling flux of water to the surface ocean decreases the silicic acid concentrations of the deep (Figure 5.10a and b show the response to either doubling or halving of the upwelling term). The higher rate of exchange supplies more silicic acid to the surface, allowing the diatoms to drawdown a larger portion through enhanced opal burial. As a result, when steady state is reached, the whole ocean has a lower silicic acid concentration, which is expressed dominantly in the concentration of the deep box. The sensitivity of this result to changes in preservation efficiency, diatom silicic acid utilisation, and surface dissolution are considered in Table 5.2. The only mechanisms tested which could act to counter an increase in sponge $\delta^{30}Si$ associated with increased surface-deep exchange are; a lower preservation efficiency, decreased diatom utilisation coupled with lower preservation efficiency, and higher surface dissolution. As previously discussed in section 5.4.2.1, mechanisms involving changing preservation efficiency are suggested to enter a negative feedback loop. For example decreased

preservation efficiency actually increases the total biogenic production because silicic acid concentration increases – increased production and silicic acid concentration would both be expected to drive preservation efficiency back towards higher values. Thus the first two mechanisms are not considered to be major caveats to this hypothesis. Increasing surface dissolution to 75% (which is within the range of modern ocean observations, Nelson et al., 1995) has the potential to dampen the increase in sponge $\delta^{30}Si$ caused by faster surface-deepwater exchange. However, as increased surface-deepwater exchange does not change silicic acid concentration or diatom production in the surface ocean compared to the 'Quaternary' situation (Table 5.2), higher surface dissolution requires an alternative driving mechanism, for example changes in diatom specific surface area, grazing or aggregation, the likelihood of which are difficult to assess. Thus, increased surface-deepwater exchange still seems a plausible mechanism to drive a steady state baseline of lower silicic acid concentrations during the Oligocene and Miocene relative to the modern day (Figure 5.6).

Is there any evidence for a change in circulation between 4 Ma and today? The work of Haug et al. (1999), Sigman et al. (2004), and Haug et al. (2005) provides sedimentary evidence for enhanced stratification resulting from colder temperatures in both the sub−Arctic North Pacific and the Southern Ocean from 2.7Ma. Therefore, we have evidence that prior to this time, during the Oligocene and Miocene, the rate of surface-deepwater exchange may have been substantially higher than today. This fits well with the lower silicic acid concentrations we observe, and with the hypothesis that a greater rate of surface-deepwater exchange drove a steady state ocean containing less silicon. The evidence for a change in stratification at 2.7Ma is actually part of a larger body of evidence suggesting that in general enhanced stratification in these regions is a feature of cold periods (Francois et al., 1997; Robinson, 2004; Jaccard et al., 2005; Brunelle et al., 2007). The modelling work of de Boer et al. (2007) indicates that this is due to a lessening of the importance of the surface ocean temperature gradient, relative to the salinity gradient, in controlling the formation of deepwater as water temperatures approach freezing (although the

Southern Ocean mechanism may alternatively or additionally be related to decreased buoyancy flux during cold periods; Watson and Naveira-Garabato, 2006). This leads to decreased convection in regions that have strong haloclines, such as the North Pacific and the Southern Ocean. On the other hand, overturning increases in the North Atlantic because the positive salinity buoyancy is smallest among the polar regions. The overall effect is to decrease surface-deepwater exchange, creating a build up of nutrients in the deep ocean as the rate of nutrient supply to the surface is reduced significantly.

Indeed, there is also evidence that this switch in stratification affected changes in the silicon cycle. Decreased deposition of opal is documented in the Southern Ocean and the North Pacific at 2.7Ma (Haug et al., 1999; Sigman et al., 2004; Haug et al., 2005). The work of Cortese et al. (2004) shows additionally that subsequent to 2.7Ma, the main opal burial sinks of the global ocean become limited to the polar front of the Southern Ocean and the Eastern Equatorial Pacific, which correspond to the modern day burial pattern. Today, these are the only major regions where silicic acid can escape the deep ocean via upwelling. The available data suggest that, prior to the onset of northern hemisphere glaciation, when surface-deepwater exchange was not so effectively capped by the salinity of the North Pacific and the resupply of nutrients was faster in the Southern Ocean, opal deposition was possible in other regions of the world oceans. What is inferred at 2.7Ma is limitation of silicic acid supply to the Southern Ocean and EEP, and the sequestration of the silicic acid pool into the deep ocean. It is noted that in order to further substantiate this hypothesis a record spanning the gap in the Cenozoic sponge $\delta^{30}Si$ record is required.

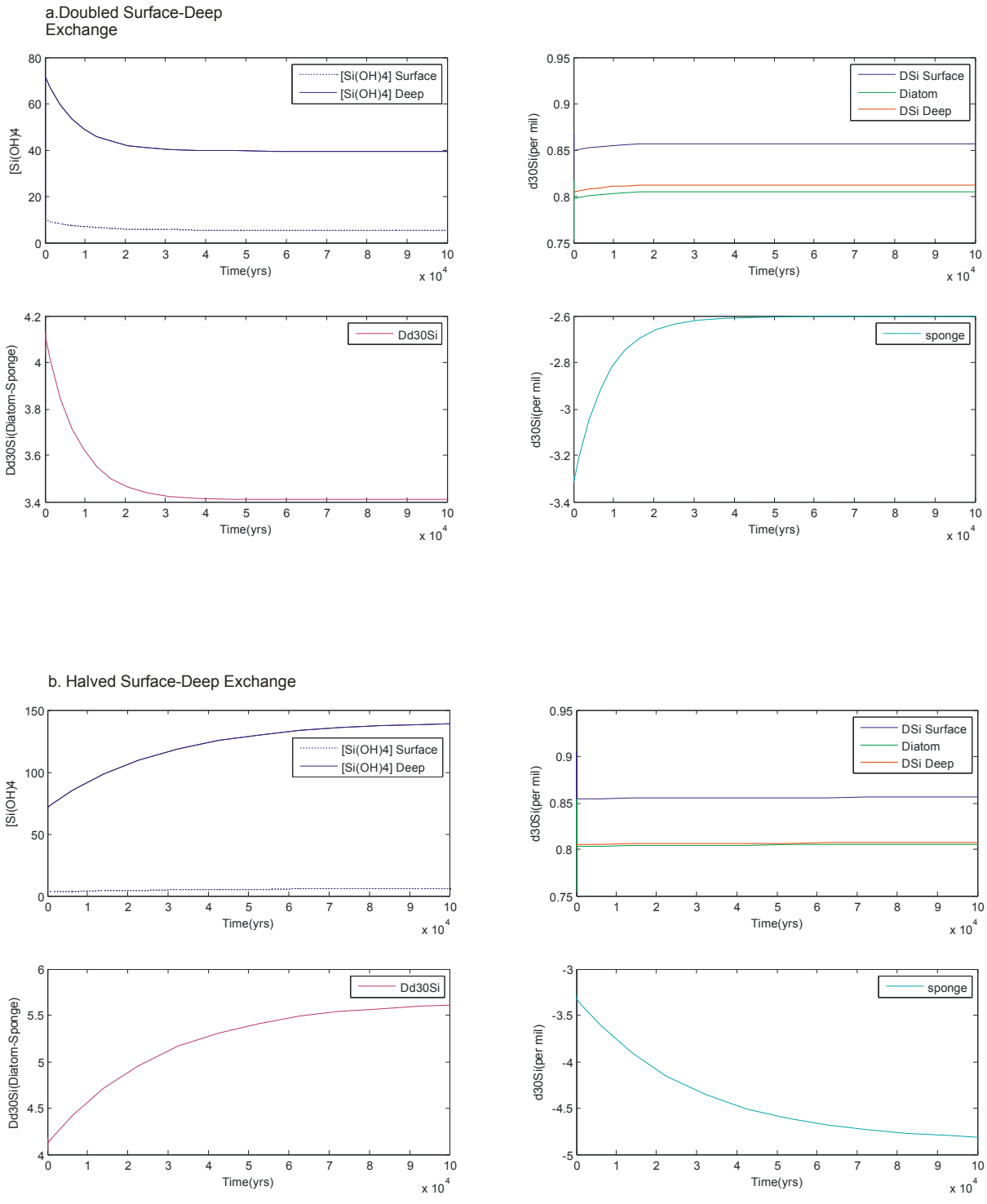


Figure 5.10 Response of the two box model to; **a.** a doubling of the rate of exchange between the deep and surface boxes and; **b.** a halving of the rate of exchange between the deep and surface boxes. Increasing the rate of exchange decreases the concentration of silicic acid in the deep ocean, whilst a halving causes an increase.

It is interesting to consider that this sequestration of silicic acid into the deep ocean, and particularly into SCW, may entail a positive feedback process. Today the Southern Ocean contains very heavily silicified diatoms that contain up to 6 times more Si by volume than those in other regions of the world oceans and, as a result, drive more efficient removal of silicic acid from the surface (Baines et al., 2010). Baines et al. (2010) show this high silicification is a characteristic of the resident diatom community, which they infer to have been shaped over time in response to the prevailing ecological, chemical and physical settings. The onset of stratification in the polar regions, associated with the onset of northern hemisphere glaciation, may have driven this ecological development, further limiting silicic acid to this region. This would be an interesting area for further study, as it has implications not only for understanding the geological silicon cycle, but also changes in the biological pump. The high ratio of Si:N of diatoms in the Southern Ocean leads to the export of waters relatively enriched in nitrate to lower latitudes, suppressing lower latitudes diatom production and having key implications for the efficiency of the global biological pump and climate (Sarmiento and Orr, 1991; Sarmiento et al., 2004; Marinov et al., 2006).

5.4.2.3 Middle−Late Miocene increase in North Atlantic Deepwater Formation

There is the hint of a trend towards more positive values of sponge $\delta^{30}Si$ in our record between ~10 Ma and 5 Ma. This occurs during a period when the strength of NADW formation is thought to have been increasing, both due to deepening of the Greenland−Iceland sill and the closure of the Central American Seaway (Poore et al., 2006; Cramer et al., 2011). It is possible that the increase in sponge $\delta^{30}Si$ could be related to the influx of an increasing amount of silicic acid poor NADW to the South Atlantic. However, because NADW supplies low silicic acid to the Southern Ocean, and its strength is considered to have increased from ~15Ma to the modern day, it is unlikely to be able to explain the low stable values of the Oligocene and Miocene or the shift to higher modern concentrations subsequent to 4Ma.

5.4.3 Synthesis of Cenozoic Silicon Cycle Evolution

Many studies document an increase in the strength of ocean overturning subsequent to the Eocene (e.g. Diester-Haass, 1995; Diester-Haass and Zahn, 1996; Diester-Haass and Zahn 2001; Katz et al., 2005; Scher and Martin 2006; Cramer et al., 2009). These changes are inferred to result from the opening of Southern Ocean gateways to circum−Antarctic current flow. Taken at face value, the increasing silicic acid concentrations documented by sponge $\delta^{30}Si$ through the Late Eocene and Early Oligocene (Figure 5.6) would appear to be at odds with the theory presented for the latter Cenozoic; increasing circulation should act to drawdown silicic acid from the subsurface ocean. However, the key difference during the late Eocene is evidence for the incursion of a new Pacific sourced water mass into the high latitude South Atlantic (Scher and Martin, 2006). Prior to the onset of upwelling, sedimentological and modelling studies have shown that the Southern Ocean was likely to have been a region dominated by sinking of surface water (Diester-Haass, 1995; Heinze and Crowley, 1997; Sijp et al., 2011). This would have created a southern hemispheric circuit that drew in warm and salty water from the low latitudes, in a situation analogous to the modern day North Atlantic. Without circum−polar water flow, there would have been little to no upwelling in the Southern Ocean, no exchange between the Pacific and Atlantic Basins, and thus ocean overturning would have been sluggish (Cramer et al., 2009). During this time of decreased circulation, this theory suggests that silicic acid would have been locked in the deep ocean, and, being the largest of the Eocene basins, may well have been concentrated in old deep Pacific waters (Cramer et al., 2009). With increased upwelling caused by the development of a circum−Antarctic current and an influx of waters from the Pacific, nutrients would have been supplied to the Southern Atlantic and hence to site 689. This in agreement with the work of Schumacher and Lazarus which suggests that at or before the Eocene Oligocene boundary there was a shift from opal deposition in the Equatorial Pacific to the Southern Ocean. As such, the change at site 689 is actually dependant on the sequestration of nutrients resulting from reduced Eocene deepwater ventilation, in agreement with our hypothesis

that during the latter Cenozoic changes in this parameter dictate the silicic acid content of the subsurface ocean.

In summary, evolution of the Southern Ocean Cenozoic silicon cycle can be outlined in three main stages:

1) 38−31.5Ma: Incursion of silicic acid rich deepwater into the Southern Ocean resulting from the subsidence of gateways and coincident with the radiation of diatoms numbers to near modern values (blue arrow, Figure 5.6);

2) 31Ma−2.7Ma: Sustained lower silicic acid concentrations caused by relatively high rates of surface-deepwater exchange that resulted from the onset of circum-Antarctic current flow and which were possibly exacerbated by increased meridional temperature gradients (note this is a whole ocean decline which only became visible at site 689 when the inflow of water from the Pacific, and its silicic acid concentration, have reached a stable level, yellow arrow in Figure 5.6);

3) 2.7Ma onward: Return to higher silicic acid concentrations caused by reduced rates of overturning circulation associated with the onset of Northern Hemisphere glaciation (green arrow in Figure 5.6).

The overarching inference is that the oceans circulation regime, coupled with intense diatom silicic acid utilisation, played a dominant role in defining marine silicon cycling through the Cenozoic.

5.4.4 Links to pCO_2 through the Cenozoic

The two phases of change in the marine silicon cycle, documented across the Eocene-Oligocene Boundary and inferred at 2.7Ma, are both periods of declining pCO_2 (Figure 5.11; Pagani et al., 2005; Seki et al., 2010; Pagani et al., 2011). Association between the Eocene radiation of diatoms and declining atmospheric pCO_2 has already been extensively discussed in Chapter 4. Because

the 2.7Ma shift is based largely on inference, discussion of pCO_2 decline is limited to simply note that the sequestration of nutrients (and hence silicic acid) in deepwater, associated with the slowdown of overturning circulation, may drawdown pCO_2 through enhanced carbon storage in the deep ocean (Sigman et al., 2004; de Boer et al., 2007). It is also worth pointing out a fundamental difference in the link between the silicon and carbon cycles between the Eocene-Oligocene boundary and 2.7Ma. Across the Eocene-Oligocene boundary the silicon cycle perturbs the long term carbon cycle through diatom driven organic carbon burial and thus is interpreted to be a driver of atmospheric pCO_2 decline. Conversely, the changes in silicon cycling from the earliest Pliocene to the modern day act as a tracer of abyssal nutrient storage. Nutrient storage in the deep ocean is a mechanism driving short term fluctuations in the carbon cycle, and is associated with smaller shifts in atmospheric pCO_2. In this case deepwater silicic acid concentration is tracing a process that can effect atmospheric CO_2, rather than being itself a driver.

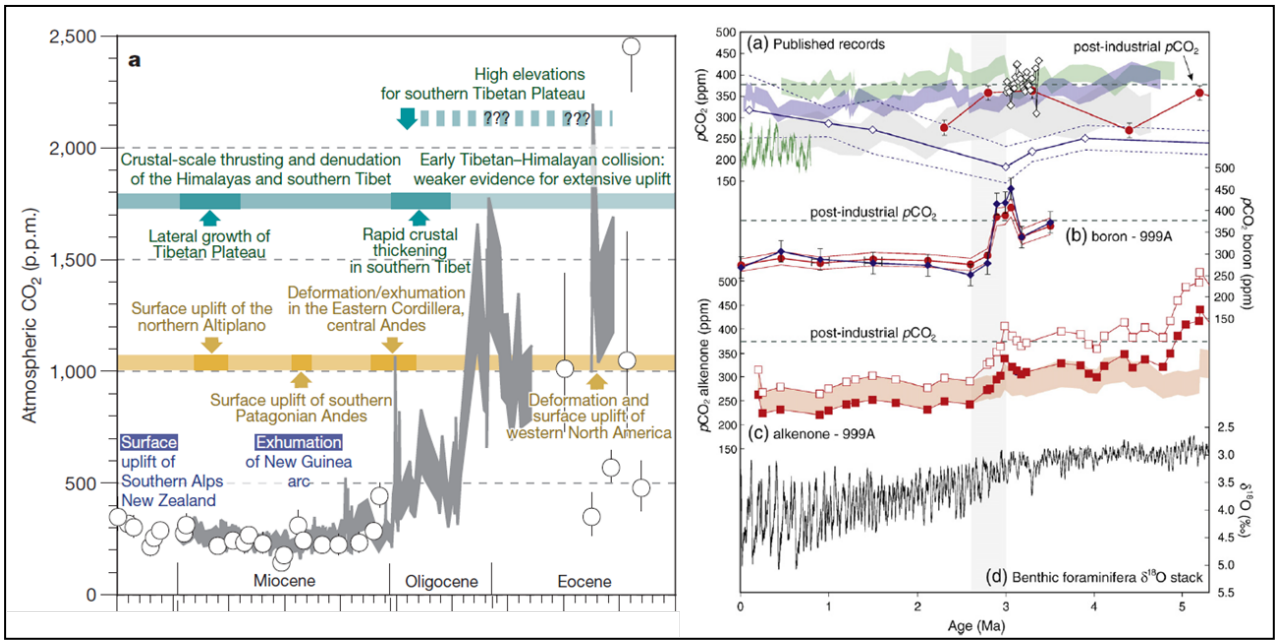


Figure 5.11 pCO_2 reconstructions from Pagani et al (2005 left) and Seki et al (2010 right), showing drops in pCO_2 across the Late Eocene–Early Oligocene and at ~2.7Ma. Note the large difference in the magnitude of the shifts.

5.5 Conclusions

I have presented the first long term record of sponge $\delta^{30}Si$. This has facilitated the reconstruction of subsurface silicic acid concentration in the high latitude south Atlantic and yields an unprecedented window on the functioning of the Cenozoic silicon cycle. The cause of a Late Eocene to Earliest Oligocene influx of silicic acid rich deep water from the Pacific is hypothesised to have been the subsidence of Southern Ocean gateways and coincidence diatom radiation. The record subsequently infers a stasis in average silicic acid concentration over around 27 Ma spanning the Oligocene and Miocene. The low silicic acid concentrations documented through this period, relative to the modern day, are interpreted to result from higher rates of deepwater ventilation. The greater supply of silicic acid to the surface, and its utilisation by the diatoms, output a greater proportion of the whole ocean silicic acid content relative to today. A steady state shift to an ocean with higher deepwater silicic acid concentration is hypothesised to have occurred as a result of increased Polar stratification associated with the onset of northern hemisphere glaciation. These are preliminary findings, and should in future be substantiated through higher resolution study, in particular of the period between 3Ma and the modern day. Additionally, further valuable insight into the Cenozoic silicon cycle could be gained from combined diatom and sponge $\delta^{30}Si$ records from the extremes of the modern overturning circulation, i.e. the sub−Arctic North Pacific and the North Atlantic.

Chapter 6. Conclusions

This thesis encompasses three bodies of work that together represent a significant advancement in the use of silicon isotope based proxies in palaeoceanographic reconstructions. A method has been developed to ensure the generation of consistent diatom $\delta^{30}Si$ values that represent robustly the environmental parameter of interest. Coupled with the first core top calibration of this proxy, an important development has been made for those fields concerned with understanding silicic acid utilisation, and more broadly, nutrient cycling. Further, the only application, thus far, of combined diatom and sponge $\delta^{30}Si$ records has proved to be a valuable investment in attempting to reconstruct the geological history of marine silicon cycling. This type of combined record paves the way towards a better understanding of the links between the silicon cycle and Earth's climate. In the following, the main conclusions taken from each chapter are laid out, and are followed by suggestions for future avenues of study.

6.1 Development of diatom $\delta^{30}Si$ as a proxy for silicic acid utilisation

Extensive work has been undertaken to develop diatom $\delta^{30}Si$ as a proxy for silicic acid utilisation in the surface ocean. Core top calibration of the Southern Ocean, entailing a first assessment of the contribution made by different components to measured $\delta^{30}Si$, has been presented. Through comparison of this latitudinal transect of core top diatom $\delta^{30}Si$ with modern surface water silicic acid concentrations, the extent to which simple models may allow quantitative reconstruction of past silicic acid utilisation has been assessed.

Size fraction purity exerts a major control over measured $\delta^{30}Si$ largely due to the inclusion of non-diatom components such as radiolaria, sponge spicules, and clay minerals that have distinct isotopic compositions. A consistent relationship between size and $\delta^{30}Si$, related to the proportions of diatom and non-diatom components in a sample, has been demonstrated. This study highlights

the potential for small amounts of non-diatom silica to significantly offset measured $\delta^{30}Si$ to lower values than diatom $\delta^{30}Si$. In order to create reliable downcore records of diatom $\delta^{30}Si$, it is essential to eliminate such contamination by selecting the correct size fraction for analysis. In general the 2-20μm fraction has been found most appropriate for core tops in this study, although this is not a hard and fast rule, and rather must be tailored to the sediment composition of each sample set.

When a pure diatom size fraction is selected, an extremely good correlation with in situ surface water minimum annual silicic acid concentration is documented (R^2=0.92). In comparison, larger size fractions (~20-50μm) exhibit a poorer correlation (R^2=0.66), again emphasising the need for size targeted analyses. Correlation with surface silicic acid concentration, and a good agreement between core top diatom $\delta^{30}Si$ and surface filtered diatom $\delta^{30}Si$, are highly supportive of the use of sedimentary diatom $\delta^{30}Si$ as a proxy for surface water silicic acid utilisation and indicate no significant effect of dissolution or early diagenesis. The better correlation with minimum annual silicic acid reflects the fact that diatom $\delta^{30}Si$ records the seasonal extent of silicic acid utilisation by diatoms, which should be kept in mind when interpreting diatom $\delta^{30}Si$ records. Core top diatom $\delta^{30}Si$ can be satisfactorily explained using steady state or Rayleigh fractionation without the need to invoke a variable diatom fractionation factor, as long as changes in the silicic acid concentration and $\delta^{30}Si$ from which diatom uptake occurs are properly accounted for i.e. it is not possible to model the entire Southern Ocean with a single set of initial conditions. This represents a major source of error in quantitative silicic acid utilisation reconstructions. However, it should not detract from the strong relationship that exists between sedimentary diatom $\delta^{30}Si$ and surface water silicic acid concentration, proving this to be a reliable qualitative proxy for silicic acid utilistaion.

6.2 The role of the Southern Ocean silicon cycle in the onset of Antarctic glaciation

The novel combination of the two opal based proxies, diatom $\delta^{30}Si$ and sponge $\delta^{30}Si$, has allowed the definition of a new parameter, $\Delta\delta^{30}Si$ (= diatom $\delta^{30}Si$ – sponge $\delta^{30}Si$). As diatom $\delta^{30}Si$ can be broadly interpreted as a measure of the surface silicic acid concentration, and sponge $\delta^{30}Si$ is dependent on the silicic acid concentration of bottom waters at the site of measurement, $\Delta\delta^{30}Si$ represents an approximation of the oceans vertical silicic acid gradient. One major benefit of this parameter is to eliminate the effect of long term changes in whole ocean $\delta^{30}Si$ from individual sponge and diatom $\delta^{30}Si$ records. Further, the $\Delta\delta^{30}Si$ record produced for the Eocene-Oligocene Boundary teases from the individual records powerful information regarding the development of the Antarctic Circumpolar Current and diatom radiation.

Increasing diatom $\delta^{30}Si$, interpreted in light of both opal accumulation rates and sponge $\delta^{30}Si$, has provided convincing evidence for diatom radiation during the Late Eocene of the Southern Ocean. Sponge $\delta^{30}Si$ shows increasing silicic acid concentrations at intermediate depths in the Antarctic Zone throughout the Late Eocene and Early Oligocene, coincident with the subsidence of Southern Ocean land bridges. The concomitant development of these two components, which are key in controlling the marine silicic acid distribution, also had major implications for organic carbon burial and global climate. A mechanistic link between the development of this system and Eocene-Oligocene pCO_2 drawdown exists through diatom driven burial of organic carbon triggered by intensified upwelling, supportive of the hypothesis that the biological carbon pump may have had a role to play in the onset of Antarctic glaciation.

6.3 The Cenozoic silicon cycle

The Eocene-Oligocene sponge $\delta^{30}Si$ record has been extended into the Oligocene, Miocene and very earliest Pliocene, yielding a long term reconstruction of silicic acid concentrations in Southern Ocean subsurface waters and providing a window to the functioning of the Cenozoic silicon cycle. The cause of a Late Eocene to Earliest Oligocene influx of silicic acid rich deep water from the Pacific is hypothesised to have been the subsidence of Southern Ocean gateways and coincident diatom radiation. The record subsequently infers a stasis of the average silicic acid concentration over around 27 Ma spanning the Oligocene and Miocene. The low silicic acid concentrations documented through this period, relative to the modern day, are interpreted to result from higher rates of surface-deepwater exchange. The greater supply of silicic acid to the surface, and its utilisation by the diatoms, output a greater proportion of the whole ocean silicic acid content relative to that of today. A steady state shift to an ocean with higher deepwater silicic acid concentration is hypothesised to have occurred as a result of increased Polar stratification associated with the onset of northern hemisphere glaciation. These are preliminary findings, and should in future be substantiated through higher resolution study, in particular of the period between 3 Ma and the modern day.

6.4 Future Directions

The work presented in this thesis has been based on a single key region of the global ocean, and has already furthered our understanding of the Cenozoic silicon cycle. However in order to tease apart changes in the overall deep water silicic acid concentration from the redistribution of silicic acid between water masses, and to gain a deeper understanding of the links between the silicon and carbon cycles, a more global perspective is required. The generation of coupled diatom-sponge $\delta^{30}Si$ records from the extremities of the meridional overturning circulation, in the North Atlantic and the North Pacific, may prove invaluable in this regard. They have not only the potential to develop our knowledge of the silicon cycle and its role in climate change, but also to provide insight into the timing and nature of perturbations and shifts in the meridional overturning circulation.

This work has suggested that diatom production was an important driver of organic carbon burial and climatic change at the Eocene-Oligocene boundary. However diatoms are thought to have evolved long before this, in the Jurassic, and the preservation of their frustules on the ocean floor suggests that radiation also took place through the Cretaceous and Early Cenozoic. Characterisation of diatom evolution and radiation, through the extension of diatom and sponge $\delta^{30}Si$ records into the Cretaceous, could further our understanding of how these micro-organisms may have played a role in both the long and short term carbon cycles and therefore in climate regulation. Records from time periods such as the Early Eocene Climatic Optimum would provide fascinating insight into the operation of the silicon cycle in a fundamentally different greenhouse world.

7. References

Anderson, L. D. and Delaney, M. L., (2005) Middle Eocene to early Oligocene paleoceanography from Agulhas Ridge, Southern Ocean (Ocean Drilling Program Leg 177, Site 1090). Paleoceanography. 20, doi: 10.1029/2004PA001043.

Baines, S. B., Twining, B. S., Brzezinski, M. A., Nelson, D. M., Fisher, N. S., (2010) Causes and biogeochemical implications of regional differences in silicification of marine diatoms. Global Biogeochemical Cycles. 24, doi:10.1029/2010GB003856.

Barker, P. F., Kennett, J. P., O'Connell, S., Berkowitz, S. P., Bryant, W. R., et al., (1990) Initial Report Leg 113. Proceedings of the Ocean Drilling Program: College Station, Texas, Initial Reports. 113, doi:10.2973/odp.proc.ir.113.1988.

Basile-Doelsch, I., (2006) Si stable isotopes in the Earth's surface: A review. Journal of Geochemical Exploration. 88, 252-256.

Berner, R. A., (2003) The long-term carbon cycle, fossil fuels and atmospheric composition. Nature. 426, 323-326.

Berner, R. A., (1990) Atmospheric Carbon Dioxide Levels Over Phanerozoic Time. Science. 249, 1382-1386.

Berner, R. A. and Caldeira, K., (1997) The need for mass balance and feedback in the geochemical carbon cycle. Geology. 25, 955-956.

Beucher, C. P., Brzezinski, M. A., Crosta, X., (2007) Silicic acid dynamics in the glacial sub-Antarctic: Implications for the silicic acid leakage hypothesis. Global Biogeochemical Cycles. 21, doi: 10.1029/2006GB002746.

Beucher, C. P., Brzezinski, M. A., Jones, J. L., (2011) Mechanisms controlling silicon isotope distribution in the Eastern Equatorial Pacific. Geochimica Et Cosmochimica Acta. 75, 4286-4294.

Beucher, C. P., Brzezinski, M. A., Jones, J. L., (2008) Sources and biological fractionation of Silicon isotopes in the Eastern Equatorial Pacific. Geochimica et Cosmochimica Acta. 72, 3063-3073.

Bohaty, S. M. and Zachos, J. C., (2003) Significant Southern Ocean warming event in the late middle Eocene. Geology. 31, 1017-1020.

Bohaty, S. M., Zachos, J. C., Delaney, M. L., (2012) Foraminiferal Mg/Ca evidence for Southern Ocean cooling across the Eocene–Oligocene transition. Earth and Planetary Science Letters. 317–318, 251-261.

Boyd, P. W., Watson, A. J., Law, C. S., Abraham, E. R., Trull, T., et al., (2000) A mesoscale phytoplankton bloom in the polar Southern Ocean stimulated by iron fertilization. Nature. 407, 695-702.

Broecker, W. S., (1991) The Great Ocean Conveyor. Oceanography. 4, 79-89.

Brunelle, B. G., Sigman, D. M., Cook, M. S., Keigwin, L. D., Haug, G. H., et al., (2007) Evidence from diatom-bound nitrogen isotopes for subarctic Pacific stratification during the last ice age and a link to North Pacific denitrification changes. Paleoceanography. 22, doi:10.1029/2005PA001205.

Brzezinski, M. A., Pride, C. J., Franck, V. M., Sigman, D. M., Sarmiento, J. L., et al., (2002) A switch from Si(OH)4 to NO- 3 depletion in the glacial Southern Ocean. Geophysical Research Letters. 29, 5-1 - 5-4.

Brzezinski, M. A., Dickson, M., Nelson, D. M., Sambrotto, R., (2003) Ratios of Si, C and N uptake by microplankton in the Southern Ocean. Deep Sea Research Part II: Topical Studies in Oceanography. 50, 619-633.

Brzezinski, M. A. and Nelson, D. M., (1996) Chronic substrate limitation of silicic acid uptake rates in the western Sargasso Sea. Deep Sea Research Part II: Topical Studies in Oceanography. 43, 437-453.

Buesseler, K. O., (1998) The decoupling of production and particulate export in the surface ocean. Global Biogeochemical Cycles. 12, 297-310.

Cande, S. C. and Kent, D. V., (1995) Revised calibration of the geomagnetic polarity timescale for the Late Cretaceous and Cenozoic. Journal of Geophysical Research. 100, 6094-6095.

Cardinal, D., Alleman, L. Y., De Jong, J., Ziegler, K., André, L., (2003) Isotopic composition of silicon measured by multicollector plasma source mass spectrometry in dry plasma mode. Journal of Analytical Atomic Spectrometry. 18, 213-218.

Cardinal, D., Alleman, L. Y., Dehairs, F., Savoye, N., Trull, T. W., André, L., (2005) Relevance of silicon isotopes to Si-nutrient utilization and Si-source assessment in Antarctic waters. Global Biogeochemical Cycles. 19, 1-13.

Cardinal, D., Savoye, N., Trull, T. W., Dehairs, F., Kopczynska, E. E., et al., (2007) Silicon isotopes in spring Southern Ocean diatoms: Large zonal changes despite homogeneity among size fractions. Marine Chemistry. 106, 46-62.

Carlisle, E. M., (1988) Silicon as a trace nutrient. Science of the Total Environment. 73, 95-106.

Casey, T. R. and Bamforth, C. W., (2010) Silicon in beer and brewing. Journal of the Science of Food and Agriculture. 90, 784-788.

Censarek, B. and Gersonde, R., (2002) Miocene diatom biostratigraphy at ODP Sites 689, 690, 1088, 1092 (Atlantic sector of the Southern Ocean). Marine Micropaleontology. 45, 309-356.

Channell, J. E. T., Galeotti, S., Martin, E. E., Billups, K., Scher, H. D., Stoner, J. S., (2003) Eocene to Miocene magnetostratigraphy, biostratigraphy, and chemostratigraphy at ODP Site 1090 (sub-Antarctic South Atlantic). Geological Society of America Bulletin. 115, 607-623.

Chapligin, B., Leng, M. J., Webb, E., Alexandre, A., Dodd, J. P., et al., (2011) Inter-laboratory comparison of oxygen isotope compositions from biogenic silica. Geochimica et Cosmochimica Acta. 75, 7242-7256.

Clarke, A., Meredith, M. P., Wallace, M. I., Brandon, M. A., Thomas, D. N., (2008) Seasonal and interannual variability in temperature, chlorophyll and macronutrients in northern Marguerite Bay, Antarctica. Deep-Sea Research Part II: Topical Studies in Oceanography. 55, 1988-2006.

Cortese, G., Gersonde, R., Hillenbrand, C., Kuhn, G., (2004) Opal sedimentation shifts in the World Ocean over the last 15 Myr. Earth and Planetary Science Letters. 224, 509-527.

Coxall, H. K., Wilson, P. A., Pälike, H., Lear, C. H., Backman, J., (2005) Rapid stepwise onset of Antarctic glaciation and deeper calcite compensation in the Pacific Ocean. Nature. 433, 53-57.

Coxall, H. K. and Wilson, P. A., (2011) Early Oligocene glaciation and productivity in the eastern equatorial Pacific: Insights into global carbon cycling. Paleoceanography. 26, doi: 10.1029/2010PA002021.

Cramer, B. S., Miller, K. G., Barrett, P. J., Wright, J. D., (2011) Late Cretaceous-Neogene trends in deep ocean temperature and continental ice volume: Reconciling records of benthic foraminiferal geochemistry ($\delta^{18}O$ and Mg/Ca) with sea level history. Journal of Geophysical Research C: Oceans. 116, doi: 10.1029/2011JC007255.

Cramer, B. S., Toggweiler, J. R., Wright, J. D., Katz, M. E., Miller, K. G., (2009) Ocean overturning since the late cretaceous: Inferences from a new benthic foraminiferal isotope compilation. Paleoceanography. 24, doi: 10.1029/2008PA001683.

Crosta, X. and Shemesh, A., (2002) Reconciling down core anticorrelation of diatom carbon and nitrogen isotopic ratios from the Southern Ocean. Paleoceanography. 17, doi: 10.1029/2000PA000565.

de Boer, A. M., Sigman, D. M., Toggweiler, J. R., Russell, J. L., (2007) Effect of global ocean temperature change on deep ocean ventilation. Paleoceanography. 22, doi: 10.1029/2005PA001242.

De La Rocha, C.L., (2007) The Biological Pump, in: Editors-in-Chief: Heinrich D. Holland, Karl K. Turekian (Eds.), Treatise on Geochemistry. Pergamon, Oxford, pp. 1-29.

De la Rocha, C. L., (2003) Silicon isotope fractionation by marine sponges and the reconstruction of the silicon isotope composition of ancient deep water. Geology. 31, 423-426.

De La Rocha, C. L. and Bickle, M. J., (2005) Sensitivity of silicon isotopes to whole-ocean changes in the silica cycle. Marine Geology. 217, 267-282.

De La Rocha, C. L., Brzezinski, M. A., Deniro, M. J., (2000) A first look at the distribution of the stable isotopes of silicon in natural waters. Geochimica et Cosmochimica Acta. 64, 2467-2477.

De La Rocha, C. L., Brzezinski, M. A., DeNiro, M. J., (1997) Fractionation of silicon isotopes by marine diatoms during biogenic silica formation. Geochimica et Cosmochimica Acta. 61, 5051-5056.

De La Rocha, C. L., Brzezinski, M. A., DeNiro, M. J., Shemesh, A., (1998) Silicon-isotope composition of diatoms as an indicator of past oceanic change. Nature. 395, 680-683.

De La Rocha, C. L., (2006) Opal-based isotopic proxies of paleoenvironmental conditions. Global Biogeochemical Cycles. 20, doi:10.1029/2005GB002664.

De La Rocha, C. L., (2002) Measurement of silicon stable isotope natural abundances via multicollector inductively coupled plasma mass spectrometry (MC-ICP-MS). Geochemistry Geophysics Geosystems. 3, doi: 10.1029/2002GC000310.

De La Rocha, C. L., Bescont, P., Croguennoc, A., Ponzevera, E., (2011) The Silicon Isotopic Composition of Surface Waters in the Atlantic and Indian Sectors of the Southern Ocean. Geochimica et Cosmochimica Acta. 75, 5283-5295.

de Souza, G. F., Reynolds, B. C., Rickli, J., Frank, M., Saito, M. A., et al., (2012) Southern Ocean control of silicon stable isotope distribution in the deep Atlantic Ocean. Global Biogeochemical Cycles. 26, doi: 10.1029/2011GB004141.

DeConto, R. M. and Pollard, D., (2003) Rapid Cenozoic glaciation of Antarctica induced by declining atmospheric CO_2. Nature. 421, 245-249.

Demarest, M. S., Brzezinski, M. A., Beucher, C. P., (2009) Fractionation of silicon isotopes during biogenic silica dissolution. Geochimica et Cosmochimica Acta. 73, 5572-5583.

Diekmann, B., Kuhn, G., Gersonde, R., Mackensen, A., (2004) Middle Eocene to early Miocene environmental changes in the sub-Antarctic Southern Ocean: Evidence from biogenic and terrigenous depositional patterns at ODP Site 1090. Global and Planetary Change. 40, 295-313.

Diester-Haass, L., (1995) Middle Eocene to Early Oligocene paleoceanography of the Antarctic Ocean (Maud Rise, ODP Leg 113, Site 689): Change from a low to a high productivity ocean. Palaeogeography, Palaeoclimatology, Palaeoecology. 113, 311-334.

Diester-Haass, L., (1991) Eocene/Oligocene paleoceanography in the Antarctic Ocean, Atlantic sector (Maud Rise, ODP leg 113, Site 689B and 690B). Marine Geology. 100, 249-276.

Diester-Haass, L., Robert, C., Chamley, H., (1993) Paleoceanographic and paleoclimatic evolution in the Weddell Sea (Antarctica) during the middle Eocene-late Oligocene, from a coarse sediment fraction and clay mineral data (ODP Site 689). Marine Geology. 114, 233-250.

Diester-Haass, L. and Zahn, R., (2001) Paleoproductivity increase at the Eocene–Oligocene climatic transition: ODP/DSDP sites 763 and 592. Palaeogeography, Palaeoclimatology, Palaeoecology. 172, 153-170.

Ding, T., Wan, D., Li, Y., Li, J., Song, H., Liu, Z., Yao, X., (1996) Silicon Isotope Geochemistry. Geological Publishing House, Beijing, China.

Douthitt, C. B., (1982) The geochemistry of the stable isotopes of silicon. Geochimica et Cosmochimica Acta. 46, 1449-1458.

EFSA, (2011) EFSA Panel on Dietetic Products, Nutrition and Allergies (NDA). EFSA Journal 2011. 9, 1-28.

Ehrmann, W. U. and Mackensen, A., (1992) Sedimentological evidence for the formation of an East Antarctic ice sheet in Eocene/Oligocene time. Palaeogeography, Palaeoclimatology, Palaeoecology. 93, 85-112.

Elderfield, H. and Rickaby, R. E., (2000) Oceanic Cd/P ratio and nutrient utilization in the glacial Southern Ocean. Nature. 405, 305-310.

Ellwood, M. J. and Hunter, K. A., (1999) Determination of the Zn/Si ratio in diatom opal: A method for the separation, cleaning and dissolution of diatoms. Marine Chemistry. 66, 149-160.

Ellwood, M. J., Wille, M., Maher, W., (2010) Glacial Silicic Acid Concentrations in the Southern Ocean. Science. 330, 1088-1091.

Epstein, S. and Taylor, H. P., (1971) $^{18}O/^{16}O$, $^{30}Si/^{28}Si$, D/H and $^{13}C/^{12}C$ ratios in lunar samples. Proceedings of the Lunar Science Conference. 2, 1421-1441.

Erez, J., (1978) Vital effect on stable-isotope composition seen in foraminifera and coral skeletons. Nature. 273, 199-202.

Falkowski, P. G., Katz, M. E., Knoll, A. H., Quigg, A., Raven, J. A., et al., (2004) The evolution of modern eukaryotic phytoplankton. Science. 305, 354-360.

Falkowski, P. G., Barber, R. T., Smetacek, V., (1998) Biogeochemical Controls and Feedbacks on Ocean Primary Production. Science. 281, 200-206.

Florindo, F. and Roberts, A. P., (2005) Eocene-Oligocene magnetobiochronology of ODP Sites 689 and 690, Maud Rise, Weddell Sea, Antarctica. Geological Society of America Bulletin. 117, 46-66.

Franois, R., Altabet, M. A., Yu, E., Sigman, D. M., Bacon, M. P., Frank, M., et al., (1997) Contribution of Southerin Ocean surface-water stratification to low atmopheric CO_2 during the last glacial period. Nature. 389, 929 - 935.

Fripiat, F., Cardinal, D., Tison, J., Worby, A., André, L., (2007) Diatom-induced silicon isotopic fractionation in Antarctic sea ice. Journal of Geophysical Research G: Biogeosciences. 112, doi:10.1029/2006JG000244.

Fripiat, F., Cavagna, A., Dehairs, F., de Brauwere, A., André, L., Cardinal, D., (2011a) Processes controlling the Si-isotopic composition in the Southern Ocean and application for paleoceanography. Biogeosciences Discussions. 8, 10155 - 10185.

Fripiat, F., Cavagna, A., Dehairs, F., Speich, S., André, L., Cardinal, D., (2011b) Silicon pool dynamics and biogenic silica export in the Southern Ocean, inferred from Si-isotopes. Ocean Science Discussions. 8, 639 - 674.

Fripiat, F., Cavagna, A., Savoye, N., Dehairs, F., André, L., Cardinal, D., (2011c) Isotopic constraints on the Si-biogeochemical cycle of the Antarctic Zone in the Kerguelen area (KEOPS). Marine Chemistry. 123, 11-22.

Georg, R. B., Reynolds, B. C., Frank, M., Halliday, A. N., (2006) New sample preparation techniques for the determination of Si isotopic compositions using MC-ICPMS. Chemical Geology. 235, 95-104.

Gersonde, R., Hodell, D. A., Blum, P., Andersson, C., Austin, W. E. N., et al., (1999) Leg 177 Initial Report. Proceedings of the Ocean Drilling Program, Initial Reports. 177, 1-67.

Harper, H. E. and Knoll, A. H., (1975) Silica, diatoms, and Cenozoic radiolarian evolution. Geology. 3, 175-177.

Haug, G. H., Ganopolski, A., Sigman, D. M., Rosell-Mele, A., Swann, G. E. A., et al., (2005) North Pacific seasonality and the glaciation of North America 2.7 million years ago. Nature. 433, 821-825.

Haug, G. H., Sigman, D. M., Tiedemann, R., Pedersen, T. F., Sarnthein, M., (1999) Onset of permanent stratification in the subarctic Pacific Ocean. Nature. 401, 779 - 782.

Heinze, C. and Crowley, T. J., (1997) Sedimentary response to ocean gateway circulation changes. Paleoceanography. 12, 742.

Hendry, K. R., Georg, R. B., Rickaby, R. E. M., Robinson, L. F., Halliday, A. N., (2010) Deep ocean nutrients during the Last Glacial Maximum deduced from sponge silicon isotopic compositions. Earth and Planetary Science Letters. 292, 290-300.

Hendry, K. R. and Rickaby, R. E. M., (2008) Opal (Zn/Si) ratios as a nearshore geochemical proxy in coastal Antarctica. Paleoceanography. 23, doi:10.1029/2007PA001576.

Hendry, K. R., Robinson, L. F., Meredith, M. P., Mulitza, S., Chiessi, C. M., Arz, H., (2012) Abrupt changes in high-latitude nutrient supply to the Atlantic during the last glacial cycle. Geology. 40, 123-126.

Hendry, K. R., Leng, M. J., Robinson, L. F., Sloane, H. J., Blusztjan, J., et al., (2011) Silicon isotopes in Antarctic sponges: an interlaboratory comparison. Antarctic Science. 23, 34-42.

Hendry, K. R. and Robinson, L. F., (2012) The relationship between silicon isotope fractionation in sponges and silicic acid concentration: Modern and core-top studies of biogenic opal. Geochimica et Cosmochimica Acta. 81, 1-12.

Hodell, D. A., Mueller, P. A., Garrido, J. R., (1991) Variations in the strontium isotopic composition of seawater during the Neogene. Geology. 19, 24-27.

Horn, M. G., Beucher, C. P., Robinson, R. S., Brzezinski, M. A., (2011) Southern ocean nitrogen and silicon dynamics during the last deglaciation. Earth and Planetary Science Letters. 310, 334-339.

Ito, T., (2005) The Antarctic Circumpolar Productivity Belt. Geophysical Research Letters. 32, doi:10.1029/2005GL023021.

Jaccard, S. L., Haug, G. H., Sigman, D. M., Pedersen, T. F., Thierstein, H. R., Röhl, U., (2005) Glacial/Interglacial Changes in Subarctic North Pacific Stratification. Science. 308, 1003-1006.

Katz, M. E., Cramer, B. S., Toggweiler, J. R., Esmay, G., Liu, C., et al., (2011) Impact of Antarctic Circumpolar Current Development on Late Paleogene Ocean Structure. Science. 332, 1076-1079.

Knox, F. and McElroy, M. B., (1984) Changes in atmospheric CO_2: influence of the marine biota at high latitude. Journal of Geophysical Research. 89, 4629-4637.

Kohfeld, K. E., Quéré, C. L., Harrison, S. P., Anderson, R. F., (2005) Role of Marine Biology in Glacial-Interglacial CO_2 Cycles. Science. 308, 74-78.

Kumar, N., Anderson, R. F., Mortlock, R. A., Froelich, P. N., Kubik, P., et al., (1995) Increased biological productivity and export production in the glacial Southern Ocean. Nature. 378, 675 - 680.

Latimer, J. C. and Filippelli, G. M., (2002) Eocene to Miocene terrigenous inputs and export production: Geochemical evidence from ODP Leg 177, Site 1090. Palaeogeography, Palaeoclimatology, Palaeoecology. 182, 151-164.

Lazarus, D. B., Hollis, C. J., Apel, M., (2008) Patterns of Opal and Radiolarian change in the Antarctic Mid-Paleogene: Clues to the Origin of the Southern Ocean. Micropaleontology. 54, 41-48.

Lear, C. H., Bailey, T. R., Pearson, P. N., Coxall, H. K., Rosenthal, Y., (2008) Cooling and ice growth across the Eocene-Oligocene transition. Geology. 36, 251-254.

Leng, M. J. and Barker, P. A., (2006) A review of the oxygen isotope composition of lacustrine diatom silica for palaeoclimate reconstruction. Earth-Science Reviews. 75, 5-27.

Leng, M. J. and Sloane, H. J., (2008) Combined oxygen and silicon isotope analysis of biogenic silica. Journal of Quaternary Science. 23, 313-319.

Livermore, R., Hillenbrand, C., Meredith, M., Eagles, G., (2007) Drake Passage and Cenozoic climate: An open and shut case? Geochemistry Geophysics Geosystems. 8, doi: 10.1029/2005GC001224.

Mackensen, A., (2004_ Changing Southern Ocean palaeocirculation and effects on global climate. Antarctic Science. 16, 369 - 386.

Maldonado, M., Carmona, M. C., Uriz, M. J., Cruzado, A., (1999) Decline in Mesozoic reef-building sponges explained by silicon limitation. Nature. 401, 785 - 788.

Marinov, I., Gnanadesikan, A., Toggweiler, J. R., Sarmiento, J. L., (2006) The Southern Ocean biogeochemical divide. Nature. 441, 964-967.

McCartney, L., (1990) Siliceous sponge spicules from Ocean Drilling Program Leg 113. Proceedings of the Ocean Drilling Program, Scientific Results. 113, 963-970.

Milligan, A. J., Varela, D. E., Brzezinski, M. A., Morel, F. M. M., (2004) Dynamics of silicon metabolism and silicon isotopic discrimination in a marine diatom as a function of pCO_2. Limnology and Oceanography. 49, 322-329.

Minoletti, F., Hermoso, M., Gressier, V., (2009) Separation of sedimentary micron-sized particles for palaeoceanography and calcareous nannoplankton biogeochemistry. Nature Protocols. 4, 14-24.

Misra, S. and Froelich, P. N., (2012) Lithium Isotope History of Cenozoic Seawater: Changes in Silicate Weathering and Reverse Weathering. Science. 335, 818 - 823.

Morley, D. W., Leng, M. J., Mackay, A. W., Sloane, H. J., Rioual, P., Battarbee, R. W., (2004) Cleaning of lake sediment samples for diatom oxygen isotope analysis. Journal of Paleolimnology. 31, 391-401.

Nelson, D. M., Treguer, P., Brzezinski, M. A., Leynaert, A., Queguiner, B., (1995) Production and dissolution of biogenic silica in the ocean: revised global estimates, comparison with regional data and relationship to biogenic sedimentation. Global Biogeochemical Cycle. 9, 359-372.

Nelson, D. M. and Smith Jr., W. O., (1986) Phytoplankton bloom dynamics of the western Ross Sea ice edge—II. Mesoscale cycling of nitrogen and silicon. Deep Sea Research Part A.Oceanographic Research Papers. 33, 1389-1412.

Orsi, A. H., Whitworth III, T., Nowlin Jr., W. D., (1995) On the meridional extent and fronts of the Antarctic Circumpolar Current. Deep Sea Research Part I: Oceanographic Research Papers. 42, 641-673.

Pagani, M., Zachos, J. C., Freeman, K. H., Tipple, B., Bohaty, S., (2005) Atmospheric science: Marked decline in atmospheric carbon dioxide concentrations during the Paleogene. Science. 309, 600-603.

Pagani, M., Huber, M., Liu, Z., Bohaty, S. M., Henderiks, J., et al., (2011) The role of carbon dioxide during the onset of Antarctic glaciation. Science. 334, 1261-1264.

Pegram, W. J., Krishnaswami, S., Ravizza, G. E., Turekian, K. K., (1992) The record of sea water $^{187}Os/^{186}Os$ variation through the Cenozoic. Earth and Planetary Science Letters. 113, 569-576.

Pichevin, L. E., Reynolds, B. C., Ganeshram, R. S., Cacho, I., Pena, L., et al., (2009) Enhanced carbon pump inferred from relaxation of nutrient limitation in the glacial ocean. Nature. 459, 1114-1118.

Pollard, R. T., Lucas, M. I., Read, J. F., (2002) Physical controls on biogeochemical zonation in the Southern Ocean. Deep Sea Research Part II: Topical Studies in Oceanography. 49, 3289-3305.

Poore, H. R., Samworth, R., White, N. J., Jones, S. M., McCave, I. N., (2006) Neogene overflow of Northern Component Water at the Greenland-Scotland Ridge. Geochemistry Geophysics Geosystems. 7, doi: 10.1029/2005GC001085.

Prescha, A., Zabłocka-Słowińska, K., Hojka, A., Grajeta, H., (2012) Instant food products as a source of silicon. Food Chemistry. 135, 1756-1761.

Rabosky, D. L. and Sorhannus, U., (2009) Diversity dynamics of marine planktonic diatoms across the Cenozoic. Nature. 457, 183-186.

Ragueneau, O., Savoye, N., Del Amo, Y., Cotten, J., Tardiveau, B., Leynaert, A., (2005) A new method for the measurement of biogenic silica in suspended matter of coastal waters: Using Si:Al ratios to correct for the mineral interference. Continental Shelf Research. 25, 697-710.

Ragueneau, O., Tréguer, P., Leynaert, A., Anderson, R. F., Brzezinski, M. A., et al., (2000) A review of the Si cycle in the modern ocean: recent progress and missing gaps in the application of biogenic opal as a paleoproductivity proxy. Global and Planetary Change. 26, 317-365.

Raymo, M. E., (1994) The Initiation of Northern Hemisphere Glaciation. Annual Review of Earth and Planetary Sciences. 22, 353-383.

Raymo, M. E. and Ruddiman, W. F., (1992) Tectonic forcing of late Cenozoic climate. Nature. 359, 117-122.

Reynolds, B.C., (2011) Silicon Isotopes as Tracers of Terrestrial Processes, in: Bakaran, M. (Ed.), Advances in Isotope Geochemistry. Springer, pp. 87-104.

Reynolds, B. C., Frank, M., Halliday, A. N., (2008) Evidence for a major change in silicon cycling in the subarctic North Pacific at 2.73 Ma. Paleoceanography. 23, doi: 10.1029/2007PA001563.

Reynolds, B. C., Georg, R. B., Oberli, F., Wiechert, U., Halliday, A. N., (2006a) Re-assessment of silicon isotope reference materials using high-resolution multi-collector ICP-MS. Journal of Analytical Atomic Spectrometry. 21, 266-269.

Reynolds, B. C., Aggarwal, J., Andre, L., Baxter, D., Beucher, C., et al., (2007) An inter-laboratory comparison of Si isotope reference materials. Journal of Analytical Atomic Spectrometry. 22, 561.

Reynolds, B. C., Frank, M., Halliday, A. N., (2006b) Silicon isotope fractionation during nutrient utilization in the North Pacific. Earth and Planetary Science Letters. 244, 431-443.

Robert, C., Diester-Haass, L., Chamley, H., (2002) Late Eocene–Oligocene oceanographic development at southern high latitudes, from terrigenous and biogenic particles: a comparison of Kerguelen Plateau and Maud Rise, ODP Sites 744 and 689. Marine Geology. 191, 37-54.

Robinson, R. S., (2004) Revisiting nutrient utilization in the glacial Antarctic: Evidence from a new method for diatom-bound N isotopic analysis. Paleoceanography. 19, doi: 10.1029/2003PA000996.

Salamy, K. A. and Zachos, J. C., (1999) Latest Eocene–Early Oligocene climate change and Southern Ocean fertility: inferences from sediment accumulation and stable isotope data. Palaeogeography, Palaeoclimatology, Palaeoecology. 145, 61-77.

Sarmiento, J.L., Gruber, N., (2006) Ocean Biogeochemical Dynamics. Princeton University Press, Princeton and Oxford.

Sarmiento, J. L., Gruber, N., Brzezinski, M. A., Dunne, J. P., (2004) High-latitude controls of thermocline nutrients and low latitude biological productivity. Nature. 427, 56-60.

Sarmiento, J. L. and Orr, J. C., (1991) Three-dimensional simulations of the impact of Southern Ocean nutrient depletion on atmospheric CO_2 and ocean chemistry. Limnology & Oceanography. 36, 1928-1950.

Sarmiento, J. L., Simeon, J., Gnanadesikan, A., Gruber, N., Key, R. M., Schlitzer, R., (2007) Deep ocean biogeochemistry of silicic acid and nitrate. Global Biogeochemical Cycles. 21, doi:10.1029/2006GB002720.

Sarmiento, J. L. and Toggweiler, J. R., (1984) A new model for the role of the oceans in determining atmospheric pCO_2. Nature. 308, 621-624.

Scher, H. D. and Martin, E. E., (2006) Timing and climatic consequences of the opening of drake passage. Science. 312, 428-430.

Schmitz, W. J., (2005) On the world ocean circulation. Volumn II, the Pacific and Indian Oceans/a global update. WHOI Technical Reports, doi:10.1575/1912/355.

Schumacher, S. and Lazarus, D., (2004) Regional differences in pelagic productivity in the late Eocene to early Oligocene—a comparison of southern high latitudes and lower latitudes. Palaeogeography, Palaeoclimatology, Palaeoecology. 214, 243-263.

Seki, O., Foster, G. L., Schmidt, D. N., Mackensen, A., Kawamura, K., Pancost, R. D., (2010) Alkenone and boron-based Pliocene pCO_2 records. Earth and Planetary Science Letters. 292, 201-211.

Shemesh, A., Burckle, L. H., Hays, J. D., (1995) Late Pleistocene oxygen isotope records of biogenic silica from the Atlantic sector of the Southern Ocean. Paleoceanography. 10, 179-196.

Shemesh, A., Mortlock, R. A., Smith, R. J., Froelich, P. N., (1988) Determination of Ge/Si in marine siliceous microfossils: Separation, cleaning and dissolution of diatoms and radiolaria. Marine Chemistry. 25, 305-323.

Sigman, D. M. and Boyle, E. A., (2000) Glacial/interglacial variations in atmospheric carbon dioxide. Nature. 407, 859-869.

Sigman, D. M., Jaccard, S. L., Haug, G. H., (2004) Polar ocean stratification in a cold climate. Nature. 428, 59-63.

Sigman, D. M., Altabet, M. A., Francois, R., McCorkle, D. C., Gaillard, J., (1999) The isotopic composition of diatom-bound nitrogen in Southern Ocean sediments. Paleoceanography. 14, 118-134.

Sigmon, D. E., Nelson, D. M., Brzezinski, M. A., (2002) The Si cycle in the Pacific sector of the Southern Ocean: seasonal diatom production in the surface layer and export to the deep sea. Deep Sea Research Part II: Topical Studies in Oceanography. 49, 1747-1763.

Sijp, W. P., England, M. H., Huber, M., (2011) Effect of the deepening of the Tasman Gateway on the global ocean. Paleoceanography. 26, doi: 10.1029/2011PA002143.

Singer, A. J. and Shemesh, A., (1995) Climatically linked carbon isotope variation during the past 430,000 years in Southern Ocean sediments. Paleoceanography. 10, 171-177.

Smetacek, V., (1999) Diatoms and the ocean carbon cycle. Protist. 150, 25-32.

Speer, K. G., Rintoul, S. R., Solyan, B., (2000) The diabatic Deacon Cell. Journal of Physical Oceanography. 22, 93-104.

Spiess, V., (1990) Cenozoic magnetostratigraphy of Leg 113 drill sites, Maud Rise, Weddell Sea, Antarctica. In Barker, P.F., Kennett, J.P., Et Al., Proc. ODP, Sci. Results. 113, 261-315.

Stickley, C. E., Brinkhuis, H., Schellenberg, S., Sluijs, A., Rohl, U., et al., (2004) Timing and nature of the deepening of the Tasmanian Gateway. Paleoceanography. 19, doi:10.1029/2004PA001022.

Swann, G. E. A. and Leng, M. J., (2009) A review of diatom $\delta^{18}O$ in palaeoceanography. Quaternary Science Reviews. 28, 384-398.

Swann, G. E. A., Leng, M. J., Sloane, H. J., Maslin, M. A., (2008) Isotope offsets in marine diatom $\delta^{18}O$ over the last 200 ka. Journal of Quaternary Science. 23, 389-400.

Takahashi, T., Sutherland, S. C., Sweeney, C., Poisson, A., Metzl, N., et al., (2002) Global sea–air CO2 flux based on climatological surface ocean pCO_2, and seasonal biological and temperature effects. Deep Sea Research Part II: Topical Studies in Oceanography. 49, 1601-1622.

Tozzi, S., Schofield, O., Falkowski, P., (2004) Historical climate change and ocean turbulence as selective agents for two key phytoplankton functional groups. Marine Ecology Progress Series. 274, 123-132.

Tréguer, P., Nelson, D. M., Van Bennekom, A. J., DeMaster, D. J., Leynaert, A., Quéguiner, B., (1995) The silica balance in the world ocean: A reestimate. Science. 268, 375-379.

Van Cappellen, P., (2002) Biogenic silica dissolution in the oceans: Reconciling experimental and field-based dissolution rates. Global Biogeochemical Cycles. 16, doi:10.1029/2001GB001431.

Varela, D. E., Pride, C. J., Brzezinski, M. A., (2004) Biological fractionation of silicon isotopes in Southern Ocean surface waters. Global Biogeochemical Cycles. 18, GB1047 1-8.

Volk, T., Hoffert, M.I., (1985) Ocean carbon pumps: analysis of relative strengths and efficiencies in ocean-driven atmospheric CO_2 changes, in: Sundquist, E. T., Broecker, W. S. (Eds.), The Carbon Cycle and Atmospheric CO_2: Natural Variations Archean to Present. American Geophysical Union, Washington, 99-110.

Watson, A. and Naveira Garabato, A. C., (2006) The role of Southern Ocean mixing and upwelling in glacial-interglacial atmospheric CO_2 change. Tellus B. 58, 73-87.

Whitworth III, T., Nowlin Jr, W. D., Orsi, A. H., Locarnini, R. A., Smith, S. G., (1994) Weddell Sea shelf water in the Bransfield Strait and Weddell-Scotia Confluence. Deep Sea Research Part I: Oceanographic Research Papers. 41, 629-641.

Wille, M., Sutton, J., Ellwood, M. J., Sambridge, M., Maher, W., Eggins, S., Kelly, M., (2010) Silicon isotopic fractionation in marine sponges: A new model for understanding silicon isotopic variations in sponges. Earth and Planetary Science Letters. 292, 281-289.

Young, E. D., Galy, A., Nagahara, H., (2002) Kinetic and equilibrium mass-dependent isotope fractionation laws in nature and their geochemical and cosmochemical significance. Geochimica Et Cosmochimica Acta. 66, 1095-1104.

Zachos, J., Pagani, H., Sloan, L., Thomas, E., Billups, K., (2001) Trends, rhythms, and aberrations in global climate 65 Ma to present. Science. 292, 686-693.

Zachos, J. C., Lohmann, K. C., Walker, J. C. G., Wise, S. W., (1993) Abrupt climate change and transient climates during the Paleogene: a marine perspective. Journal of Geology. 101, 191-213.

Zachos, J. C. and Kump, L. R., (2005) Carbon cycle feedbacks and the initiation of Antarctic glaciation in the earliest Oligocene. Global and Planetary Change. 47, 51-66.

Appendix 1: Silicon Isotope Data Tables

In the main text and figures, all errors are quoted as the external reproducibility (0.25‰), unless the internal 2σSD calculated on the 6-8 standard sample brackets was larger, in which case this is quoted. For samples having replicate analyses, an average value used in the main manuscript and figures was calculated as an average weighted by the internal 2 σSD error on each replicate measurement, and the new internal 2σSD was then calculated as $1/\sqrt{\sum(1/(2\sigma)^2)}$. ***^{30}Si** is the expected $\delta^{30}Si$ calculated from measured $\delta^{29}Si$ assuming mass dependent isotope fractionation, and is equal to **δ^{29}Si*0.5092. No.** is the number of standard sample brackets.

Table 1. Silicon isotope data from Chapter 3; core top diatom $\delta^{30}Si$ study of the Southern Ocean. Replicates between OXF-NIGL are splits of the same batch of dry opal, NIGL-NIGL are replicates of the same batch of dry opal, and OXF-OXF are replicates on the same solution of dissolved opal.

Sample	Size Fraction (μm)*[1,2]	Latitude	Longitude	$\delta^{30}Si$	2SD $\delta^{30}Si$	$\delta^{29}Si$	2SD $\delta^{29}Si$	($\delta^{30}Si$*0.5092)	Location
BC383		-66.72	-70.44						
	<2			0.7	0.1	0.34	0.02	0.36	NIGL
	2-5			1.04	0.1	0.53	0.02	0.53	NIGL
	5-8			1.01	0.1	0.5	0.02	0.51	NIGL
	5-8			0.93	0.1	0.49	0.02	0.47	NIGL
	8-10			0.96	0.1	0.47	0.02	0.49	NIGL
	12-20			0.78	0.1	0.39	0.02	0.4	NIGL
	12-20			0.8	0.14	0.41	0.07	0.41	OXF
	20-50			-0.53	0.1	-0.25	0.02	-0.27	NIGL
	>50			-1.21	0.07	-0.59	0.11	-0.62	OXF
	Bulk			0.39	0.1	0.18	0.03	0.3	NIGL
385		-68.02	-70.52						
	<2			0.37	0.12	0.20	0.07	0.19	OXF
	2-5			0.91	0.15	0.47	0.07	0.48	OXF
	5-8			0.78	0.07	0.41	0.05	0.40	OXF
	8-12			0.93	0.24	0.52	0.11	0.47	OXF
	12-20			0.82	0.15	0.39	0.09	0.42	OXF
	20-50			0.7	0.17	0.29	0.17	0.36	OXF

	Bulk			0.59	0.11	0.32	0.07	0.32	OXF
391		-67.86	-68.23						
	<2			0.37	0.12	0.2	0.06	0.19	NIGL
	2-5			0.77	0.12	0.34	0.06	0.39	NIGL
	5-8			0.76	0.12	0.34	0.06	0.39	NIGL
	8-12			0.64	0.12	0.31	0.06	0.29	NIGL
	8-12			0.56	0.12	0.27	0.06	0.23	NIGL
	12-20			0.46	0.12	0.22	0.06	0.23	NIGL
	20-50			-0.53	0.18	-0.13	0.14	-0.27	OXF
	>50			-1.84	0.21	-0.88	0.18	-0.27	OXF
	Bulk			0.47	0.12	0.24	0.06	0.24	NIGL
KC08A		-63.34	-55.87						
	<2			-1.14	0.16	-0.56	0.11	-0.58	OXF
	2-5			0.28	0.16	0.13	0.08	0.14	OXF
	5-8			0.49	0.26	0.25	0.1	0.25	OXF
	8-12			0.05	0.16	-0.03	0.11	0.03	OXF
	12-20			-0.47	0.1	-0.26	0.08	-0.24	OXF
	20-41			-1.02	0.07	-0.53	0.09	-0.52	OXF
	>41			-0.74	0.2	-0.4	0.1	-0.38	OXF
	Bulk			-0.81	0.11	-0.44	0.07	-0.41	OXF
TAN127		-57.56	160.87						
	<2			2.36	0.31	1.30	0.29	1.20	OXF
	2-5			1.84	0.30	0.94	0.18	0.94	OXF
	2-5			1.69	0.15	0.85	0.21	0.86	OXF
	5-8			1.78	0.25	0.91	0.22	0.91	OXF
	8-12			1.32	0.26	0.75	0.22	0.67	OXF
	12-20			1.46	0.26	0.78	0.22	0.74	OXF
	12-20			1.38	0.17	0.67	0.11	0.7	OXF
	20-41			0.86	0.26	0.42	0.22	0.44	OXF
	20-41			1.18	0.14	0.67	0.09	0.60	OXF
	41-50			0.8	0.19	0.4	0.21	0.41	OXF
	41-50			0.9	0.24	0.49	0.13	0.46	OXF
	>50			0.45	0.19	0.28	0.09	0.23	OXF
	Bulk			1.21	0.24	0.61	0.14	0.62	OXF
	Bulk			1.68	0.26	0.88	0.25	0.86	OXF
TAN124		-58.69	160.23						
	2-5			1.88	0.27	0.94	0.12	0.96	OXF
	2-5			1.8	0.21	1.03	0.15	0.92	OXF
	5-8			1.71	0.3	0.93	0.19	0.87	OXF
	5-8			1.76	0.15	0.93	0.13	0.9	OXF
	8-12			1.99	0.26	1.07	0.16	1.01	OXF

	12-20			1.34	0.29	0.71	0.18	0.68	OXF
	20-41			1.24	0.22	0.62	0.15	0.63	OXF
	41-50			1.40	0.21	0.81	0.17	0.71	OXF
	>50			-0.05	0.15	0.00	0.15	-0.03	OXF
	Bulk			1.67	0.39	1.02	0.22	0.85	OXF
NZ4		-61.77	174.42						
	2-20			2.02	0.26	1.02	0.2	1.03	OXF
	2-20			1.89	0.22	0.98	0.19	0.96	OXF
	20-63			0.72	0.16	0.37	0.16	0.37	OXF
NZ5		-63.11	-169.74						
	2-20			1.58	0.33	0.84	0.2	0.81	OXF
	2-20			1.52	0.18	0.79	0.12	0.46	OXF
	20-63			0.9	0.16	0.47	0.12	0.46	OXF
NZ6		-63.29	174.78						
	2-20			1.14	0.2	0.6	0.13	0.58	OXF
	20-63			1.36	0.16	0.67	0.08	0.69	OXF
	20-63			1.32	0.12	0.63	0.07	0.67	OXF
NZ7		-60.42	-170.19						
	2-20			1.8	0.15	0.96	0.14	0.92	OXF
	20-63			1.38	0.12	0.7	0.1	0.7	OXF
	20-63			1.15	0.2	0.57	0.1	0.59	OXF
NZ11		-63.63	-169.32						
	2-20			1.55	0.14	0.77	0.12	0.79	OXF
	2-20			1.27	0.2	0.64	0.11	0.65	OXF
	20-63			1.62	0.15	0.82	0.12	0.82	OXF
1090-18		-41.81	8.9						
	2-10			1.87	0.18	0.92	0.09	0.95	OXF
	10-20			1.87	0.16	0.94	0.05	0.95	OXF
	20-41			0.08	0.15	0.07	0.05	0.04	OXF
		-41.81	8.9						
1090-20	2-10			2.07	0.17	1.10	0.08	1.05	OXF
	10-20			1.75	0.21	0.89	0.16	0.89	OXF
	20-41			0.28	0.15	0.15	0.06	0.20	OXF
		-41.81	8.9						
1090-26	2-10			1.89	0.15	0.97	0.12	0.96	OXF
	20-41			0.71	0.07	0.36	0.03	0.36	OXF
		-41.81	8.9						
1090-31	2-10			1.36	0.07	0.72	0.08	0.69	OXF
	20-41			0.00	0.12	-0.02	0.05	0.00	OXF

Table 2. Diatom $\delta^{30}Si$ values for Southern Ocean core top calibration, Chapter 3d

Core	Section	Interval (cm)	Depth (mbsf)	Depth (mcd)	Age (Ma Channell, CK95)	Size Fraction (µm) *[1,2]	$\delta^{30}Si$ (‰)	2SD	$\delta^{29}Si$ (‰)	2SD	*30 Si	no.	date
16	4	80-81	142.5	149.15	24.23	2-10	2.02	0.26	1.05	0.08	1.03	8	13 Jun 11
17	6	50-51	154.07	161.57	24.94	2-10	1.92	0.19	1.01	0.12	0.98	8	13 Jun 11
18	3	112-113	160.32	168.1	25.50	2-10	1.87	0.18	0.92	0.09	0.95	8	13 Jun 11
20	3	55-56	178.75	186.36	27.07	2-10	1.99	0.20	1.04	0.12	1.01	4	13 Jun 11
20	3	55-56	178.75	186.36	27.07	2-10	2.05	0.20	1.08	0.13	1.05	4	13 Jun 11

20	3	55-56	178.75	186.36	27.07	2-10	2.20	0.32	1.14	0.11	1.12	8	14 Jun 11
21	6	70-71	192.9	200.95	28.05	2-10	1.62	0.11	0.81	0.06	0.82	8	14 Jun 11
22	7	11-12	203.51	211.12	28.66	2-10	1.97	0.20	1.04	0.09	1.00	8	14 Jun 11
23	7	115-116	213.15	221.55	32.85	2-10	1.88	0.13	0.99	0.08	0.96	8	14 Jun 11
24	1	125-126	215.05	226.01	33.11	2-10	1.55	0.18	0.79	0.11	0.79	8	22 Oct 11
24	2	125-126	216.45	227.41	33.15	2-10	1.70	0.31	0.87	0.24	0.87	7	22 Oct 11
24	4	10-11	218.4	229.36	33.20	2-10	1.91	0.15	0.99	0.09	0.97	8	14 Jun 11
24	5	15-16	220.05	231.01	33.25	2-10	1.70	0.22	0.96	0.14	0.87	8	22 Oct 11
24	6	120-121	222.5	233.46	33.31	2-10	1.76	0.12	0.85	0.19	0.89	8	22 Oct 11
25	2	45-46	225.45	236.16	33.39	2-10	1.89	0.17	0.99	0.07	0.96	8	14 Jun 11
25	5	47-48	229.97	240.68	33.51	2-10	1.79	0.16	0.92	0.12	0.91	8	22 Oct 11
26	2	94-95	235.7	247.64	33.69	2-10	1.52	0.24	0.71	0.16	0.78	8	22 Oct 11
26	5	11-12	239.31	251.3	33.79	2-10	1.89	0.15	0.97	0.12	0.96	8	14 Jun 11
27	4	47-48	247.87	259.86	34.02	2-10	1.57	0.09	0.82	0.10	0.80	8	29 Jul 11
27	5	21-22	250.61	262.6	34.09	2-10	1.32	0.16	0.67	0.12	0.67	8	22 Oct 11
27	5	21-22	250.61	262.6	34.09	2-10	1.22	0.13	0.61	0.08	0.62	8	9 Nov 11
28	1	103-104	253.63	265.62	34.17	2-10	1.59	0.17	0.80	0.09	0.81	8	22 Oct 11
28	4	86-87	257.96	269.95	34.28	2-10	1.68	0.18	0.90	0.14	0.85	8	30 Jul 11
29	3	14-15	265.44	277.43	34.48	2-10	1.76	0.11	0.91	0.12	0.89	8	30 Jul 11
29	3	14-15	265.44	277.43	34.48	2-10	1.66	0.16	0.83	0.07	0.85	8	31 Jul 11
30	6	138-139	280.88	292.87	35.50	2-10	1.82	0.19	0.95	0.20	0.93	6	29 Jul 11
30	6	138-139	280.88	292.87	35.50	2-10	1.79	0.17	0.93	0.11	0.91	8	30 Jul 11
31	5	62-63	288.32	300.31	35.90	2-10	1.36	0.07	0.72	0.08	0.69	8	14 Jun 11
33	1	16-17	295.06	307.05	36.24	2-10	1.16	0.14	0.64	0.12	0.59	8	30 Jul 11
34	1	55-56	301.65	313.64	36.46	2-10	1.65	0.14	0.90	0.10	0.84	8	29 Jul 11
35	2	36-37	312.66	324.65	36.82	2-10	1.79	0.12	0.91	0.10	0.91	8	30 Jul 11
36	6	49-50	328.39	340.38	37.50	2-10	1.30	0.19	0.68	0.13	0.66	8	29 Jul 11
37	3	108-109	334.08	346.07	38.04	2-10	1.19	0.10	0.58	0.11	0.61	8	22 Oct 11
16	4	80-81	142.5	149.15	24.23	10-20	2.04	0.13	1.02	0.11	1.04	8	31 Jul 11
17	6	50-51	154.07	161.57	24.94	10-20	1.95	0.22	1.03	0.10	0.99	7	27 Aug 11
18	3	112-113	160.32	168.1	25.50	10-20	1.87	0.16	0.94	0.05	0.95	8	30 Aug 11
19	2	5-6	167.25	176.74	26.17	10-20	1.77	0.10	0.93	0.07	0.90	8	30 Jul 11
20	3	55-56	178.75	186.36	27.07	10-20	1.75	0.21	0.89	0.16	0.89	8	27 Aug 11
21	6	70-71	192.9	200.95	28.05	10-20	1.49	0.15	0.77	0.08	0.76	8	31 Jul 11
22	7	11-12	203.51	211.12	28.66	10-20	2.08	0.11	1.08	0.12	1.06	8	30 Jul 11
23	7	115-116	213.15	221.55	32.85	10-20	1.68	0.18	0.78	0.12	0.85	8	31 Jul 11
24	4	10-11	218.4	229.36	33.20	10-20	1.99	0.08	1.02	0.08	1.01	8	30 Aug 11
25	2	45-46	225.45	236.16	33.39	10-20	1.90	0.21	0.97	0.11	0.97	8	30 Aug 11
26	5	11-12	239.31	251.3	33.79	10-20	2.09	0.38	1.08	0.09	1.06	8	30 Aug 11
27	4	47-48	247.87	259.86	34.02	10-20	1.67	0.21	0.88	0.17	0.85	5	30 Jul 11
27	4	47-48	247.87	259.86	34.02	10-20	1.68	0.20	0.82	0.07	0.85	8	31 Jul 11

28	4	86-87	257.96	269.95	34.28	10-20	1.76	0.13	0.84	0.10	0.90	8	31 Jul 11
30	6	138-139	280.88	292.87	35.50	10-20	1.66	0.13	0.88	0.08	0.85	8	30 Jul 11
33	1	16-17	295.06	307.05	36.24	10-20	1.65	0.14	0.89	0.07	0.84	8	30 Aug 11
34	1	55-56	301.65	313.64	36.46	10-20	1.60	0.18	0.79	0.09	0.81	8	31 Jul 11
35	2	36-37	312.66	324.65	36.82	10-20	1.69	0.16	0.89	0.12	0.86	8	27 Aug 11
36	6	49-50	328.39	340.38	37.50	10-20	1.28	0.21	0.61	0.07	0.65	8	31 Jul 11
37	3	108-109	334.08	346.07	38.04	10-20	0.96	0.22	0.52	0.18	0.49	8	27 Aug 11

Table 3. Sponge silicon isotope values (Chapters 4 and 5), all samples from ocean drilling project core ODP113-689B. CHEMISTRY/ANALYSIS indicated a replicate measurement of the same solution of dissolved sponge spicules which has undergone separate column chemistry and analysis. REPICKED indicates a complete methodological repeat, where a new batch of sponge spicules have been picked, cleaned, dissolved, put through column chemistry and analysed.

Core	Section	Interval	Depth	Age	δ^{30}Si (‰)	2σSD	δ^{29}Si (‰)	2σSD	*30Si	No.	Date	Type of replicate
2	4	18cm	9.98	4.16	-2.39	0.26	-1.14	0.27	-1.22	7	20th Feb 2012	
3	2	39-40	16.69	5.20	-1.78	0.19	-0.9	0.12	-0.91	8	9th Mar 2012	
3	2	39-40	16.69	5.20	-2.38	0.5	-1.17	0.32	-1.21	8	23rd Feb 2012	CHEMISTRY/ANALYSIS
3	3	20-21	18.00	5.39	-2.29	0.12	-1.19	0.13	-1.16	8	18th July 2012	
3	3	120-121	19.00	6.77	-2.56	0.16	-1.29	0.15	-1.3	8	18th July 2012	
3	4	70-71	20.00	7.38	-2.59	0.16	-1.34	0.1	-1.32	8	18th July 2012	
4	2	120-121	27.00	9.82	-2.57	0.22	-1.31	0.1	-1.31	8	16th Jun 2012	
4	3	70-71	28.00	9.92	-2.95	0.13	-1.48	0.14	-1.5	8	9th Mar 2012	
4	4	20-21	29.00	10.03	-2.45	0.28	-1.28	0.15	-1.25	8	15th Jun 2012	
4	5	70-71	31.00	10.23	-2.98	0.13	-1.54	0.16	-1.52	8	16th Jun 2012	
5	1	120-121	34.00	10.54	-2.77	0.34	-1.39	0.09	-1.41	7	15th Jun 2012	
5	3	116-117	37.96	10.95	-2.6	0.16	-1.34	0.14	-1.32	8	10th Mar 2012	
5	3	145-146	38.25	11.00	-2.94	0.13	-1.48	0.19	-1.5	8	16th Jun 2012	
6	2	50-51	45.30	12.60	-2.14	0.26	-1.1	0.14	-1.09	8	10th Mar 2012	
6	2	120-121	46.00	12.68	-2.73	0.47	-1.43	0.3	-1.39	8	20th Feb 2012	
6	2	120-121	46.00	12.68	-2.95	0.19	-1.46	0.24	-1.5	8	20th Feb 2012	REPICKED
6	4	20-21	48.00	12.91	-2.22	0.23	-1.16	0.14	-1.13	7	9th Mar 2012	
6	4	120-121	49.00	13.09	-2.86	0.24	-1.45	0.13	-1.46	8	10th Mar	

											2012	
6	5	70-71	50.00	13.36	-2.49	0.24	-1.56	0.14	-1.5	8	21st Feb 2012	
6	5	70-71	50.00	13.36	-2.39	0.2	-1.22	0.13	-1.22	8	21st Apr 2012	CHEMISTRY/ANALYSIS
6	6	20-21	52.00	13.74	-2.95	0.12	-1.48	0.06	-1.5	8	8th Mar 2012	
7	1	110-111	54.00	14.17	-2.62	0.16	-1.33	0.1	-1.34	8	21st Feb 2012	
7	1	110-111			-2.28	0.59	-1.18	0.4	-1.16	5	22nd Feb 2012	REPICKED
7	3	10-11	56.00	14.98	-1.93	0.23	-1.04	0.11	-0.98	8	21st Feb 2012	
7	3	110-111	57.00	15.10	-2.71	0.2	-1.35	0.12	-1.38	8	8th Mar 2012	
7	4	93-94	58.33	15.72	-2.89	0.15	-1.53	0.16	-1.47	8	20th Feb 2012	
7	4	93-94	58.33	15.72	-2.78	0.17	-1.43	0.07	-1.42	8	20th Feb 2012	REPICKED
7	6	0-1	60.40	17.72	-2.67	0.24	-1.33	0.1	-1.36	8	10th Mar 2012	
7	6	66-67	61.06	17.99	-3.32	0.12	-1.7	0.07	-1.69	8	8th Mar 2012	
7	6	66-67	61.06	17.99	-3.45	0.14	-1.75	0.1	-1.75	7	29th Apr 2012	
8	4	109-110	68.09	25.47	-2.86	0.23	-1.46	0.18	-1.46	8	29th Apr 2012	
8	4	109-110	68.09	25.47	-2.99	0.33	-1.62	0.16	-1.52	8	29th Apr 2012	REPICKED
8	6	60-61	70.60	25.98	-2.41	0.18	-1.23	0.14	-1.23	7	29th Apr 2012	
9	3	80-81	75.90	26.50	-3.35	0.22	-1.73	0.11	-1.7	8	14th May 1012	
9	3	80-81	75.90	26.50	-3.04	0.23	-1.54	0.16	-1.55	8	14th May 1012	CHEMISTRY/ANALYSIS
9	5	110-111	79.20	26.99	-2.41	0.17	-1.17	0.16	-1.23	6	20th Apr 2012	
9	5	110-111	79.20	26.99	-2.66	0.24	-1.36	0.16	-1.35	7	29th Apr 2012	CHEMISTRY/ANALYSIS
10	1	81-82	82.51	27.50	-2.9	0.08	-1.44	0.08	-1.48	6	29th Apr 2012	
12	2	71-72	103.21	30.00	-2.71	0.1	-1.38	0.12	-1.38	8	18th July 2012	
12	3	36-37	104.36	30.46	-3.01	0.29	-1.46	0.23	-1.53	6	20th Apr 2012	
12	6	101-102	109.51	31.51	-2.83	0.25	-1.37	0.15	-1.44	7	20th Apr 2012	
12	6	101-102	109.51	31.51	-3.31	0.11	-1.72	0.12	-1.69	8	29th Apr 2012	CHEMISTRY/ANALYSIS
12	6	101-102	109.51	31.51	-2.89	0.13	-1.5	0.13	-1.47	8	29th Apr 2012	REPICKED
13	1	75	110.91	31.81	-3.35	0.19	-1.71	0.13	-1.71	8	18th July 2012	
13	3	15	113.75	32.42	-2.3	0.33	-1.22	0.22	-1.17	8	18th July 2012	
13	4	78	115.88	32.88	-2.86	0.15	-1.49	0.07	-1.46	8	8th Nov 2011	
13	5	80	117.4	33.17	-2.93	0.16	-1.51	0.11	-1.49	8	18th July 2012	
13	5	80	117.4	33.17	-2.15	0.19	-1.1	0.13	-1.09	8	26th Nov 2011	REPICKED
13	6	75	118.85	33.41	-2.18	0.33	-1.15	0.16	-1.11	8	26th Nov 2011	
13	6	75	118.85	33.41	-2.55	0.14	-1.28	0.11	0.66	8	9th Nov 2011	REPICKED
13	7	15	119.76	33.56	-2.59	0.23	-1.24	0.12	-1.32	8	26th Nov 2011	
13	7	15	119.76	33.56	-2.59	0.24	-1.36	0.2	-1.32	7	8th Nov	REPICKED

											2011	
14	1	75	120.95	33.86	-2.83	0.2	-1.39	0.31	-1.44	4	23rd Nov 2011	
14	1	75	120.95	33.86	-2.59	0.16	-1.31	0.18	-1.32	6	26th Nov 2011	CHEMISTRY/ANALYSIS
14	1	75	120.95	33.86	-2.52	0.11	-1.28	0.08	-1.28	8	8th Nov 2011	REPICKED
14	3	43	123.63	34.54	-3.05	0.14	-1.56	0.1	-1.55	8	8th Nov 2011	
14	3	43	123.63	35.54	-3.39	0.09	-1.71	0.07	1.73	8	8th Nov 2011	REPICKED
14	3	122	124.42	34.77	-2.55	0.25	-1.3	0.15	-1.3	7	8th Nov 2011	
14	4	75	125.45	35.00	-2.49	0.21	-1.23	0.18	-1.27	8	18th July 2012	
14	5	75	126.95	35.18	-2.45	0.18	-1.3	0.11	-1.25	8	18th July 2012	
15	3	75	133.65	36.25	-2.73	0.11	-1.39	0.12	-1.39	8	23rd Nov 2011	
15	4	75	135.15	36.56	-2.35	0.23	-1.2	0.2	-1.2	8	26th Nov 2011	
15	5	125	137.15	36.78	-1.26	0.24	-0.69	0.21	-0.64	8	27th Nov 2011	
16	1	75	140.15	37.07	-2.21	0.11	-1.06	0.12	-1.12	8	18th July 2012	
16	1	75	140.15	37.07	-1.79	0.16	-0.87	0.11	-0.91	8	27th Nov 2011	REPICKED
OUTLERS												
3	2	120-121	17.54	6.7	-4.2	0.2	-2.18	0.12	-2.14	8	18th July 2012	REPICKED
4.00	3.00	70-71	28	9.9	-3.79	0.22	-1.89	0.16	-1.93	8	20th Feb 2012	REPICKED
5	3	116-117	37.96	10.9	-3.5	0.26	-1.77	0.2	-1.78	8	15th Jun 2012	REPICKED

Appendix 2: Fragmentation during Microseparation

To minimise fragmentation during microseparation, a low power ultrasonic bath (Fisherbrand FB11002 fitted with A emitters at 40 watts, total ultrasonic power 40 Hz) is employed in the ultrasonic filtration technique. However, diatom valve fragmentation occurring during sonication is still a cause for concern, and would decrease the ability of the technique to separate diatom species and non-diatom components. To investigate optimal sonication settings and potential biogenic opal fragmentation, an assessment of fragmentation was carried out as follows: A suspension of mainly centric diatoms (dominantly *Thalassiosira lentiginosa*) in the size range 20-50μm was subjected to the two lowest (20% and 40%) power settings for up to 2 hours. The suspension was placed in a beaker and on the bottom of the bath. Smear slides were made from material removed at 5min, 15min, 20min, 1hr and 2hrs and of the sample prior to sonication. Fragmentation was then analysed by counting the numbers of fragments in the ranges >75% of a valve (i.e. whole valves), 50-<75%, 25-<50%, and <25%. Fragmentation at 20% power does not become significant until greater than 30 minutes of sonication, with the number of whole valves decreasing from 50% to 45% in that time, but subsequently to 25% after 1hour (Figure 1a). However, at 40% power (Figure 1b), fragmentation is much quicker, with the number of whole valves decreasing from the initial 50% to 30% after 15 minutes, 20% after 30 minutes and to only 10% after 2 hours.

These are maximum estimates of the fragmentation which may occur during ultrasonic filtration for two reasons; firstly, the large centric diatoms that make up the bulk of this sample are probably the most susceptible to fragmentation, and secondly because the suspension is placed directly in the bath and is subjected to sonication for the entire 2 hours. In the real situation, the suspension moves through the beaker suspended in the bath into another beaker which is not in the bath – so the suspension is not subjected to sonication for the entire time the separation is

taking place. Nonetheless the experiment shows that fragmentation is a justified concern, and likely does occur to some extent during the filtrations. As such the time material is subjected to sonication should be kept as minimal as possible and only the lowest power (20%) setting should be used. It should be noted however, that filtrations at >20μm take less than 5 minutes, and therefore are highly unlikely to fragment large, non- diatom components such as radiolaria, which would lead to their fragments being incorporation into smaller size fractions than for normal sieving.

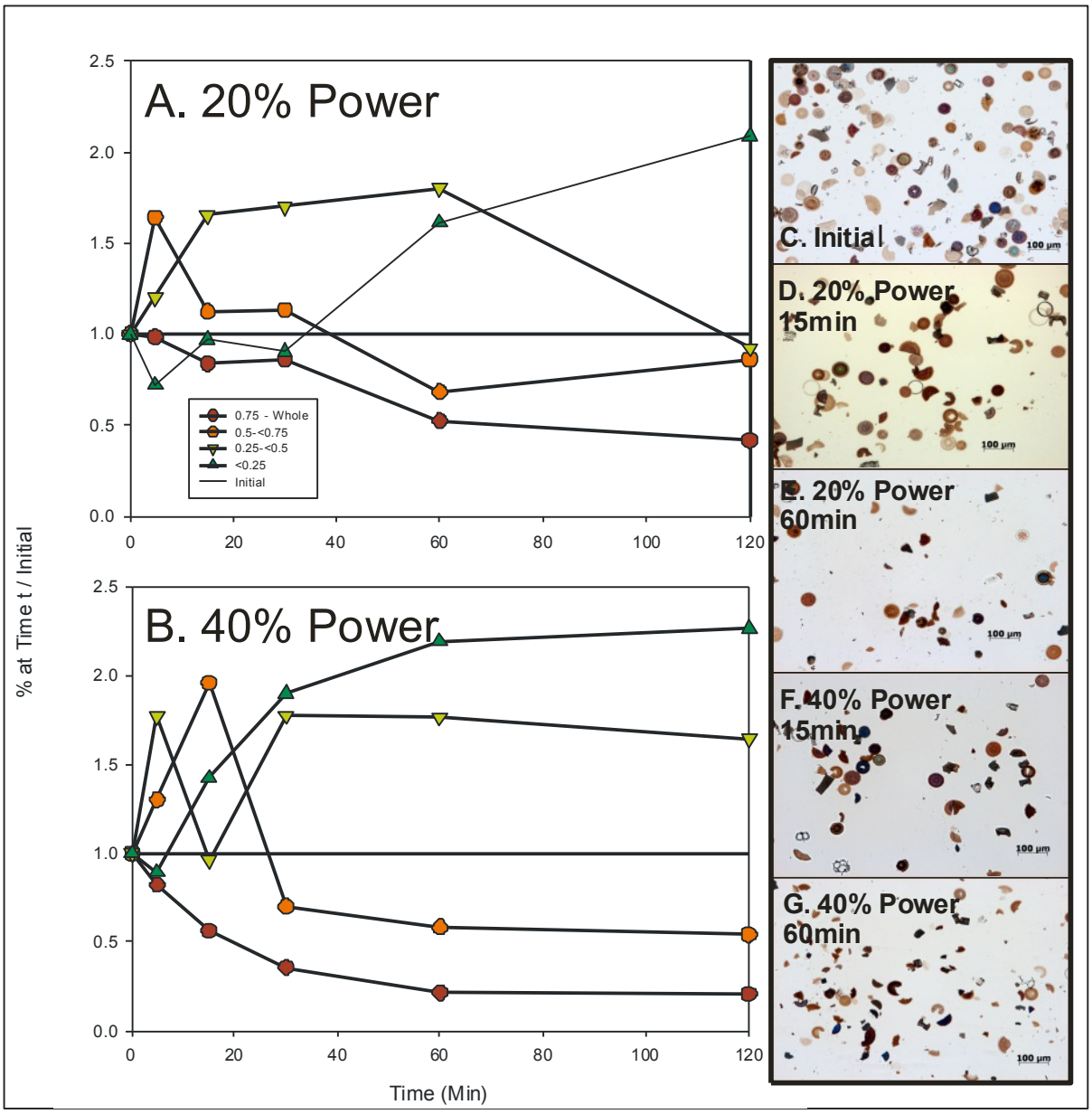


Figure A1. Fragmentation with time. Fragmentation was determined by counting the number of valves in the ranges >0.75, 0.5-0.75, 0.25-0.5 and <0.25 at each time interval. The percentage of valves in each range at time t is plotted over the initial number of valves in that range before ultrasonication (i.e. a value of 1 means no fragmentation has occurred. For whole valves, values <1 means valves have been fragmented, for <0.25, valves >1 mean fragments have been gained from the breakup of larger valves). Fragmentation is minimised if valves are only subjected to 20% power for up to an hour. This is a maximum estimate of fragmentation.

Appendix 3: Diatom Species Composition of Size Fractions

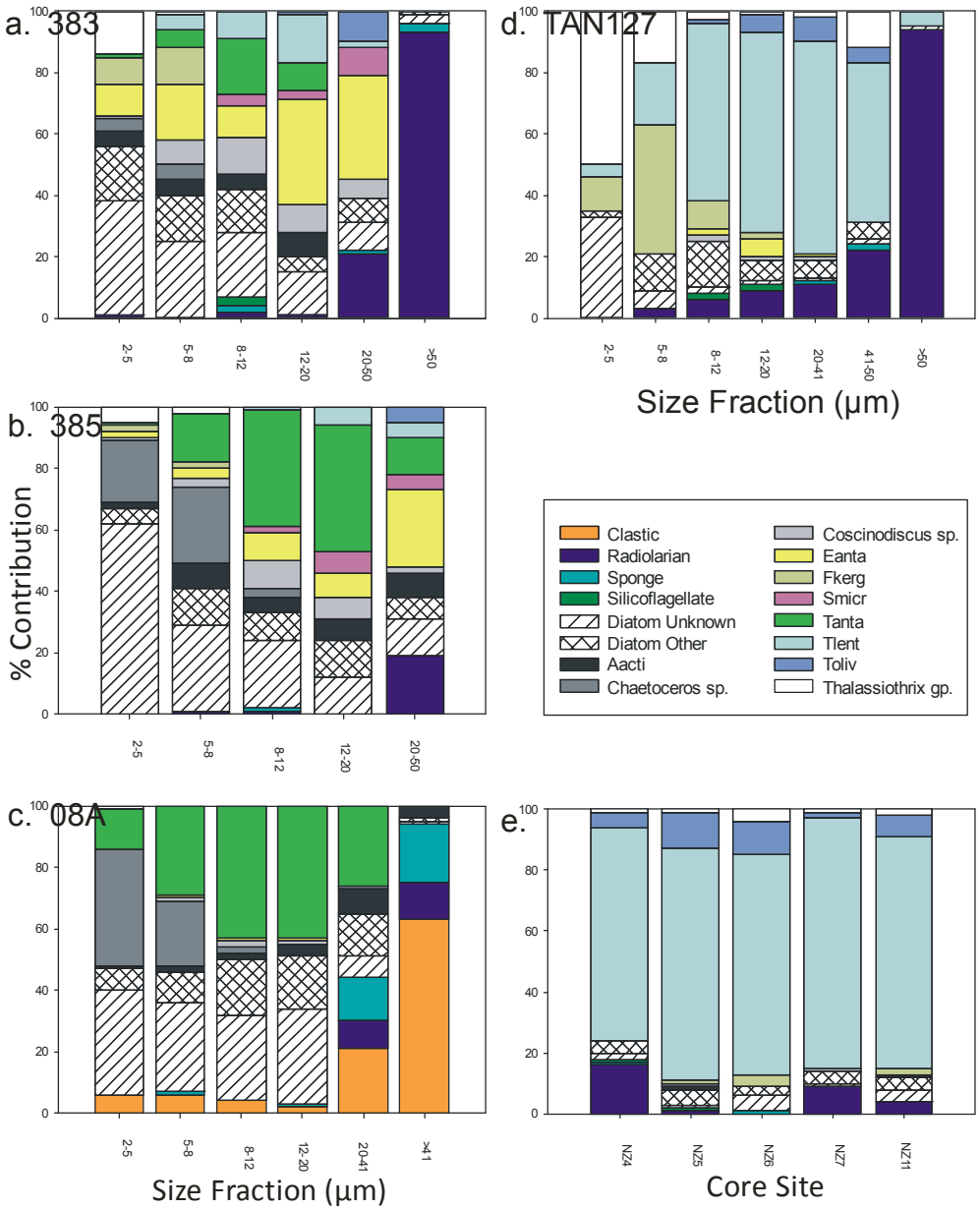


Figure 9. Size fraction assemblage showing both diatom and non-diatom components **a.** 383; **b.** 385; **c.** 08A; **d.** TAN127; **e.** NZ Sites, 20-63µm fraction. Total diatom percentage is lowest in the >50µm size fraction, which is dominated by radiolaria (or clastic grains at site KC08A), and is highest between 2 and 20µm. The diatom species assemblage is most diverse at site 383,

compared to the Pacific sector sites which are dominated by only three main diatoms; *Thalassiosira lenitginosa*, *Thalassiothrix* gp. species and *Fragilariopsis kerguelensis*. High numbers of unidentifiable diatom fragments occur in the smaller size fractions of the Antarctic Peninsula sites. On the Antarctic Peninsula, a separation can be made between *Thalassiosira antarctica* and *Cheatoceros* resting spores (sites 385 and KC08A), and in the Pacific Sector between *T. lentiginsoa*, *F. kerguelensis* and *Thalassiothrix* group species (site TAN127). Aacti = *Actinocyclus actinochilus*, Eanta = *Eucampia antarctica,* Fkerg = *Fragilariopsis kerguelensis,* Smicr = *Stellarima microtrias,* Tanta = *Thalassiosira antarctica,* Toliv = *Thalassiosira oliveriana*.

Acknowledgements

These have, of course, been done at the last minute in an incredible rush. But don't let the inevitable typos and nonsensical sentences detract from the gratitude I have to all the people included here.

Mum, Dad, Clare, Eleanor – Thank you, I couldn't have put this together without your support. I'm still swimming. Ros, thank you for giving me the opportunity – I don't think that many people would have! And for putting up with the endless mad dashes to finish presentations, posters, written documents.... Micheäl, please learn to speak properly (but there wouldn't have been so much of a thesis without your help, please thank you sorry). Kate, your efficiency amazes me, and I'm so so grateful for you all of your insight and support. Thanks to all those people who have taught me and put up with me in the labs/on the mass spec, and to Jorn for his selfless help with my maths. Thanks to Alex Halliday for supervision. And finally Shamita, thank you for accepting me, even without maths!

To the people who taught me to play politics: I didn't enjoy the lessons, but the skills will last me for life, thank you.

BGC, I've got a code red! Laura, Dan, Chris – living you guys was great, but I still don't think I'm doing my washing up quite right.... can anyone help?? Richard – can't believe this is finally the end Tristan – thanks for the chat. To everyone else and the people I have certainly missed, sorry and thank you.